UNIVERSITAT
POLITÈCNICA
DE VALÈNCIA

Analysis and Design of Reconfigurable Antennas Using the Theory of Characteristic Modes

Zakaria Mahlaoui Boudallaa

Advisor: Pr Eva Antonino Daviu

Universitat Politècnica de Valéncia

A thesis submitted for the degree of

Philosophiæ Doctor (PhD)

December 2023

Day of the defense: 1^{st} **of December 2023**
Valencia, Spain

To My Mom Hana, Sara, Zayd, Doha, and Yassine.
For their endless love, support and encouragement

Acknowledgements

Personal Acknowledgements:

First and foremost, I'd like to thank my mother and my wife for their understanding, patience, support and energy during my doctorate, and merely to be by my side. Without you, I wouldn't be at this point.

I warmly thank my advisors Pr Eva for her guidance, helpful comments, informative advises, and especially for her constructive criticisms. The fields of research I have covered in this thesis are still young and in growing demand. I very much appreciate your undertaking to guide me in this thesis.

I greatly appreciate all the comments, thoughts and stimulating questions, and, last not least, the LaTeX help of my dear friends and research colleagues. That was, that is, and it will be an honour working with you..

Finally, I would like to offer my sincere thanks to my parents and brothers who turned me into the person I am today. I learned from my parents not to choose easily, though stuffs may at times sound tempting, just try harder and never give up. This dissertation is also for you.

To cite this document:

```
@phdthesis{zakaria2023mahlaoui,
 author = {Zakaria Mahlaoui Boudallaa},
 title = {Analysis and Design of Reconfigurable Antennas Using
          the Theory of Characteristic Modes},
 year = {2023},
 school = {Universitat Politècnica de València}
 }
```

Abstract

The Theory of Characteristic Modes, originally formulated in 1968, allows to obtain a set of real eigenvalues and real current modes that can be used to expand the total current on a conducting or dielectric body. The information provided by characteristic eigencurrents (modes) and eigenvalues can be used to perform antenna design in a systematic way. The great advantage of the Theory of Characteristic Modes over other traditional design methods is the clear physical vision provided about the phenomena that contribute to the radiation of the antenna. This physical vision allows to better understand the operation of the antenna, so that the design and the optimization of it can be carried out quickly and coherently.

The objective of this Thesis is to extend the use of the Theory of Characteristic Modes to the design of reconfigurable antennas in a systematic way. The use of reconfigurable antennas has become more and more important during the last years, as a way to meet the imposed requirements and desired performance of novel wireless communication systems. The approach of making an antenna reconfigurable implies the capability of an antenna system to adjust its characteristic such as operating frequency, radiation pattern and polarization. Active components such as varactor diodes, PIN diodes, MEMS, RF switches, photoconductive elements or smart materials can be used to change these base characteristics.

The dynamic reconfigurability of the operating parameters of an antenna leads to a flexible communication system. Frequency reconfigurable antennas enable multi-standard performances to be maintained

while preserving the same physical characteristics of the antennas. Radiation reconfigurable and polarisation diversity antennas enable to increase the efficiency of indoor communications by significantly decreasing the level of interference.

In this thesis, the research is turning around the analysis and design of antenna structures with the Theory of Characteristic Modes in a way that the antenna parameters will be tuneable, so the final design of the structure is a reconfigurable antenna that modifies dynamically its performance in a reasoned and coherent way. Characteristic modes and their properties will be analysed in order to design reconfigurable antennas, which combine different modes and produce different radiation characteristics. A systematic method to obtain the required characteristics of the antenna will be implemented during this work. Moreover, different switching techniques will be analysed and evaluated in order to asses their real effect on the antenna and on the characteristic modes. In this work, small reconfigurable antenna prototypes will be designed for IoT applications and 5G systems.

Resumen

La Teoría de los Modos Característicos, formulada originalmente en 1968, permite obtener un conjunto de valores propios reales y modos de corriente reales que se pueden utilizar para expandir la corriente total en un cuerpo conductor o dieléctrico. La información proporcionada por las corrientes características (modos) y los valores propios se puede utilizar para realizar el diseño de la antena de una manera sistemática. La gran ventaja de la Teoría de los Modos Característicos sobre otros métodos de diseño tradicionales es la clara visión física que se proporciona sobre los fenómenos que contribuyen a la radiación de la antena. Esta visión física permite comprender mejor el funcionamiento de la antena, de modo que el diseño y la optimización de la misma se pueden llevar a cabo de forma rápida y coherente.

El objetivo de esta Tesis es extender el uso de la Teoría de los Modos Característicos al diseño de antenas reconfigurables de manera sistemática. El uso de antenas reconfigurables se ha vuelto cada vez más importante en los últimos años, como una forma de cumplir con los requisitos impuestos y el rendimiento deseado en los nuevos sistemas de comunicaciones inalámbricas. El enfoque de hacer una antena reconfigurable implica la capacidad de una antena para ajustar sus características, como la frecuencia de operación, el diagrama de radiación y la polarización. Diversos componentes activos como diodos varactor, diodos PIN, MEMS, interruptores de RF, elementos fotoconductores o materiales inteligentes pueden usarse para cambiar estas características básicas de la antena.

La reconfiguración dinámica de los parámetros operativos de una antena conduce a un sistema de comunicación flexible. Las antenas reconfigurables por frecuencia permiten el mantenimiento de múltiples estándares mientras se mantienen las mismas características físicas de las antenas. La antena reconfigurable por radiación y la diversidad de polarización permiten aumentar la eficiencia de las comunicaciones interiores al reducir significativamente el nivel de interferencia.

En esta tesis, la investigación gira en torno al análisis y diseño de estructuras de antenas con la Teoría de los Modos Característicos de manera que los parámetros de las antenas sean sintonizables, por lo que el diseño final de la estructura es una antena reconfigurable que modifica dinámicamente su rendimiento de una forma razonada y coherente. Se analizarán los modos característicos y sus propiedades para diseñar antenas reconfigurables, que combinarán diferentes modos y producirán diferentes características de radiación. En este trabajo se implementará un método sistemático para obtener las características requeridas de la antena. Además, se analizarán y evaluarán diferentes técnicas de conmutación para evaluar su efecto real en la antena y en los modos característicos. El trabajo se centrará en el diseño de pequeñas antenas reconfigurables para aplicaciones IoT y sistemas 5G.

Resum

La Teoria dels Modes Característics, formulada originalment el 1968, permet obtenir un conjunt de valors propis reals i modes de corrent reals que es poden utilitzar per expandir el corrent total en un cos conductor o dielèctric. La informació proporcionada pels corrents característics (modes) i els valors propis es pot utilitzar per fer el disseny de l'antena d'una manera sistemàtica. El gran avantatge de la Teoria dels Modes Característiques sobre altres mètodes de disseny tradicionals és la clara visió física que es proporciona sobre els fenòmens que contribueixen a la radiació de l'antena. Aquesta visió física permet comprendre millor el funcionament de l'antena, de manera que el disseny i l'optimització de la mateixa es poden dur a terme de forma ràpida i coherent.

L'objectiu d'aquesta Tesi és estendre l'ús de la Teoria dels Modes Característics al disseny d'antenes reconfigurables de manera sistemàtica. L'ús d'antenes reconfigurables s'ha tornat cada cop més important en els darrers anys, com una forma de complir amb els requisits imposats i el rendiment desitjat en els nous sistemes.temes de comunicacions sense fil. L'enfocament de fer una antenna reconfigurable implica la capacitat duna antena per ajustar les seves característiques, com la freqüència d'operació, el diagrama de radiació i la polarització. Diversos components actius com va donar dos varactor, díodes PIN, MEMS, interruptors de RF, elements fotoconductors o materials intel·ligents poden utilitzar-se per canviar aquestes característiques bàsiques de l'antena.

La reconfiguració dinàmica dels paràmetres operatius duna antena condueix a un sistema de comunicació flexible. Les antenes reconfigurables per freqüència permeten el manteniment de múltiples estàndards mentre es mantenen les mateixes característiques físiques de les antenes. L'antena reconfigurable per radiació i diversitat de polarització permeten augmentar l'eficiència de les comunicacions interiors en reduir significativament el nivell dinterferència.

En aquesta tesi, la investigació gira al voltant de l'anàlisi i el disseny de estructures d'antenes amb la Teoria dels Modes Característics de manera que els paràmetres de les antenes siguin sintonitzables, per això que el disseny final de lestructura és una antena reconfigurable que modifica dinàmicament el seu rendiment d'una forma raonada i coherent. S'analitzaran els modes característics i les propietats per dissenyar antenes reconfigurables, que combinaran diferents maneres i produiran diferents característiques de radiació. En aquest tractament baix s'implementarà un mètode sistemàtic per obtenir les característiques requerides de l'antena. A més, s'analitzaran i avaluaran diferents tècniques de commutació per avaluar el seu efecte real a la antena i en les maneres característiques. El treball se centrarà en el disseny de petites antenes reconfigurables per a aplicacions IoT i sistemes 5G.

Contents

List of Figures

List of Tables

Glossary

CA Characteristic Angle

CM Cavity Model

CM Characteristic Modes

CMA Characteristic Modes Analysis

CP Circular Polarization

CST Computer Simulation Technology

DC Direct current

DGS Defected Ground Structure

DWM Dielectric Waveguide Model

FEKO Feldberechnung für Körper mit beliebiger Oberfläche (Field calculations involving bodies of arbitrary shape)

FRA Frequency Reconfigurable Antenna

IMD Intermodulation Distortion

IoT Internet of things

LP Linear Polarization

MS Modal Significance

MWC Modal Weighting Coefficient

PCB Printed Circuit Board

PIN P-type layer, intrinsic layer, and N-type layer

RA Reconfigurable antenna

RPRA Radiation Pattern Reconfigurable Antenna

SM Spherical Mode

SPDT Single pole, double throw

TCM Theory of Characteristic Modes

VCTL DC control voltage

VDD DC supply voltage

Chapter 1

Introduction

1.1 State of the art of reconfigurable antennas

Over the past decades, wireless technologies and communication systems have become increasingly advanced. Communications have developed not just as a technology, but also in a socially and economically omnipresent way. The growing demand for mobile cell phone services, wireless high-speed Internet access and associated enabling technologies, for example location-based service delivery, video streaming and smart cities, etc, forced operators to look at wide band widths, and multi-access user terminals.

To meet the imposed requirements and desired performance of these systems, the use of reconfigurable antennas has become more and more important during the last years [1, 2, 3, 4]. Making antennas reconfigurable can improve the wireless communication performance by adding a degree of freedom to the system.

The transition to greater broadband has led to a constant migration to higher radio frequency bands, along with the continued advancement of higher microwave frequencies for ground links and specialized services. In the moderately higher frequency bands (1,5 to 3.5 GHz) [5, 6, 7], slot antennas have frequently been considered a standard design option. Nevertheless, the basic slot designs are limited bandwidth, and the mitigation of this issue has been thoroughly researched,

where the antenna response is adjusted by changing the dimensions of the antenna. [8]. Even so, this is not practical for the majority of antenna types, that may require significant differences when business requirements are changed or added. It is thus desirable to obtain the same answer through an electrical setting.

Microstrip antennas are often seen as the starting point for small antenna designs, especially in portable devices, due to their light-weight structure and ease of manufacture. More generally, low profile or compact module designs are universally required in these applications [9, 10]. Fundamentally, microstrip antennas are resonant structures. Direct microstrip antennas are formed as rectangular, circular, or triangular patches. Many techniques exist for miniaturisation of these basic microstrip antennas, and modified geometries are popular, e.g. ring structures or slotted L-shaped structures. The main disadvantage of the resulting structures is the associated loss of bandwidth. However, bandwidth may be recovered by adding lossy elements, but these will adversely affect the efficiency of the antenna. The use of lossy elements may be avoided with a tuneable antenna or re-configurable antenna concept [11].

The use of PIN diodes [12, 4, 13] and varactor [14, 1, 7, 15] diodes are ones of the most extended techniques to achieve reconfigurability. However, the great development of electronics systems during the last decade has brought new elements like RF switches, photo-conductive elements, mechanical actuators or smart materials. Varactor diodes are also considered to be one of the most used techniques to overcome the inherent constraints of some antennas like narrow bandwidth and low gain.

Antenna reconfigurability can thus involve the radiation pattern [12], the frequency band [16], or the polarization of the radiated field [17]. In [13], a simple compact planar Reconfigurable Radiation Pattern Antenna (RRPA) based on arc dipoles is proposed. The antenna is made up of four similar arc dipoles and a broadband reconfigurable feeding network, that are printed respectively on the bottom and the top layers of the substrate. Switching the states ON/OFF

of the PIN diodes, which are implemented in the reconfigurable feeding circuit, four different modes with endfire radiation patterns may be obtained in the azimuth plane. Besides, in [18], a dual-band frequency reconfigurable multiple-input multiple-output (MIMO) patch slotted antenna structure is presented. The antenna has a planar configuration and comprises four symmetrically placed rectangular patch antenna elements. Varactor diodes are integrated within the feed-line to achieve frequency reconfigurability. Also, a simple microstrip-line-fed wideband polarization reconfigurable antenna (PRA) is introduced in in [19]. A circular metal ring with gaps and modified ground plane is inicialy designed for wide-band circular polarization (CP). Two PIN diodes are implemented to control the polarization attitudes. The attainment of right-hand CP, left-hand CP, and linear polarization (LP) can be achieved by controlling the state of the PIN diodes.

1.2 Motivation

The motivation of this PhD is to join the potential and flexibility given by reconfigurable systems and the use of characteristic modes. In the last recent years, some authors have started to work in this concept. In [20, 21, 22, 23, 24], different radiation pattern reconfigurable antennas have been designed using characteristic modes, while in [25] a polarization-reconfigurable antenna has been proposed. These works have focused in MIMO applications and mobile communication systems, while we will focus more on the design of reconfigurable integrated antennas for small devices for IoT applications.

To fulfil this expectation, CM (Characteristic Mode) theory [26, 27, 28] has been taken into account, which is a relatively new approach in the antenna field, presents an easy way to understand the physics behind several antenna features, such as the radiation pattern shape, beamwidth and direction, polarization, bandwidth and operating frequency. This physical understanding provides information about how modes operate and helps in the practical antenna design process, making it easier [29, 30].

1.3 Objectives of the thesis

The main goal of this research is to model and analyse the operation of novel reconfigurable antennas using Characteristic Mode analysis. In order to attain this objective, different switching techniques (varactor diodes, PIN diodes, RF switches) will be analysed and evaluated in order to achieve the required performance. A systematic method to obtain the required characteristics of the reconfigurable antenna based on the characteristic modes will be devised.

The present work is also devoted to analyse with the TCM and design reconfigurable antennas based on switching elements, which can be used for small IoT devices and 5G wireless communications devices applications. For this, the initial research is carried out with different reconfigurable designs. Different antenna geometries are considered, but the analysis is not only limited to the study of antenna geometries, but also the tuning strategies are investigated within the set limits.

This research deals with slots and microstrip printed patch antennas for different wireless communication bands. Different switching techniques will be analysed and evaluated in order to assess their real effect on the antenna and on its characteristic modes.

Some of these applications require fixed antenna, where the antenna is designed and optimised to operate at particular frequencies. In present mobile devices, the space allocated to antenna design is often commercially restricted. Depending upon the fundamental physical limitations, it is a big challenge to construct an antenna in the small space available that covers only one very wide frequency band or multiple frequency bands. To a certain extent, the issue of wide bandwidth coverage can be solved by the use of multiple antennas, but then more space and interconnections are needed for the antennas, and the mutual coupling between the individual antennas can cause serious problems [31, 32].

To overcome this issue, adaptive antennas (reconfigurable) where the antenna's operating frequencies can change to other bands by using reconfigurable elements (multifunctional antenna) were introduced and investigated. This type of antenna will not cover all bandwidths at the same time, it can provide several dynamic selective narrow frequency bands, and among those bands, it is more efficient than conventional broadband and multiband antenna solutions. This approach can help reduce the size of antennas while maintaining the operating bandwidth, or, alternatively, increase the available bandwidth of the antenna without increasing the physical size.

The following points are considered during this thesis:

- **Literature**: identifying main methodologies and research techniques on the topic of antennas.
- **Hypothesis and Simulation**: Starting by formulating hypothesis, design and simulating antennas.
- **Analysis and optimization**: The analysis using the characteristic modes provide some physical insights to more understand the antenna structure, that lead to optimizing antennas for a better performance.
- **Experiment and Validation**: Many prototypes are manufactured to verify the simulated results.
- **Publication**: Results as available to be share with the scientific society, an ongoing paper writing for publication.

1.4 Structure of the thesis

The thesis is organized into six chapters, including this introductory chapter 1, as follows:

In chapter 2,the fundamental mathematical formulation of the characteristic mode theory will be reviewed. An approach of how TCM is applied to reconfigurable antennas will be presented. Also the fundamental aspects of some regular geometric bodies as dipole and rectangular structures will be analyzed based on CM. The objective is not really to study deeply the two structures, but on the basis of its simplicity, it allows to understand the fundamentals of the modal theory.

In chapter 3 will be dedicated to present the electronic components used in reconfigurable antennas. The three main components PIN diode, Varactor diode and SPDT switch are implemented in a different antennas and modeled in simulation following various approaches. Resulting to this modeling simulation a nearest results to the fabricated model and that taking into account some secondary effects of the electronic components.

In chapter 4, a Defected Ground Structure (DGS) consisting in a rectangular shape slot embedded in the ground plane, is proposed and has been studied using characteristic mode analysis, which provides interesting physical insight into the antenna behavior. Varactor diodes are used to perform the selectivity over the frequency band. The understandings are successfully applied to design a reconfigurable antenna that entirely covers the 2 GHz band and with a steady band that is centered at 5 GHz. Moreover, a prototype has been fabricated and measurements have been performed to validate the simulated results.

In chapter 5, the application of CMA on two rectangular parallel plates generated a better understanding and shows how modes operate. Based on that findings, a proposed design consists to switch between a bidirectional and unidirectional radiation pattern, depending on the state of the PIN diodes. The aim of using a SPDT switch is to reach a common operating frequency (2.5 GHz) at both states, avoiding the modification of the basic geometry. Hence, the proposed antenna proposes a convenient solution for several IoT applications, as it can produce different beam conditions in a sensor without changing physically the antenna structure.

Finally, chapter 6 summarises the most important findings of this thesis and includes proposals for future work.

Chapter 2

Antennas from Characteristic Mode Theory perspective

The Theory of Characteristic Modes (TCM) has become a new matter in antenna society in the last decade. The great advantage of the TCM over other classical design methods is the clear physical vision provided about the phenomena that contribute to the radiation of the antenna. This physical insight allows to better understand the operation of the antenna, so that the design and the optimization of it can be carried out quickly and coherently. Afterwards, some fundamental questions will be discussed: What are the classical modal analysis methods? What are characteristic modes and why the characteristic modes were proposed? Which is the most advisable antenna for a distinct application from the characteristic mode theory perspective?

2.1 Classical modal analysis in antenna design

In antenna design, there are three main popular modal analysis methods for distinct antenna structures: Spherical Modes (SM), Cavity Modes (CM) and Dielectric Wave-guide Modes (DWM). A short review is presented in the next sections to show the features and the restraints of the three main modal analysis methods.

2.1.1 Spherical Modes

The first modal analysis method to determine antenna problems was the spherical modes (SM) method, proposed by Chu in 1948 [33], where the physical limitations of omnidirectional antennas is discussed. With the use of the spherical wave functions to describe the field, the gain G and the Q factor of an unspecified antenna are calculated under idealized conditions. Later in 1960 [34], Harrington applies the SM method to determine the fundamental limitations of an antenna with respect to the gain, bandwidth, and efficiency. Based on the assumption that any radiating field can be written as a sum of spherical vector waves, a sphere can completely enclose the antenna. Then, the radiated power of the antenna is calculated from the propagating modes within the sphere. When the sphere enclosing the antenna is very small, the limitations of an electrically small antenna in terms of the Q factor can be determined from the size of the antenna. However, to take into account all the propagating modes, the enclosing sphere has to be large enough. If the size of the antenna increases, it gives rise to many propagating modes. On the other hand, it is difficult to calculate the modal coefficients for all the propagating modes in a large sphere. Hence, the spherical mode method is limited to antennas with very small electrically size [35].

2.1.2 Cavity Modes

The cavity model (CM) was developed by Lo in 1979 [36] to analyze microstrip antennas. The model considers that the microstrip antenna resembles a lossy resonant cavity. As shown in Figure 2.1, the normalized fields inside the dielectric substrate (between the radiating patch and the ground plane) can be found more accurately by treating that region as a cavity bounded by electric conductors (above and below it) and by magnetic walls (to simulate an open circuit) along the perimeter of the radiating patch. In general, the dielectric substrate is assumed to be very thin in terms of thickness. The thin substrate thickness ensures the suppression of the surface wave. It also ensures that the field inside the cavity is uniform in the direction of the substrate thickness [36, 37].

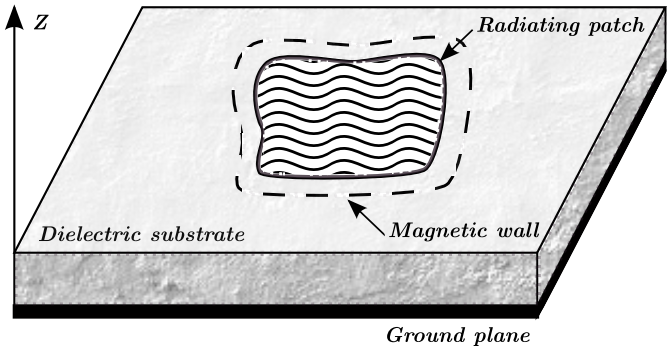

Figure 2.1: General geometry of a microstrip antenna with the cavity model.

The cavity model assumes that the fields underneath the patch are expressed as the summation of various resonant modes. As well, the cavity model takes into account the fringing fields along the perimeter by extending a small offset distance out of the patch periphery. The far-fields are computed from the equivalent magnetic currents around the periphery. The cavity model also accounts for the higher-order resonant modes and the feed inductance [35].

As an advantage, the cavity model offers an easy clear physical insight into the resonant behavior of microstrip antennas. The model has limitations as well, as it is only applicable to regular patch shapes such as the rectangular, triangular, circular and elliptical patches. The computation of resonant modes for complex-shaped patches using cavity model is a challenging task. In addition, the cavity model is not suitable for the analysis of multilayered or thick substrate microstrip antennas [8].

2.1.3 Dielectric Waveguide Modes

Dielectric Waveguide Model (DWM) is an approximate but accurate method for computing the characteristics of dielectric resonators (DR) [38]. It was developed to identify the lowest-order modes of a resonator and to define the resonant frequencies of various lower-order modes [39, 40]. According to the DWM analysis method, it can be assumed that the resonator is a truncated section of an infinite dielectric waveguide, as shown in Figure 2.2. The standing wave pattern in x and

y directions is still controlled by the characteristic equations that are the same as those valid for the isolated infinite dielectric waveguide. Marcatili's approximation technique [41] has been widely used for the analysis of the rectangular dielectric waveguide.

As stated in [39, 41, 35], the modes of a rectangular dielectric waveguide can

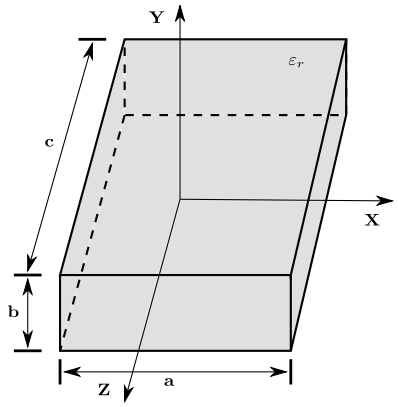

Figure 2.2: Isolated dielectric waveguide resonator.

be divided into TM^y_{mn} and TE^y_{mn} families of modes. As the analysis method for all of these modes is similar, only the resonant frequency determination for the TM^y_{mn} mode is being provided. According to Marcatili's approximation, the characteristic equations for the wave numbers k_x and k_y of the TM^y_{mn} modes are as follows:

$$k_y b = n\pi - 2tan^{-1}\left(\frac{k_y}{\varepsilon_r k_{y0}}\right) \qquad n = 1, 2, 3, \ldots \tag{2.1a}$$

where

$$k_{y0} = [(\varepsilon_r - 1)k_0^2 - k_y^2]^{1/2} \tag{2.1b}$$

$$k_x a = m\pi - 2tan^{-1}\left(\frac{k_x}{k_{x0}}\right) \qquad m = 1, 2, 3, \ldots \tag{2.2a}$$

where

$$k_{x0} = [(\varepsilon_r - 1)k_0^2 - k_x^2]^{1/2} \tag{2.2b}$$

and where k_{x0} and k_{y0} represent the ecay constants of the field along the x and y directions outside the dielectric waveguide, and k_0 is the free-space wave

number. The propagation constant k_z can be resolved by using the following separation equation:

$$k_x^2 + k_y^2 + k_z^2 = \varepsilon_r k_0^2 \tag{2.3}$$

By solving the characteristic equations simultaneously, one can determine the resonant frequencies of the TM_{mn}^y modes.

However, the advantage of the DWM, as mentioned before, is the accuracy in computing the characteristics of dielectric resonators (DR). However, it is only applicable to rectangular DRAs. For cylindrical DRAs and other DRAs with more sophisticated shapes, some basic approaches and engineering formulas [42] or full-wave simulations can be an alternative.

To conclude, the modal analysis methods hand over interesting physical insights into the performance and modal radiation nature of radiating structures. However, these modal analysis methods are theoretically developed for solving a particular set of problems, thus they are not compatible for the rest of antenna problems. Therefore, it is crucial to employ a general and versatile modal theory for the diversity of antenna problems.

2.2 Theory of characteristic modes: Definition and mathematical review of the modal attributes

The Characteristic Modes (CM) theory was initially developed by Garbacz in 1968 [26] and later refined by Harrington and Mautz in 1971 [28]. It consists of a versatile modal analysis tool for antennas with arbitrary shapes and materials. The CM, together with its metric parameters or modal attributes, provide the following effective information for antenna analysis and design:

- Resonant frequencies of the dominant mode and higher-order modes for a radiating structure.
- Modal radiation fields in the far-field range.

- Modal currents on the surface of the analyzed structure.
- Significances of the modes at a given frequency.

2.2.1 Surface integral equation

Surface integral equation (SIE), jointly with the Method of Moments (MoM), is widely used for solving time harmonic electromagnetic radiation and scattering problems from PEC structures. There are two basic SIEs for PEC ojects: The Electric Field Integral Equation (EFIE) and the Magnetic Field Integral Equation (MFIE). In the EFIE, the boundary condition is enforced on the tangential electric field, while in the MFIE, the boundary condition is enforced on the tangential magnetic field. The next section starts with a review of the basic theory related to the electromagnetic fields, from Maxwell's equations and the boundary conditions, to go to the formulation of the two basic SIEs.

a) Maxwell's equations

As known, Maxwell's equations are the fundamental equations in electromagnetics [8, 35]. Considering an electromagnetic wave within a homogeneous medium with constituent parameters ε (permittivity) and μ (permeability), the electric and magnetic fields, electric and magnetic currents have to satisfy the following frequency-domain Maxwell's equations (a time dependence factor $e^{j\omega t}$ is suppressed [43]):

$$\nabla \times \vec{E} = -\vec{M} - j\omega\mu\vec{H} \tag{2.4}$$

$$\nabla \times \vec{H} = \vec{J} + j\omega\varepsilon\vec{E} \tag{2.5}$$

$$\nabla \cdot \vec{D} = \rho_e \tag{2.6}$$

$$\nabla \cdot \vec{B} = \rho_m \tag{2.7}$$

where $\vec{E}$ is the electric field intensity, $\vec{H}$ is the magnetic field intensity, $\vec{D} = \varepsilon\vec{E}$ is the electric flux density, $\vec{B} = \mu\vec{H}$ is the magnetic flux density, ρ_e is the electric charge density, and ρ_m is the magnetic charge density, respectively.

In addition to the Maxwell's equations, there are another two continuity equations relating the change of the current density and the charge density(2.8)-(2.9):

$$\nabla \cdot \vec{J} = -j\omega\rho_e \tag{2.8}$$

$$\nabla \cdot \vec{M} = -j\omega\rho_m \tag{2.9}$$

In Equations (2.4)–(2.9), only four of the six equations are independent. We can use the two curl equations and two of the divergence equations in (2.6)–(2.9) to describe an electromagnetic problem.

b) Electromagnetic Boundary Condition

The electromagnetic fields may be discontinuous on the interface of two mediums. They are controlled by the following boundary conditions:

$$\hat{n} \times (E_1 - E_2)|_s = -M_s \tag{2.10}$$

$$\hat{n} \times (H_1 - H_2)|_s = J_s \tag{2.11}$$

$$\hat{n} \cdot (D_1 - D_2)|_s = \rho_{es} \tag{2.12}$$

$$\hat{n} \cdot (B_1 - B_2)|_s = \rho_{ms} \tag{2.13}$$

where the subscripts 1 and 2 represent the medium 1 and medium 2, respectively, and $\hat{n}$ is the unit normal vector on the boundary and is pointing from medium 2 to medium 1. In particular, when the medium 2 is a perfect electric conductor, the electromagnetic fields have to satisfy the following boundary conditions:

$$\hat{n} \times E|_s = 0 \tag{2.14}$$

$$\hat{n} \times H|_s = J_s \tag{2.15}$$

$$\hat{n} \cdot D|_s = \rho_{es} \tag{2.16}$$

$$\hat{n} \cdot B|_s = 0 \tag{2.17}$$

c) Magnetic Vector Potential and Electric Scalar Potential

In a source-free region, Equation (2.7) shows that $\vec{H}$ is always solenoidal. Therefore, it can be written as the curl of another arbitrary vector:

$$\vec{H} = \frac{1}{\mu}\nabla \times \vec{A} \tag{2.18}$$

where $\vec{A}$ is referred to as the magnetic vector potential. Substitution of (2.18) into (2.4) gives:

$$\nabla \times \vec{E} = -j\omega\nabla \times \vec{A} \tag{2.19}$$

Therefore, we have:

$$\nabla \times (\vec{E} + j\omega\vec{A}) = 0 \tag{2.20}$$

Applying the vector identity formulation $\nabla \times (-\nabla\Phi) = 0$, the electric field is given by:

$$\vec{E} = -j\omega\vec{A} - \nabla\Phi \tag{2.21}$$

where Φ is an arbitrary electric scalar potential. Taking the curl of both sides of Equation (2.18), and using the vector identity $\nabla \times \nabla \times \vec{A} = \nabla(\nabla \cdot \vec{A}) - \nabla^2\vec{A}$, we have:

$$\mu\nabla \times \vec{H} = \nabla(\nabla \cdot \vec{A}) - \nabla^2\vec{A} \tag{2.22}$$

Substituting (2.22) into (2.5), we get:

$$\nabla(\nabla \cdot \vec{A}) - \nabla^2\vec{A} = \mu\vec{J} + j\omega\mu\varepsilon\vec{E} \tag{2.23}$$

Combining (2.21) and (2.23) leads to the following:

$$\nabla^2\vec{A} + k^2\vec{A} = -\mu\vec{J} + \nabla(\nabla \cdot \vec{A} + j\omega\varepsilon\mu\nabla\Phi) \tag{2.24}$$

where k is the wavenumber and is defined by $k = \omega\sqrt{\varepsilon\mu}$. The curl of $\vec{A}$ has already been defined in Equation (2.18). The Helmholtz theorem illustrates that to uniquely define the vector field $\vec{A}$, the divergence of $\vec{A}$ must be defined. Considering the right-hand side of Equation (2.24), the Lorentz gauge is adopted to simplify Equation (2.24):

$$\nabla \cdot \vec{A} = -j\omega\varepsilon\mu\Phi \tag{2.25}$$

Therefore, Equation (2.24) reduces to an inhomogeneous vector Helmholtz equation:

$$\nabla^2 \vec{A} + k^2 \vec{A} = -\mu \vec{J} \tag{2.26}$$

The electric field in the source-free region thus can be expressed as follows:

$$\vec{E} = -j\omega \vec{A} - \nabla \Phi = -j\omega \vec{A} - \frac{j}{\omega \varepsilon \mu} \nabla (\nabla \cdot \vec{A}) \tag{2.27}$$

d) Diffraction problem analysis

Let's consider an incident plane wave E^i illuminating a PEC structure. As shown in Figure2.3, the incident wave induces surface currents $\vec{J}$ on the PEC body. The induced surface current $\vec{J}$ will then generate a scattering field E^s. The boundary condition in (2.14) illustrates that the tangential electric field vanishes on PEC surfaces S. This boundary condition gives an integral equation from which the surface current $\vec{J}$ can be solved:

$$(E^i(r) + E^s(r))_{tan} = 0, r \in S \tag{2.28}$$

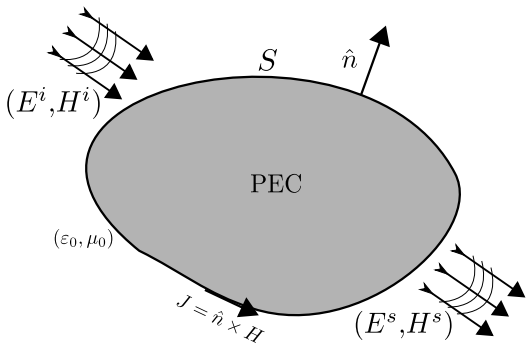

Figure 2.3: Surface equivalence principle of PEC structure

where the subscript *tan* represents the tangential component of the electric field.

The scattered electric field E^s can be expressed in terms of the induced surface current:

$$\begin{aligned} \vec{E}^s &= -j\omega \vec{A}(r) - \nabla \Phi(r) \\ &= -\frac{j\omega\mu_0}{4\pi} \int_s G(r,r') \vec{J}(r') dS' - \frac{j}{4\pi\varepsilon_0\omega} \nabla \int_s G(r,r') \nabla' \cdot \vec{J}(r') dS' \end{aligned} \tag{2.29}$$

where ε_0 and μ_0 are the permittivity and permeability of the free space, respectively. $G(r, r')$ is the Green's function multiplied by 4π in the free space and is given by:

$$G(r, r') = \frac{e^{jkR}}{4\pi R} \tag{2.30}$$

where $R = \mid r - r' \mid$ denotes the distance between the source point r' and observation point r.
Combining the scattering field expression (2.29) with (2.28), we obtain:

$$[L(J)]_{tan} = E^i_{tan}(r), \ r \in S \tag{2.31}$$

where $L(.)$ is an integro-differential operator to express the scattering field in terms of the electric current and can be written as follows:

$$L(J) = -\vec{E}^s(r) = \frac{jk_0\eta_0}{4\pi}\left\{\int_s G(r, r')\vec{J}(r')dS' + \frac{1}{k_0^2}\nabla\int_s G(r, r')\nabla'\cdot\vec{J}(r')dS'\right\} \tag{2.32}$$

where $k_0 = \sqrt{\varepsilon_0\mu_0}$ and $\eta_0 = \sqrt{\mu_0/\varepsilon_0}$ are the wave number and wave impedance in free space, respectively. Equation (2.29) is developed using the boundary condition of the electric field, and hence it is usually termed as the EFIE.
Once the induced currents J are solved from Equation (2.31), the scattered electric field in the far-field range can be calculated from the following:

$$\vec{E}^s(r) = -jk_0\eta_0\frac{e^{-jkr}}{4\pi r}\int_s \vec{J}(r')e^{-jkr'.\hat{r}}dS' \tag{2.33}$$

where $r = |r|$ and $\hat{r}$ is the unit vector in the direction of r. The scattered magnetic field in the far-field range can be readily obtained from:

$$\vec{H}^s(r) = \frac{1}{\eta_0}\hat{r}\times\vec{E}^s(r) \tag{2.34}$$

Once arrived to this stage, the integral equations (2.33) and (2.34) can then be solved by a numerical technique appropriate for integral equations, such as the Method of Moments(MoM).

e) Method of moments

The MoM is a numerical method for solving an integral equation by transforming it into a matrix equation. In electromagnetics, MoM is particularly well suited to open problems, like radiation and scattering problems. In the MoM, there are initially three steps in discretizing an integral equation into a matrix equation. First, the three-dimensional PEC surface will be modeled by dividing the surface into many small elements. Second, appropriate basis functions should be assigned to the elements such that the unknown currents in the integral equation are expanded. Third, testing procedure is used to transfer the integral operator into a MoM impedance matrix.

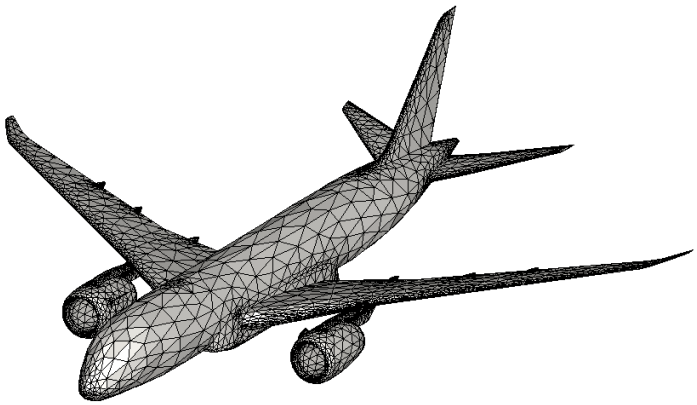

Figure 2.4: Triangular meshing of a 787 Dreamliner aircraft with CST.

In the initial step, triangular shapes are especially reasonable to demonstrate discretionary molded three-dimensional PEC surface. The triangular element is a basic two-dimensional surface and it is easy to deal with any bended surface. Many simulation software packages such as the CST [44] and FEKO [45] are able to generate high-quality triangular meshes. Figure 2.4 illustrates the triangular element mesh produced by CST software for an aircraft model.

In general, quasi-equilateral triangular elements with uniform element size are preferred to guarantee the exactness and the accuracy in geometry modeling and furthermore well-conditioned MoM matrix. In general, $\lambda/10$ mesh size is usually sufficient to obtain accurate results in scattering and conventional radiation problems, where λ is the wavelength in the free space. However, in the Characteristic

Mode Analysis (CMA), modal currents generally change radically in the higher-order modes. In this sense, to precisely catch the behavior of very high-order modes, it is proposed to model the PEC surface with a generally dense mesh in beyond of $\lambda/15$.

The following step in the MoM is to characterize basis functions on the triangular meshes. In the MoM, the most popular basis function for PEC surfaces is the Rao-Wilton-Glisson (RWG) basis function [13]. As presented in Figure 2.5, the RWG basis function is defined over a pair of triangular elements that share a common edge l_n, and it is given by the following vector function:

$$f(r) = f_n^+(r) + f_n^-(r) \tag{2.35}$$

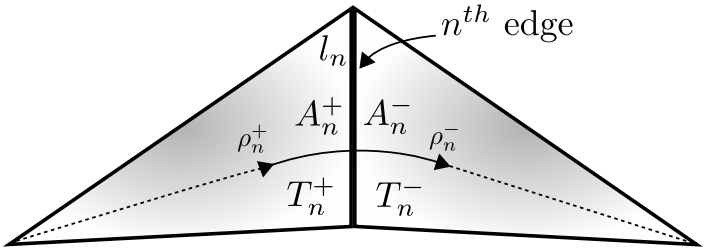

Figure 2.5: A RWG basis function defined over a set of two adjacent triangles.

$$f_n^\pm(r) = \begin{cases} \frac{l_n}{2A_n^\pm}\rho_n^\pm & , r \in T_n^\pm \\ 0 & , r \notin T_n^\pm \end{cases} \tag{2.36}$$

where T_n^+ and T_n^- are the two triangles that share the common edge l which is indexed by n, l_n is the length of the edge, A_n^+ and A_n^- are the areas of the two triangles, and ρ_n^+ and ρ_n^- are the position vectors defined with regard to the free vertices. Specifically, ρ_n^+ points are way from the free vertex of T_n^+, and ρ_n^- points are toward the free vertex of T_n^-. The plus and minus designations of the two triangles are based on the supposition that the positive currents are flowing from T_n^+ to T_n^-.

Additionally, taking the surface divergence of the RWG basis function in Equation (2.36), we get:

$$\nabla_S \cdot f_n^\pm(r) = \begin{cases} \pm\frac{l_n}{A_n^\pm} & , r \in T_n^\pm \\ 0 & , r \notin T_n^\pm \end{cases} \tag{2.37}$$

The divergence of the current density is proportional to the electric charge density. Besides, Equation (2.37) shows that the total charge density associated with the triangle pairs equals to zero. Therefore, there is no fictitious charge accumulated on the common edge, and the RWG basis function is known as a divergence conforming basis function. With the RWG basis function, the electric surface currents on the PEC body can be expanded as:

$$J(r) = \sum_{n=1}^{N} J_n f_n(r) \tag{2.38}$$

where J_n is the unknown weighting coefficient for the n^{th} basis function and N denotes the number of common edges.

The last step in discretizing an integral equation into a matrix equation is to test the integral equation with expanded current representation. The substitution of Equation (2.38) into the $EFIE$ formulation gives:

$$\vec{E}^{i}_{tan}(r) = \frac{jk_0\eta_0}{4\pi}\left(\sum_{n=1}^{N} J_n \int_s f_n(r')G(r,r')dS' + \frac{1}{k_0^2}\sum_{n=1}^{N} J_n \nabla \int_s \nabla' \cdot f_n(r')G(r,r')dS'\right)_{tan} \tag{2.39}$$

f) Characteristic Modes formulation

Adopting the RWG basis function $f_m(r)$ as the testing function, and applying the vector identity $\nabla \cdot (\phi\vec{A}) = \vec{A} \cdot (\nabla\phi) + \phi(\nabla \cdot \vec{A})$ to Equation (2.39), the following matrix equation is obtained:

$$\left[Z_{mn}\right]\left[J_n\right] = \left[V_m\right] \tag{2.40}$$

where

$$Z_{mn} = \frac{jk_0\eta_0}{4\pi}\left(A_{mn} - \frac{1}{k_0^2}B_{mn}\right) \tag{2.41}$$

$$A_{mn} = \int_s f_m(r) \cdot \int_s f_n(r')G(r,r')dS'dS \tag{2.42}$$

$$B_{mn} = \int_s \nabla_S \cdot f_m(r) \int_s \nabla'_s \cdot f_n(r')G(r,r')dS'dS \tag{2.43}$$

$$V_m = \int_s f_m(r) \cdot E^i(r) dS \tag{2.44}$$

g) Conventional Derivation

The $EFIE$ presented in Equation (2.31) uncovers that the $L(\cdot)$ operator constructs the relationships between the electric fields $\vec{E}$ and the surface currents $\vec{J}$. Because the $L(\cdot)$ operator highlights with the impedance property, an impedance operator $Z(\cdot)$ is defined to exhibit this impedance property:

$$\left[Z(\vec{J})\right] = \left[L(\vec{J})\right]_{tan} \tag{2.45}$$

As can be seen, $Z(\cdot)$ describes the tangential component of the electric field due to the induced currents $\vec{J}$. It is obvious that the MoM matrix calculated from Equation (2.41) is a discretization form of the $Z(\cdot)$ operator. In the next equation, the impedance matrix Z is used to describe the $EFIE$ MoM matrix, as given in Equation (2.41).

$$\left[Z\right] = \left[R\right] + j\left[X\right] \tag{2.46}$$

The impedance matrix Z can be expressed in terms of its real and imaginary self-adjoint matrices. As seen in Equation (2.41), both R and X are real and symmetric matrices. The following generalized eigenvalue equation can be derived for the CMA:

$$\left[X\right](\vec{J}_n) = \lambda_n \left[R\right](\vec{J}_n) \tag{2.47}$$

where $\vec{J}_n$ and λ_n are the real eigenvectors (CM) and real eigenvalues, respectively; and n is the index of the order of each mode.

2.2.2 Physical interpretation of CM parameters

CM ($\vec{J}_n$ in Equation (2.47)) are defined as a set of orthogonal current modes that are supported on a conducting surface. The eigenvalue equation is derived from the MoM impedance matrix [28, 46, 35], as seen in the previous section. A set of orthogonal eigencurrents ($\vec{J}_n$) together with their associated eigenvalues (λ_n) are obtained. Due to the orthogonality of the eigencurrents, the total current

on the surface of the conductor can be expanded into a set of modes ($\vec{J}_n$). The eigenvalues (λ_n) provide information about the radiating behavior of the associated mode. Morevover, other modal attributes such as the ***Characteristic Angle*** and ***Modal Significance*** can be calculated, which are associated to an ***Eigenvalue***.

In the following section, a brief review of the parameters used in the Characteristic Mode Analysis (CMA), which are provided by the eigenvalues, will be described. This parameters provide physical insight associated to the radiating behavior of an antenna with arbitrary shape. The preliminary developments of the equations are presented in the previous sections and in [46, 35, 28] the mathematical formulation of CM is presented.

a) Physical interpretation of Eigenvalue

Based on the approach developed in [28, 46], characteristic current modes can be obtained as the eigenfunctions of the following particular weighted eigenvalue equation:

$$XJ_n = \lambda_n R J_n \tag{2.48}$$

where J_n and λ_n are the real eigenvectors and eigenvalues, respectively, n is the index of the order of each mode, R and X are the real and imaginary parts of the impedance matrix of the MoM. The electric fields E_n, produced by the characteristic currents J_n on the surface of a conducting body, are called characteristic fields [28]. Following the developments in [28, 46], we obtain:

$$\omega \iiint_V (\mu H_m \cdot H_n^* - \varepsilon E_m \cdot E_n^*) dV = \lambda_n \delta_{mn} \tag{2.49}$$

where

$$\delta_{mn} = \begin{cases} 1, & \text{if } m = n \\ 0, & \text{if } m \neq n \end{cases} \tag{2.50}$$

Choosing $m = n$ in Equation (2.50), it gives the following physical interpretations of the eigenvalues:

- The total stored field energy within a radiation or scattering problem is proportional to the magnitude of the eigenvalues (λ_n).

- In the case of $\lambda_n = 0$, it demonstrates that $\iiint_V \mu H_n \cdot H_n^* = \iiint_V \varepsilon E_m \cdot E_n^* dV$. It corresponds to the case of resonance and the associated modes are known as **resonant modes**.

- In the case of $\lambda_n > 0$, it demonstrates that $\iiint_V \mu H_n \cdot H_n^* > \iiint_V \varepsilon E_m \cdot E_n^* dV$. Because the stored magnetic field energy dominates over the stored electric field energy, the associated modes are known as **inductive modes**.

- In the case of $\lambda_n < 0$,it demonstrates that $\iiint_V \mu H_n \cdot H_n^* < \iiint_V \varepsilon E_m \cdot E_n^* dV$. Because the stored electric field energy dominates over the stored magnetic field energy, the associated modes are known as **capacitive modes**.

b) Physical interpretation of the Modal Significance

The modal significance (MS) is defined as shown in Equation (2.51). As observed, it is a function of the operating frequency and the dimension of the conducting object [47], and it measures the contribution of each mode in the total electromagnetic response.

$$MS = \left| \frac{1}{1 + j\lambda_n} \right| \tag{2.51}$$

As can be observed from Equation (2.51), the MS transforms the $[-\infty, +\infty]$ value range of eigenvalues (λ_n) into a much smaller range of $[0, 1]$. In many cases, it is more convenient to use the MS other than the eigenvalues to investigate the resonant behavior across a wide frequency band.

In addition, the MS also provides a convenient way to measure the bandwidth (BW_n) of each CM when the power radiated by the mode is more than one-half the power radiated at resonance. As shown in Equation (2.52), half-power (HP) at resonance corresponds to a cutback of the normalized current by a factor $\sqrt{2}$. Moreover, the MS is also used to identify the significant modes and non-significant modes of a radiating structure. Characteristic modes with $MS \geq 0.707$ are referred to as significant modes, whereas characteristic modes with $MS \leq 0.707$ are considered as non-significant modes.

$$MS_{HP_n} = \left| \frac{1}{1 + j\lambda_n} \right| = \frac{1}{\sqrt{2}} = 0.707 \tag{2.52}$$

Hence, a half-power BW_n can be defined according to the MS as:

$$BW_n = \frac{f_U - f_L}{f_{res}} \tag{2.53}$$

where f_{res}, f_U, and f_L are respectively the resonant frequency, upper-band frequency, and lower-band frequency.

c) Physical interpretation of the Characteristic Angle

According to the CM theory, any PEC structure with surface S is associated to an infinite set of characteristic currents J_n on S. Each J_n radiates a characteristic electric field E_n into free space. The tangential component of E_n on S is equiphase. The Characteristic Angle (CA), expressed by Equation (2.54), defines the phase lag between J_n and E_n^{tan}, and it is an important metric parameter in the CM theory, as it indicates the resonant behavior and the energy stored by each mode [48].

$$\alpha_n = 180° - tan^{-1}(\lambda_n) \tag{2.54}$$

Moreover, the CA provides a way to better understand the mode behavior close the resonance. CA varies within the range $[90°, 270°]$. If the modal current J_n and the tangential electric field E_n^{tan} on S are 180° out of phase ($\alpha_n = 180°$), the mode is labelled external, the behaviour is in resonance and the PEC structure is an active radiator. However, if J_n and E_n^{tan} on S are 90° or 270° out of phase ($\alpha_n = 90°$ *or* $\alpha_n = 270°$), the mode is said to be in internal (cavity) resonance. In this case, the modal current yields a null field in the exterior region.

Then, following the physical interpretation of the eigenvalues, the characteristic modes can be also categorized using the CA:

- If $\alpha_n = 180°$, the associated modes are **resonant modes**.
- If $90° < \alpha_n < 180°$, the associated modes are **inductive modes**.
- If $180° < \alpha_n < 270°$, the associated modes are **capacitive modes**.

d) Physical interpretation of the modal weighting coefficient

The eigencurrent or characteristic current J_n, provides useful insight into the field response of each modes and the modes overall contribution to the response of the antenna structure. The surface current on the structure is the weighted sum of all the characteristic currents and since the electric and magnetic fields are linearly related to the currents [28], that same relationship can be established:

$$\begin{aligned} J &= \sum_n \alpha_n J_n \\ E &= \sum_n \alpha_n E_n \\ H &= \sum_n \alpha_n H_n \end{aligned} \tag{2.55}$$

where α_n is the Modal Weighting Coefficient (MWC) defined by (2.56). The MWC is important as it combines the eigenvalue, an intrinsic property of each mode and independent of an excitation source, with an excitation source. Therefore, as stated in (2.55), it expresses the contribution of each mode's characteristic current or fields the overall response of the antenna.

$$\alpha_n = \frac{\mathrm{V}_n^i}{1 + j\lambda_n} \tag{2.56}$$

The modal excitation coefficient V_n^i, represents the coupling between an external excitation source E^i, and the characteristic current J_n. The coupling is dependent on the position, magnitude, phase, and polarization of the excitation source and the characteristic current [35].

2.3 TCM applied to reconfigurable antennas

As presented in Figure 2.6, the workflow for the design of a reconfigurable antenna based on a CMA is divided to three basic processes: Simulation, fabrication and measurement.

1. **Simulation**: This step is fundamental, and all the CMA is performed at this step. It is divided in the following sub-steps:

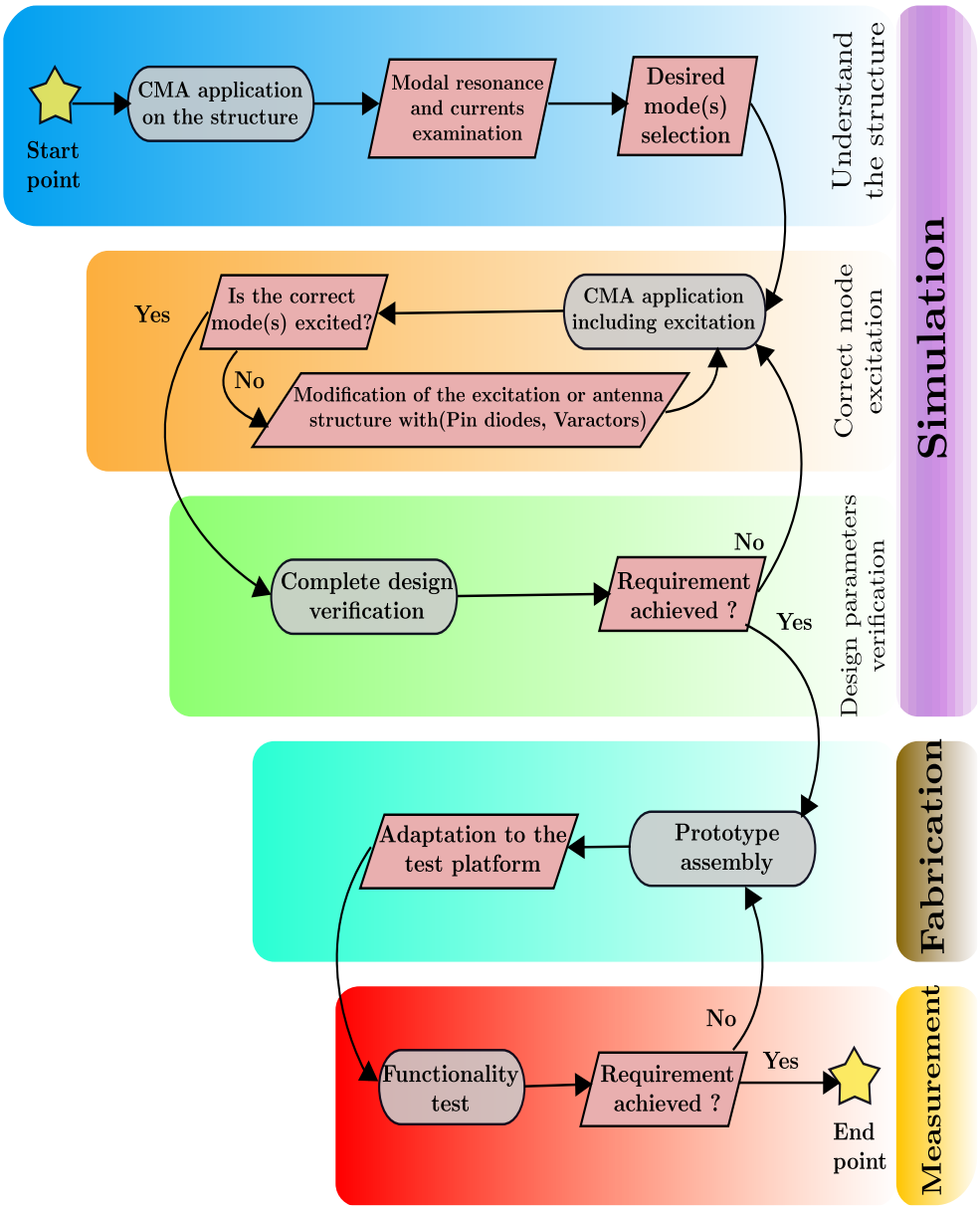

Figure 2.6: Workflow for the design of a Reconfigurable antenna based on CMA.

(a) *Understand the structure*: The first sub-step concerns the initial investigation to understand the behavior of the structure. The structure can be basic and simple, or very complex. At this stage, the excitation can be excluded, as CM are computed in absence of any excitation. The CMA will find out which modes are consistently in or near resonance

within the frequency range of interest. Besides, CMA can determine the attributes of a single mode or a combination of modes that are convenient for the application under study.

(b) *Correct mode excitation*: As a second sub-step and once a mode or a combination of modes have been selected, an excitation must be chosen to excite these modes. A detailed CMA of the structure can be performed to determine the appropriate antenna feeding location or modify the antenna geometry including PIN diodes or varactors. Through evaluation of the modal weighting coefficient 2.2.2, the analysis will find out how well the structure was able to achieve the desired modal behavior.

(c) *Design parameters verification*: The third sub-step deals with the verification action, where a full-wave solver can be used to compute the performance of the designed antenna (S-parameters, radiation pattern, gain, directivity, efficiency, and so on).

2. **Fabrication**: This step is practical and requires a good handmade. This step will allow to validate the results obtained at the previous steps. Additional parameters may affect at this step, such as the tolerances of electronic components, effect of the temperature, interference among biasing wires or effect of the feeding connector.

3. **Measurement**: Finally, this step will give the effectiveness of the previous design steps and will shows the accuracy in the performance of the designed structure.

2.4 Characteristic mode analysis of some basic planar structures

In this section, the fundamental aspects of some regular geometric bodies will be analyzed, which are the surface current distribution in the structure and the stability of the radiation patterns due to the modes in the structure. Companies developing commercial electromagnetic simulators such as CST [44] and FEKO

[45] have incorporated CMA into their products a few years ago. This analysis tool has led to a very notable increase in the use of CMA by many antenna designers. That is why these simulators will be used for the development of this work.

Therefore, in this section we will provide, for the sake of introduction, the CMA of basic structure examples, such a dipole, rectangular and loop structures [49, 46], and the interpretation of the modal attributes will be shown using these examples.

2.4.1 Dipole structure

In this section, the CMA applied to the dipole shown in Figure 2.7a is presented. The structure consists of a PEC dipole of length L = 50 mm and width W = 0.5 mm. Figure 2.7 shows the dipole structure and the current distributions of the first three modes. The radiation pattern at the resonance frequency of each mode is shown in Figure 2.8. In a frequency band ranging from 0 to 10 GHz, the first three modes are resonating at 2.8 GHz, 5.8 GHz and 8.8 GHz, respectively, as shown in Figure 2.9c when α_n = 180°. The first mode (mode 1), which is the main mode, shows an omnidirectional radiation pattern, as depicted in Figure 2.8. At this point, knowing the current distributions and the associated radiation patterns of each mode, we can gain the flexibility of choosing the adequate antenna behavior. Thus, in a simple structures such as the dipole, the excitation point can turn on the desired mode or in a combination of modes.

Moreover, Figure 2.9b presents the Modal Significance of the first three modes. From a first glance, it is seen that the 3 modes have a narrow band, and applying the equation 2.53, we obtain the results presented in Table 2.1.

2.4.2 Rectangular structure

The rectangular shape is one of the most used geometries in antennas. To better understand the rectangular structure, the CMA is performed for the first five modes. Figure 2.10a shows a rectangular conducting plate of dimension W x L =

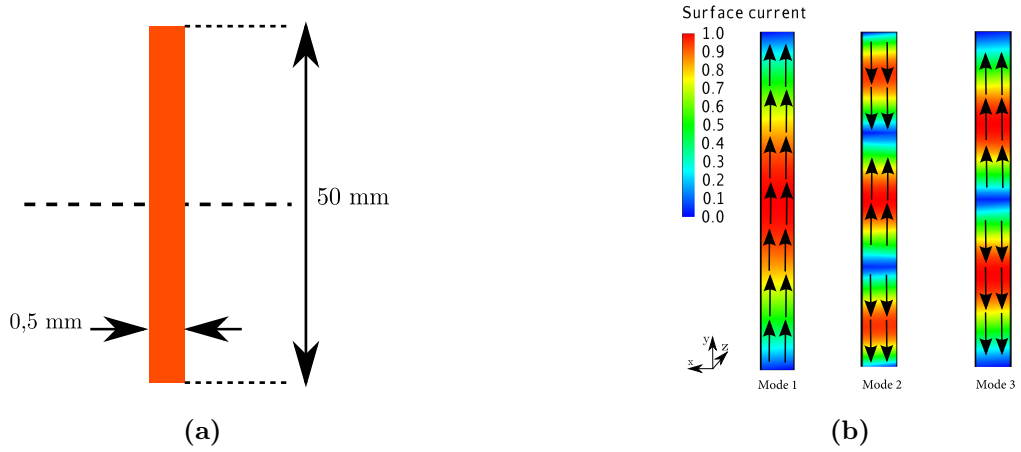

Figure 2.7: (a) Dimensions of the dipole structure; (b) Current distribution of the first three modes of the dipole.

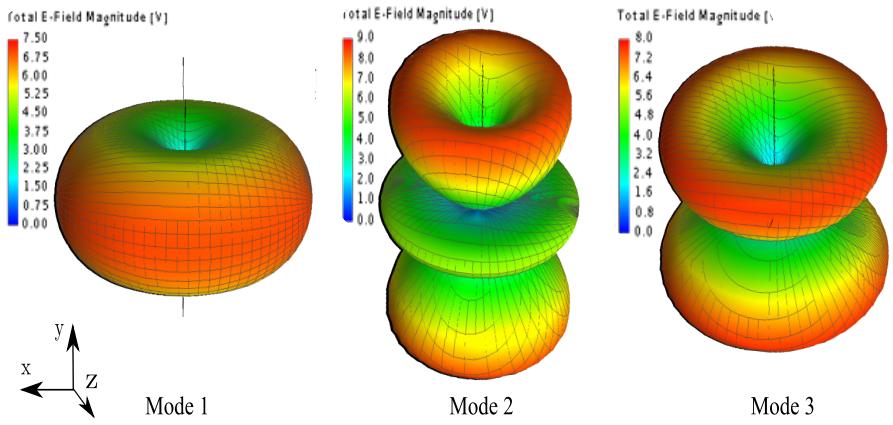

Figure 2.8: Radiation pattern of the first three modes of the dipole.

Table 2.1: Resonance frequency and bandwidth of the first three modes of the dipole.

Mode	f_{res} (GHz)	f_L (GHz)	f_U (GHz)	$BW(\%)$
Mode 1	2.8	2.6	3.1	17.86
Mode 2	5.8	5.5	6.2	12.07
Mode 3	8.8	8.4	9.3	10.23

62.5 mm x 125 mm. The current distribution of the first five modes is illustrated in Figure 2.10b, where mode 1 and mode 2 presents horizontal and vertical current distribution, respectively, and they are commonly excited in rectangular antenna structures, such as the rectangular patch antenna. As shown in Figure 2.10b, the current of mode 3 follows a loop path along the perimeter of the structure, and presents an inductive behaviour. Therefore this is a non-resonating mode. Mode 4 and mode 5 are higher-order modes presenting a complex current distribution, and therefore they exhibit complex-shaped radiation patterns, as shown in Figure 2.11.

Note that mode 1 of the rectangular plate is showing the same characteristics (current distribution and radiation pattern) as mode 1 of the dipole, provided in Figure 2.7b and 2.8, respectively. However, modal bandwidth is much bigger in the rectangular plate due to the larger radiation surface, as it will be shown.

Furthermore, the CM physical interpretation provides significant information, and hence we will focus firstly on mode 1.

Figure 2.12a shows the Eigenvalues of the modes versus frequency. Taking into account mode 1, we can see that $\lambda_{mode\ 1} < 0$, so the stored electric field energy dominates over the stored magnetic field energy. The associated modes are known as the capacitive modes. Basically this mode could be a good candidate to be reconfigurable using Varactor o PIN diodes, which contribute to modify the inner capacitance of the structure and therefore change parameters such as its resonance frequency or its radiation pattern.

To investigate the resonant behavior along the frequency band, the Characteristic Angle is the adequate parameter to analyse this behavior, as shown in Figure 2.12b. The corresponding resonant frequency of mode 1 ($\alpha_{mode\ 1} = 180°$) is $f_{res} = 1.1\ GHz$. In addition, mode 1 exhibits a large bandwidth, since its Characteristic Angle curve is close to 180° in a wide frequency range after resonance.

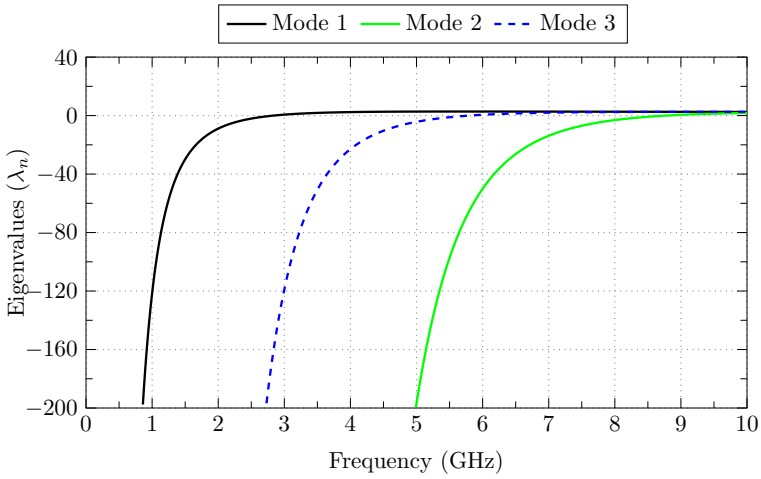

(a) Eigenvalue

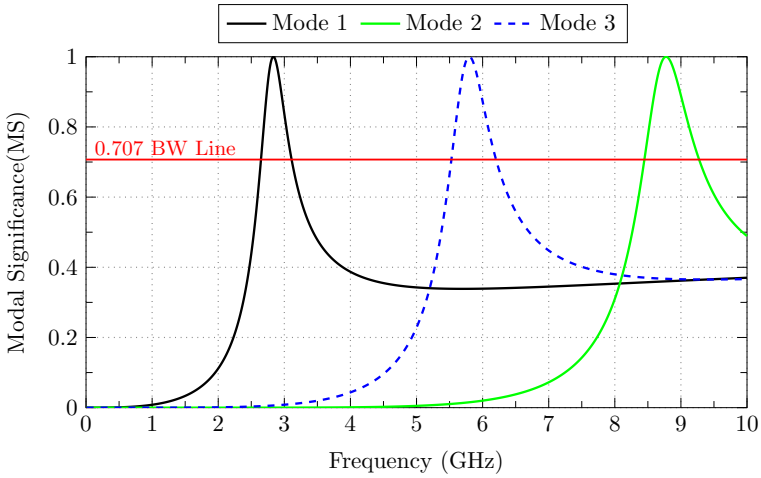

(b) Modal significance

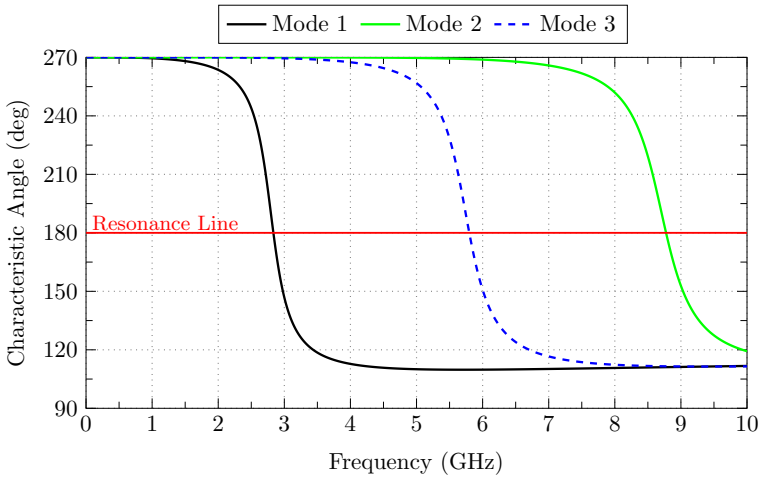

(c) Characteristic angle

Figure 2.9: CM parameters of the first three modes of the dipole versus frequency.

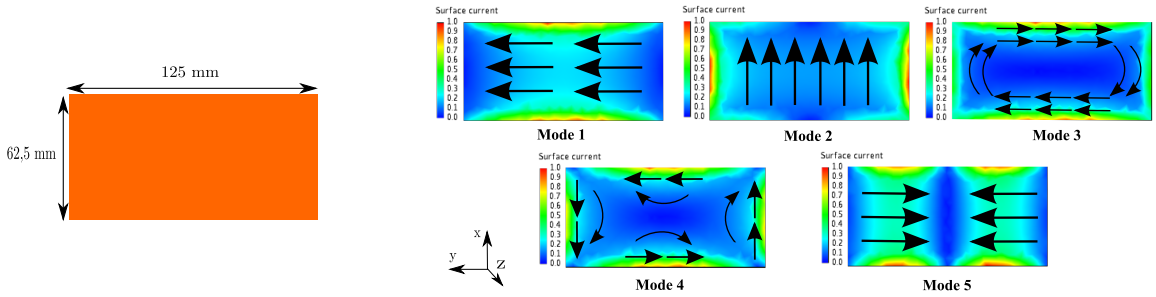

(a) (b)

Figure 2.10: (a) Geometry of the rectangle metallic plate under CMA; (b) Current distributions of the first five modes of the rectangular plate. Black arrows are added to show the direction of the current flow.

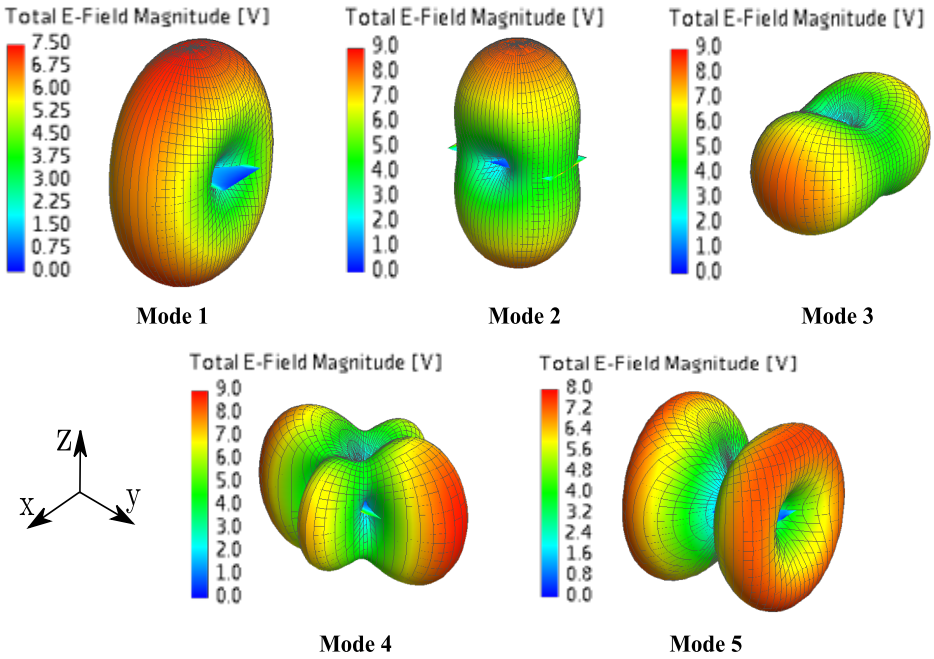

Figure 2.11: Radiation patterns of the first five modes of the rectangular plate: (a) Mode 1, (b) Mode 2, (c) Mode 3, (d) Mode 4 and (e) Mode 5.

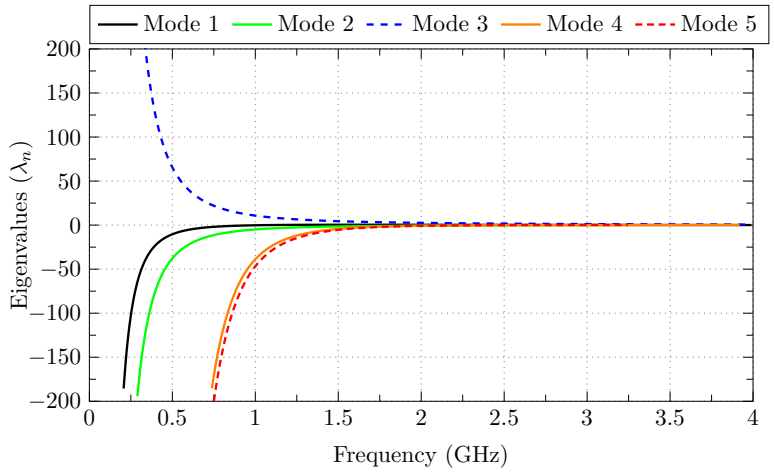

(a) Eigenvalue

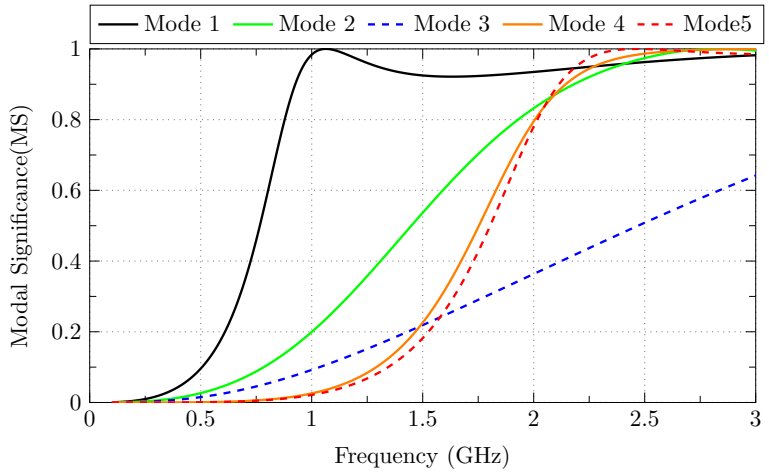

(b) Modal significance

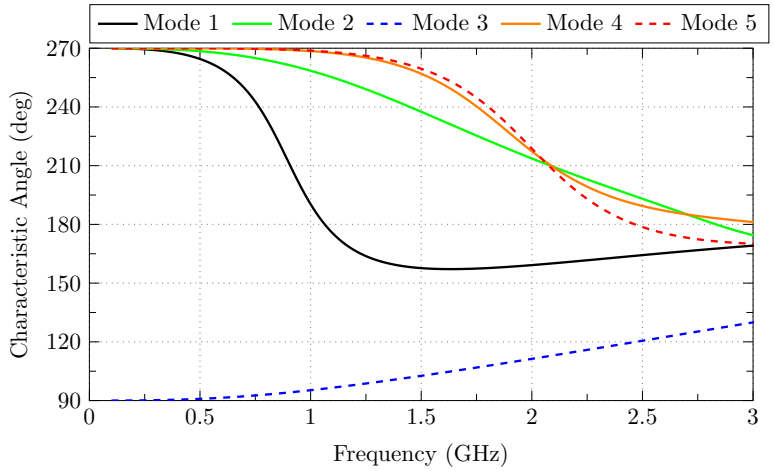

(c) Characteristic angle

Figure 2.12: CM parameters of the first five modes of the rectangular plate versus frequency.

Chapter 3

Modelling of switching electronic components employed in reconfigurable antennas

3.1 Introduction

The evolution of wireless communication systems in the last years requests new techniques and concepts to design antennas that cope with the more and more demanding challenges. Reconfigurable antennas have greatly contributed over recent years to provide to requirements demanded by market and customers. Reconfigurable antennas allows to dynamically modify the antenna performance, in terms of operating frequency, polarization or radiation pattern, among others.

Reconfigurable antennas can use active components such as PIN diodes, varactor diodes, SPDT (Single Pole Double Throw) switches, photoconductive components, or can achieve reconfiguration by changing the material properties using smart materials [50, 51, 3]. Therefore, those components are able to change the antenna basic characteristics like the operating frequency [52, 53, 54], type of polarization [55] and radiation pattern [56, 12].

In this chapter, the focus will be on the electronic components that will be used to achieve the reconfigurability of an antenna. Several advantages are pre-

sented from using reconfigurable antenna with a great ability to check more than one wireless requirement using electronic components such as the PIN diode, varactor diode and SPDT switch. The proposed designs was simulated using CST(Computer Simulation Technology) Studio Suite software taking into account the electronic components. The incorporation of this components was based on data provided from the manufacturer. Starting from a basic simulation level approach and ending with a full model that considered the switching components and the biasing network system, delivers an accurate investigation and reduce manufacturing cost.

3.2 PIN diode

The PIN diode is a silicon semiconductor with a high-resistivity intrinsic area I, interceding between a doped P-type and N-type region, as presented in Figure 3.1. Forward biasing the PIN diode provokes a low resistance at high frequencies. On the other hand, reverse biasing the diode generates a high resistance and causes an open circuit. The PIN diode is a current controlled resistor at radio frequencies and microwave circuits or can be defined as a switch that open or close the current flow. When the PIN diode is forward biased, the state is labeled ON, and the current flow reaches the required path. Nevertheless, reverse biasing causes an open circuit, and ,as a result, there is no current flow and the case is identified as OFF state [4].

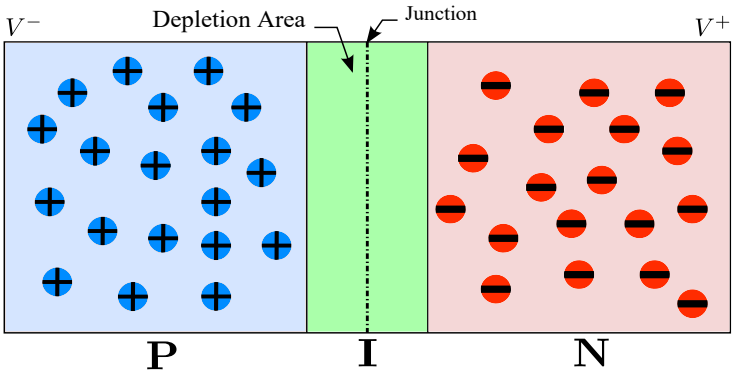

Figure 3.1: PIN diode diagram.

In Figure 3.2, the geometry of a Frequency Reconfigurable Antenna (FRA) proposed by the author in [53] is presented. The antenna covers the 5 GHz U-NII band using PIN diodes, and allows to switch between three different configurations. As it is known, many applications use only one range of four from this unlicensed band in order to avoid the communication at the same frequency range of some other application. In this way, the proposed antenna provides a convenient solution, as it can be employed at different frequency bands without physically changing the antenna structure.

The simulated antenna, shown in Figure 3.2, consists of a rectangular planar dipole over a ground plane, with a substrate height of H =3.175 mm and a relative dielectric constant ε_r = 2.2. The feeding point is positioned at the top plate, on a gap of G =2 mm that separates the negative from the positive side. It should be noted that the bending at the end of the gap slot is for matching purposes, and the full dimensions of the antenna are $W \times L$ = 40 mm × 25 mm.

The reconfigurable antenna has four PIN diodes at each corner of the ground plane, as depicted in Figure 3.2. Because of the different paths of the current flow achieved by the three configurations, the operating frequency is altered when switching the PIN diodes.

Table 3.1 shows the appropriate configurations of the PIN diodes to obtain the successive frequency bands. As shown, the first configuration consists of turning OFF all the PIN diodes, the second configuration contains two PIN diodes in ON state and the other two that are in OFF state, and the last configuration includes all the PIN diode in ON state.

The biasing circuit consists of four narrow slots surrounding the PIN diodes to separate the DC area and RF zone, and eight DC block capacitors to preserve the continuity of the RF current across the structure. Next, different approaches followed to analyse the effect of the PIN diodes at the simulation stage will be shown, and a comparison between them will be given.

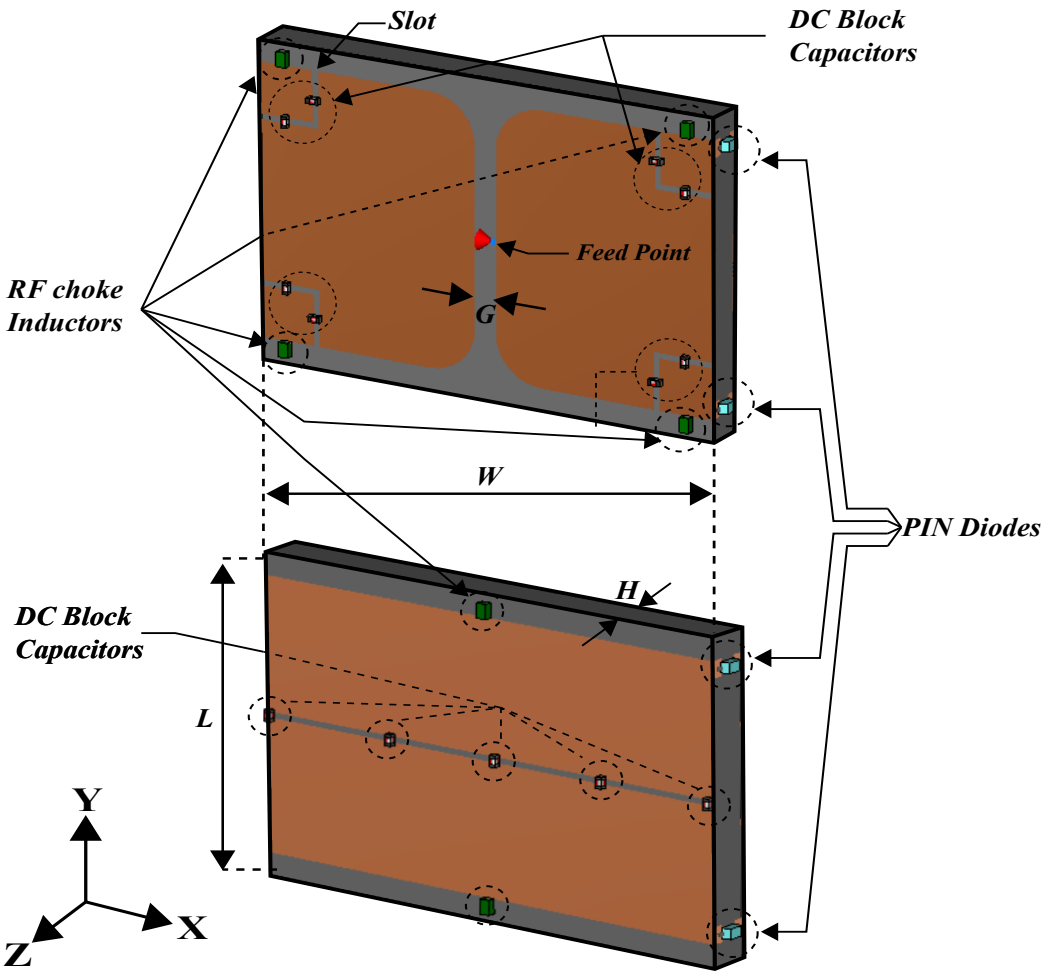

Figure 3.2: 3D Antenna structure with PIN diodes, DC Block Capacitors and RF Chokes.

First approach: Ideal case. As a first approach, wires can replace the PIN Diodes during the electromagnetic simulation. It consists of adding a wire in palce of the PIN diode which generates a very low resistance and that resembles to the ON state, allowing the current to spread on the antenna. In the other side, disabling wires from simulation generates a very high resistance and causes an open circuit, which leads to an OFF state, where currents cease to flow in the back side of the antenna. Results for the simulated S_{11} parameter in this ideal case are shown in Figure 3.4 for the three PIN diodes configurations.

Table 3.1: Proposed configuration for the PIN diodes.

	1^{st} configuration	2^{nd} configuration	3^{rd} configuration
PIN diode 1	OFF	ON	ON
PIN diode 2	OFF	ON	ON
PIN diode 3	OFF	OFF	ON
PIN diode 4	OFF	OFF	ON
Central frequency	5,20 GHz	5,50 GHz	5,70 GHz
Bandwidth	480 MHz	380 MHz	370 MHz

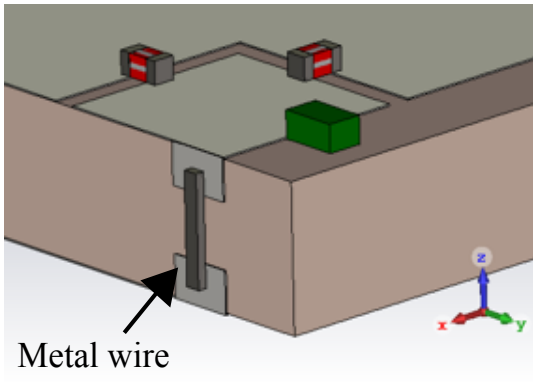

Figure 3.3: Wire in place of Pin Diode as Ideal approach.

Second approach: PIN diodes equivalent circuit case: As a second approach, the PIN diode model given by the manufacturer can be used in the simulation. The model adopted for the proposed design is the one of *Infineon BAR50-02V* diode [57]. For the forward bias, the equivalent circuit is shown in Figure 3.5 (b), that comprises a series inductance L of 0.6 nH and a parallel capacitor C of 0.15 pF, with a resistance R_2 of 3 Ω. In the reverse bias state, the parallel resistor R_1 turns to 5 $k\Omega$ 3.5 (a).

Figure 3.6 shows the schematic used with CST Studio Suite for the simulation of the antenna using the equivalent circuit model for the four PIN diodes. Results for the simulated S_{11} parameter are shown in Figure 3.7 for the three configurations. By comparing both S_{11} parameters in 3.4 and 3.7, it can be seen that the two approaches have good agreement in term of the frequency scope (5 Ghz

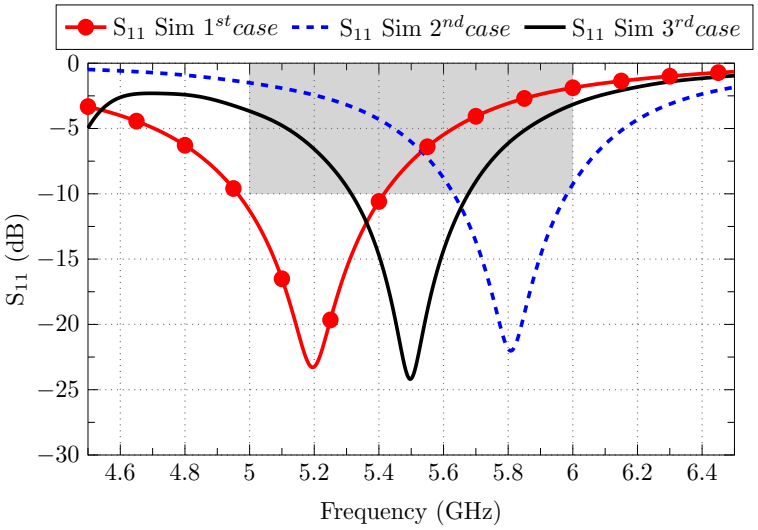

Figure 3.4: Simulated S_{11} parameter (dB) for the ideal case using metal wires.

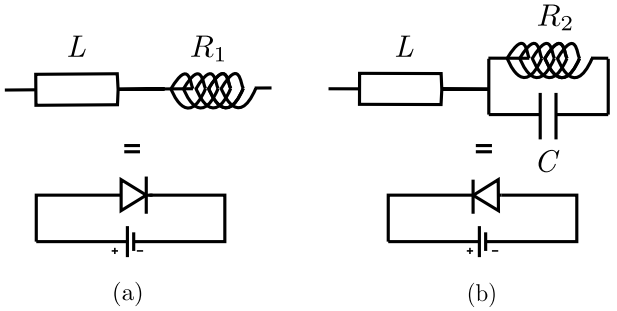

Figure 3.5: PIN diode equivalent circuit:(a)Reverse biasing;(b)Forward biasing [57].

band) even with a small shift in the central frequency. It can be mentioned that the second approach it is the more convenient approach as the characteristics of the pin diode are included in the simulation.

To validate the previous simulation approach (Second approach), which is the most convenient in term of accuracy. As shown in figure 3.8, the fabricated FRA was made a Neltec substrate model NY9220ST3175 with a thickness of H =3.175 mm and a relative dielectric constant ε_r = 2.2. A 50 Ω port cable was bent toward the ground plane of the antenna. The four PIN diodes model used in this antenna is the Infineon BAR50-02V SC79 package [57]. Thirteen DC block Capacitors of

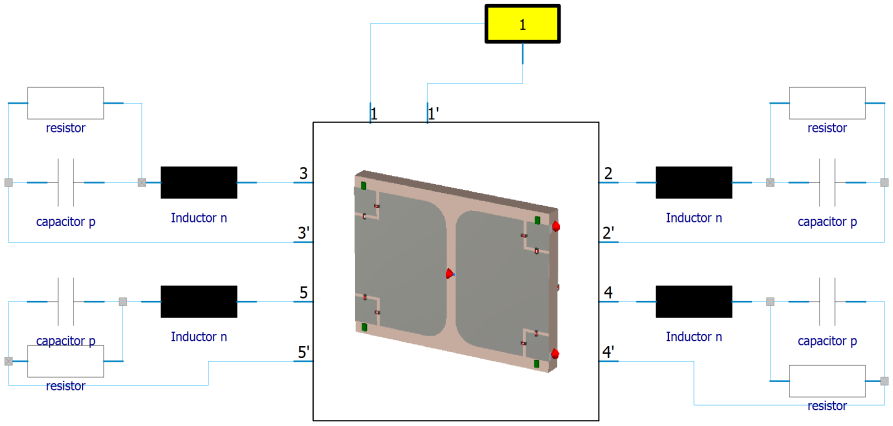

Figure 3.6: Antenna schematic with PIN diodes equivalent circuit.

20 pF was implemented and six RF choke inductors of 16 nH to perform the DC signal isolation from the RF signal.

The measured and simulated radiation patterns of the three configurations are plotted in 3.10. It can be seen that the experimental data exhibit an excellent agreement with the simulation results in the (YZ) plan at the three configurations frequency points. Some discrepancies were observed in the (XZ) plan, largely due to the manufacture tolerance and the effects of coaxial cable that crosses this plane. As it can be observed in 3.10, the switch between the three configurations does not affect remarkably the pattern beam.

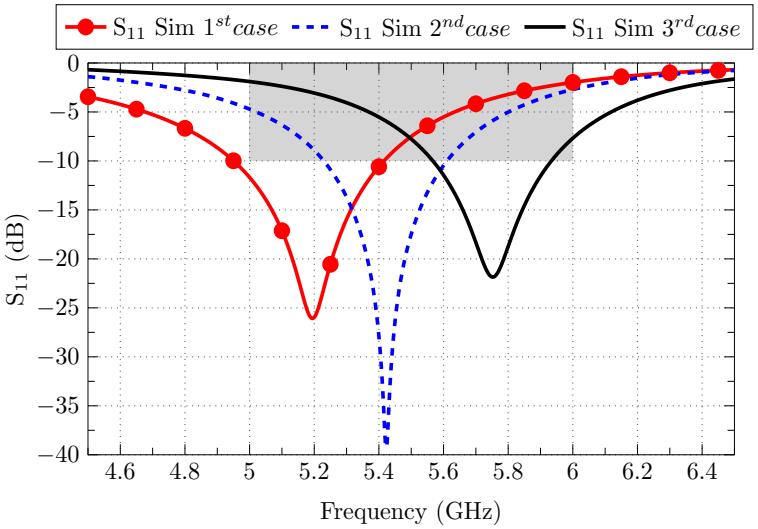

Figure 3.7: Simulated S_{11} parameter (dB) with the PIN diodes equivalent circuit.

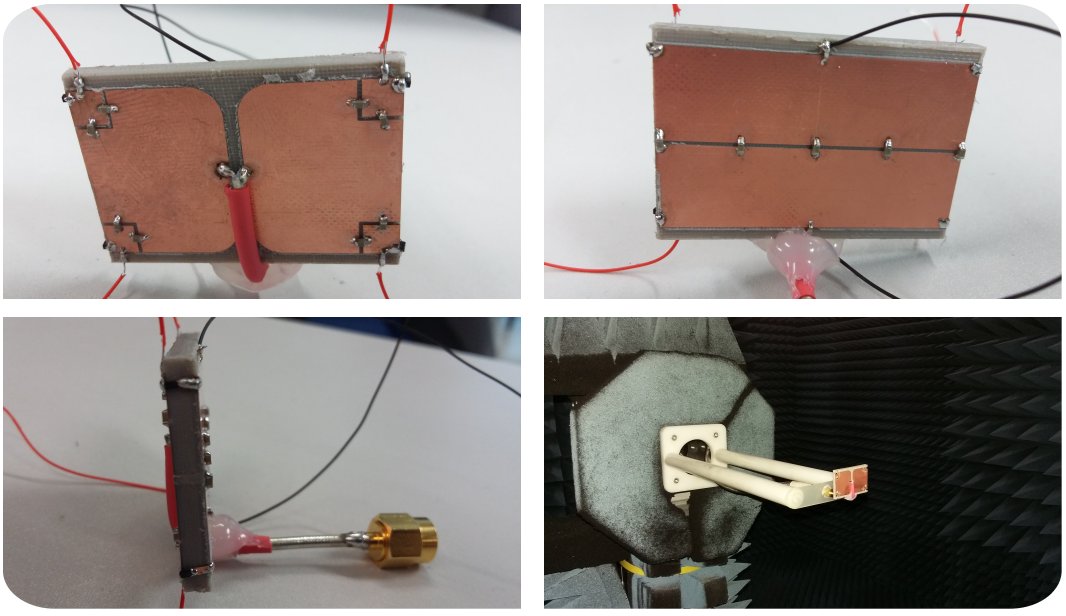

Figure 3.8: FRA Fabricated antenna.

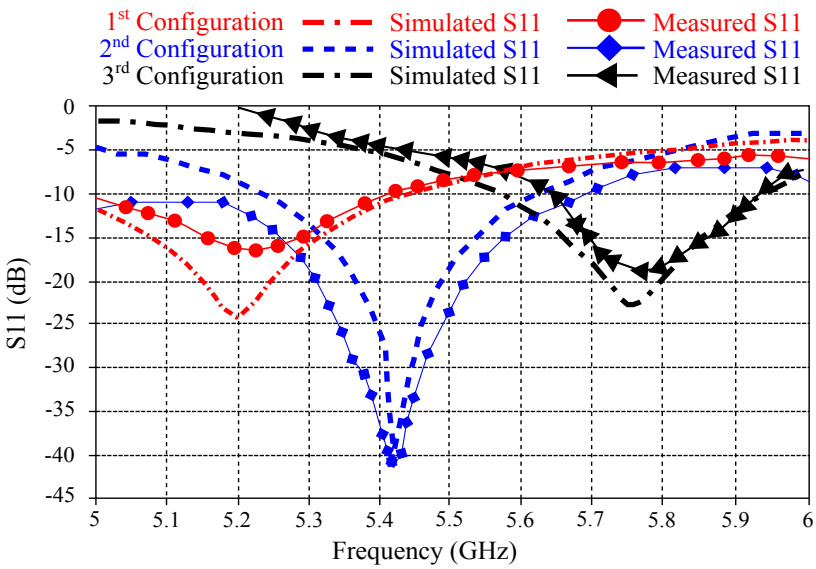

Figure 3.9: S11 parameters of the simulated results vs the measured results.

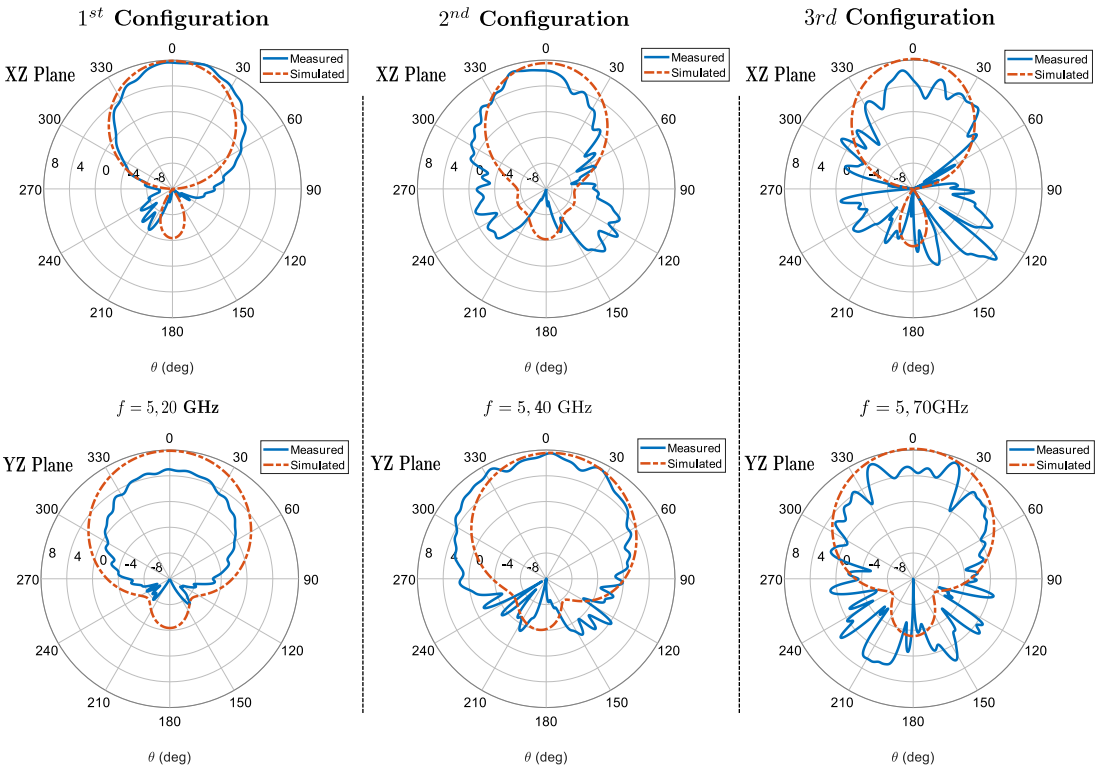

Figure 3.10: Simulated and measured radiation patterns for the three configurations using PIN diodes.

3.3 Varactor diode

Dissimilar to the PIN diode, when the varactor diode is forward biased, the depletion area disappears as shown in Figure 3.11 (a), and the diode works as a conducting plate. On the other hand, when a reverse bias is applied to the varactor, the reverse voltage expands the width of the depletion area as shown in Figure 3.11 (b). When the thickness of the depletion area increases with the reverse bias, the exhibited capacitance is inversely relative with the square root of the operated voltage.

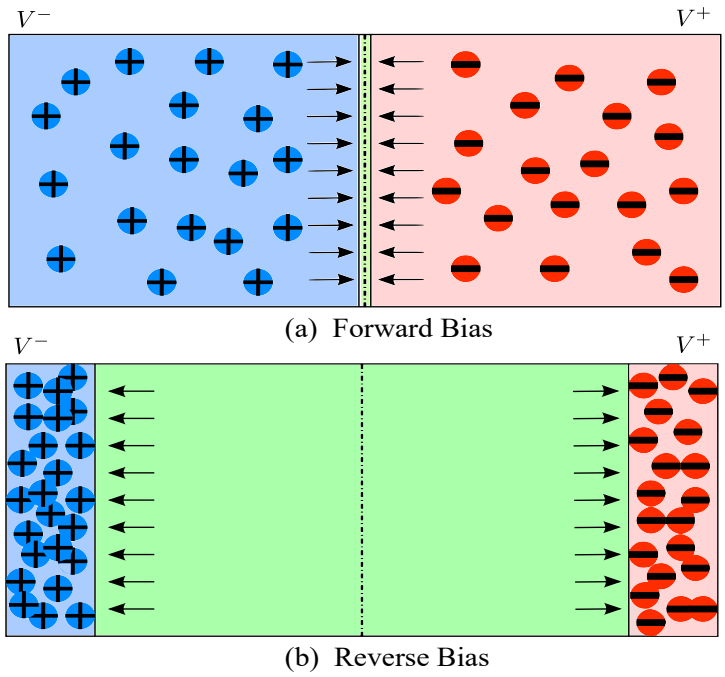

Figure 3.11: Varactor diode operation diagram.

Varactor diodes are suitable components for tuning the operating frequency range of an antenna. In order to achieve this objective, a varactor diode can be used to achieve the required tuning when reverse bias is applied [4]. The advantages of using varactor diodes for tuning are, for instance, reducing the antenna size without drastically modifying the basic geometry, enabling the radiator to

be resonant over a greater frequency band.

In [52] the author proposed a frequency reconfigurable antenna using varactor diodes. The proposed antenna is shown in Figure 3.12, and consists of a rectangular microstrip patch antenna, whose parameters can be obtained by using the formulas in [8]. As observed, the proposed antenna employs a Defected Ground Structure (DGS). The proposed antenna is designed on a RT/duroid 5880 substrate with a thickness h = 1.575 mm and a relative dielectric constant ε_r = 2.2. The length and width of the rectangular resonator are L = 11 mm and W = 19 mm, respectively. The width of the 50 Ω microstrip feeding line (W_m) is 1.5 mm. The total dimensions of the antenna are 30 mm × 30 mm.

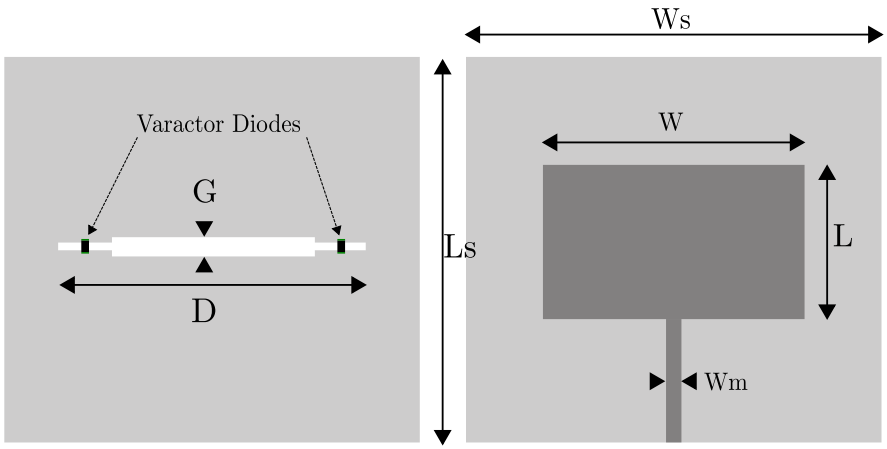

Figure 3.12: Geometry of the proposed frequency reconfigurable antenna structure: Bottom part, consisting in a Defected Ground Structure (left), and Top structure (right).

Conventionally, in a planar microstrip circuit, the DGS is located underneath the microstrip feeding line, disturbing the current distribution around the defect. As shown in Figure 3.12, the defected shape in our case is a rectangular slot with a variable width, with an initial value of G = 1 mm and a length of D = 22 mm. The slot is located under the rectangular resonator, and at each side of the slot, a varactor is positioned to change the electrical length of the slot when a reversed bias voltage is applied. The capacitance of the varactor is inversely proportional

to the reversed bias, as shown in Table 3.2.

Table 3.2: Capacitance versus Reverse voltage (for varactor SMV1232) [58].

$V_R(V)$	0	1	2	3	4	5	6	7
$C_J(pF)$	4,15	2,67	1,97	1,51	1,22	1,05	0,94	0,86

For the simulation of the reconfigurable antenna, three models are proposed:

First approach: Ideal case. It consists of using lumped elements to model the varactor diodes. It is based on the use of a pair of capacitors located at each side of the slot, at the point of the antenna where the electric field is high, as shown in Figure 3.13. Based on the datasheet of the varactor diode SMV1232-079LF [58] and Table 3.2, a series of simulations have been done by varying the capacitance value. Figure 3.14 shows the frequency tuning range achieved, from 5 GHz to 6.7 GHz.

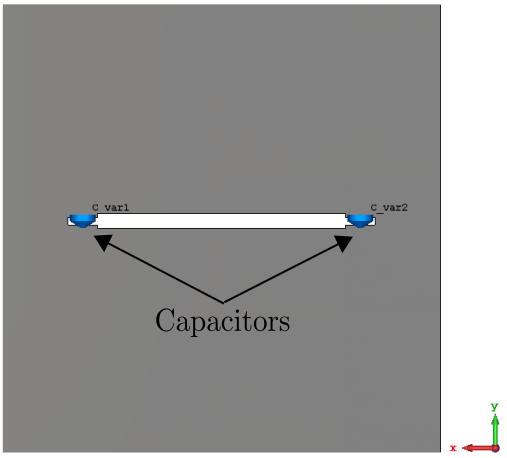

Figure 3.13: Bottom part of the antenna (DGS), using lumped capacitors as an ideal case.

Second approach: Varactor equivalent circuit case. This model consists of including the equivalent circuit of the varactor diode (SMV1232- 079LF model), given by the manufacturer, and depicted in Figure 3.15 and Figure 3.16. In these

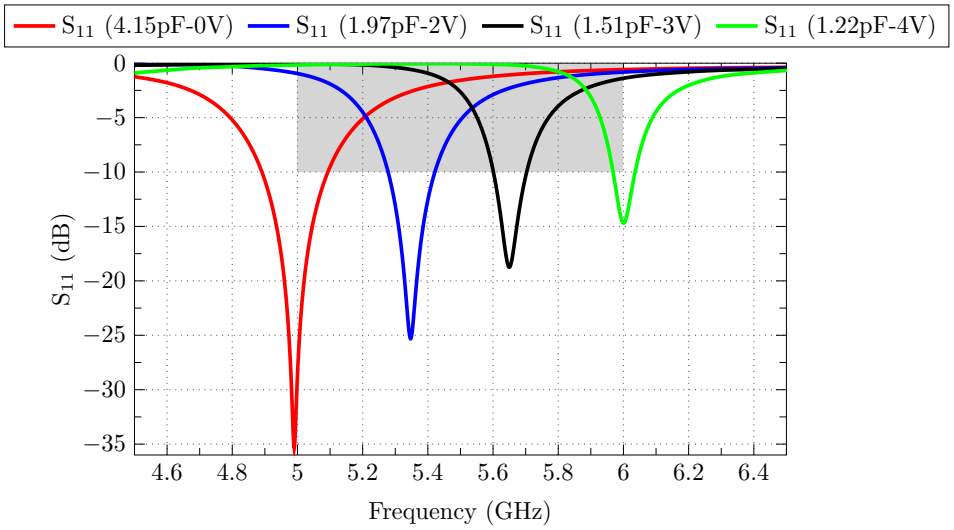

Figure 3.14: Simulated S_{11} parameter (dB) in the ideal case using capacitors.

figures, C_J is the variable junction capacitance of the diode, and can be varied from 4.15 pF to 0.72 pF with a reverse voltage between 0 and 15 V; R_S is the variable series resistance of the diode, L_S is the parasitic inductance and C_P is the parasitic capacitance arising from the installation of the package material, geometry and the bonding wires or ribbons. C_P has been neglected in the equivalent circuit of the simulation, as seen in the schematic used for the simulation shown in Figure 3.16. The values of R_S and L_S are 1.5 Ω and 0.7 nH respectively [58]. Figure 3.17 shows the frequency tuning range achieved, from 5 GHz to 6 GHz.

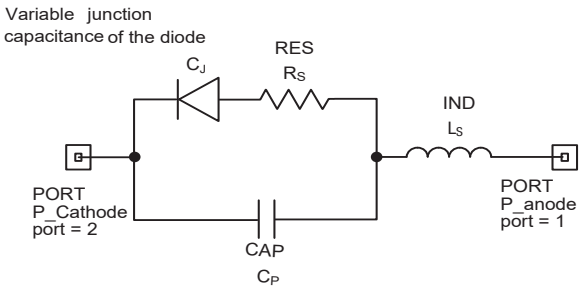

Figure 3.15: Varactor equivalent circuit (SMV1232-079LF model) [58].

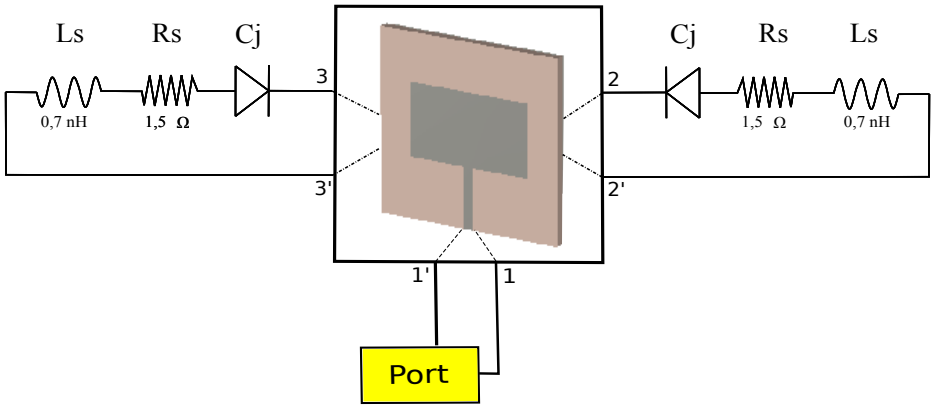

Figure 3.16: Antenna schematic used for the antenna simulation employing the varactor equivalent circuit.

Third approach: Varactor S-Parameter data files case. This approach is based on the S-Parameters data files provided by the manufacturer of the varactor [58]. The manufacturer provides different files containing the S-Parameters measured for several voltage values. Figure 3.18 shows the simulation schematic using these data files. Moreover, Figure 3.19 presents the simulated results, where it can be observed that different operating frequencies are obtained by switching between the files, from 0 to 13 V.

By comparing the three cases (Figure 3.14, Figure 3.17 and Figure 3.19), it is observed that the reflection coefficient in the first case does not perfectly match the others cases. This is due to the fact that the first case is an ideal approximation, with no parasitic effects.

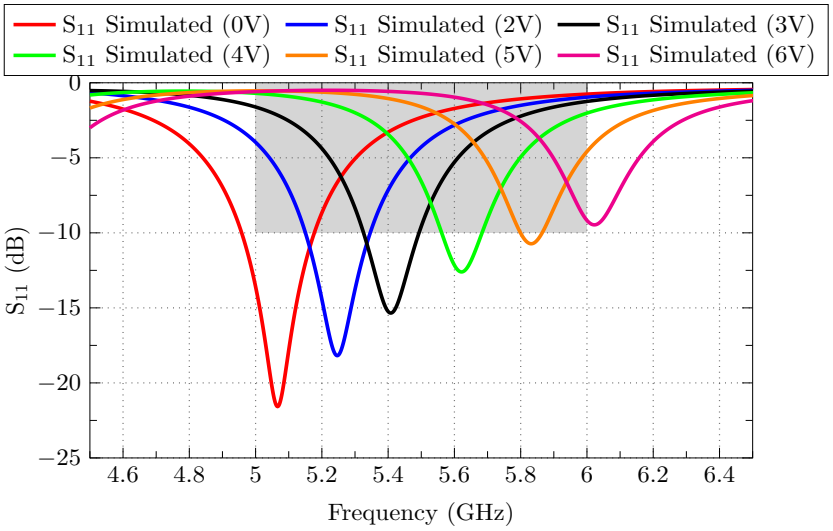

Figure 3.17: Simulated S_{11} parameter (dB) using the varactor equivalent circuit.

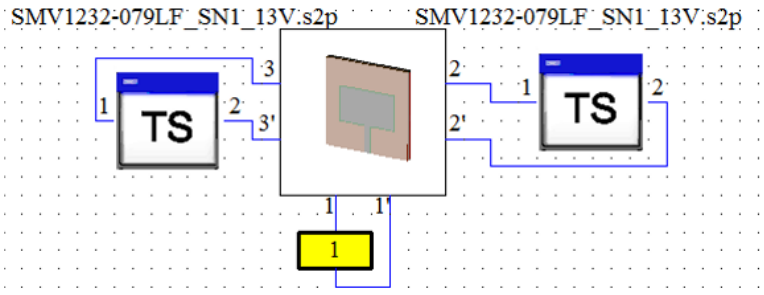

Figure 3.18: Antenna simulation schematic using the S_{11} data files of the varactor diode provided by the manufacturer [58].

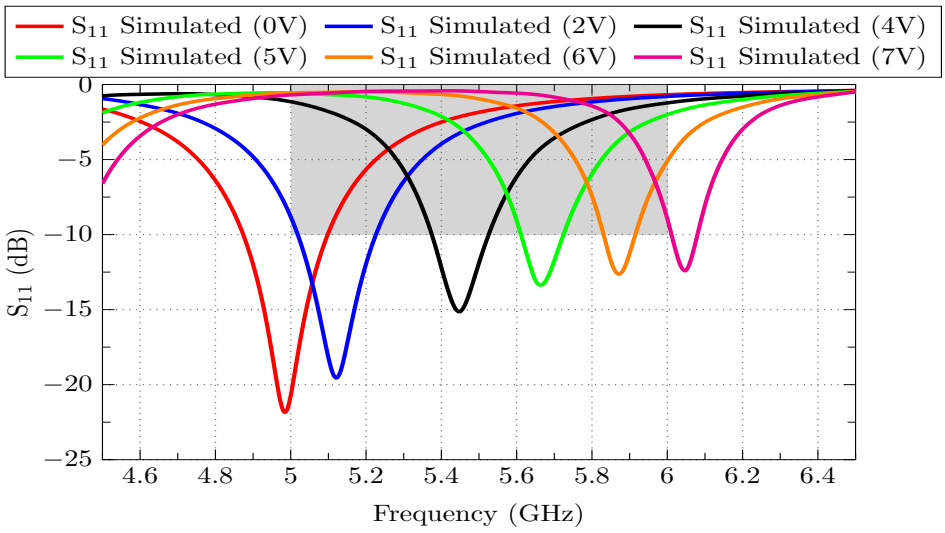

Figure 3.19: Simulated S_{11} parameter (dB) using the varactor data files.

3.4 PIN diode and Varactor diode

A radiation pattern reconfigurable antenna, combining PIN and varactor diodes, was presented by the author in [59]. The combination of PIN and varactor diodes is feasible in a way that each component has a specific role. The geometry of the proposed antenna is shown in Figure 3.20 and Figure 3.21, and consists of a rectangular patch antenna printed on Neltec substrate with thickness of 1.524 mm, relative permittivity ε_r = 2.2 and loss tangent $tan\ \delta$ = 0.0009. The dimensions of the structure are $W1$ = 18mm, $W2$ = 22.6 mm, L = 13 mm, S = 1mm and E = 1.3 mm.

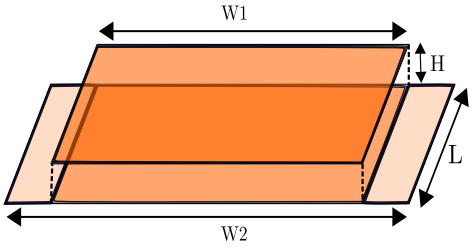

Figure 3.20: Geometry of the structure.

Two PIN diodes are connecting the bottom plate to the lateral edges, as shown in Figure 3.21(b). The two PIN diodes states, labeled as ON and OFF, allow or disallow the current to flow through the lateral edges, respectively. Hence, and as shown in the modal analysis presented in next chapter, the radiation pattern can get varied.

By switching the PIN diodes from ON to OFF state, a shift in the operating frequency occurs. This is due to the increase on the length of the edges of the lower plate of the antenna. To settle this issue, an optimized configuration is proposed that consists of applying a minor modification by adding a varactor on the top plate, as show in Figure 3.21(a). The use of varactor diodes is considered one of the most used techniques to overcome the inherent constraint of narrow bandwidth and therefore extend the operation frequency range. As shown in Figure 3.23, a common operating frequency is achieved between 5.3 GHz and 5.7

GHz for the two PIN diode states, ON and OFF.

Table 3.3: Proposed configuration for the pattern reconfigurable antenna.

	Case1	Case2
Pin Diodes	ON	OFF
Varactor	3V	6V
Pattern	Directional	Bidirectional

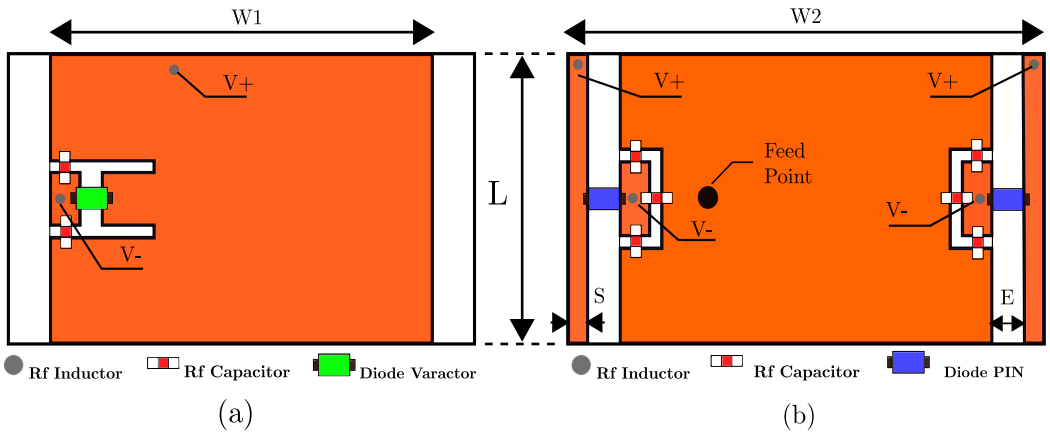

Figure 3.21: (a) Antenna top view; (b) Antenna bottom view.

The RF switch model adopted is the Infineon BAR50-02V silicon PIN diode [57]. As shown in Figure 3.21, to perform the DC biasing supply, additional components are fitted nearby the PIN diodes and the varactor diode 3.3. The DC voltage is isolated from the RF signal using four RF inductors of 27 nH. A total of eight DC block capacitor of 47 pF are used in order to conserve the continuity of the RF current crosswise the metal structure. The varactor diode model adopted in the design is MA46H120 [60], which has a tunable capacitance from 0.14 pF to 1.1 pF over the range of 0 to 10 V reverse bias voltage.

The proposed radiation pattern reconfigurable antenna is fabricated and assembled with the electronic components as presented in Figure 3.22. In this first prototype, wires are adopted in a classic manner to bias the diodes. Figure 3.23

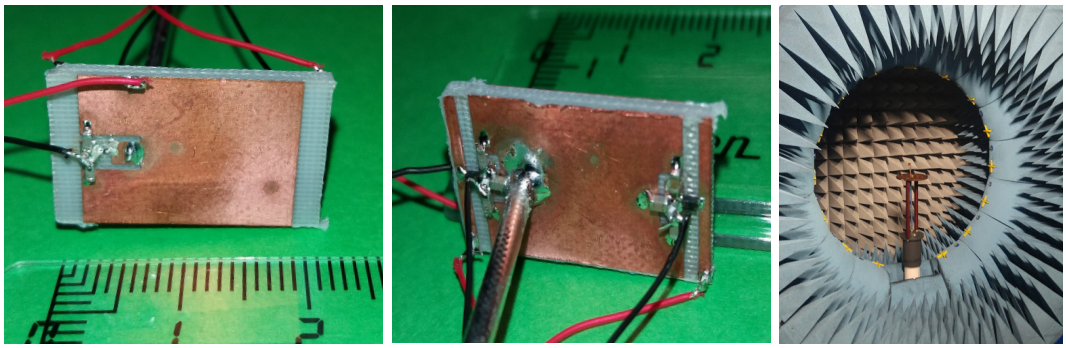

Figure 3.22: Fabricated radiation pattern reconfigurable antenna: Top plate (left), bottom plate (center) and measurement setup of the antenna (right).

shows the measured versus simulated S_{11} parameter of the proposed radiation pattern reconfigurable antenna, when the PIN diodes are at the ON/OFF state. In addition, the varactor is reverse biased with 6 V when the state is OFF, and 3 V at the ON state in order to match the impedance and to obtain a common operating frequency. From this figure, it is observed that the proposed antenna shows good measured impedance matching at the 5.3-5.7 GHz band that is suitable for WLAN applications.

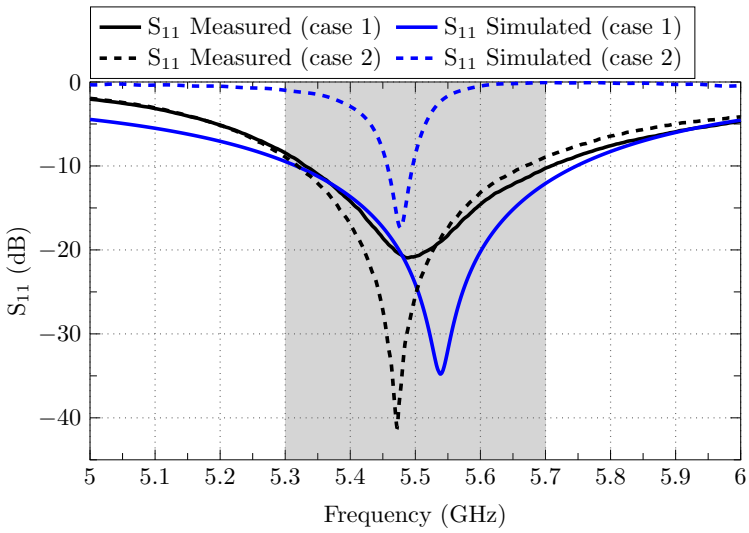

Figure 3.23: Simulated and measured S_{11} parameter for the two cases ON/OFF.

The radiation pattern measurements of the radiation pattern reconfigurable

antenna are plotted in Figure 3.24, for both XZ and YZ planes, at 5.5 GHz. As observed, by turning the PIN diodes to ON state leads to a directional beam, whereas by switching the PIN diodes to OFF state conducts to a bidirectional pattern. Therefore, a radiation pattern reconfigurable antenna is achieved.

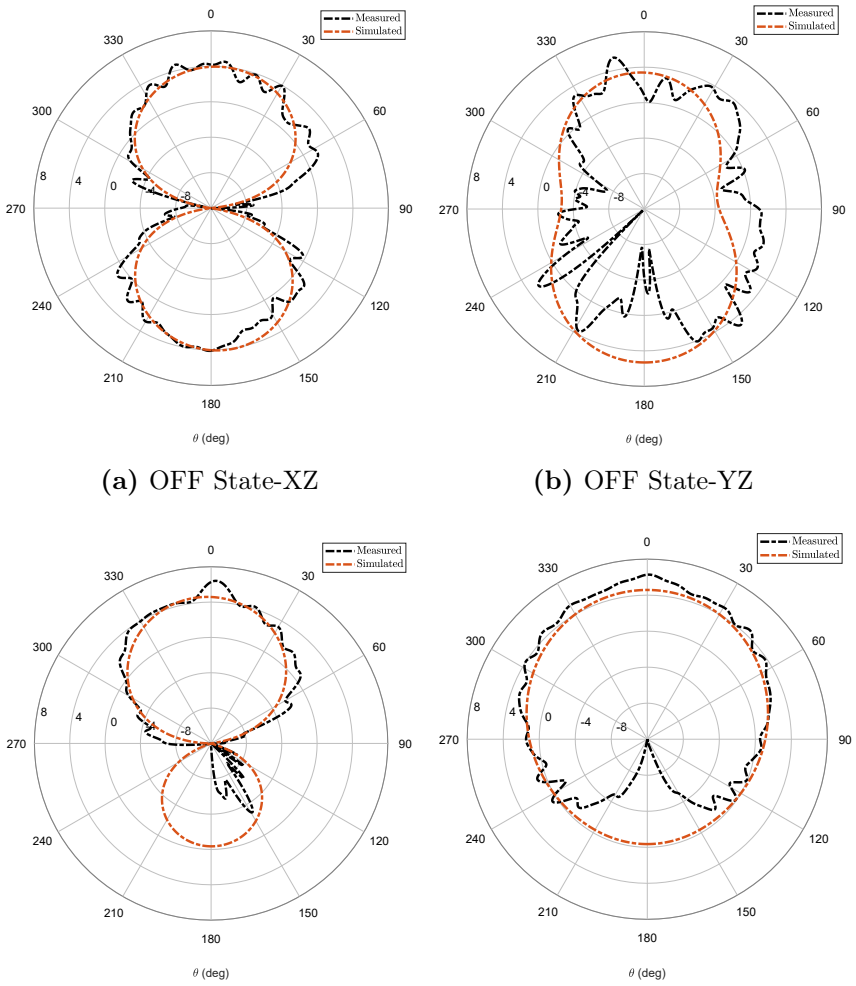

(a) OFF State-XZ **(b)** OFF State-YZ

(c) ON State-XZ **(d)** ON State-YZ

Figure 3.24: Measured radiation patterns at 5.5 GHz for both states of the radiation pattern reconfigurable antenna shown in Figure 3.22 .

3.5 Single-Pole Double-Throw (SPDT) switch

A Single-Pole Double-Throw (SPDT) switch can also be used for mode switching in wireless applications [61, 62]. Depending on the logic voltage applied to the control pin (VCTL) (see the SPDT block diagram in Figure 3.25), the INPUT pin is connected to one of the two switched RF outputs (OUTPUT1 or OUTPUT2) using a low insertion loss path, while the path between the INPUT pin and the other OUTPUT pin is in a high-isolation state. The switch is *reflective short* on the isolated port.

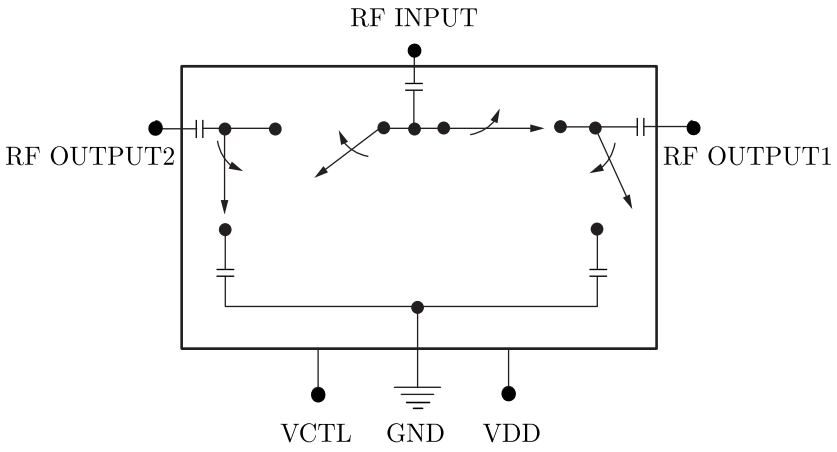

Figure 3.25: SPDT switch block diagram.

The antenna presented in previous section and shown in Figure 3.21 has been redesigned using a SPDT switch. The new proposed structure was presented by the author in [63], and its geometry is shown in Figure 3.26. Dimensions are presented in Table 3.4. The top side of the antenna contains the matching switching network. It comprises the main antenna 50 Ω input port that is controlled by a SPDT to choose the appropriate sub-input, depending on the configuration (case 1 or case 2). Configuration of the PIN diodes and SPDT switch for the two cases is shown in Table 3.5. The inferior plate is considered as the ground plane, and its dimension can be increased by means of two PIN diodes connected to two edge arms at the each side, as shown in Figure 3.26(b).

Table 3.4: Antenna dimensions.

Parameter	W	L	WS	LS	H	ε_r
Value (mm)	28	41	47.6	35	1.524	2.2

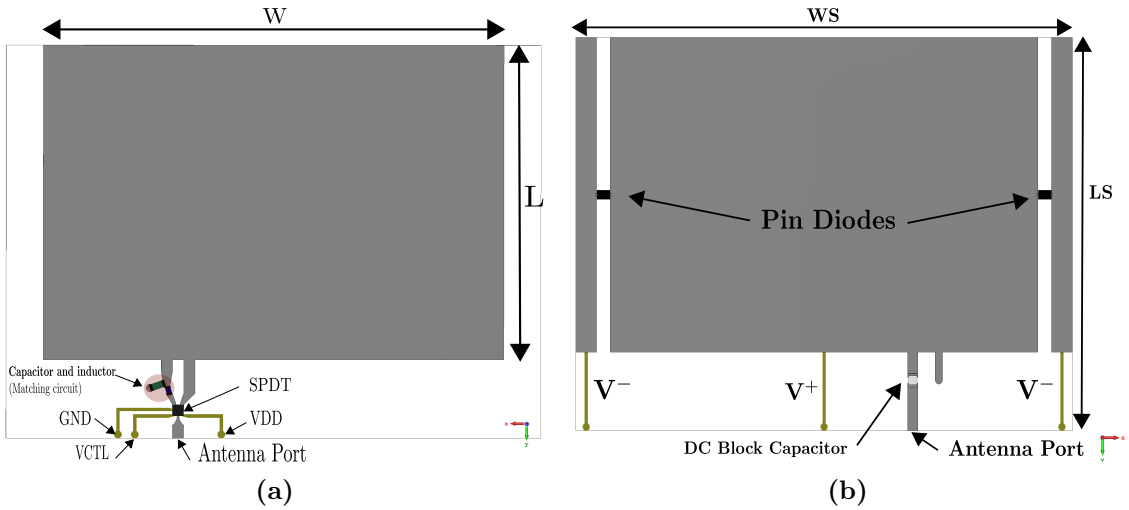

Figure 3.26: Geometry of the radiation pattern reconfigurable antenna with SPDT switch: (a) Antenna top view; (b) Antenna bottom view.

The antenna switches perform two functions: PIN diodes provide the switching between the two Cases or configurations, giving two different radiation patterns, whereas the SPDT switch is intended for impedance matching switching. To achieve a good DC biasing supply to the PIN diodes, a DC block capacitor is introduced between the input port and the ground plane. To decrease the number of matching lumped elements in the structure, Case 1 is matched by putting the feeding input at the appropriate position in the antenna. Then, Case 2 is matched by a series and a shunt capacitors of 0.6 pF.

A full-wave simulation is carried out using CST Microwave Suite simulator. All the electronic components are taken into consideration in the simulation to provide the most precise results. The antenna design and the switches setup are optimized to be controlled with a microcontroller. As aforementioned, the radiation pattern reconfigurable antenna structure is based on two configurations,

Table 3.5: Antenna switches configuration.

Case	PIN Diodes	SPDT
1	OFF	VDD = 5 V , VCTL = 0 V
2	ON	VDD = 5 V , VCTL = 3.3 V

as shown in Table 3.5:

Case 1: The PIN diodes are reverse biased and a nought given to the SPDT V_{CTL} (0 V). The simulated S_{11} parameter is depicted in Figure 3.27 with blue line, and shows the obtained band at 2.44 GHz with this configuration. As a result, a bidirectional radiation pattern is achieved at this frequency, with a directivity of 4.8 dB in both directions ($\theta = 0\,^{\circ}$ and $\theta = 180^{\circ}$), as presented in Figure 3.28(a).

Case 2: The PIN diodes are forward biased and V_{CTL} of the SPDT is set to 3.3 V. This second configuration gives a simulated S_{11} parameter with a bandwidth larger than the first configuration, as shown in Figure 3.27. Both configurations cover the 2.4 GHz band. However, with this second configuration a directional radiation pattern is obtained with a directivity of 5 dB, as displayed in Figure 3.28(b).

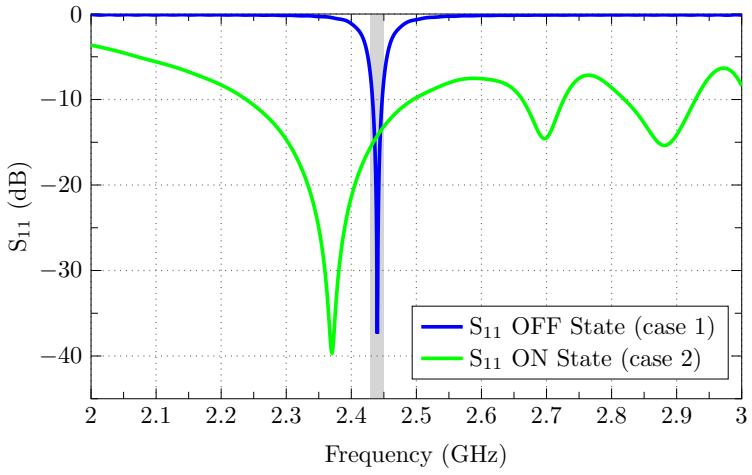

Figure 3.27: Simulated S_{11} parameter for the antenna shown in Figure 3.26, for Case 1 and Case 2.

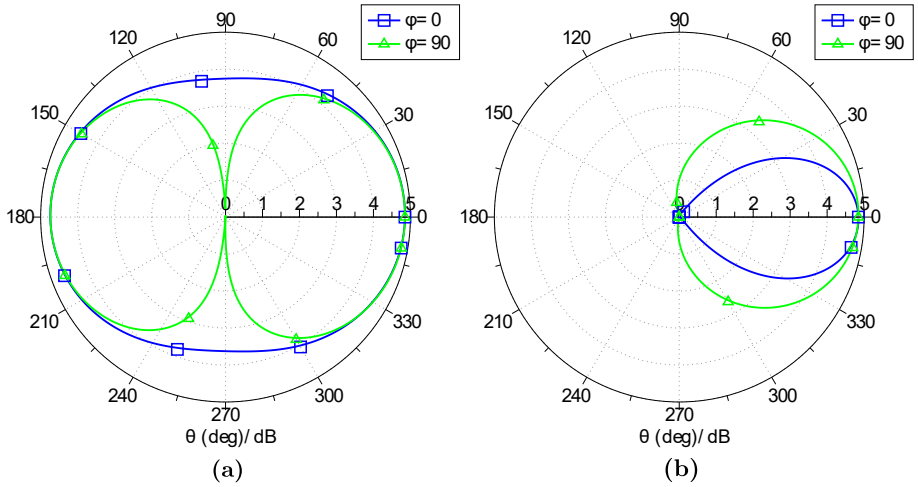

Figure 3.28: Simulated radiation patterns for the antenna shown in Figure 3.26: (a) Case 1; (b) Case 2.

3.6 Conclusion

In the present chapter, the implementation of different type of switches in antenna structure to achieve a tuning requirement was demonstrated. The modeling and conceptions has been based on a comprehensive approach and a simple structure with single layer and a single feed, this is the most desirable in wireless communication systems.

The frequency reconfigurable antenna with PIN diodes presented in the first section 3.2, provides coverage across all the the 5 GHz U-NII bands. The antenna has a low profile and it is very small volume and can be used inside WiFi or IoT terminals. Meanwhile in section 3.3, another frequency reconfigurable antenna using varactor diodes was proposed in the same 5 GHz U-NII bands. From a functional view with respect to the frequency adjustment, using varactors diode hands over a large varied frequency bands, as any alter in the variable junction capacitance of the diode can shift the frequency. This wide frequency reconfigurable band gives more flexibility to the communication system. In the other hand, the shift between frequencies can leads to an antenna mode mutation 4, which can not guarantee the consistency of the radiation pattern along the shift frequency range.

Moreover, in sections 3.4 and 3.5, the proposed radiation pattern reconfigurable antenna was upgraded from using the combination of Pin and varactor diodes in 5GHz band to SPDT switch in 2 GHz band. The first prototype presents the combination possibility of two types of diode, each one has its own role, the PIN diode provides the alteration functionality of the radiation pattern, and the varactor diode tunes the frequency in such a way to obtain a common band for both radiation patterns directional and bidirectional. In the second prototype, a SPDT switch was adopted instead of varactor diode, the enhance includes the feeding network, the same antenna design will be more developed in Chapter 5.

Thus, various types of reconfigurable antennas have been outlined. Taking into account the network bias system and switching components in the structure design reduces the cost of fabrication. To achieve several objectives, with switching components, it is feasible to use a single reconfigurable antenna.

Chapter 4

Design of frequency reconfigurable antennas using the TCM

4.1 Introduction

In a wireless system, the antenna is a decisive component. A simple and appropriate design can fulfil the system requirements and improve the global system performance. Patch antennas are one of the simplest antenna structures, and they have been widely used over the years due to their characteristics of low cost, light weight, low profile, and ease of integration.

Nevertheless, interference to/with other communication systems can exist because of the presence of different wireless applications that are using the same frequency band. As an example, in the Industrial, Scientific, and Medical (ISM) radio bands and the Unlicensed National Information Infrastructure (referred to as U-NII) bands used by IEEE 802.11 devices, the use of those bands is sometimes excessive by the Wi-Fi customers and leads to the presence of interferences because the access to this radio spectrum is without any restrictions and regulations that might be applicable elsewhere.

In addition, this unlicensed band operates over many frequencies, and from an antenna design perspective, UWB antenna with a band suppression feature can be one solution [64] for this problem. However, the cost and the design difficulty here are increased. To overcome this issue, frequency reconfigurable antennas

are proposed, where a dynamic modification of the operating frequency of the antenna brings flexibility to the communication system.

This kind of antenna will not cover all the frequency bands simultaneously but provides several dynamically selectable narrow frequency bands and, within these bands, exhibits higher flexibility than that achievable with conventional wideband and multiple band antenna solutions [54, 52]. Reconfigurability can be achieved by using electronic components to tune antenna characteristics such as PIN diodes [65, 66, 67], varactors [68, 69], and MEMS switches [70, 71] or changing material properties [72], as commented in previous chapters.

This chapter presents the design process of a reconfigurable antenna with two bands, suitable for WLAN applications. Work done in [52] proposed a similar simulation approach but only at 5 GHz band. However, the antenna proposed here operates at 2 GHz band, which will be a reconfigurable band, and at a second one that ranges from 5.3 GHz to 5.8 GHz, which is a steady band. A Defected Ground Structure (DGS) [73] consisting in a rectangular shape slot embedded in the ground plane is proposed and has been studied using characteristic mode analysis (CMA), which provides interesting physical insight into the antenna behavior [29]. Varactor diodes are used to perform the selectivity over the frequency band. In this part, two simulation approaches for the diodes, presented in Chapter 3, are followed: The ideal case and the equivalent circuit case.

At the end, a prototype has been fabricated and measurements have been performed to validate the simulated results.

4.2 Characteristic Mode Analysis of a Patch Antenna over a Finite Ground Plane

Let us perform the characteristic mode analysis (CMA) of a metallic rectangular plate of 29 mm × 31 mm over a rectangular ground plane of 35 mm × 50 mm. Figure 4.1 shows the geometry of the structure under analysis, where the separation between the two plates is $h = 1\ 524$ mm. No substrate is used.

The characteristic angle α_n associated to the first six Characteristic Modes (CM) of the structure is shown in Figure 4.2. Current distribution corresponding

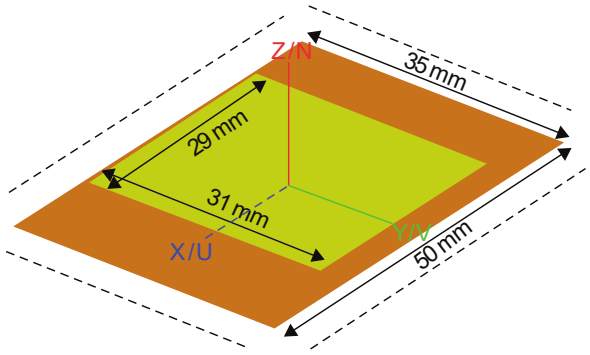

Figure 4.1: Patch antenna over a finite rectangular ground plane, to be analyzed with CMA. Separation between the two plates is 1.524 mm.

to these six modes at its resonance frequency (α_n = 180°) is plotted in Figure 4.3. As it can be observed, each mode presents a specific current distribution, with vertical and/or horizontal currents.

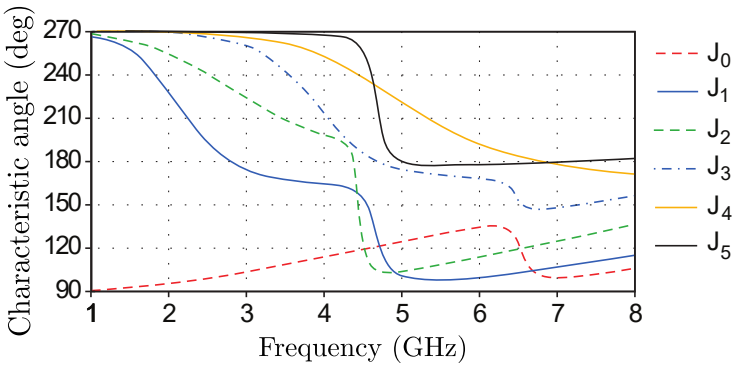

Figure 4.2: Characteristic angle associated to the first six CM of the patch antenna shown in Figure 4.1.

CM are intrinsic to any structure but their excitation depends on the feeding mechanism used. If the patch antenna is excited at its longer edge by a microstrip line, modes with current distributed along the x-axis and with opposite flow direction in the patch and in the ground plane will be excited. Therefore, according to Figure 4.3, modes J_1 and J_4 are the ones that will be excited. As each mode resonates at a different frequency (α_n = 180°), two operating bands will be achieved, obtaining a dual-band antenna.

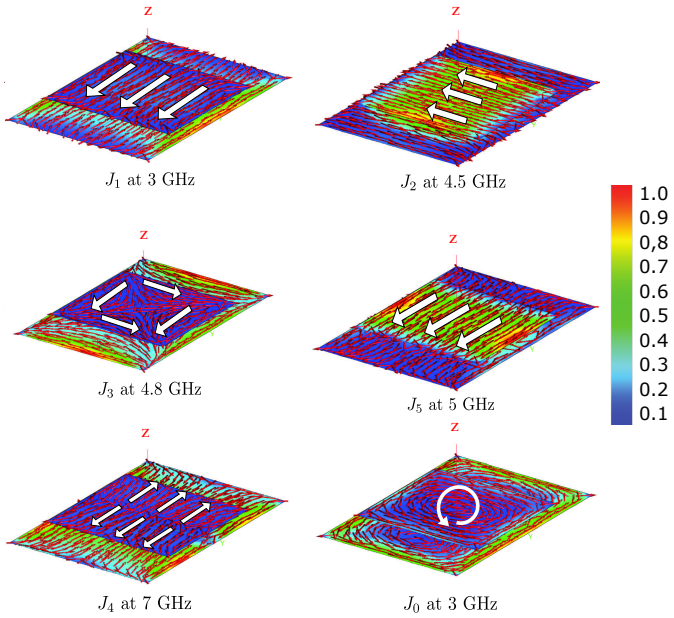

Figure 4.3: Current distribution of the first six CM of a patch antenna over a rectangular ground plane, near their resonance frequency.

Now, in order to create a tunable band for the first operating band, a narrow rectangular slot with two tunable capacitors could be inserted in the antenna at the appropriate place, so as to not disturb the second operating band that should be fixed. Looking at the current distribution associated to modes J_1 and J_4, we can see that the slot should be inserted at the center of the ground plane, along the y-axis. Remark that the unidirectional radiation behavior of the patch is then lost when the slot is etched in the ground plane, as back radiation will appear in this case. For applications where bidirectional radiation is needed, the proposed antenna with this DGP (slotted ground plane) can be used.

Figure 4.4 depicts the geometry of the proposed defected ground plane of the patch antenna. As a null of current is present at the position of the slot for mode J_4, this mode will not be affected by the presence of the slot, whereas mode J_1 will be. This fact can be observed in Figure 4.5, where a comparison of the characteristic angle of the original structure and the structure including the slot is shown. As it can be seen, the resonant frequency of mode J_1 is shifted down due to the presence of the slot, whereas mode J_4 is not perturbed.

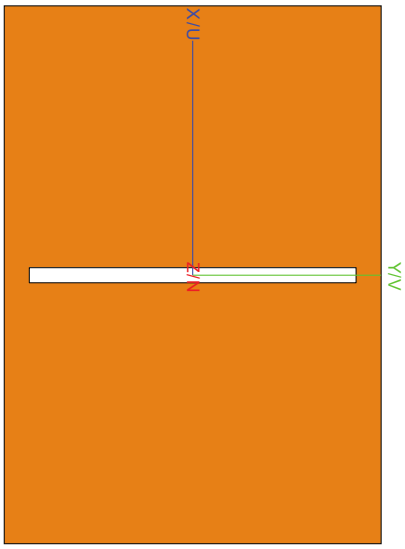

Figure 4.4: Defected ground plane (DGP) for the reconfigurable dual-band antenna.

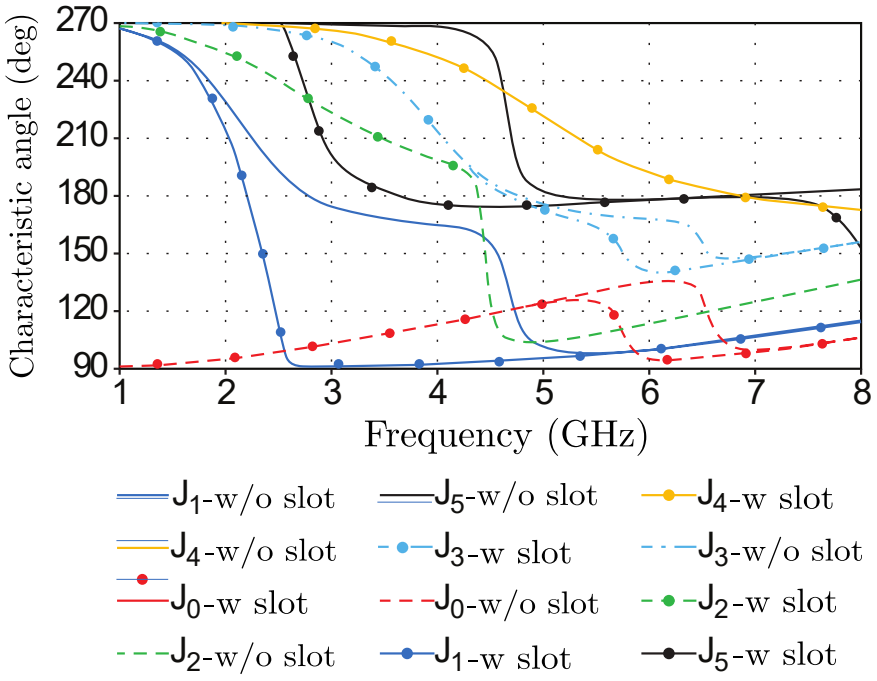

Figure 4.5: Comparison of the characteristic angle associated to the first six CM of the patch antenna over a ground plane with (-w) and without (-w/o) slot.

Moreover, Figure 4.6 shows the characteristic angle of the first six modes when varying the slot length (S). As seen, the variation of the slot length affects modes J_1 and J_5, modifying their characteristic angle. Modes J_0, J_2, J_3, and J_4 are showing a constant behavior as they are conserving the same characteristic angle and resonant frequency even though the slot length is changing.

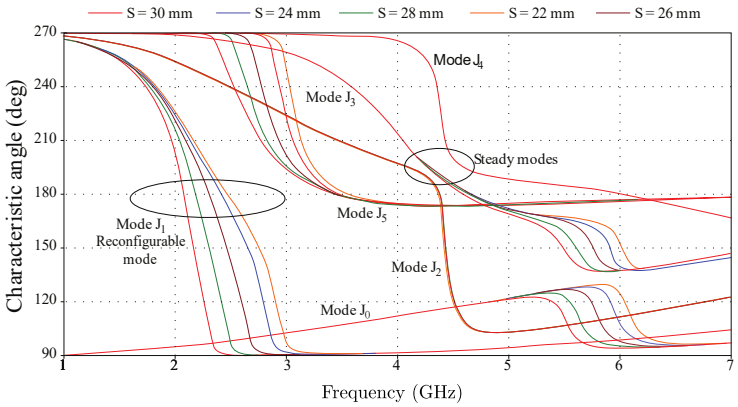

Figure 4.6: Characteristic angle variation with the slot length (S) for the first six CM over frequency.

As modes J_1 and J_4 are excited in the proposed antenna, if the slot is loaded with variable capacitors, the resonance frequency of mode J_1 can be tuned, keeping the resonance frequency of mode J_4 steady. This will be shown in the next section.

4.3 Antenna Description and Simulations

4.3.1 Antenna Geometry

Figure 4.7 shows the geometry of the proposed reconfigurable dual-band antenna. As observed, the antenna consists of a rectangular patch with length L and width W, where entire dimensions of the ground plane are $L_s \times W_s$. The substrate used is Rogers $RO3003$, which is a lossy substrate with a dielectric constant of $\varepsilon_r = 3$ and loss tangent $tan\ \delta$=0.001. The patch antenna is fed at the longer edge by a microstrip line of width W_M connected to a coaxial SMA port of 50 Ω. As the objective is to obtain two bands (lower band at 2 GHz and upper band centered

Table 4.1: Dimension of the designed antenna.

Parameter	W	L	W_S	L_S	W_M	G	S	h
Value (mm)	31	29	35	50	1.25	1	30	1.524

at 5 GHz), a slot of length S and width G is etched in the ground plane, as described in the previous section. Each side of the slot is loaded with a varactor diode, in order to keep the symmetry. The model of the varactor adopted in this work is the Skyworks $SMV2025$ surface mount hyperabrupt tuning varactor diode [74].

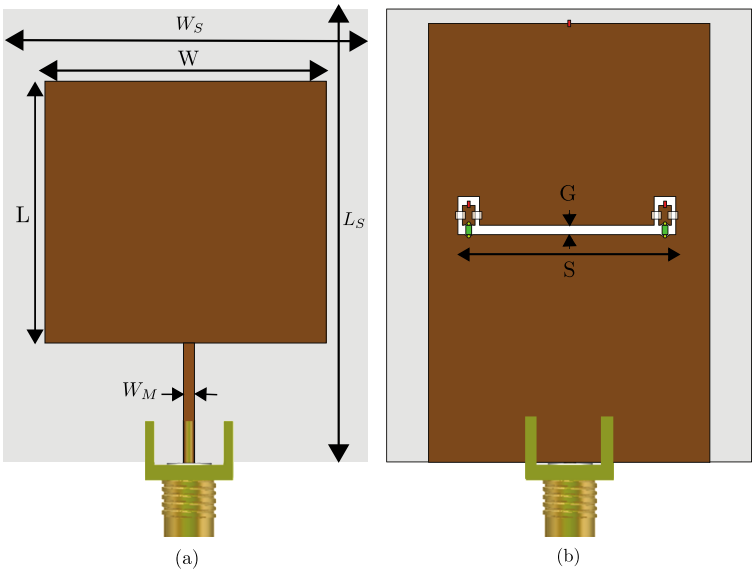

Figure 4.7: Dual-band frequency reconfigurable antenna geometry: (a) Front view; (b) Back view.

The simulation design is performed by using CST Microwave Suite software, based on the simplified theoretical formulations that have been described in [8]. The final dimensions of the proposed antenna are shown in Table 4.1.

4.3.2 Simulation Results

In this section, simulated results for the proposed antenna will be presented. Firstly, a parametric study of the slot parameters will be shown to observe how its dimensions and position is affecting the S_{11} parameter associated to the antenna. Then, different simulation methods, presented already in Chapter 3, will be explained for modelling the PIN and varactor diodes used in the proposed antenna. Simulated results will be presented for both models.

a) Parametric Study of the Slot

In Figure 4.6, it has been presented the characteristic angle variation of the modes when varying the slot length S, showing a variation in the resonance frequency of mode J_1 (mode of the tunable band). In Figure 4.8(a), the S_{11} parameter for different slot lengths is shown. As it can be observed, the slot length affects the first frequency band (reconfigurable band). In order to obtain good results, the slot should be inserted in the center of the ground plane.

Figure 4.8(b) shows the S_{11} parameter for different slot positions on the y-axis, with respect to the center of the ground plane (i.e., $GP\ center$ is the distance from the center of the slot to the center of the ground plane along the y-axis). Finally, Figure 4.8(c) presents the S_{11} parameter for different slot widths G. As observed, the slot width affects the matching of the frequency bands.

b) Reconfigurable Antenna Simulation Methods

Figure 4.9 shows the simulated return loss of the antenna without slot and with slot. As shown by the CMA and as can be observed in Figure 4.9, the effect of adding a slot in the ground plane of the antenna shifts down the lower band, from 2.8 GHz to 2.2 GHz. It should be mentioned that the band achieved by the slot could be obtained by using a slot length of 0.165λ. Likewise, the second frequency band holds in a steady regime without any disturbance coming from the slot, as seen before.

To be noted, the second band is a combination of several modes, as seen in the previous section, and it is observed that the length (L) and width (W) of the rectangular patch affect this band. As a suggestion, this band could be tuned as

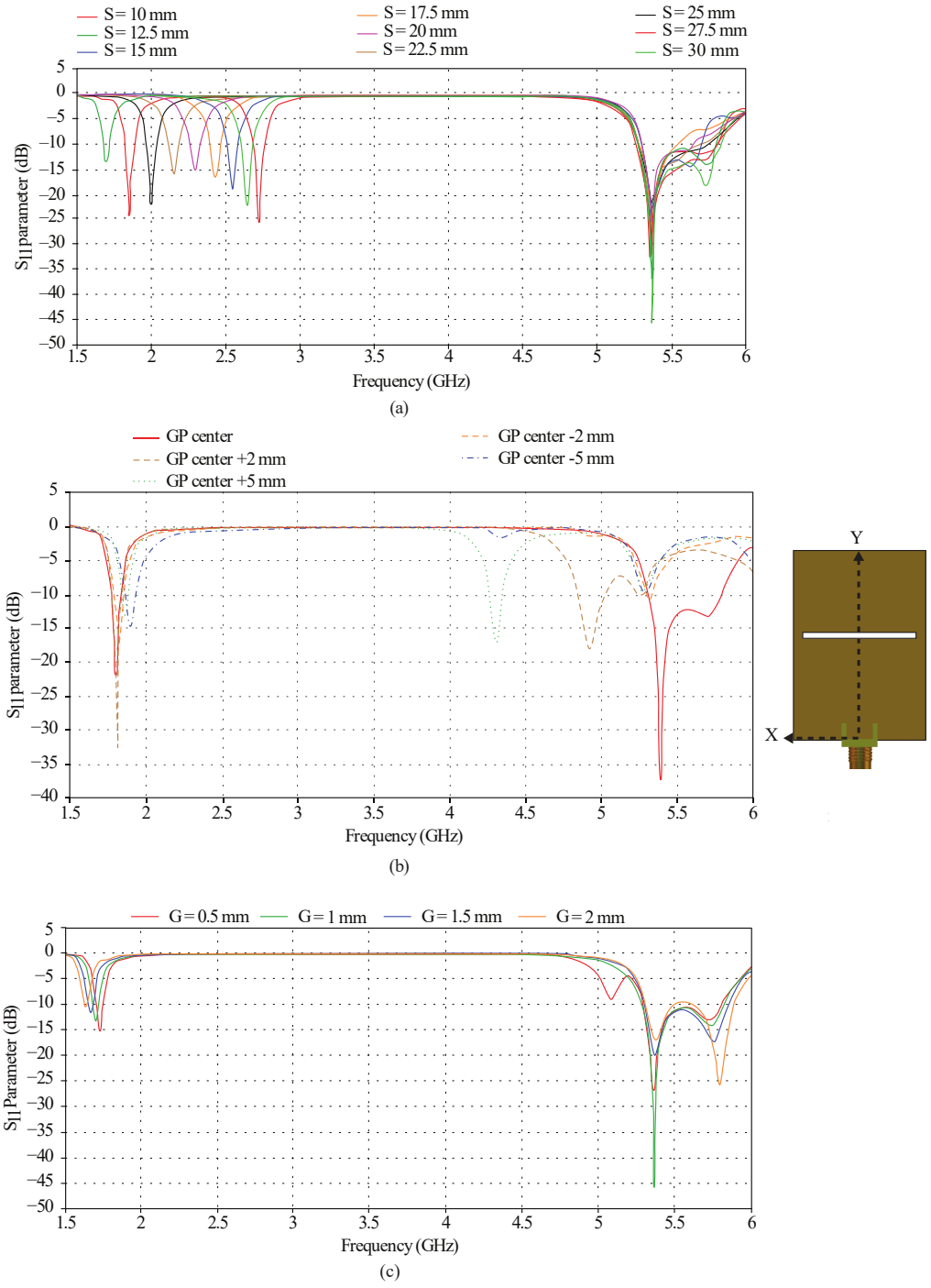

Figure 4.8: Simulated S_{11} parameter variation with: (a) The slot length (S); (b) The slot position along the y-axis ($GP\ center$); (c) The slot width (G).

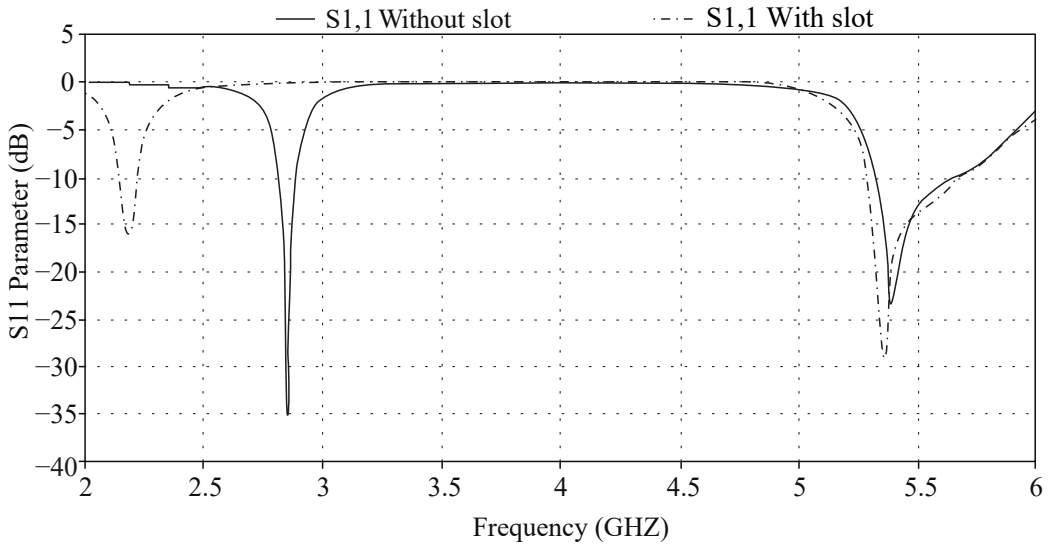

Figure 4.9: Simulated S_{11} parameter of the antenna without slot and with slot.

well by following the approach in [75], by embedding a pair of capacitors in the two opposite corners of the rectangular patch.

For the simulation of the structure including varactors, two approaches are followed in order to obtain good simulation performance. The first method consists of using the fundamental lumped element of the varactor diode, which is purely a capacitor. The second manner is based on using the equivalent circuit of the varactor diode given by the manufacturer, which include capacitors, inductance, and resistance, as shown in Chapter 3. Therefore, two cases are used for the simulation:

(1) Case 1: Ideal Circuit. It is based on using the nominal capacitance for each voltage given in the datasheet of the Skyworks $SMV2025$ varactor diode model. Thus, a capacitor is used to simulate the diode varactor function. In Figure 4.10, the simulated S_{11} parameter of the antenna for different capacitance values (*cap* parameter) is shown. As seen, by altering the capacitance values, the frequency of the first band is shifted reversely to the capacitor value and a smooth variation in a wide frequency range can be achieved. Meanwhile, the second band keeps it constancy when the capacitors are varied. Remark that this simulation approach (ideal case) does not include any parasitic element.

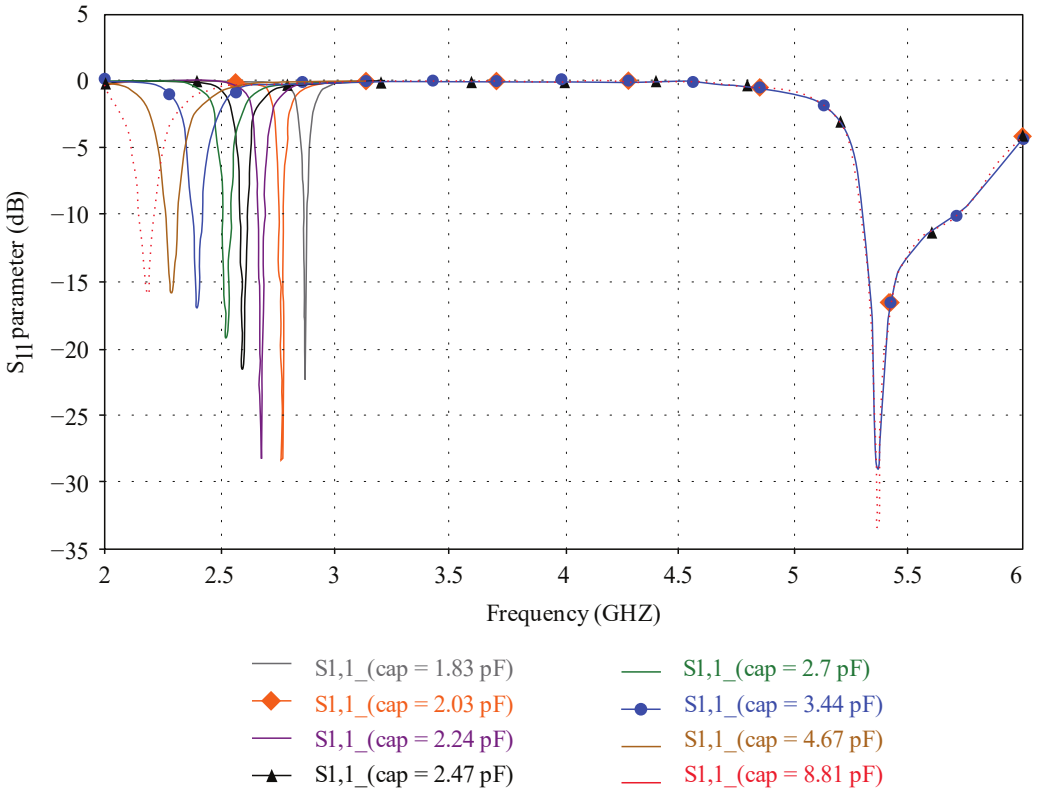

Figure 4.10: Simulated S_{11} parameter of the antenna considering the ideal case for the varactor diode using capacitors.

(2) Case 2: Equivalent Circuit. To improve the simulation performance, this case includes lumped elements in the equivalent circuit model of the varactor. Figure 4.11(a) shows the equivalent circuit of the varactor diode [74], where LS is the parasitic inductance, RS is the series resistance of the diode, CT is the variable junction capacitance of the diode, and CP is the parasitic capacitance arising from the installation of the package material. The tuning capacitance CT ranges from 8.81 pF to 1.15 pF and can be achieved by the means of a reverse bias from 0 V to 20 V. The varactor diode model adopted in this antenna offers very low parasitic inductance and capacitance. Figure 4.11 (b) shows the antenna schematic with the equivalent circuit of the varactor diode used for simulation.

Finally, Figure 4.12 shows the capacitor variation with frequency. It can be seen that with this varactor model, a wide reconfigurable frequency band is achieved, from 2 GHz to 3.8 GHz.

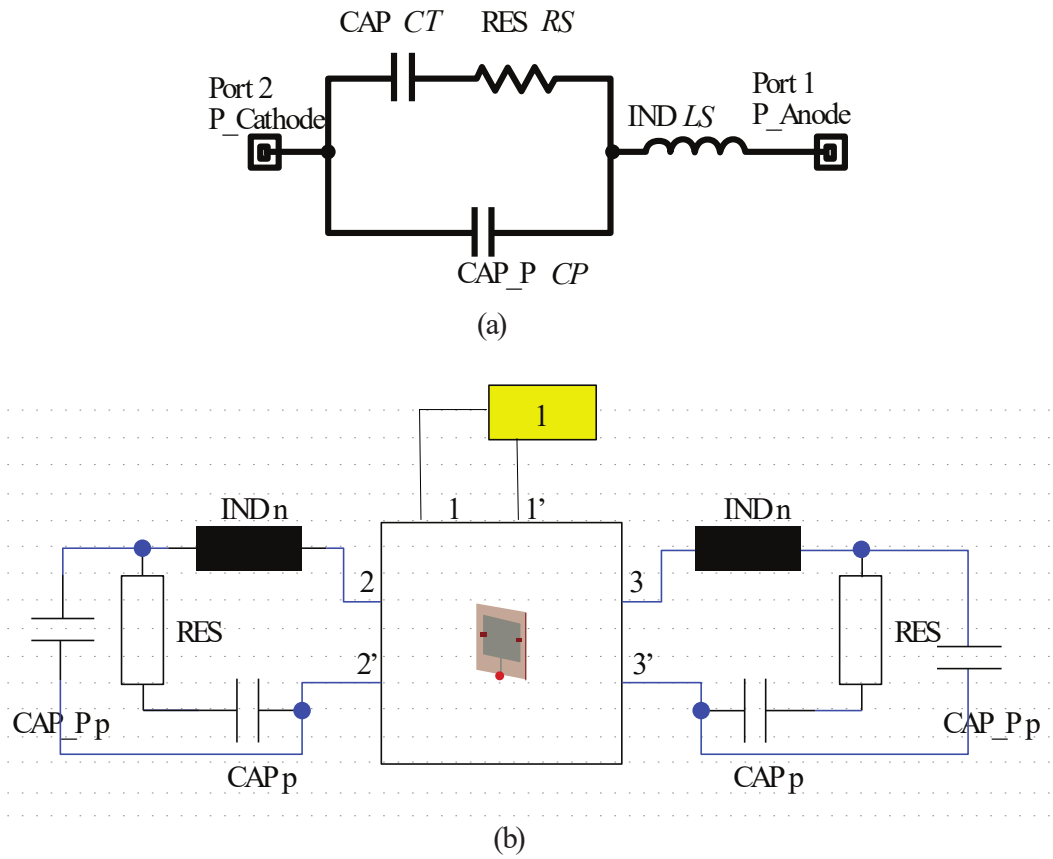

Figure 4.11: (a) Equivalent circuit of the varactor diode [74]. (b) Schematic design of the antenna used for simulation.

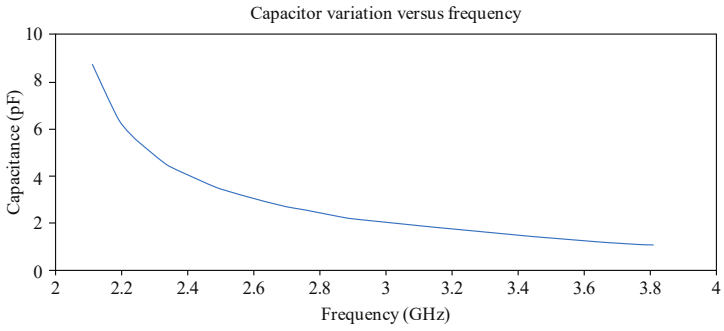

Figure 4.12: Variation of the varactor capacitance over frequency [74].

The S_{11} parameter for both approaches are shown in Figure 4.10 and Figure 4.13, respectively, showing a good agreement. The first band is a reconfig-

urable band, while the second is a steady band. A small shift in frequency can be observed in the second case, due to the additional parasitic components added to the model. It can be seen that the S_{11} (dB) is below -10 dB for all the bands. The bandwidth for the reconfigurable bands varies from 50 MHz to 10 MHz, whereas for the steady band the impedance bandwidth reaches 500 MHz, considering $S_{11} \leq$ -10 dB.

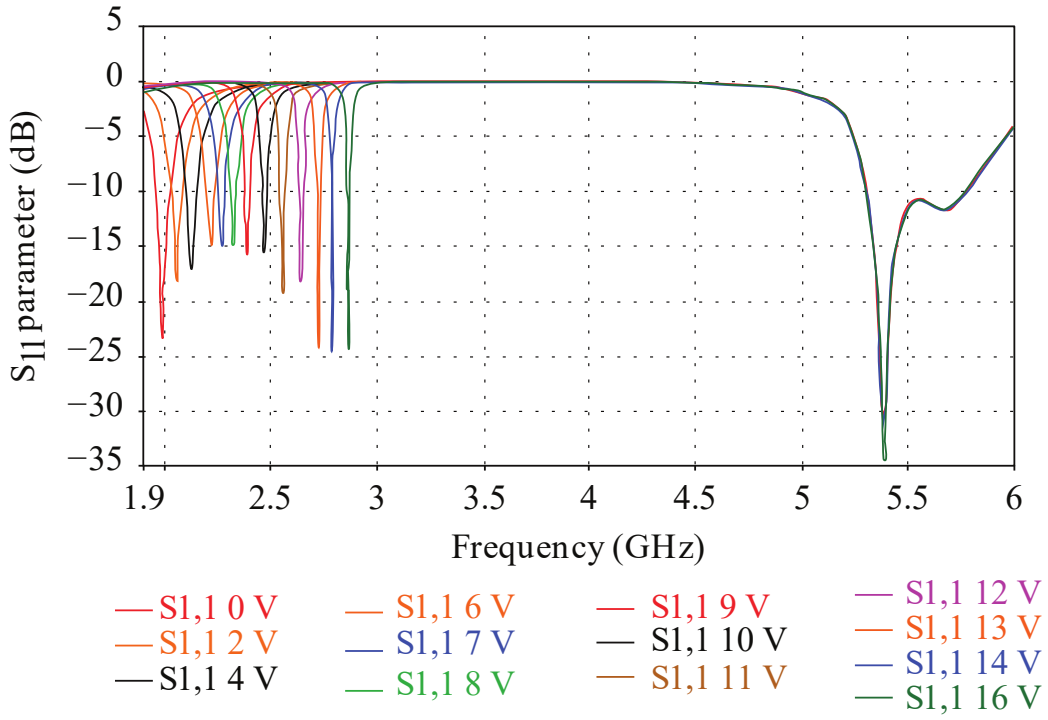

Figure 4.13: Simulated S_{11} parameter of the antenna using the varactor equivalent circuit.

4.4 Prototype and Measurement Results

The bias circuit of the varactor diodes has been implemented and DC components for controlling the varactor diodes are fitted in the ground plane. As illustrated in Figure 4.14, four DC block capacitors of 40 pF are used, in order to conserve the continuity of the RF current in the ground plane and provide DC blocking.

DC voltage is isolated from the RF signal using three RF inductors of 40 nH. The cathode of the varactor diodes is connected to a small copper area and supplied with the positive DC voltage, while the anodes of the varactor diodes are connected to the ground plane, where the negative terminal is connected. The prototype of the antenna is depicted in Figure 4.15 and has been tested and analyzed.

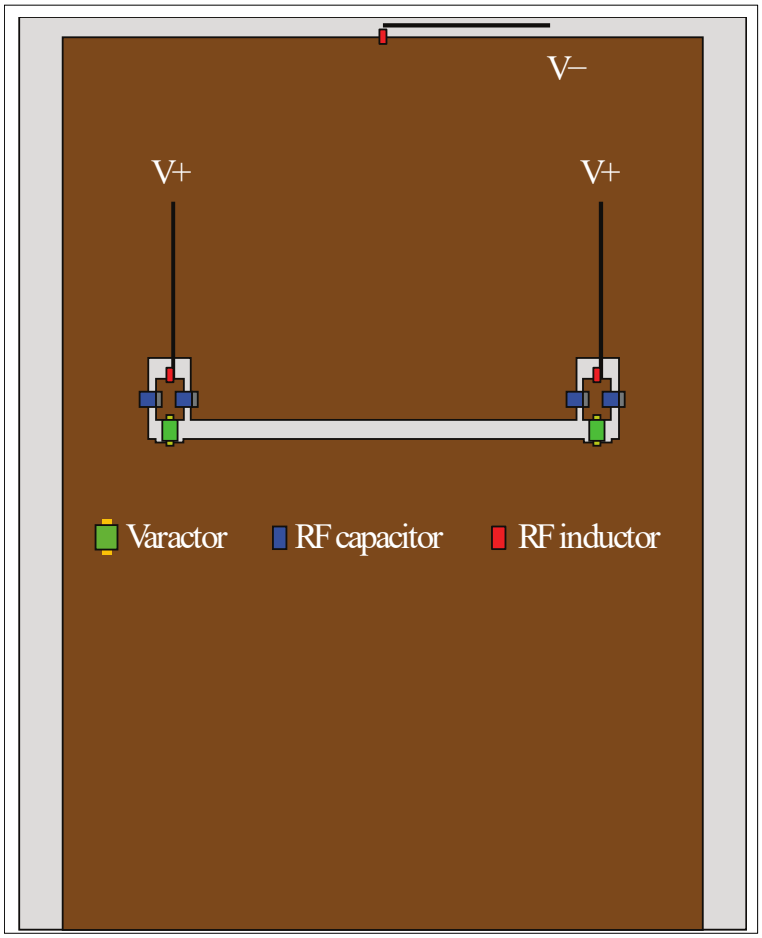

Figure 4.14: Biasing circuit configuration for the varactor diodes.

Figure 4.16 illustrates a comparison between the simulated and measured S_{11} parameter for three different biasing voltages of 0 V, 2 V and 4 V. As the bias voltage increases, the capacitance decreases and the lower operating band is shifted to upper frequencies. It can be seen that at the reconfigurable band (lower band), a good agreement between the first configuration shown in Figure 4.16(a) (lower

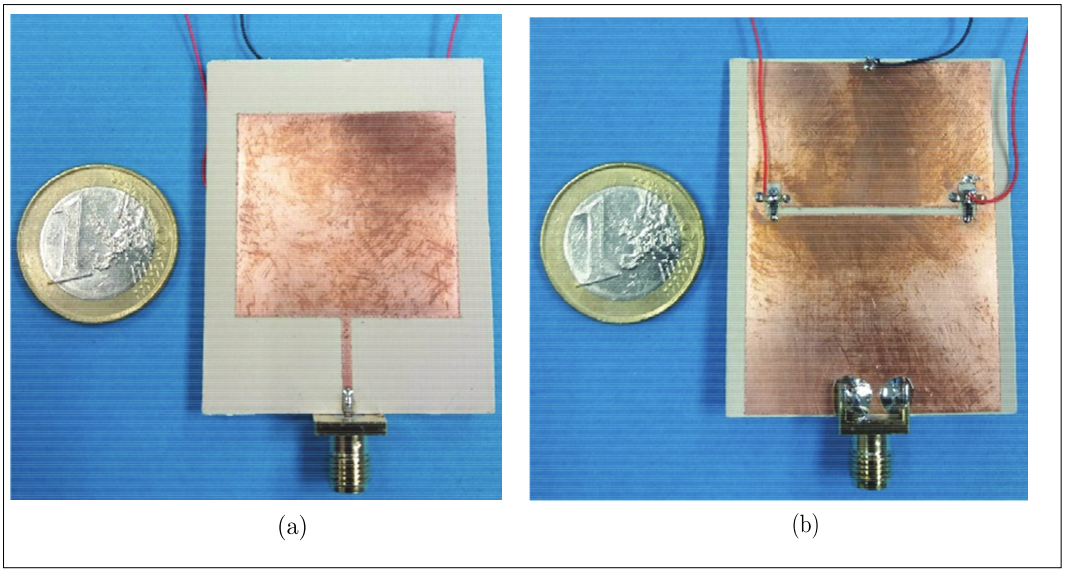

Figure 4.15: Fabricated antenna with the DC biasing circuit: (a) Front view; (b) Back view.

band centered at 2 GHz) and the second configuration shown in Figure 4.16(b) (lower band centered at 2.15 GHz) is observed. The corresponding equivalent capacitance to the biasing voltages of 0 V and 2 V is 8.81 pF and 4.67 pF, respectively. The third configuration in Figure 4.16(c) (lower band centered at 2.25 GHz) does not meet a perfect match between simulation and measurement, due to the unstable behavior of the biasing circuit as the frequency increases. However, any selectable frequency at the 2 GHz band can be achieved by slightly biasing reversely the varactor.

The radiation patterns of the antenna prototype were measured for two biasing voltages (0 V and 4 V). The 3D patterns were taken at three selected operating frequencies within the reconfigurable band: $f_1 = 2$ GHz for 0 V and $f_1 = 2.3$ GHz for 4 V, and two frequencies (f_2 and f_3) within the steady band ($f_2 = 5.4$ GHz and $f_3 = 5.67$ GHz).

As shown in Figure 4.17, the majority of the measured radiation patterns agree well with the simulated ones. Remark that some difference between the simulated and measured patterns for the first configuration (f_1, 0 V) exists, due to slight differences between the simulated and physical feeding adjustments.

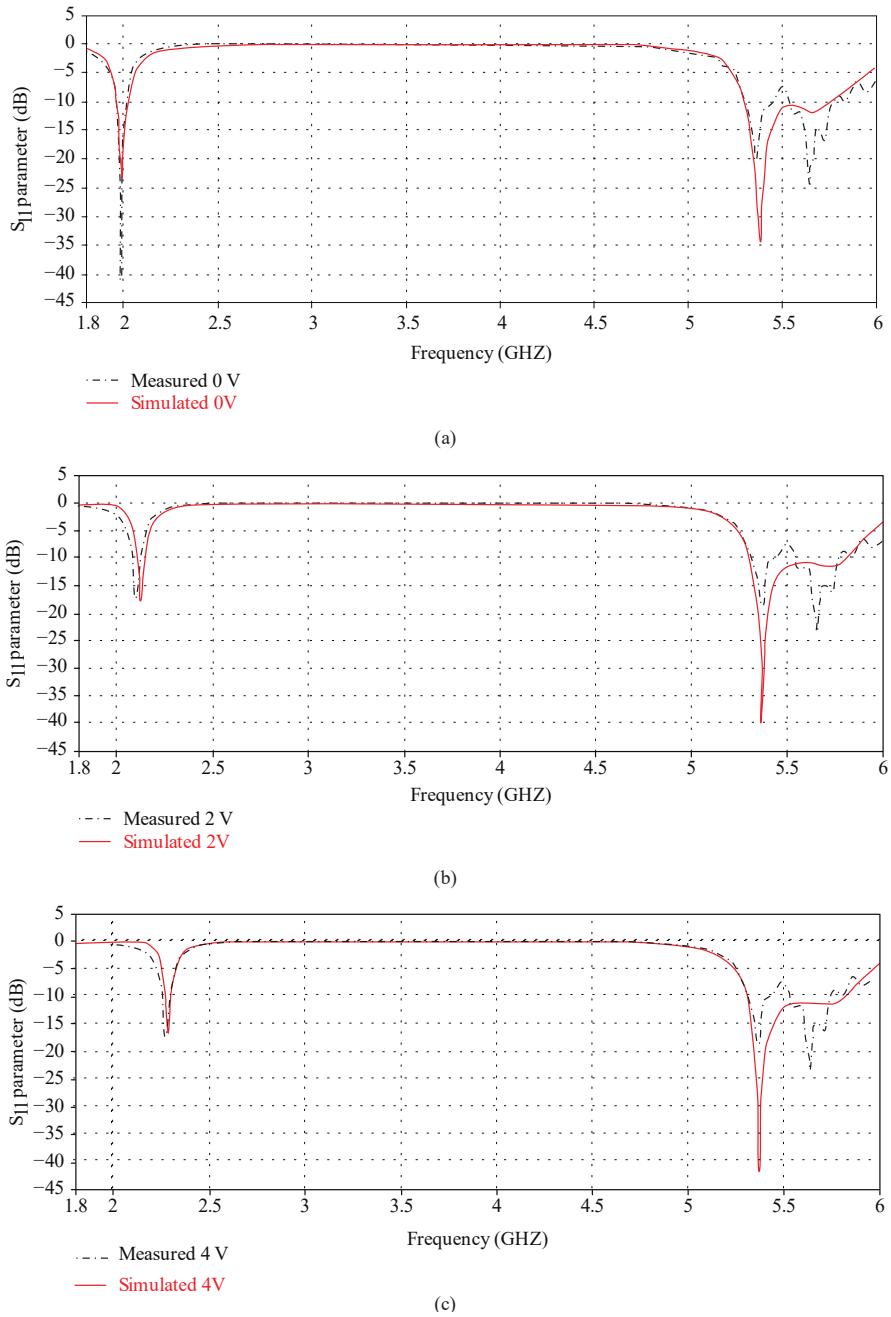

Figure 4.16: Simulated vs. measured S_{11} parameter for different biasing voltages: (a) 0 V; (b) 2 V; (c) 4 V.

Measured efficiency for the antenna in the steady band is above 66%, whereas

the efficiency of the reconfigurable bands when the varactor is biased with 0 V and 4 V is 49% and 89%, respectively. These values are acceptable for real applications. In addition, the measured gain of the first and second bands are 3.16 dBi and 6.56 dBi, respectively (when 0 V is applied), and 6.33 dBi and 5.67 dBi, respectively (when 4 V is applied).

4.5 Conclusion

A practical approach to design a dual-band frequency reconfigurable antenna has been proposed. Based on the Characteristic Mode Analysis, the ability to tune a particular mode keeping the rest of modes unaltered has been demonstrated. Two simulation methods have been proposed for the varactor diode: ideal case and equivalent circuit case. The models are successfully applied to design a reconfigurable antenna that entirely covers the 2 GHz band and with a steady band centered at 5 GHz. The simulated results using the equivalent circuit of the varactor diode and the measured results are in good agreement.

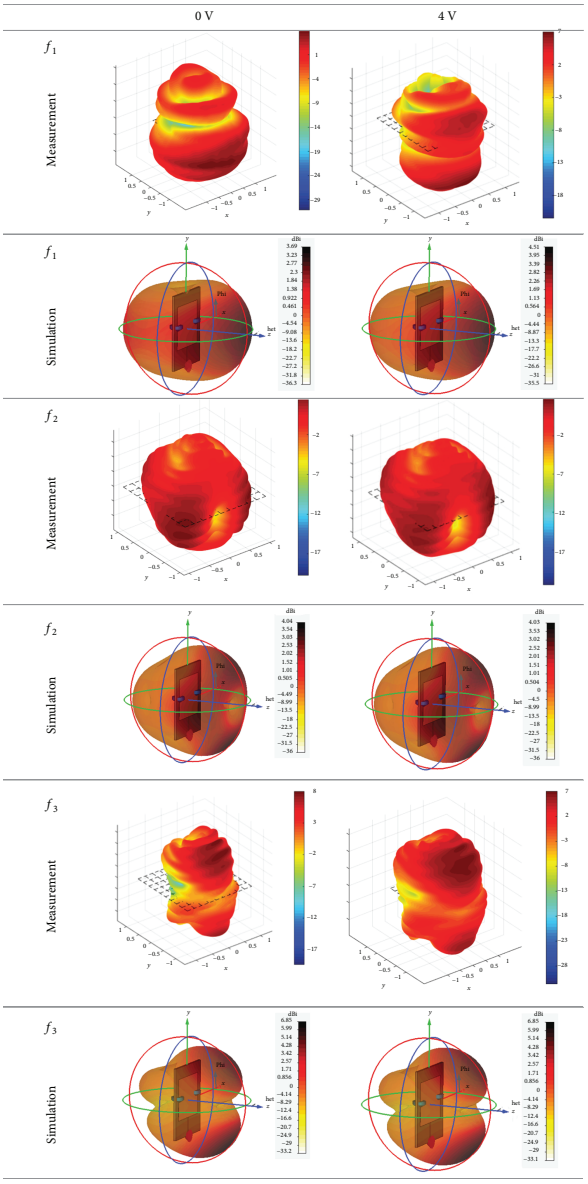

Figure 4.17: Simulated and measured 3D radiation patterns for frequencies: f_1 = 2 GHz for 0 V and f_1 = 2.3 GHz for 4 V, f_2 = 5.4 GHz and f_3 = 5.67 GHz.

Chapter 5

Design of radiation pattern reconfigurable antennas using the TCM

5.1 Introduction

This chapter describes the design of a radiation pattern reconfigurable antenna based on the use of two rectangular parallel plates. The design is based on that presented by the author in [59], but a significant improvement has been provided with the current design. Firstly, the geometry is proposed and a CMA is performed in order to explain the behavior of the antenna from a modal perspective. Then, a reconfigurable radiating structure using PIN diodes and a SPDT switch [61] is proposed.

The goal of the proposed design is to switch between a bidirectional and unidirectional radiation pattern, depending on the state of the PIN diodes. The aim of using a SPDT switch is to reach a common operating frequency (2.5 GHz) at both states, avoiding the modification of the basic geometry. Hence, the proposed antenna proposes a convenient solution for several IoT applications, as it can produce different beam conditions in a sensor without changing physically the antenna structure.

CMA, antenna simulation and design of the structure have been performed by means of *FEKO* [45] and *CST Microwave Studio* [44] simulation softwares.

5.2 Design of a rectangular parallel plate antenna based on Characteristic Mode Analysis

Let us consider two rectangular metallic plates separated a distance $H = 1.5\ mm$, as shown in Figure 5.1. Two cases are analysed, corresponding to two plates with the same dimensions ($W1 \times L = 62.5\ mm \times 42\ mm$), and two plates with a small variation in the length of the lower plate ($W2 \times L = 68.5\ mm \times 42\ mm$).

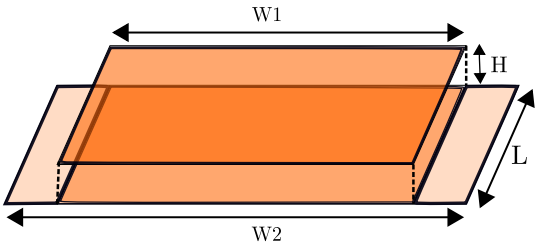

Figure 5.1: Geometry of the structure under analysis.

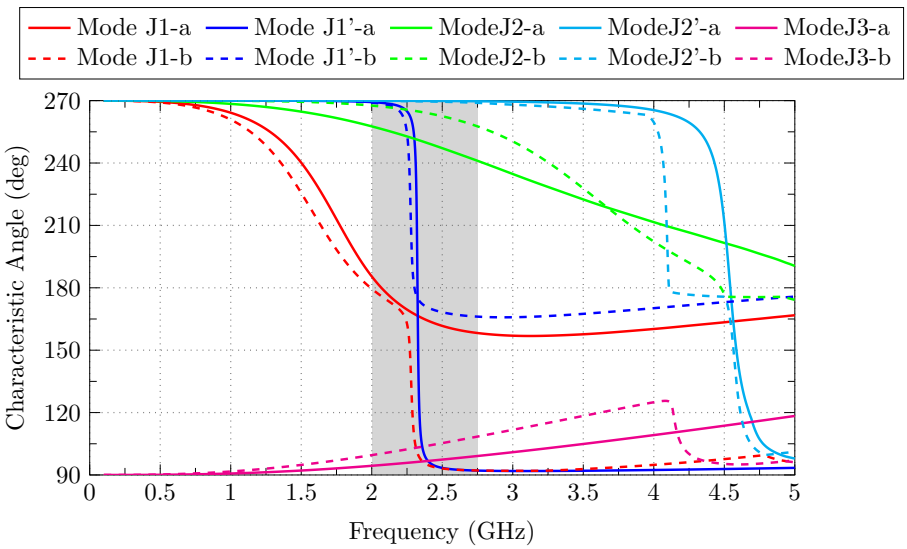

Figure 5.2: Characteristic angle associated to the first five modes of the structure shown in Figure 5.1. Mode-a case 1: parallel plates with the same dimensions, Mode-b case 2: parallel plates with different size.

Let us now analyse these two parallel plates applying the CMA. Figure 5.2

presents the characteristic angle (α_n) analysis carried out over the 0-5 GHz frequency range, for the plates with the same and with different dimensions. As seen in Figure 5.2, the observation of the curves at α_n = 180° shows that, for both cases, there are two main resonant modes at the 2.5 GHz band: Antenna mode $J1$ (where current flows in the same direction in both plates) and transmission line mode $J1'$ (where current flows in opposite direction in both plates), as depicted in Figure 5.3, where the current distribution associated to the first five modes of the structure is shown.

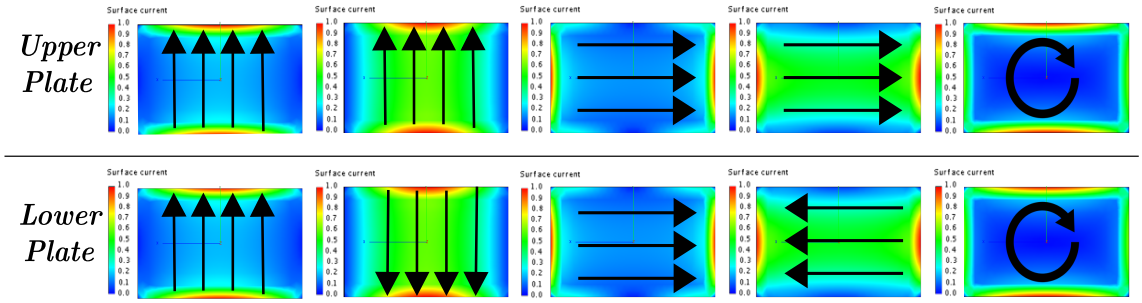

Figure 5.3: Current distribution associated to the first five modes of the structure shown in Figure 5.1, at the resonance frequency of each mode. Black arrows have been added to show easier the current flow.

Figure 5.4 shows the radiation pattern associated to different modes and to the structure, when it is excited. At resonance frequency, antenna mode $J1$ and transmission line mode $J1'$ are presenting two different radiation patterns, as shown in Figure 5.4(a). However, by exciting the structure using a probe from the lower plate to the upper plate, a different combination of these two fundamental modes can be obtained by means of slightly expanding the dimensions of one plate. As shown in Figure 5.4(b) and Figure 5.4(c), it can be observed that the resulting radiation pattern when exciting the structure with a probe feed gets varied from a bidirectional beam to a directional pattern, when slightly increasing the size of the lower plate.

The different modal contribution to the total radiated power in the two cases can be observed in Figure 5.5 and Figure 5.6. As seen in Figure 5.5, mode $J1'$

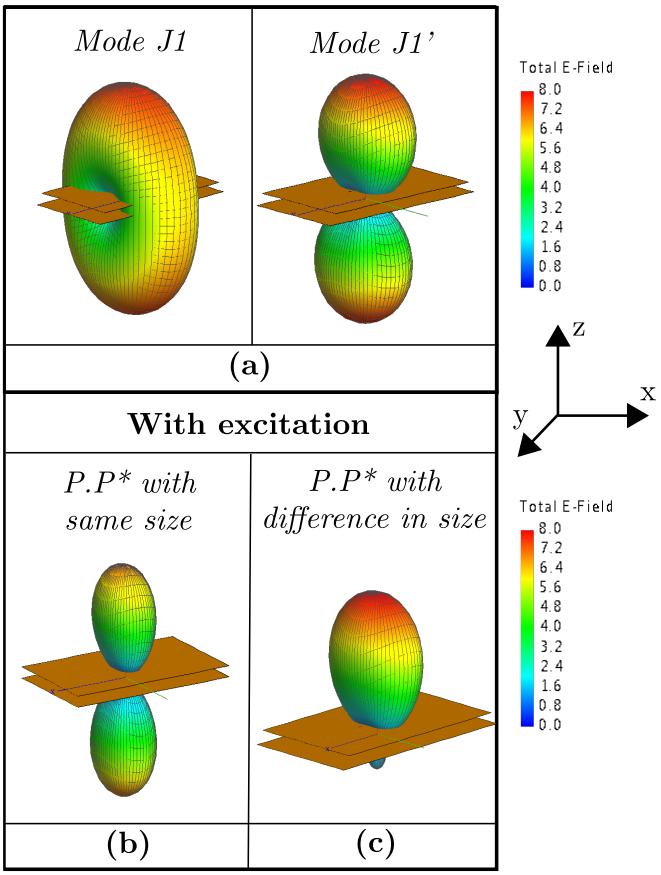

Figure 5.4: Radiation pattern associated to: (a) Fundamental modes $J1$ and $J1'$; (b) Parallel plates (P.P*) with the same size; (c) Parallel plates (P.P*) with different size.

(narrow band transmission line mode) dominates the total radiation power at 2.5 GHz frequency band and leads to the bidirectional radiation pattern shown in Figure 5.4(b). Conversely, in Figure 5.6, when the dimensions of the parallel plates are slightly different, the total radiated power results in a combination of mode $J1$ (antenna mode) and $J1'$ (transmission line mode) and, therefore, the combination of these two modes under excitation produces a directional pattern, as shown in Figure 5.4(c).

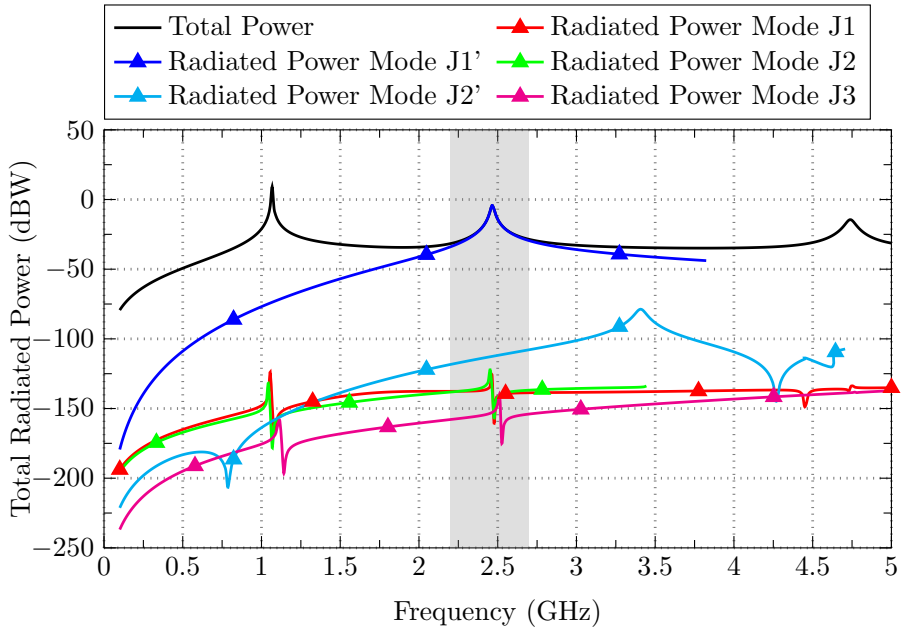

Figure 5.5: Total power and modal radiated power for two parallel plates with the same size.

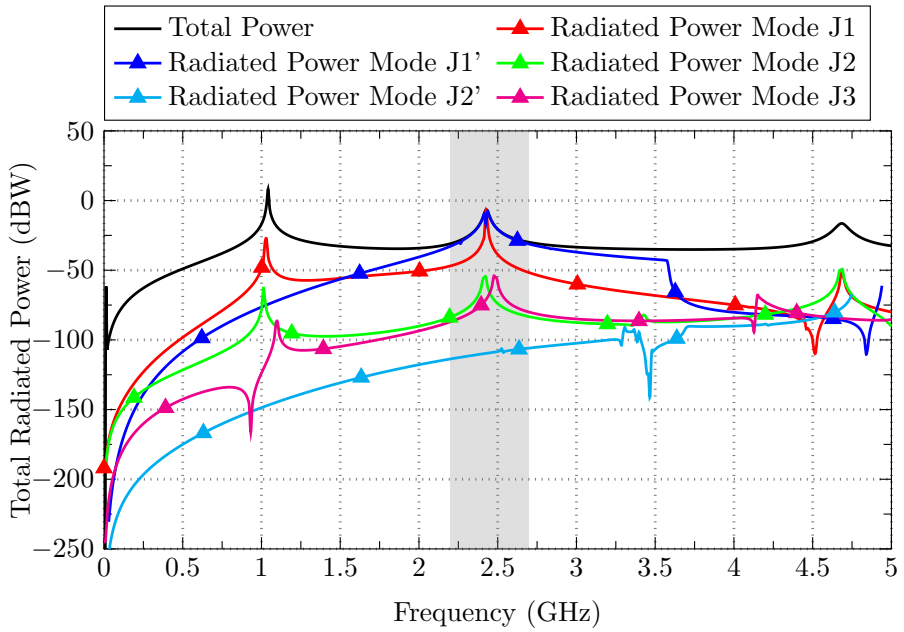

Figure 5.6: Total power and modal radiated power for two parallel plates with different size.

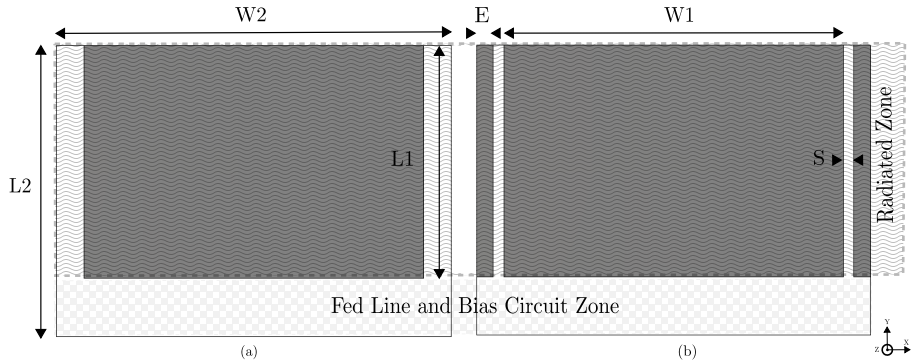

Figure 5.7: (a) Antenna top view, (b) Antenna back view.

5.3 Results and discussion

5.3.1 Reconfigurable antenna description

The proposed radiation pattern reconfigurable antenna is presented in Figure 5.7 and consists of a rectangular patch antenna printed on a Neltec substrate with a thickness H =1.524 mm, ε_r = 2.2 and tangent loss $tan\ \delta$ =0.0009. The dimensions of the structure are $W1$= 41mm, $W2$= 47.6 mm, $L1$= 28 mm, $L2$= 35 mm, S= 1.3 mm and E= 2 mm.

The idea is to implement an antenna consisting in two parallel plates, where the length of the lower plate is variable. Therefore, two PIN diodes ($D1$ and $D2$) are connecting the bottom plate to the lateral edges, as shown in Figure 5.8(c). The two PIN diodes states, labeled as ON and OFF, enable or disable the current to flow through the lateral edges. Hence, and as shown in the modal analysis, the radiation pattern can get varied.

Nevertheless, by switching the PIN diodes from ON to OFF state, it is noted a shift in the operating frequency, due to a change in the input impedance of the antenna at the excitation point. To settle this issue, a SPDT switch is added on the top plate. The aim of using a SPDT switch is to guarantee a common frequency operating band on the ON to OFF states, by switching the RF input signal to the adequate position related to the PIN diodes state, as show in Figure 5.8(a) and (b).

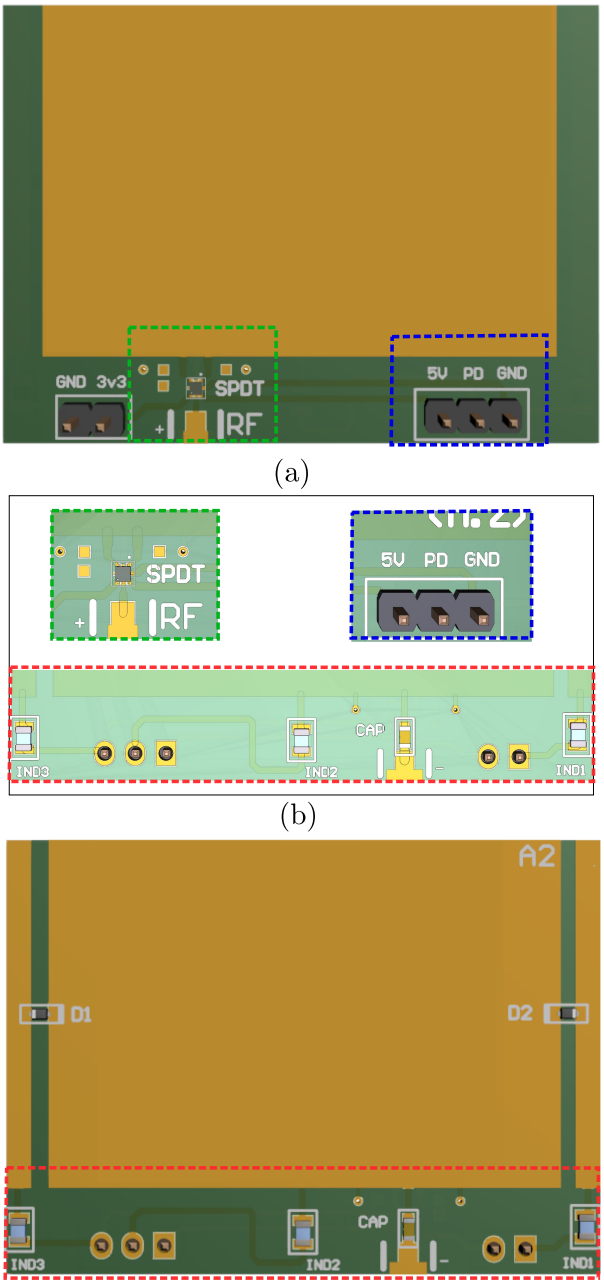

Figure 5.8: (a) Antenna top view; (b) Biasing circuit; (c) Antenna back view.

Table 5.1: Electronic components used in the proposed reconfigurable antenna.

Symbol	Value	Unit	Manufacturer	Comment
D1	BAR64-02V	-	Infineon	PIN Diode
D2	BAR64-02V	-	Infineon	PIN Diode
SPDT	SKY13585-679LF	-	Skyworks	Switch
CAP	12	pF	Murata MLCC	DC Block
IND1	68	nH	Murata LQW	DC Return
IND2	68	nH	Murata LQW	RF Choke
IND	68	nH	Murata LQW	DC Return

5.3.2 Bias circuit configuration

Figure 5.9 shows the equivalent circuit of the PIN diode for forward and reverse biasing. The PIN diode model considered for the design is the Infineon BAR64-02V silicon PIN diode, with low insertion loss and fast switching time [76]. As shown in Figure 5.9, the equivalent circuit consists of an inductor and a parallel capacitor resistor. To obtain the first configuration (PIN diodes are reverse biased), the values of the elements are L = 0,6 nH, C = 0,35 pF and R = 3,3 kΩ. In the other hand, the elements values of the second configuration (PIN diodes are forward biased) are L = 0,6 nH and R =1,35 Ω.

The SPDT switch (Figure 5.10) model adopted in the design is SKY13585-679LF [61], with a low insertion loss (0.5 dB typically at 2.45 GHz) for mode switching at ISM band. A remarkable advantage about using this model is that it has integrated DC blocking capacitors, so no external DC blocking capacitors are required.

As illustrated in Figure 5.8(b), to perform the DC bias supply to the PIN diodes $D1$ and $D2$, additional components are fitted in the feed line and bias circuit zone (see also Figure 5.7). A DC block capacitor CAP of 12 pF is used in order to preserve the continuity of the RF current throughout the metal structure. The inductors $IND1$ and $IND3$ of 68 nH provide the DC return path for the bias current. The DC voltage is isolated from the RF signal using a RF choke inductor $IND2$ of 68 nH. Table 5.1 summarizes the models and values used for

the different components in the proposed design.

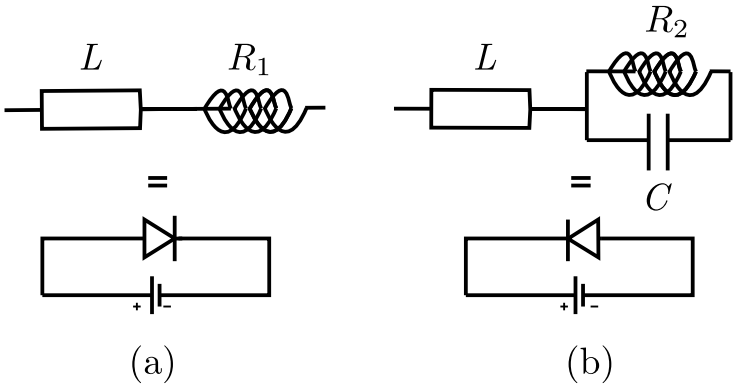

Figure 5.9: Equivalent circuit of the PIN diodes [76]: (a) Forward bias, (b) Reverse bias.

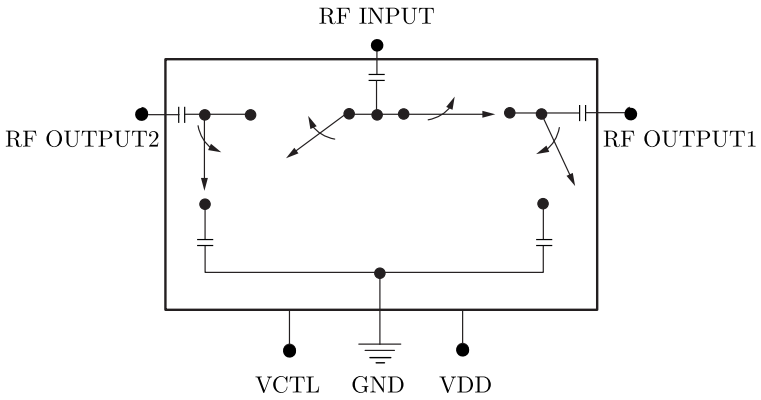

Figure 5.10: SPDT switch block diagram.

To meet the switches biasing requirements, Figure 5.11 illustrates the platform based on an nano-controller [77] with an input supply voltage V_{in} between 7V and 12V. A battery of 9V is employed to fed the whole system. In the following, it describes the setup of the two configurations:

- Configuration 1 (PIN Diode OFF)

Table 5.2: Reconfigurable antenna configuration: Case 1 (bidirectional pattern) and case 2 (unidirectional pattern).

Case	Mode(s) excited	PIN Diodes	SPDT
1	J_1'	OFF	VDD = 5 V, VCTL = 0 V
2	$J_1' + J_1$	ON	VDD = 5 V, VCTL = 3.3 V

  - PD (white) PIN Diodes connected to the Arduino 5V output intervening by a resistance of (25 ohms), to achieve $I_{F-Total}$ 200 mA (2 PIN diodes are in parallel)
  - 5v (Red) SPDT VDD connected to the Arduino 5V output
  - 3v3 (Green) SPDT $VCTL$ connected to the Arduino 3.3V output
  - GND (black and blue) Ground connected to the Arduino GND

- Configuration 2 (PIN Diode ON)
  - PD (white) PIN Diodes disconnected from the Arduino 5V output
  - 5v (Red) SPDT VDD connected to the Arduino 5V output
  - 3v3 (Red) SPDT $VCTL$ disconnected from the Arduino 3.3V output
  - GND (black and blue) Ground connected to the Arduino GND output

Table 5.2 shows the two configurations. To attain the first case, which consists of a bidirectional radiation pattern, the PIN diodes $D1$ and $D2$ were reverse biased and the SPDT $INPUT$ pin (see SPDT block diagram in Figure 5.10) is connected to the RF $OUTPUT1$ by giving to VDD and $VCLT$ a supply voltage of 5 V and 0 V, respectively. The second case corresponds to a directional radiation pattern achieved by forward biasing the PIN diodes $D1$ and $D2$, the SPDT $INPUT$ pin is connected to the RF $OUTPUT2$ by giving to VDD and $VCLT$ a supply voltage of 5 V and 3.3 V, respectively.

5.3.3 Prototype and measurement results

The proposed radiation pattern reconfigurable antenna is fabricated and assembled with the electronic components as presented in Figure 5.12. In this proto-

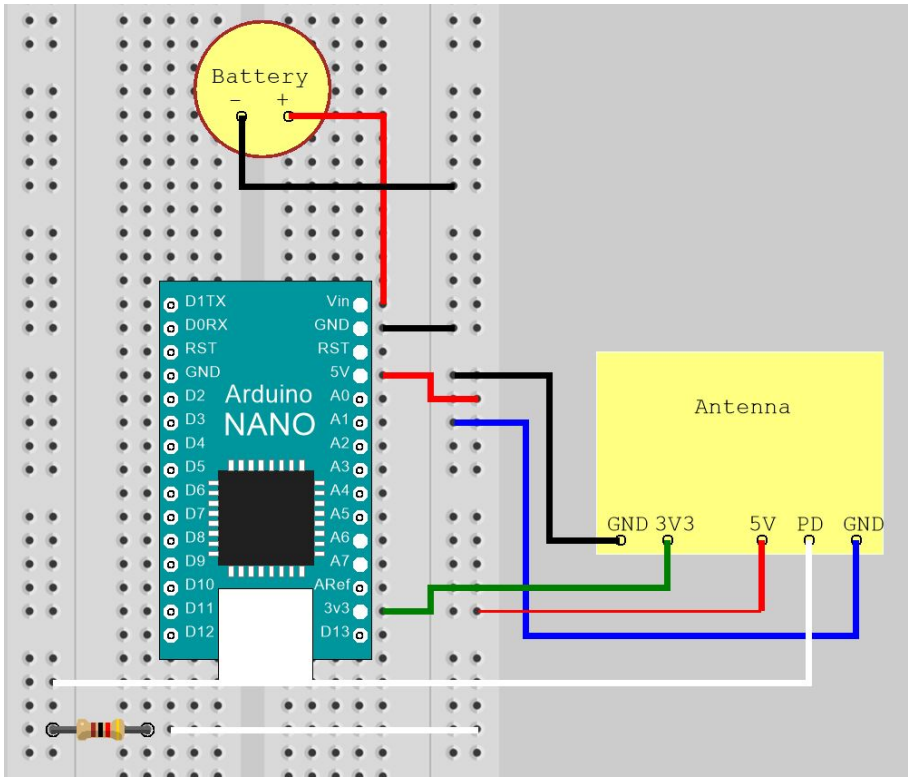

Figure 5.11: Draw of the antenna platform based on a nano-arduino and a battery.

type, connection wires are arranged in an appropriate manner to minimize the perturbation on the radiation. Figure 5.13 shows the simulated versus measured S_{11} parameter of the proposed radiation pattern reconfigurable antenna for both cases. From this Figure 5.13, it is observed that simulation and measurement perfectly agree on a common band at 2.5 GHz. It can be noted that simulated S_{11} parameter for case 2 shows a wide bandwidth. This is due to the fact that simulation files include ideal values for the lumped elements used for forward biasing the PIN diodes. The relative measured bandwidth at -10 dB for case 1 and case 2 are respectively 60 MHz and 25 MHz. However, measurement results meet the requirements, and a common operation frequency is achieved without changing physically the antenna structure.

2D radiation pattern measurements of the reconfigurable antenna at 2.45 GHz frequency band are plotted for both XZ and YZ planes in Figure 5.15. As presented by the CMA in the first section, a reconfigurable radiation pattern is

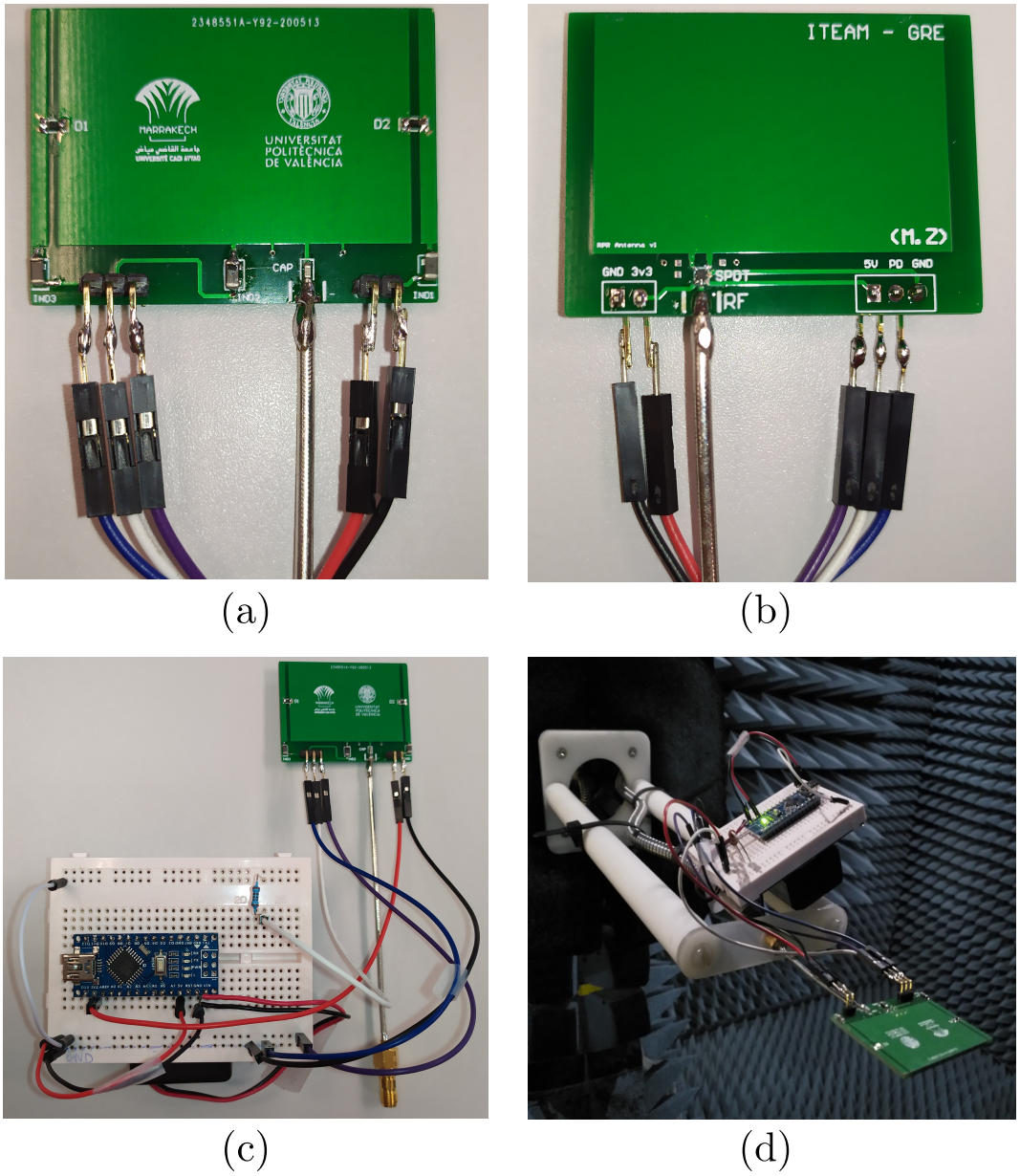

Figure 5.12: Final antenna prototype: (a) Top View, (b) Bottom View and (c) Antenna with bias platform (d) Antenna in anechoic chamber.

achieved. Turning the PIN diodes to ON state and SPDT to $OUTPUT2$ leads to a directional beam, and switching the PIN diodes to OFF state and SPDT to $OUTPUT1$ produces a bidirectional pattern. The maximum peak gain and

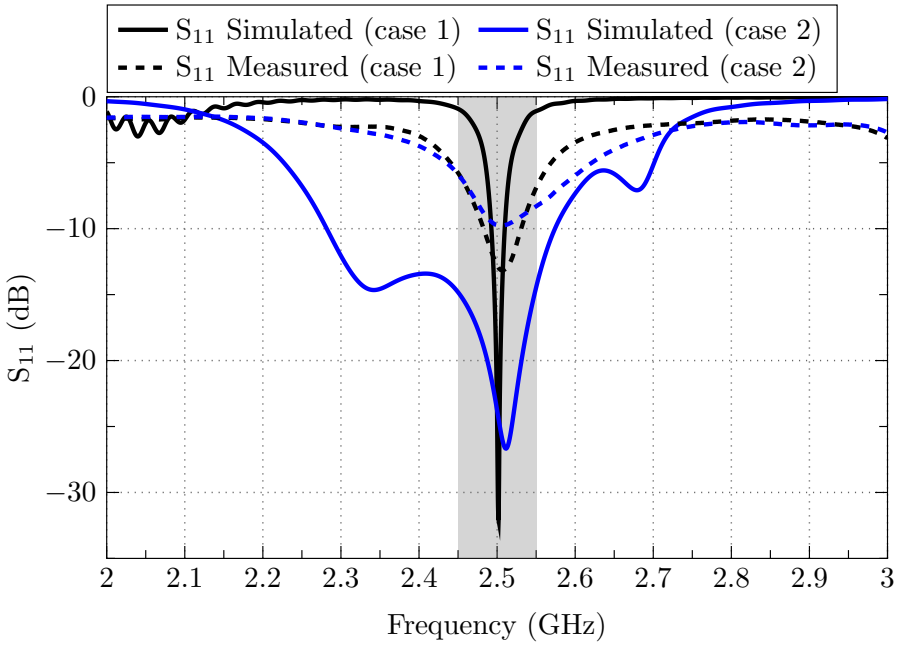

Figure 5.13: Simulated and measured S_{11} parameter for the ON/OFF cases presented in Table 5.2 .

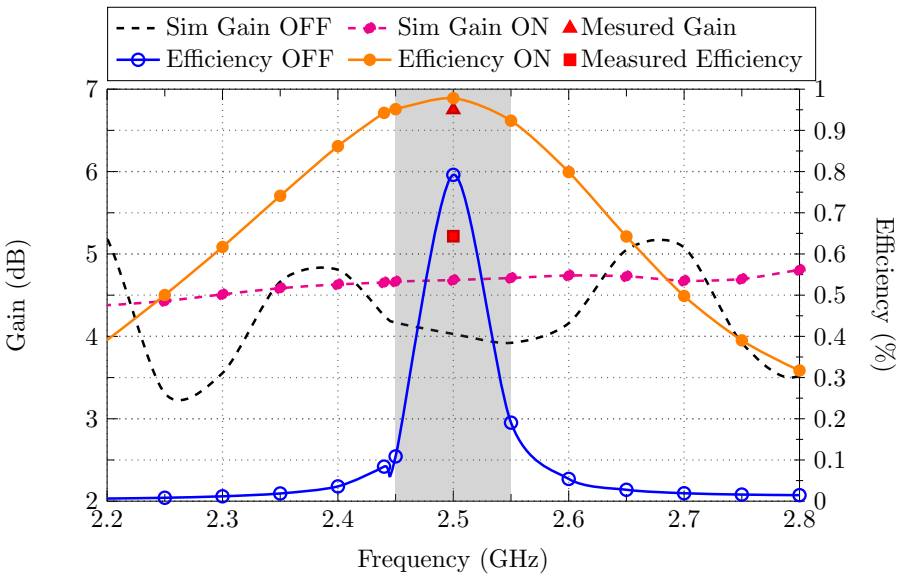

Figure 5.14: Antenna gain and efficiency.

the maximum radiation efficiency for both states have been measured as shown in 5.14 , reaching values up to 6.75 dBi and 64.31% at 2.5 GHz, respectively.

It should be noted that the efficiency is slightly low due to the diodes, SPDT switch and particularly the nano controller platform that was incorporated in the measurement environment.

The performance of the proposed design is compared in Table 5.3 with some recently published designs featuring radiation pattern reconfigurable antenna performances. It is clear that the proposed antenna has fewer PIN diodes, which it means less energy consumption and a low cost configuration. Moreover, it has the smallest size except reference [78]. In comparison with the antenna having the same beam number [79, 78], the proposed antenna has different beams at the same resonant frequency which gives it a toughness in term of adaptation to the environment. Furthermore, the fabrication of our design is robust and the complexity is modest by comparison to the selected references.

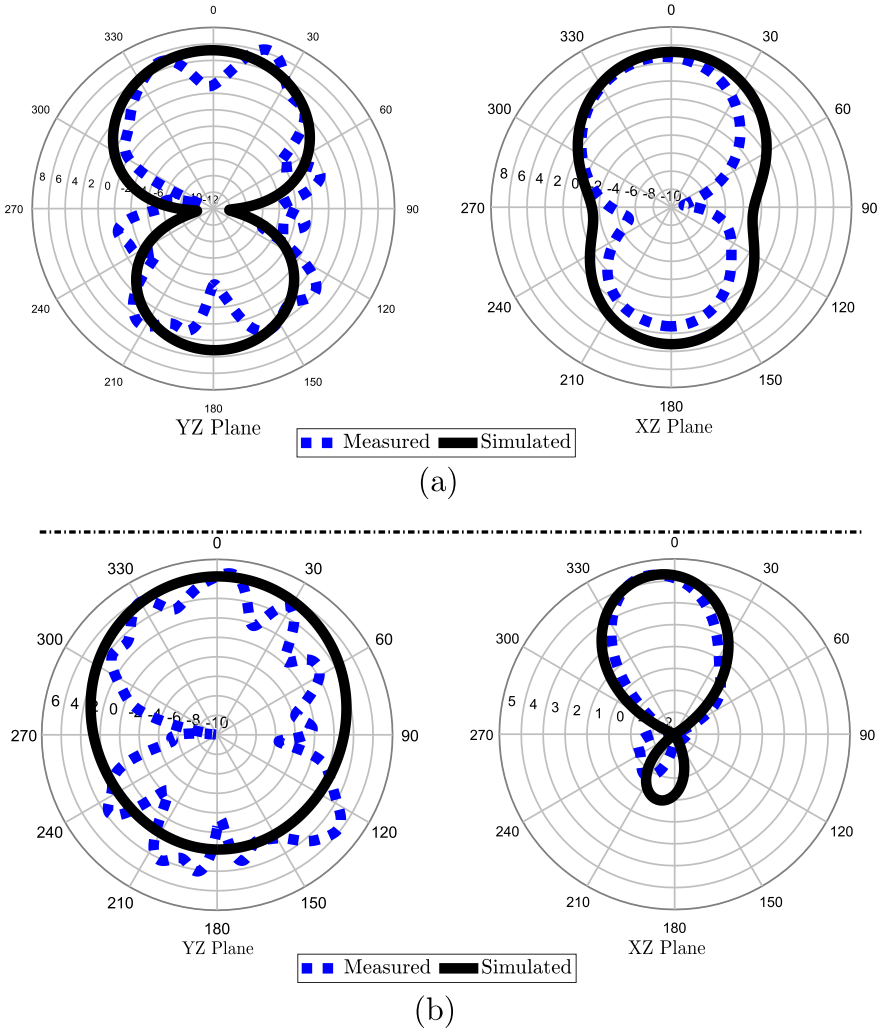

Figure 5.15: Simulated versus measured radiation patterns at 2.45 GHz: (a) case 1 (b) case 2 (see Table 5.2).

Table 5.3: Comparison of the proposed structure.

Ref.	**Beams type**	**Frequency (GHz)**	**Beams Number**	**PIN diodes**	**Size** (mm^3)
[79]	Broadside and Conical	2.25-2.85	3	2	170×170×17
[78]	Omnidirectional	3.4-3.8	3	4	40×30×1.6
[80]	Sum and Difference	3.3-5.5	2	4	144×190×0.8
[81]	Conical and Broadside	1.65-3.65	2	6	140×140×6
This work	Broadside and Bidirectional	2.28-2.58	3	2	47.6×35×1.524

5.4 Conclusion

The CM theory is able to provide a physical interpretation of the radiating behavior of an antenna. A radiation pattern reconfigurable antenna has been proposed in this paper, based on the information provided by the CMA. The design of the antenna started from the modal analysis, in which the first case of two parallel plates with the same size shows a domination of mode $J1'$ and therefore a bidirectional pattern when the structure is excited. The second case, with a small difference in size in one plate, presents a unidirectional pattern, which arise from the contribution of two modes $J1$ and $J1'$. After the analysis, a reconfigurable antenna with the same structure has been proposed with the aim of changing the radiation pattern, and two different patterns are achieved by switching ON/OFF the state of the PIN diodes. By means of introducing a SPDT switch, the operating frequency at both states is adjusted to 2.45 GHz. The bias voltage used is low, which is a significant interest for IoT sensors and mobile stations.

Chapter 6

Conclusions

6.1 Conclusions

The main purpose of this dissertation was to design reconfigurable antennas starting from the characteristic modes analysis. The proposed approach using CMA has been fully demonstrated, providing a number of antenna designs that wrap various applications. Characteristic mode analysis offers a powerful way to understand the physics behind multiple antenna features, such as the operating frequency and bandwidth, the radiation pattern shape and direction, and even the polarization, this physical understanding provides insight into how modes work and helps in the practical antenna design process.

As commented in Chapter 2, several parameters are used in CMA which are determined by the eigenvalues such as the Characteristic Angle and the Modal Weighting Coefficient. The three basic processes of design of a reconfigurable antenna based on a CMA are presented in a workflow, the first process consists of understanding the structure, achieving the desired modal behavior and design parameters verification. Later, it comes the fabrication and measurement that are presenting the second and third processes respectively.

The objective of Chapter 3 was to describe the different switching techniques (varactor diodes, PIN diodes, SPDT switches) to achieve a tuning requirement on an antenna. The electronic components was modeled and took into account

in simulation. The result of enabling the current flow to reach different path on the structure surface, is to obtain a reconfigurable antenna, hence, the PIN diode/SPDT switch will be a good candidate. In other hand, the reverse bias of the varactor diode alter the capacitance which is inversely relative with the square root of the operated voltage. at this stage, the varactor can be employed as reconfiguration factor to obtain a selective frequency.

Based on the Characteristic Mode Analysis, the ability to tune a particular mode keeping the rest of modes unaltered has been demonstrated in Chapter 4. According to this clarification on modes, the variation of the slot lengths was replaced with a varactor diode. Thus, as the reverse bias voltage increases, the capacitance decreases and the lower operating band is shifted to upper frequencies. As a result, a frequency reconfigurable antenna with a selective 2 GHz band for the reconfigurable mode, and a solid band at 5 GHz for the steady modes.

Moreover, in Chapter 5, two rectangular metallic plates are analysed. As a consequence of mode combination, the obtain of bidirectional and unidirectional radiation pattern was attained. S reconfigurable antenna with the same structure has been proposed with the aim of changing the radiation pattern, and two different patterns are achieved by switching ON/OFF the state of the PIN diodes. By introducing an SPDT switch, the operating frequency in both states is set to 2.45 GHz. The antenna and the switching network are printed as PCB laminated sandwich structure, the aim is to clean the field for a better radiation result. To meet the switches biasing requirements, a platform based on an nano-controller to control the biasing circuit network was proposed and a battery is employed to fed the whole system.

In the future works, the measurement of Intermodulation Distortion (IMD) will be introduced. In a RF system when two or more signals are used, The spectrum will consist of the original signals and the sum and difference of the input signals along with their harmonics. The 2^{nd} order intermodulation products and the original signals will be mixed together, resulting in 3^{rd} order intermodulation products. The best manner to avoid IMD products is to run the device in

the linear region before it initiates distortions. Those 3^{rd} order intermodulation products are very concerning, because it's hard to get rid of them.

Lastly, it can be concluded that the modal analysis techniques are good resources to understand the behaviour behind an antenna structure, they afford a precise physical understanding of the phenomena occurring in the antenna. Based on this insights, prototypes of reconfigurable antennas have been provided and measured, giving in all situations satisfactory results. This demonstrates that the design process using the characteristic modes analysis is appropriate for producing a reconfigurable antenna design with the requisite performance.

References

[1] Chang Jiang You, Shu Han Liu, Jin Xi Zhang, Xi Wang, Qin Yu Li, Guang Qiang Yin, et al. "Frequency- and Pattern Reconfigurable Antenna Array With Broadband Tuning and Wide Scanning Angles". In: *IEEE Transactions on Antennas and Propagation* 71.6 (2023), pp. 5398–5403. DOI: 10.1109/TAP.2023.3255647.

[2] Lyuwei Chen, Yi Huang, Hanyang Wang, Hai Zhou, and Kexin Liu. "A Reconfigurable Metal Rim Antenna With Smallest Clearance for Smartphone Applications". In: *IEEE Access* 10 (2022), pp. 112250–112260. DOI: 10.1109/ACCESS.2022.3216237.

[3] J.-M Laheurte. "Compact Antennas for Wireless Communications and Terminals: Theory and Design". In: *Compact Antennas for Wireless Communications and Terminals: Theory and Design* (Jan. 2013). DOI: 10.1002/9781118603437.

[4] H. M Al-tamimi and S Mahdi. "A Study of Reconfigurable Multiband Antenna for Wireless Application". In: *International Journal of New Technology and Research* 5.5 (2006), pp. 125–134.

[5] Zhan Zhang, Shengli Cao, and Junhong Wang. "Azimuth-Pattern Reconfigurable Planar Antenna Design Using Characteristic Mode Analysis". In: *IEEE Access* 9 (2021), pp. 60043–60051. DOI: 10.1109/ACCESS.2021.3073706.

[6] Shing-Lung Steven Yang, Ahmed A. Kishk, and Kai-Fong Lee. "Frequency Reconfigurable U-Slot Microstrip Patch Antenna". In: *IEEE Antennas and Wireless Propagation Letters* 7 (2008), pp. 127–129. DOI: 10.1109/LAWP.2008.921330.

[7] N. Behdad and K. Sarabandi. "A varactor-tuned dual-band slot antenna". In: *IEEE Transactions on Antennas and Propagation* 54.2 (2006), pp. 401–408. DOI: 10.1109/TAP.2005.863373.

[8] A. Constantine Balanis. *Antenna theory: Analysis and design*. 3rd ed. Hoboken, New Jersey.: John Wiley & Sons, Inc., 2005. ISBN: 0-471-66782-X.

[9] K Fujimoto and J. R James. *Mobile Antenna Systems Handbook*. 3rd ed. Norwood, MA: Artech House, 2008. ISBN: 978-1-59693-126-8.

[10] D. G Fang. *Antenna Theory and Microstrip Antennas*. Boca Raton, FL: Taylor and Francis Group, 2010. ISBN: 978-1-4398-0727-9.

[11] X.-S. Yang, B.-Z. Wang, and H.-L. Liu. "Reconfigurable Yagi Patch Array by Utilizing Odd-even-Mode Method". In: *Journal of Electromagnetic Waves and Applications* 20.13 (2006), pp. 1725–1738.

[12] Shengli Cao, Zhan Zhang, Xiaona Fu, and Junhong Wang. "Pattern Reconfigurable Bidirectional Antenna Design Using the Characteristic Mode Analysis". In: *IEEE Antennas and Wireless Propagation Letters* 20.1 (2021), pp. 53–57. DOI: 10.1109/LAWP.2020.3039506.

[13] Guiping Jin, Miaolan Li, Dan Liu, and Guangjie Zeng. "A Simple Planar Pattern-Reconfigurable Antenna Based on Arc Dipoles". In: *IEEE Antennas and Wireless Propagation Letters* 17.9 (2018), pp. 1664–1668. DOI: 10.1109/LAWP.2018.2862624.

[14] Yifeng Qin, Long Zhang, Chun-Xu Mao, and Hongyi Zhu. "Low-profile Compact Tri-band Multimode Reconfigurable Antenna Using Characteristic Mode Analysis". In: *IEEE Transactions on Antennas and Propagation* (2023), pp. 1–1. DOI: 10.1109/TAP.2023.3266055.

[15] C Rick. "The nuts and bolts of tuning varactors". In: *High Frequency Electronics* (2009), pp. 44–51.

[16] Chenguang Guo, Zhan Zhang, Xiaona Fu, and Junhong Wang. "A Frequency Reconfigurable Antenna With Filtering Characteristics Using Characteristic Mode Analysis". In: *IEEE Antennas and Wireless Propagation Letters* (2023), pp. 1–5. DOI: 10.1109/LAWP.2023.3264666.

[17] Wentao Li, Yi Ming Wang, Yongqiang Hei, Bo Li, and Xiaowei Shi. "A Compact Low-Profile Reconfigurable Metasurface Antenna With Polarization and Pattern Diversities". In: *IEEE Antennas and Wireless Propagation Letters* 20.7 (2021), pp. 1170–1174. DOI: 10.1109/LAWP.2021.3074639.

[18] Xiongwen Zhao and Sharjeel Riaz. "A Dual-Band Frequency Reconfigurable MIMO Patch-Slot Antenna Based on Reconfigurable Microstrip Feedline". In: *IEEE Access* 6 (2018), pp. 41450–41457. DOI: 10.1109/ACCESS.2018.2858442.

[19] A Bhattacharjee, S Dwari, and M Mandal. "Polarization-Reconfigurable Compact Monopole". In: 18.5 (2019), pp. 1041–1045.

[20] Krishna Kumar Kishor and Sean Victor Hum. "A Pattern Reconfigurable Chassis-Mode MIMO Antenna". In: *IEEE Transactions on Antennas and Propagation* 62.6 (2014), pp. 3290–3298. DOI: 10.1109/TAP.2014.2313634.

[21] Francesco Alessio Dicandia, Simone Genovesi, and Agostino Monorchio. "Null-Steering Antenna Design Using Phase-Shifted Characteristic Modes". In: *IEEE Transactions on Antennas and Propagation* 64.7 (2016), pp. 2698–2706. DOI: 10.1109/TAP.2016.2556700.

[22] Francesco Alessio Dicandia, Simone Genovesi, and Agostino Monorchio. "Advantageous Exploitation of Characteristic Modes Analysis for the Design of 3-D Null-Scanning Antennas". In: *IEEE Transactions on Antennas and Propagation* 65.8 (2017), pp. 3924–3934. DOI: 10.1109/TAP.2017.2716402.

[23] Francesco Dicandia, Simone Genovesi, and Agostino Monorchio. "Efficient Excitation of Characteristic Modes for Radiation Pattern Control by Using a Novel Balanced Inductive Coupling Element". In: *IEEE Transactions on Antennas and Propagation* PP (Jan. 2018), pp. 1–1. DOI: 10.1109/TAP.2018.2790046.

[24] Ke Li and Yan Shi. "A Pattern Reconfigurable MIMO Antenna Design Using Characteristic Modes". In: *IEEE Access* 6 (2018), pp. 43526–43534. DOI: 10.1109/ACCESS.2018.2863250.

[25] Ke Li and Yan Shi. "A Pattern Reconfigurable MIMO Antenna Design Using Characteristic Modes". In: *IEEE Access* 6 (2018), pp. 43526–43534. DOI: 10.1109/ACCESS.2018.2863250.

[26] J. Robert Garbacz. "A Generalized Expansion for Radiated and Scattered Fields". PhD thesis. Ohio State University, 1968.

[27] J. Robert Garbacz and H. Richard Turpin. "A Generalized Expansion for Radiated and Scattered Fields". In: *IEEE Transactions on Antennas and Propagation* AP-19.3 (1971), pp. 348–358. ISSN: 15582221. DOI: 10.1109/TAP.1971.1139935.

[28] F. Roger Harrington and J. R Mautz. "Theory of Characteristic Modes for Conducting Bodies". In: *IEEE Transactions on Antennas and Propagation* AP-19.5 (1971), pp. 622–628.

[29] E. Antonino-Daviu, M. Cabedo-Fabrés, M. Sonkki, N. Mohamed Mohamed-Hicho, and M. Ferrando-Bataller. "Design Guidelines for the Excitation of Characteristic Modes in Slotted Planar Structures". In: *IEEE Transactions on Antennas and Propagation* 64.12 (2016), pp. 5020–5029.

[30] Marta Cabedo-Fabres, Eva Antonino-Daviu, Alejandro Valero-Nogueira, and Miguel Ferando Bataller. "The theory of characteristic modes revisited: A contribution to the design of antennas for modern applications". In: *IEEE Antennas and Propagation Magazine* 49.5 (2007), pp. 52–68. ISSN: 10459243. DOI: 10.1109/MAP.2007.4395295.

[31] K.R. Boyle and P.J. Massey. "Nine-band antenna system for mobile phones". In: *Electronics Letters* 42 (Apr. 2006), pp. 265–266. DOI: 10.1049/el:20060061.

[32] Aliou Diallo, Cyril Luxey, Philippe Le Thuc, Robert Staraj, and Georges Kossiavas. "Study and reduction of the mutual coupling between two mobile phone PIFAs operating in the DCS1800 and UMTS Bands". In: *Antennas and Propagation, IEEE Transactions on* 54 (Dec. 2006), pp. 3063–3074. DOI: 10.1109/TAP.2006.883981.

[33] J. Len Chu. "Physical limitations of omnidirectional antennas". In: *J. Appl. Phys* 12.12 (1948), pp. 1163–1175.

[34] F. Roger Harrington. "Effect of antenna size on gain, bandwidth, and efficiency". In: *Journal of Research of the National Bureau of Standards, Section D: Radio Propagation* 64D.1 (1960), p. 1. ISSN: 1060-1783. DOI: 10.6028/jres.064d.003.

[35] Chen Yikai and Wang Chao-Fu. *Characteristic modes: Theory and applications in antenna engineering*. 1st ed. Hoboken, New Jersey.: John Wiley & Sons, Inc., 2015. ISBN: 978-1-119-03842-9.

[36] T. Yuen Lo, D. Solomon, and W. F Richards. "Theory and Experiment on Microstrip Antennas". In: *IEEE Transactions on Antennas and Propagation* 27.2 (1979), pp. 137–145. ISSN: 15582221.

[37] F. William Richards, Yuen T. Lo, and Daniel D. Harrison. "An Improved Theory for Microstrip Antennas and Applications". In: *IEEE Transactions on Antennas and Propagation* 29.1 (1981), pp. 38–46. ISSN: 15582221. DOI: 10.1109/TAP.1981.1142524.

[38] C CHANG and T ITOH. "Resonant characteristics of dielectric resonators for millimeter wave integrated circuits". In: *Arch. Elektron. ubertrag. techH* AEU-33 (1979), pp. 141–144.

[39] R. K Mongia. "Theoretical and experimental resonant frequencies of rectangular dielectric resonators". In: *IEE Proc.-H* 139.1 (1992), pp. 98–104.

[40] R. K Mongia and A Ittipiboon. "Theoretical and experimental investigations on rectangular dielectric resonator antennas". In: *IEEE Transactions on Antennas and Propagation* 45.9 (1997), pp. 348–1356.

[41] E. A.J. Marcatili. "Dielectric Rectangular Waveguide and Directional Coupler for Integrated Optics". In: *Bell System Technical Journal* 48.7 (1969), pp. 2071–2102. ISSN: 15387305. DOI: 10.1002/j.1538-7305.1969.tb01166.x.

[42] K. Wa Leung, E. Hock Lim, and X. Sheng Fang. "Dielectric resonator antennas: From the basic to the aesthetic". In: *Proceedings of the IEEE* 100.7 (2012), pp. 2181–2193. ISSN: 00189219. DOI: 10.1109/JPROC.2012.2187872.

[43] R. F. Harrington. *Time-Harmonic Electromagnetic Fields*. John Wiley & Sons, 2001.

[44] *CST Studio Suite Software*. Version 2020." Jan. 17, 2020. URL: https://www.3ds.com/es/productos-y-servicios/simulia/productos/cst-studio-suite/.

[45] *FEKO Softwaer*. Version 2018.2-338937. Oct. 25, 2018. URL: https://altairhyperworks.com/product/FEKO.

[46] M. Fabrés Cabedo. "Systematic Design of Antennas Using the Theory of Characteristic Modes". PhD thesis. Universidad Politecnica de Valencia, 2007.

[47] Brian. A Austin and Kevin. P Murray. "The application of characteristic-mode techniques to vehicle-mounted NVIS antennas". In: *IEEE Antennas and Propagation Magazine* 40.1 (1998), pp. 7–21. ISSN: 10459243. DOI: 10.1109/74.667319.

[48] E. H Newman. "The application of characteristic-mode techniques to vehicle-mounted NVIS antennas". In: *IEEE Transactions on Antennas and Propagation* AP-27.4 (1979), pp. 530–531.

[49] E. Antonino Daviu. "Analysis and design of antennas for wireless communications using modal methods". PhD thesis. Universidad Politecnica de Valencia, 2008.

[50] Dimitris E. Anagnostou, David Torres, Tarron S. Teeslink, and Nelson Sepulveda. "Vanadium Dioxide for Reconfigurable Antennas and Microwave Devices: Enabling RF Reconfigurability Through Smart Materials". In: *IEEE Antennas and Propagation Magazine* 62.3 (2020), pp. 58–73. DOI: 10.1109/MAP.2020.2964521.

[51] Jiaxiang Hao, Jian Ren, Xiaoyu Du, Jan Hvolgaard Mikkelsen, Ming Shen, and Ying Zeng Yin. "Pattern-Reconfigurable Yagi–Uda Antenna Based on Liquid Metal". In: *IEEE Antennas and Wireless Propagation Letters* 20.4 (2021), pp. 587–591. DOI: 10.1109/LAWP.2021.3058115.

[52] Zakaria Mahlaoui, Eva Antonino-Daviu, Miguel Ferrando-Bataller, Hamza Benchakroun, and Adnane Latif. "Frequency reconfigurable patch antenna with defected ground structure using varactor diodes". In: *2017 11th European Conference on Antennas and Propagation (EUCAP)*. 2017, pp. 2217–2220. DOI: 10.23919/EuCAP.2017.7928358.

[53] Zakaria Mahlaoui, Eva Antonino-Daviu, Adnane Latif, Miguel Ferrando-Bataller, and Carlos Ramiro Peñafiel-Ojeda. "Frequency Reconfigurable Patch Antenna Using Pin Diodes with Directive and Fixed Radiation Pattern". In: *2018 International Conference on Selected Topics in Mobile and Wireless Networking (MoWNeT)*. 2018, pp. 1–3. DOI: 10.1109/MoWNet.2018.8428914.

[54] H. Al-Tamimi and S. Mahdi. "A Study of Reconfigurable Multiband Antenna for Wireless Application". In: *International Journal of New Technology and Research* 2.5 (2016), pp. 125–134. ISSN: 2454-4116.

[55] Mohamed Nasrun Osman, Mohamad Kamal A Rahim, Peter Gardner, Mohamad Rijal Hamid, Mohd Fairus Mohd Yusoff, and Huda A Majid. "An electronically reconfigurable patch antenna design for polarization diversity with fixed resonant frequency". In: *radioengineering* 24.1 (2015), pp. 45–53.

[56] Zakaria Mahlaoui, Eva Antonino-Daviu, and Miguel Ferrando-Bataller. "Radiation Pattern Reconfigurable Antenna for IoT Devices". In: *International Journal of Antennas and Propagation* 2021 (Aug. 2021), pp. 1–13. DOI: 10.1155/2021/5534063.

[57] *Silicon PIN Diodes*. BAR50-02V. Infineon Technologies AG. July 2011. URL: http://www.infineon.com.

[58] *SMV123x Series: Hyperabrupt Junction Tuning Varactors*. SKY1232-079LF. Skyworks Solutions, Inc. Aug. 2015. URL: www.skyworksinc.com.

[59] Zakaria Mahlaoui, Eva Antonino-Daviu, Adnane Latif, and Miguel Ferrando-Bataller. "Radiation pattern reconfigurable antenna design using characteristic modes". In: *12th European Conference on Antennas and Propagation (EuCAP 2018)*. 2018, pp. 1–4. DOI: 10.1049/cp.2018.0462.

[60] *GaAs Constant Gamma Flip-Chip Varactor Diode, MA46H120 Series*. MA46H120 Series. Rev. V3. MA-COM Technology Solutions.

[61] *SKY13585-679LF: 1.0 to 6.0 GHz SPDT Switch*. SKY13585-679LF. Skyworks Solutions, Inc. May 2017. URL: www.skyworksinc.com.

[62] Babak Kazemi Esfeh, Martin Rack, Sergej Makovejev, Frederic Allibert, and Jean-Pierre Raskin. "A SPDT RF switch small-and large-signal characteristics on TR-HR SOI substrates". In: *IEEE Journal of the Electron Devices Society* 6 (2018), pp. 543–550.

[63] Zakaria Mahlaoui, Eva Antonino-Daviu, and Miguel Ferrando-Bataller. "Radiation Pattern Agile Antenna using PIN Diodes and SPDT Switches". In: *2020 IEEE International Symposium on Antennas and Propagation and North American Radio Science Meeting*. 2020, pp. 1771–1772. DOI: 10.1109/IEEECONF35879.2020.9329761.

[64] F. Zhu, S. Gao, A. T. Ho, R. A. Abd-Alhameed, C. H. See, T. W. C. Brown, et al. "Multiple Band-Notched UWB Antenna With Band-Rejected Elements Integrated in the Feed Line". In: *IEEE Transactions on Antennas and Propagation* 61.8 (2013), pp. 3952–3960. DOI: 10.1109/TAP.2013.2260119.

[65] Y. Cui, Zhang Panpan, and Ronglin Li. "Broadband quad-polarisation reconfigurable antenna". In: *Electronics Letters* 54 (2018), pp. 1199–1200.

[66] K. Boonying, C. Phongcharoenpanich, and S. Kosulvit. "Polarization reconfigurable suspended antenna using RF switches and P-I-N diodes". In: *The 4th Joint International Conference on Information and Communication Technology, Electronic and Electrical Engineering (JICTEE)* (2014), pp. 1–4.

[67] P. Qin, Y. Guo, and C. Ding. "A Dual-Band Polarization Reconfigurable Antenna for WLAN Systems". In: *IEEE Transactions on Antennas and Propagation* 61 (2013), pp. 5706–5713.

[68] Issa T. E. Elfergani, A. Hussaini, C. See, R. Abd-Alhameed, N. McEwan, S. Zhu, et al. "Printed monopole antenna with tunable band-notched characteristic for use in mobile and ultra-wide band applications". In: *International Journal of Rf and Microwave Computer-aided Engineering* 25 (2015), pp. 403–412.

[69] N. Nguyen-Trong, L. Hall, and C. Fumeaux. "A Frequency- and Pattern-Reconfigurable Center-Shorted Microstrip Antenna". In: *IEEE Antennas and Wireless Propagation Letters* 15 (2016), pp. 1955–1958.

[70] M. Wright, W. Baron, J. Miller, J. Tuss, D. Zeppettella, and M. Ali. "MEMS Reconfigurable Broadband Patch Antenna for Conformal Applications". In: *IEEE Transactions on Antennas and Propagation* 66 (2018), pp. 2770–2778.

[71] Q. Liu, Naizhi Wang, C. Wu, G. Wei, and A. Smolders. "Frequency Reconfigurable Antenna Controlled by Multi-Reed Switches". In: *IEEE Antennas and Wireless Propagation Letters* 14 (2015), pp. 927–930.

[72] R. Simorangkir, Y. Yang, R. Hashmi, T. Björninen, K. Esselle, and L. Ukkonen. "Polydimethylsiloxane-Embedded Conductive Fabric: Characterization and Application for Realization of Robust Passive and Active Flexible Wearable Antennas". In: *IEEE Access* 6 (2018), pp. 48102–48112.

[73] D. Guha, S. Biswas, and C. Kumar. "Printed Antenna Designs Using Defected Ground Structures : A Review of Fundamentals and State-ofthe-Art Developments". In: vol. 2. 2014, pp. 1–13.

[74] *SMV2025 series: surface mount, silicon hyperabrupt tuning varactor diodes*. SMV2025series. Skyworks Solutions, Inc. 2015. URL: www.skyworksinc.com.

[75] I. Rouissi, I. Ben Trad, J. Floc'h, H. Rmili, and H. Trabelsi. "Design of frequency reconfigurable triband antenna using capacitive loading for wireless communications". In: *2015 Loughborough Antennas Propagation Conference (LAPC)* (2015), pp. 1–5.

[76] *Low signal distortion, surface mount RF PIN diode*. BAR64-02V. Infineon Technologies AG. June 2018. URL: http://www.infineon.com.

[77] Arduino. *User Manual Arduino Nano (V2.3)*. June 26, 2008. 4 pp. URL: https://www.arduino.cc/en/uploads/Main/ArduinoNanoManual23.pdf. June 26, 2008.

[78] L. Han, Caixia Wang, Wenmei Zhang, R. Ma, and Q. Zeng. "Design of Frequency- and Pattern-Reconfigurable Wideband Slot Antenna". In: *International Journal of Antennas and Propagation* 2018 (2018), pp. 1–7.

[79] W. Lin, H. Wong, and R. W. Ziolkowski. "Wideband Pattern-Reconfigurable Antenna With Switchable Broadside and Conical Beams". In: *IEEE Antennas and Wireless Propagation Letters* 16 (2017), pp. 2638–2641. DOI: 10.1109/LAWP.2017.2738101.

[80] Seyed-Ali Malakooti and C. Fumeaux. "Pattern-Reconfigurable Antenna With Switchable Wideband to Frequency-Agile Bandpass/Bandstop Filtering Operation". In: *IEEE Access* 7 (2019), pp. 167065–167075.

[81] X. Yang, Huawei Lin, Hui Gu, L. Ge, and X. Zeng. "Broadband Pattern Diversity Patch Antenna With Switchable Feeding Network". In: *IEEE Access* 6 (2018), pp. 69612–69619.

[82] Zakaria Mahlaoui, Eva Antonino-Daviu, A. Latif, and Miguel Ferrando-Bataller. "Design of a Dual-Band Frequency Reconfigurable Patch Antenna Based on Characteristic Modes". In: *International Journal of Antennas and Propagation* 2019 (Mar. 2019), pp. 1–12. DOI: 10.1155/2019/4512532.

[83] Zakaria Mahlaoui, Eva Antonino-Daviu, A. Latif, and Miguel Ferrando-Bataller. "Radiation Pattern Reconfigurable Antenna Design Using Characteristic Modes". In: Jan. 2018, 103 (4 pp.)–103 (4 pp.) DOI: 10.1049/cp.2018.0462.

[84] Hamza Benchakroun, Marta Cabedo-Fabrés, Miguel Ferrando-Bataller, Zakaria Mahlaoui, and Adnane Latif. "New approach for the design of UWB monopoles with directive radiation for BAN applications". In: *12th European Conference on Antennas and Propagation (EuCAP 2018)*. 2018, pp. 1–5. DOI: 10.1049/cp.2018.0492.

6.7 Related publications

6.7.1 JCR indexed journals

- Zakaria Mahlaoui, Eva Antonino-Daviu, and Miguel Ferrando-Bataller. "Radiation Pattern Reconfigurable Antenna for IoT Devices". In: *International Journal of Antennas and Propagation* 2021 (Aug. 2021), pp. 1–13. DOI: 10.1155/2021/5534063.

- Zakaria Mahlaoui, Eva Antonino-Daviu, A. Latif, and Miguel Ferrando-Bataller. "Design of a Dual-Band Frequency Reconfigurable Patch Antenna Based on Characteristic Modes". In: *International Journal of Antennas and Propagation* 2019 (Mar. 2019), pp. 1–12. DOI: 10.1155/2019/4512532.

6.7.2 International conferences

- Zakaria Mahlaoui, Eva Antonino-Daviu, and Miguel Ferrando-Bataller. "Radiation Pattern Agile Antenna using PIN Diodes and SPDT Switches". In: *2020 IEEE International Symposium on Antennas and Propagation and North American Radio Science Meeting*. 2020, pp. 1771–1772. DOI: 10.1109/IEEECONF35879.2020.9329761.

- Zakaria Mahlaoui, Eva Antonino-Daviu, A. Latif, and Miguel Ferrando-Bataller. "Radiation Pattern Reconfigurable Antenna Design Using Characteristic Modes". In: Jan. 2018, 103 (4 pp.)–103 (4 pp.) DOI: 10.1049/cp.2018.0462.

- Zakaria Mahlaoui, Eva Antonino-Daviu, Adnane Latif, and Miguel Ferrando-Bataller. "Radiation pattern reconfigurable antenna design using characteristic modes". In: *12th European Conference on Antennas and Propagation (EuCAP 2018)*. 2018, pp. 1–4. DOI: 10.1049/cp.2018.0462.

- Zakaria Mahlaoui, Eva Antonino-Daviu, Adnane Latif, Miguel Ferrando-Bataller, and Carlos Ramiro Peñafiel-Ojeda. "Frequency Reconfigurable Patch Antenna Using Pin Diodes with Directive and Fixed Radiation Pattern". In: *2018 International Conference on Selected Topics in Mobile and Wireless Networking (MoWNeT)*. 2018, pp. 1–3. DOI: 10.1109/MoWNet.2018.8428914.

- Zakaria Mahlaoui, Eva Antonino-Daviu, Miguel Ferrando-Bataller, Hamza Benchakroun, and Adnane Latif. "Frequency reconfigurable patch antenna with defected ground structure using varactor diodes". In: *2017 11th European Conference on Antennas and Propagation (EUCAP)*. 2017, pp. 2217–2220. DOI: 10.23919/EuCAP.2017.7928358.

- Hamza Benchakroun, Marta Cabedo-Fabrés, Miguel Ferrando-Bataller, Zakaria Mahlaoui, and Adnane Latif. "New approach for the design of UWB monopoles with directive radiation for BAN applications". In: *12th European Conference on Antennas and Propagation (EuCAP 2018)*. 2018, pp. 1–5. DOI: 10.1049/cp.2018.0492.

Hindawi
International Journal of Antennas and Propagation
Volume 2021, Article ID 5534063, 13 pages
https://doi.org/10.1155/2021/5534063

Research Article

Radiation Pattern Reconfigurable Antenna for IoT Devices

Zakaria Mahlaoui,[1,2] **Eva Antonino-Daviu**,[1] **and Miguel Ferrando-Bataller**[1]

[1]*Instituto de Telecomunicaciones y Aplicaciones Multimedia, Universitat Politècnica de València, Valencia, Spain*
[2]*National School of Applied Sciences, Cadi Ayyad University, Marrakesh, Morocco*

Correspondence should be addressed to Eva Antonino-Daviu; evanda@upvnet.upv.es

Received 11 February 2021; Revised 1 July 2021; Accepted 7 August 2021; Published 18 August 2021

Academic Editor: Giorgio Montisci

Based on the characteristic mode theory, a versatile radiation pattern reconfigurable antenna is proposed. The analysis starts from two parallel metallic plates with the same and different dimensions. By means of two PIN diodes, the size of one of the parallel metallic plates can be modified and consequently the behavior of the radiation pattern can be switched between bidirectional and unidirectional radiation patterns. Moreover, a SPDT switch is used to adjust the frequency and match the input impedance. The reconfigurable antenna prototype has been assembled and tested, and a good agreement between simulated and measured results is obtained at 2.5 GHz band which fits the IoT applications.

1. Introduction

As a fundamental part of a wireless system and due to the strong demand of the market for diverse applications, antennas are sometimes required to change their basic characteristics with respect to the application needs. To fulfil this expectation, CM (characteristic mode) theory [1–3], which is a relatively new approach in the antenna field, presents an easy way to understand the physics behind several antenna features, such as the radiation pattern shape, beamwidth and direction, polarization, and bandwidth and operating frequency. This physical understanding provides information about how modes operate and helps in the practical antenna design process, making it easier [4, 5].

The huge growth of Internet of Things (IoT) and smart industrial applications builds up many engineering and scientific challenges that involve ingenious research efforts from both academic and industrial society for the development of cost-effective, scalable, efficient, and reliable antenna systems for IoT. This is why reconfigurable antennas (RAs) are conceived as a suitable system that can change its basic characteristics [6, 7] such as the operating frequency [8, 9], the radiation pattern [10, 11], or even the polarization [12, 13] to cope with the demand of several communication systems such as IoT sensors and mobile stations [14]. Reconfigurable antennas are classified into several types, depending on the use of semiconductors such as PIN diodes [15] and varactor diodes [11, 16], RF MEMS [17], photoconductive components [18], and reconfiguration by changing material properties [19] or by mechanical handling [20].

This paper describes a radiation pattern reconfigurable antenna based on the use of two rectangular parallel plates. The design is based on that presented in [21], but a significant improvement has been provided with the current design. Firstly, the geometry is proposed and a CM analysis (CMA) is performed in order to explain the behavior of the antenna from a modal perspective. Then, a reconfigurable radiating structure using PIN diodes and a SPDT switch [22] is proposed.

The goal of the proposed design is to switch between a bidirectional and unidirectional radiation pattern, depending on the state of the PIN diodes. The aim of using a SPDT switch is to reach a common operating frequency (2.5 GHz) at both states, avoiding the modification of the basic geometry. Hence, the proposed antenna proposes a convenient solution for several IoT applications, as it can produce different beam conditions in a sensor without changing physically the antenna structure.

CMA, antenna simulation, and design of the structure have been performed by means of *FEKO* [23] and *CST Microwave Studio* simulation software applications [24].

The paper starts with a brief overview of the CM theory and the physical interpretation of the modal parameters. Then, the general procedure for designing reconfigurable antennas using CMA is discussed, following the CMA of two rectangular parallel plates. In Section 5, a radiation pattern reconfigurable antenna is proposed, and a prototype and measurements are presented in the next section. Finally, conclusions are discussed.

2. Characteristic Mode Overview

The CM theory was initially developed by Garbacz in 1968 [1] and later refined by Harrington and Mautz in 1971 [3]. This theory has recently become a versatile modal analysis tool for antennas with arbitrary shapes and materials. The CMs together with their metric parameters provide the following effective information for antenna analysis and design:

(i) Resonant frequencies of the dominant mode and higher-order modes.

(ii) Modal radiation fields in the far-field range.

(iii) Modal currents on the surface of the analyzed structure.

(iv) Significance of the modes at a given frequency.

CMs are defined as a set of orthogonal radiating current modes that are supported by a conducting or dielectric surface. A weighted eigenvalue equation is derived from the method of moments (MoM) impedance matrix [3, 5, 25], and a set of orthogonal eigencurrents (i.e., CMs), together with their associated eigenvalues, is obtained. Due to the orthogonality of the eigencurrents, the total current on the surface of the conductor can be expanded into a set of modes. Eigenvalues provide information about the radiating behavior of the associated mode. Moreover, attributes such as the *characteristic angle* or *modal significance* can be calculated, which are associated to the eigenvalue.

In the following, a brief review of the parameters associated to the CMA will be provided, in order to obtain physical insight into the radiating behavior of an antenna with arbitrary shape.

2.1. Physical Interpretation of the Eigenvalue. Based on the approach developed in [3, 5], CMs can be obtained as the eigenfunctions of the following particular weighted eigenvalue equation:

$$XJ_n = \lambda_n R J_n, \tag{1}$$

where J_n and λ_n are the real eigenvectors and eigenvalues, respectively, n is the index of the order of each mode, and R and X are the real and imaginary parts of the impedance matrix of the MoM. The electric fields E_n and the magnetic fields H_n produced by characteristic currents J_n on the surface of a conducting body S are called characteristic fields or eigenfields associated to J_n [3].

As presented in [3], the selection of R as a weight operator in equation (1) is responsible for the orthogonality properties of characteristic modes, expressed by (2) and (3):

$$\langle \overrightarrow{J_m}, R \cdot \overrightarrow{J_n} \rangle = \langle \overrightarrow{J_m^*}, R \cdot \overrightarrow{J_n} \rangle = \delta_{mn}, \tag{2}$$

$$\langle \overrightarrow{J_m}, X \cdot \overrightarrow{J_n} \rangle = \langle \overrightarrow{J_m^*}, X \cdot \overrightarrow{J_n} \rangle = \lambda_n \delta_{mn}, \tag{3}$$

where

$$\delta_{mn} = \begin{cases} 1, & \text{if } m = n, \\ 0, & \text{if } m \neq n. \end{cases} \tag{4}$$

Choosing $m = n$ gives the following physical interpretations of the eigenvalues [5]:

(i) The total stored field energy within a radiation or scattering problem is proportional to the magnitude of the eigenvalues.

(ii) The case of $\lambda_n = 0$ corresponds to the case of resonance, and the associated modes are known as the *resonant modes.*

(iii) In the case of $\lambda_n > 0$, the stored magnetic field energy dominates over the stored electric field energy, so the associated modes are known as the *inductive modes.*

(iv) In the case of $\lambda_n < 0$, the stored electric field energy dominates over the stored magnetic field energy, so the associated modes are known as the *capacitive modes.*

2.2. Physical Interpretation of the Modal Significance. The modal significance (MS_n) is a function of the operating frequency and the dimensions of the conducting object [26]. It measures the contribution of each mode to the total electromagnetic response to a given source. As can be observed in equation (5), MS_n transforms the $[-\infty, +\infty]$ value range of eigenvalues λ_n into a much smaller range of $[0, 1]$. In many cases, it is more convenient to use the MS_n other than λ_n to investigate the resonant behavior across a wide frequency band.

$$\mathrm{MS}_n = \left| \frac{1}{1 + j\lambda_n} \right|. \tag{5}$$

In addition, MS_n also provides a convenient way to measure the bandwidth (BW_n) of each CM. This bandwidth can be defined as the frequency range where the power radiated by the mode is more than one-half of the power radiated by the same mode at resonance and can be expressed as shown in the following equation:

$$\mathrm{MS}_{\mathrm{HP}_n} = \left| \frac{1}{1 + j\lambda_n} \right| = \frac{1}{\sqrt{2}} = 0.707. \tag{6}$$

Half power (HP) at resonance corresponds to a cutback of the normalized current by a factor $\sqrt{2}$ [5]. Moreover, MS_n

is also used to identify the significant modes and nonsignificant modes. CMs with $MS_n \geq 0.707$ are referred to as significant modes, whereas CMs with $MS_n < 0.707$ are referred to as nonsignificant modes.

2.3. Physical Interpretation of the Characteristic Angle. The characteristic angle (α_n) is a modal attribute that defines the phase lag between the characteristic currents J_n and the tangential component of the characteristic electric field $E_n^{\tan}$ on the surface S. It is an important metric parameter in the CM theory, which indicates the resonant behavior or the kind of stored energy of each mode [27]:

$$\alpha_n = 180^\circ - \tan^{-1}(\lambda_n). \quad (7)$$

As α_n varies in the range $[90^\circ, 270^\circ]$, it provides an easy way to understand the mode behavior close to the resonance, especially if the mode presents narrow or large radiating bandwidth. CMs with a steep slope near 180° for α_n curve present narrow bandwidth, whereas those with a smooth slope present larger bandwidth. The smoother the slope of α_n curve at 180° is, the larger bandwidth the mode can exhibit.

According to the physical interpretation of eigenvalues, the characteristic modes can be also categorized using the characteristic angle α_n:

(i) If $\alpha_n = 180^\circ$, the associated modes are resonant modes.

(ii) If $90^\circ < \alpha_n < 180^\circ$, the associated modes are inductive modes.

(iii) If $180^\circ < \alpha_n < 270^\circ$, the associated modes are capacitive modes.

2.4. CM Applied to Reconfigurable Antennas. As presented in Figure 1, the workflow of a reconfigurable antenna design based on a CMA is divided into three basic processes: simulation, fabrication, and measurement.

(i) Simulation: this step is fundamental, since all CMA carries out this step, which presents the following substeps:

(1) *Understanding the structure*: the first substep concerns the initial investigation to understand the behavior of the structure. The excitation of the structure is excluded at this stage. The CMA will find out which modes are consistently in or near resonance within the frequency range of interest. Besides, CMA can determine the attributes of a single mode or a combination of modes that are convenient for the target application.

(2) *Correct mode excitation*: as a second substep and once a mode or a combination of modes of interest is determined, an excitation for these modes must be conceived. Analysis of the surface current distribution associated to the modes of the structure is performed and can determine the appropriate antenna location feed. By means of the evaluation of the modal weighting coefficients, the analysis will find out how well the structure was able to achieve the selected modal behavior.

(3) *Design parameter verification*: the third substep deals with the verification action, where a chosen solver is used to calculate the performance parameters of the antenna such as S-parameters, radiation pattern, gain, directivity, or efficiency.

(ii) Fabrication: this step is practical and requires a good manufacturing ability that determines the accomplishment of the previous steps results. Additional parameters must be taken into consideration in the use of electronic components such as temperature, interference among bias wires, and feed.

(iii) Measurement: finally, this step validates the previous steps and shows the performance of the design structure.

3. Geometry and Design of Rectangular Parallel Plates Based on Characteristic Mode Analysis

Let us consider two rectangular metallic plates separated a distance $H = 1.5$ mm, as shown in Figure 2. Two cases are analyzed, corresponding to two plates with the same dimensions ($W1 \times L = 62.5\,\text{mm} \times 42\,\text{mm}$) and two plates with a small variation in the length of the lower plate ($W2 \times L = 68.5\,\text{mm} \times 42\,\text{mm}$).

Let us now analyze these two parallel plates applying the CM theory. Figure 3 presents the characteristic angle (α_n) analysis carried out over the 0–5 GHz frequency range, for the plates with the same and with different dimensions. As seen in Figure 3, the observation of the curves at $\alpha_n = 180^\circ$ shows that for both cases, there are two main resonant modes at the 2.5 GHz band: antenna mode $J1$ (where current flows in the same direction in both plates) and transmission line mode $J1'$ (where current flows in opposite direction in both plates), as depicted in Figure 4.

At resonance frequency, antenna mode $J1$ and transmission line mode $J1'$ are presenting two different radiation patterns, as shown in Figure 5(a). However, by exciting the structure using a probe from the lower plate to the upper plate, a different combination of these two fundamental modes is excited by means of slightly expanding the dimensions of one plate. As shown in Figures 5(b) and 5(c), it can be observed that the resulting radiation pattern when exciting the structure with a probe feed gets varied from a bidirectional beam to a directional pattern, when slightly increasing the size of the lower plate.

The different modal contribution to the total radiated power in the two cases can be observed in Figures 6 and 7. As seen in Figure 6, mode $J1'$ (narrowband transmission line mode) dominates the total radiation power at 2.5 GHz frequency band and leads to the bidirectional radiation pattern shown in Figure 5(b). Conversely, in Figure 7, when the dimensions of the parallel plates are slightly different, the total radiated power results in a combination of mode $J1$

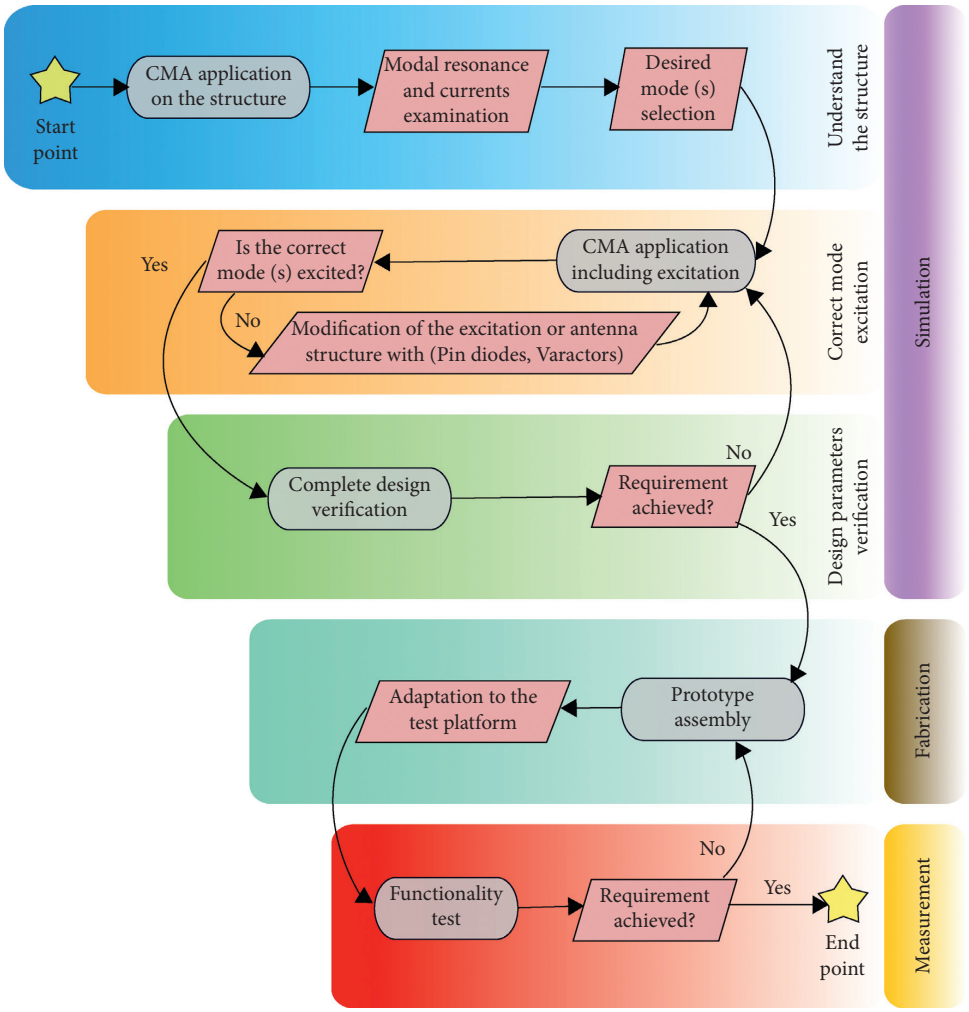

Figure 1: Workflow of a reconfigurable antenna design based on CMA.

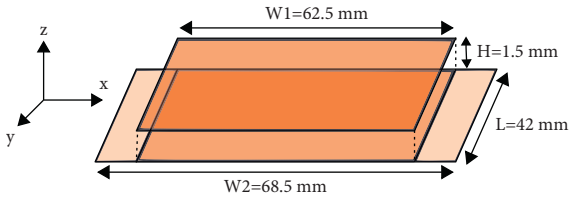

Figure 2: Geometry of the structure considered for the CMA.

(antenna mode) and $J1'$ (transmission line mode), and therefore this double mode excitation produces a directional pattern, as shown in Figure 5(c).

4. Results and Discussion

4.1. Reconfigurable Antenna Description. The proposed radiation pattern reconfigurable antenna is presented in Figure 8 and consists of a rectangular patch antenna printed on a Neltec substrate with a thickness H of 1.524 mm, $\varepsilon_r = 2.2$, and tangent loss of 0.0009. The dimensions of the

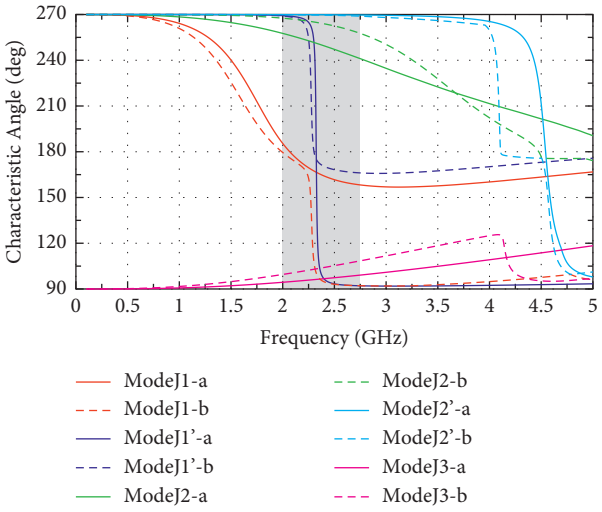

Figure 3: Characteristic angle associated to the first five modes of the structure shown in Figure 2. Mode-a case 1: parallel plates with the same dimensions. Mode-b case 2: parallel plates with different sizes.

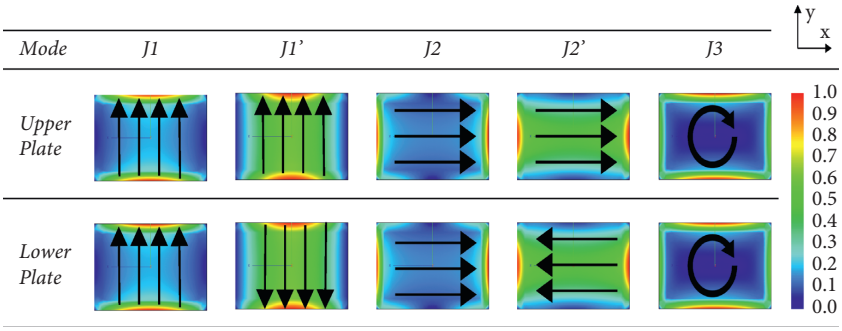

FIGURE 4: Current distribution associated to the first five modes of the structure shown in Figure 2, at the resonance frequency of each mode.

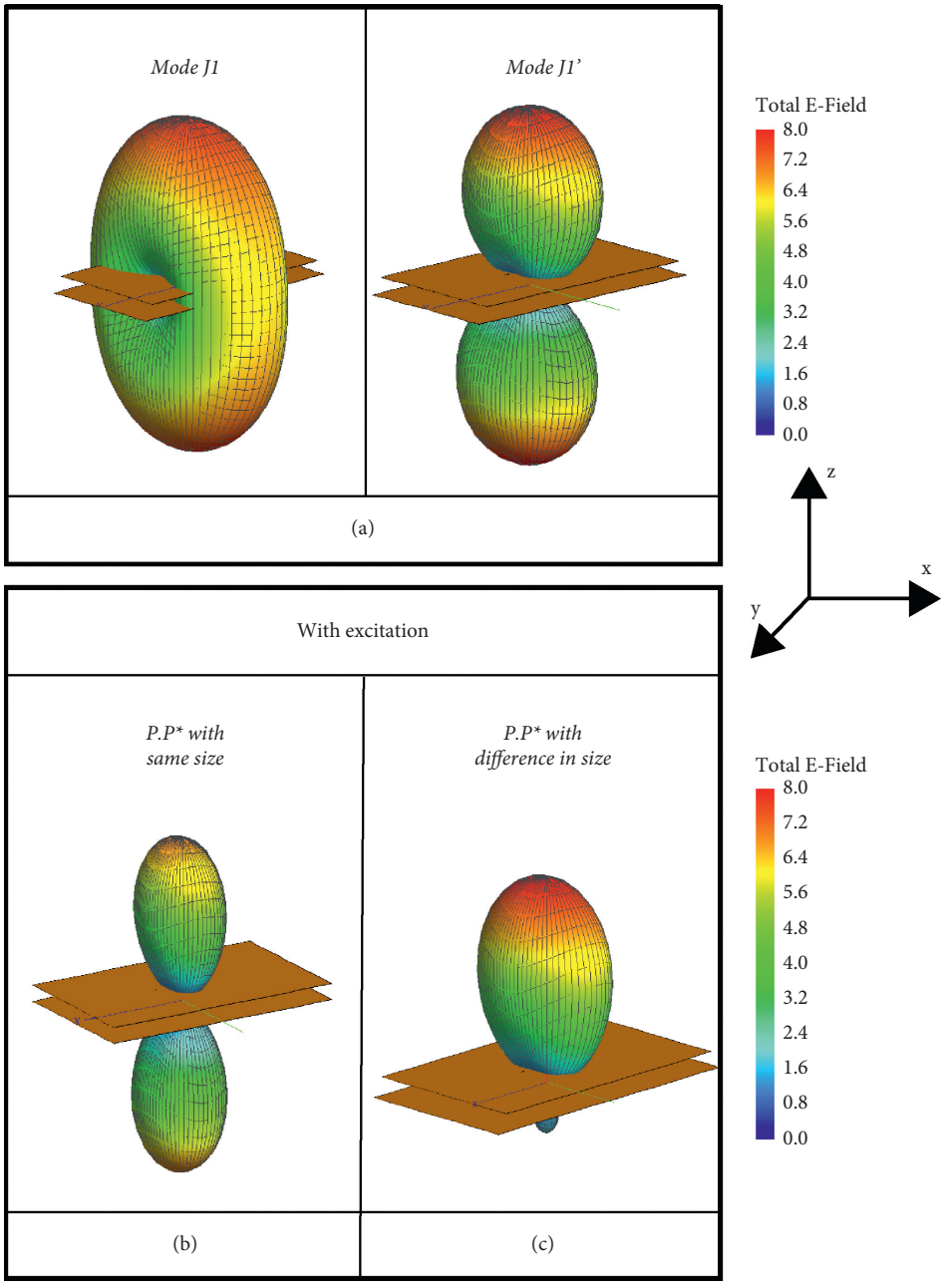

FIGURE 5: Radiation pattern associated to (a) fundamental modes $J1$ and $J1'$; (b) parallel plates (P.P*) with the same size; and (c) parallel plates (P.P*) with different sizes.

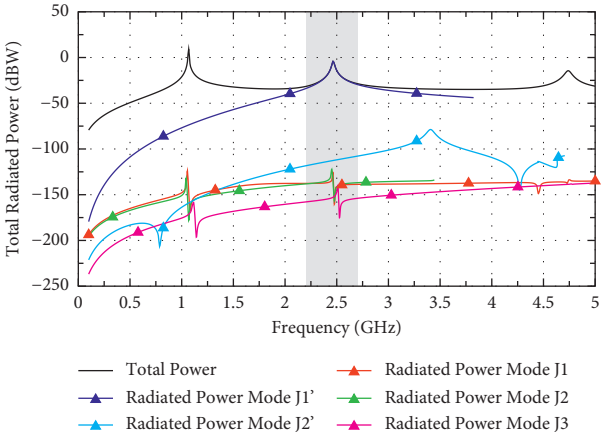

Figure 6: Total power and modal radiated power for two parallel plates with the same size.

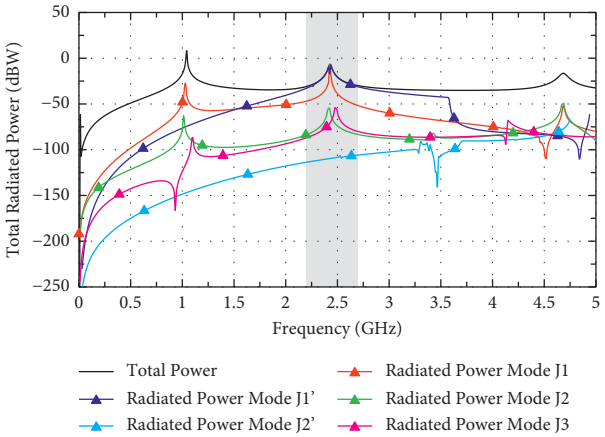

Figure 7: Total power and modal radiated power for two parallel plates with different sizes.

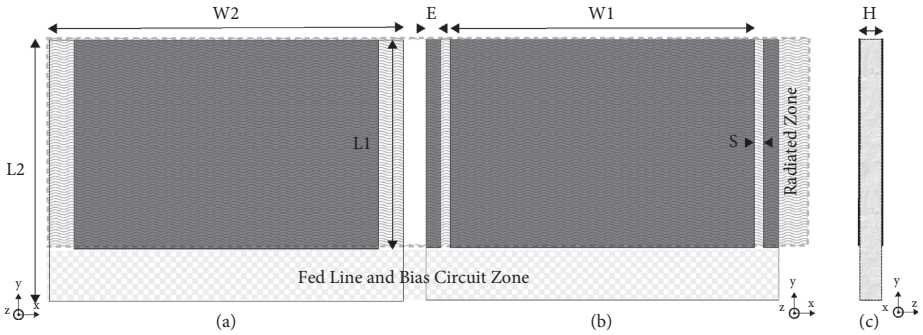

Figure 8: (a) Antenna's top view, (b) antenna's back view, and (c) antenna's lateral view.

structure are $W1 = 41$ mm, $W2 = 47.6$ mm, $L1 = 28$ mm, $L2 = 35$ mm, $S = 1.3$ mm, and $E = 2$ mm.

The idea is to implement an antenna consisting of two parallel plates, where the length of the lower plate is variable. Therefore, two PIN diodes are connecting the bottom plate to the lateral edges, as shown in Figure 9(c) (diodes $D1$ and $D2$). The two PIN diodes states, labeled as ON and OFF, enable or disable the current to flow through the lateral edges; hence, and as shown in the modal analysis, the radiation pattern can get varied.

By switching from ON to OFF state, it is noted a shift in the operating frequency, due to a change in the input

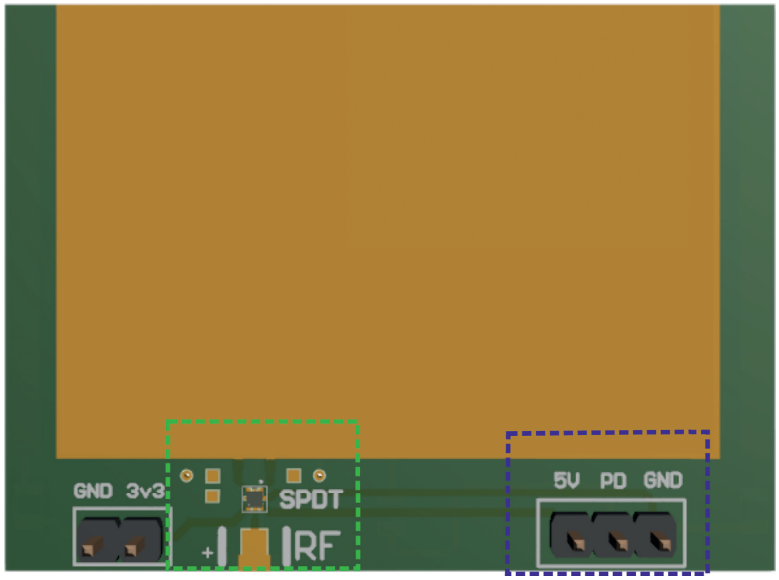

(a)

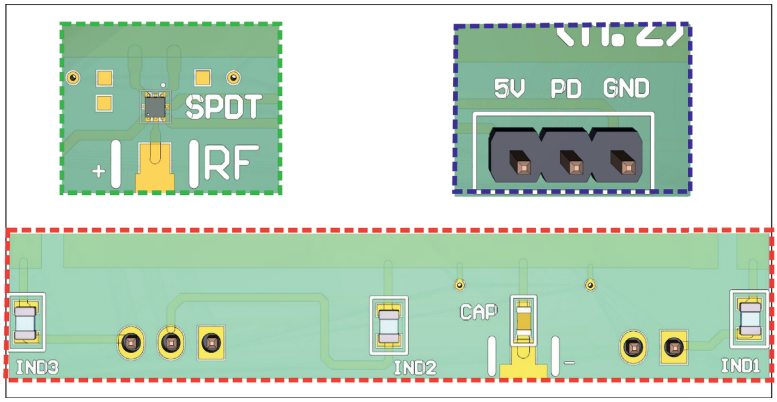

(b)

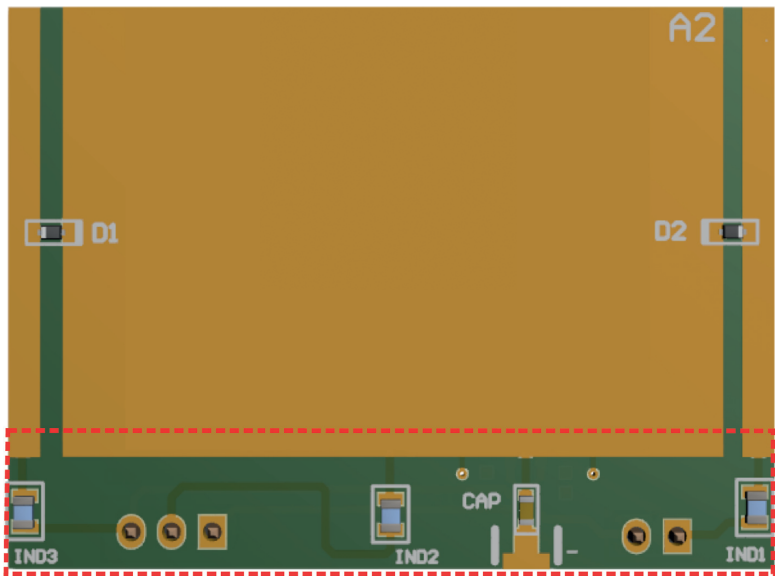

(c)

Figure 9: (a) Antenna's top view, (b) bias circuit areas, and (c) antenna's back view.

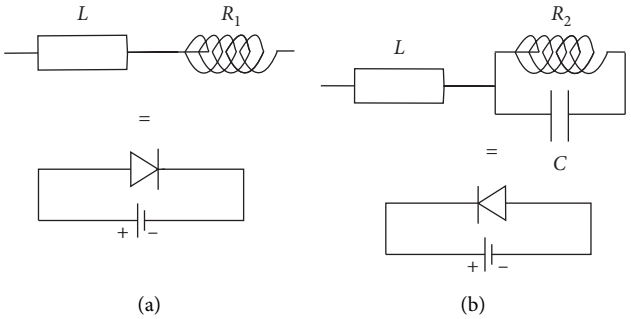

Figure 10: Equivalent circuit of the PIN diodes: (a) forward bias; (b) reverse bias.

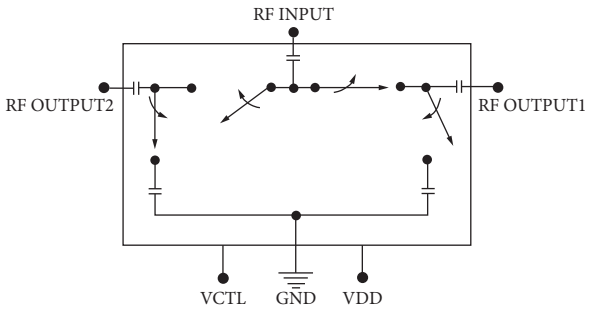

Figure 11: SPDT switch block diagram.

Table 1: Electronic components used in the proposed reconfigurable antenna.

Symbol	Value	Unit	Manufacturer	Comment
D1	BAR64-02V	—	Infineon	PIN diode
D2	BAR64-02V	—	Infineon	PIN diode
SPDT	SKY13585-679LF	—	Skyworks	Switch
CAP	12	pF	Murata MLCC	DC block
IND1	68	nH	Murata LQW	DC return
IND2	68	nH	Murata LQW	RF choke
IND	68	nH	Murata LQW	DC return

impedance of the antenna. To settle this issue, a SPDT switch is added on the top plate. The aim of using a SPDT switch is to guarantee a common frequency operating band by switching the RF input signal to the adequate position related to the PIN diodes state, as shown in Figures 9(a) and 9(b).

4.2. Bias Circuit Configuration. Figure 10 shows the equivalent circuit of the PIN diode for forward and reverse biasing. The PIN diode model considered for the design is the Infineon BAR64-02V silicon PIN diode, with low insertion loss and fast switching time [28]. As shown in Figure 10, the equivalent circuit consists of an inductor and a parallel capacitor resistor. To obtain the first configuration (PIN diodes are reverse biased), the values of the elements are ($L = 0.6$ nH, $C = 0.35$ pF, and $R = 3.3$ kΩ). On the other hand, the element values of the second configuration (PIN diodes are forward biased) are ($L = 0.6$ nH and $R = 1.35\ \Omega$).

The SPDT switch (Figure 11) model adopted in the design is SKY13585-679LF [22], with a low insertion loss (0.5 dB typically at 2.45 GHz) for mode switching at ISM band. A remarkable advantage about using this model is that it has integrated DC blocking capacitors, so no external DC blocking capacitors are required.

As illustrated in Figure 9(b), to perform the DC bias supply to the PIN diodes $D1$ and $D2$, additional components are fitted in the feed line and bias circuit zone (see also Figure 8). A DC block capacitor CAP of 12 pF is used in order to preserve the continuity of the RF current throughout the metal structure. The inductors IND1 and IND3 of 68 nH provide the DC return path for the bias current. The DC voltage is isolated from the RF signal using a RF choke inductor IND2 of 68 nH. Table 1 summarizes the models and values used for the different components in the proposed design.

To meet the switches' biasing requirements, a platform based on a nanocontroller [29] and a battery is employed to

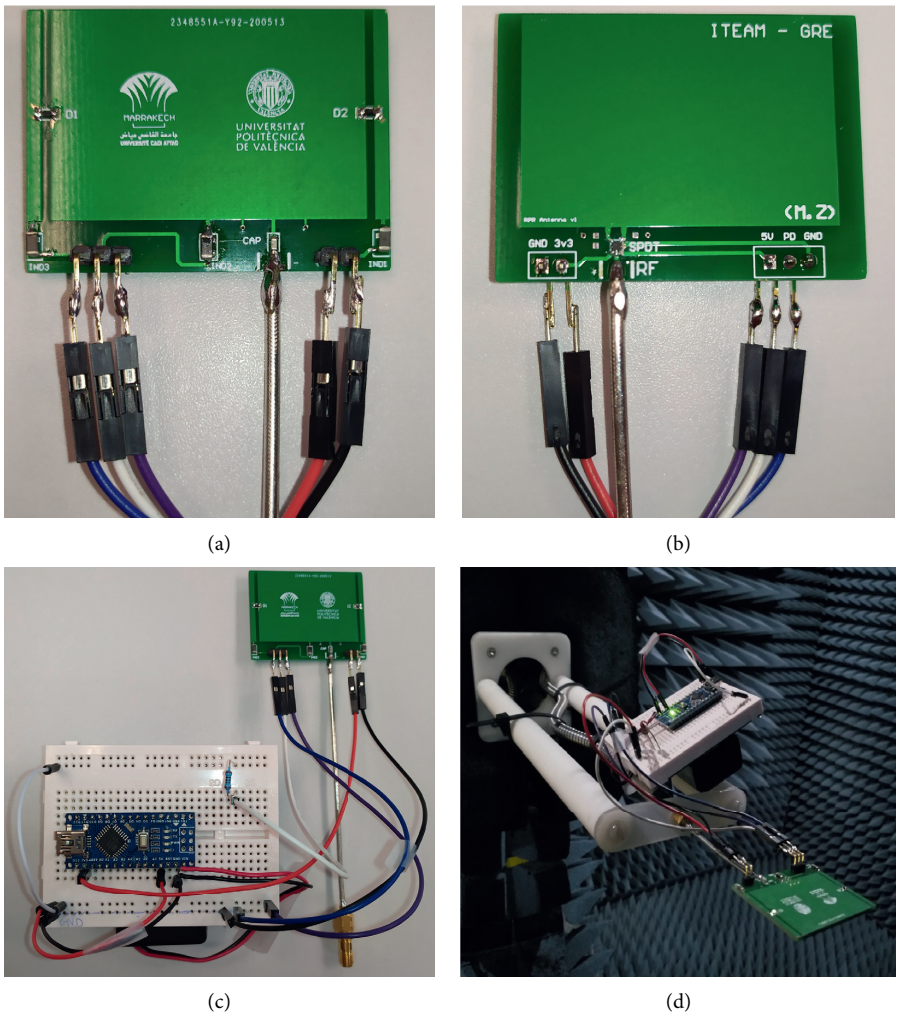

Figure 12: Final antenna prototype: (a) top view; (b) bottom view; (c) antenna with bias platform; (d) antenna in anechoic chamber.

Table 2: Reconfigurable antenna configuration: case 1 (bidirectional pattern) and case 2 (unidirectional pattern).

Case	Mode(s) excited	PIN diodes	SPDT
1	J_1'	OFF	VDD = 5 V, VCTL = 0 V
2	$J_1' + J_1$	ON	VDD = 5 V, VCTL = 3.3 V

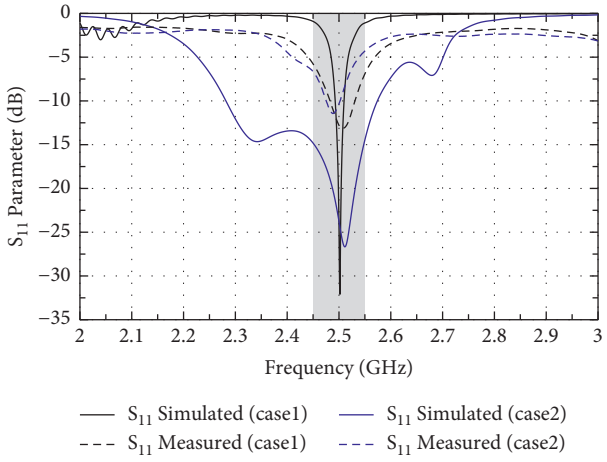

Figure 13: Simulated and measured S_{11} parameter for the ON/OFF cases presented in Table 2.

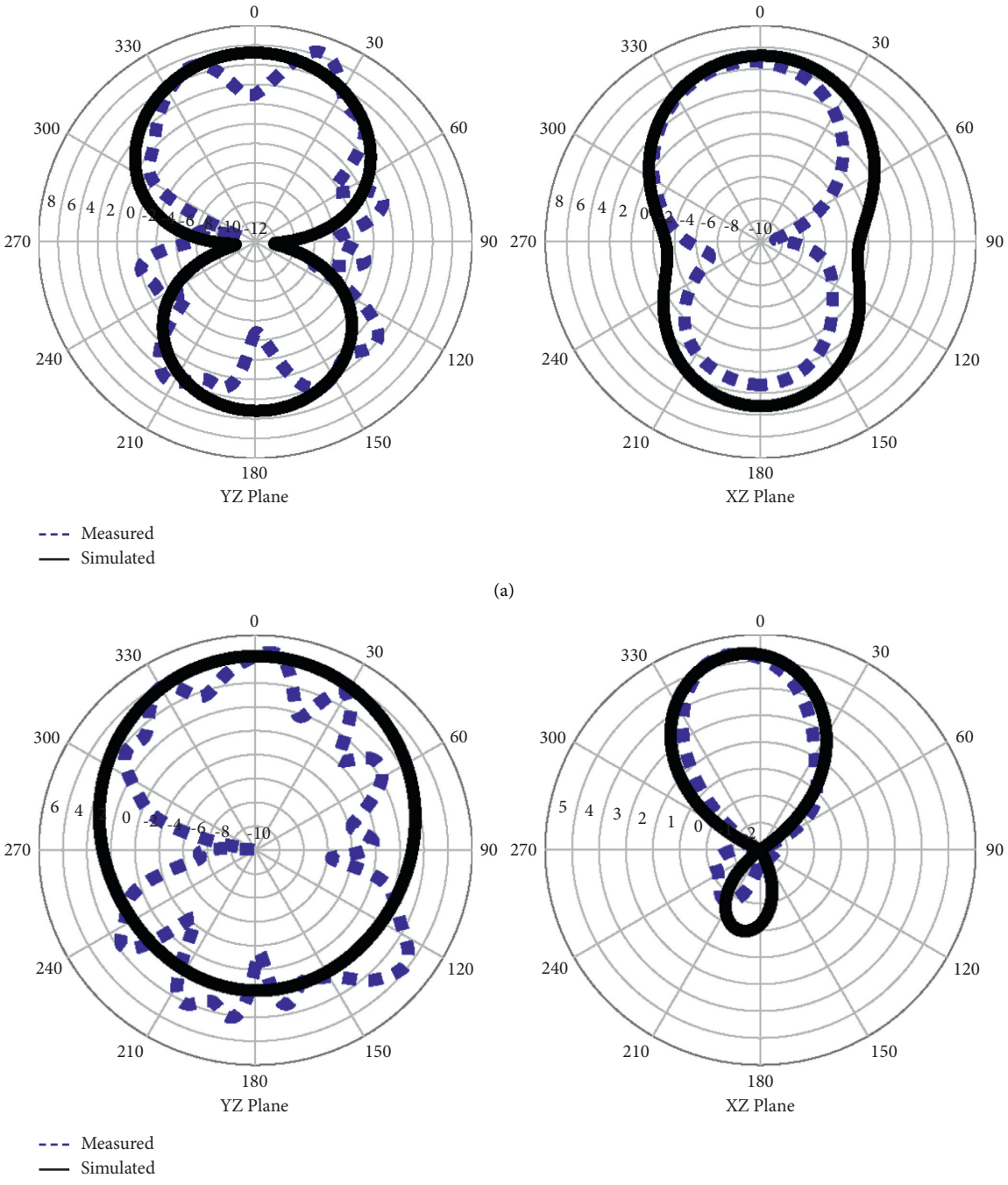

Figure 14: Simulated versus measured radiation patterns at 2.45 GHz: (a) case 1 and (b) case 2 (see Table 2).

achieve the bias signal corresponding to the two cases (case 1: bidirectional pattern and case 2: unidirectional pattern), as shown in Figure 12(c).

Table 2 shows the two configurations. To attain the first case, which consists of a bidirectional radiation pattern, the PIN diodes $D1$ and $D2$ were reverse biased and the SPDT INPUT pin (see SPDT block diagram in Figure 11) is connected to the RF OUTPUT1 by giving VDD and VCLT a supply voltage of 5 V and 0 V, respectively. The second case corresponds to a directional radiation pattern achieved by forward biasing the PIN diodes $D1$ and $D2$, and the SPDT INPUT pin is connected to the RF OUTPUT2 by giving VDD and VCLT a supply voltage of 5 V and 3.3 V, respectively.

4.3. Prototype and Measurement Results. The proposed radiation pattern reconfigurable antenna is fabricated and assembled with the electronic components as presented in Figure 12. In this prototype, connection wires are arranged

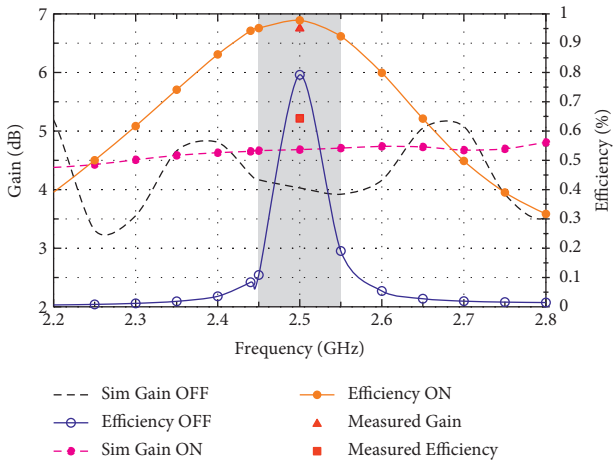

Figure 15: Antenna gain and efficiency.

Table 3: Comparison of the proposed structure.

Ref.	Beam type	Frequency (GHz)	Number of beams	PIN diodes	Size (mm^3)
[30]	Broadside and conical	2.25–2.85	3	2	$170 \times 170 \times 17$
[31]	Omnidirectional	3.4–3.8	3	4	$40 \times 30 \times 1.6$
[32]	Sum and difference	3.3–5.5	2	4	$144 \times 190 \times 0.8$
[33]	Conical and broadside	1.65–3.65	2	6	$140 \times 140 \times 6$
This work	Broadside and bidirectional	2.28–2.58	3	2	$47.6 \times 35 \times 1.524$

in an appropriate manner to minimize the perturbation on the radiation. Figure 13 shows the simulated versus measured S_{11} parameter of the proposed radiation pattern reconfigurable antenna for both cases. From Figure 13, it is observed that simulation and measurement perfectly agree on a common band at 2.5 GHz. It can be noted that simulated S_{11} parameter for case 2 shows a wide bandwidth. This is due to the fact that simulation files include ideal values for the lumped elements used for forward biasing the PIN diodes. The relative measured bandwidth at −10 dB for case 1 and case 2 is, respectively, 60 MHz and 25 MHz. However, measurement results meet the requirements, and a common operation frequency is achieved without changing physically the antenna structure.

2D radiation pattern measurements of the reconfigurable antenna at 2.45 GHz frequency band are plotted for both *XZ* and *YZ* planes in Figure 14. As presented by the CMA in the first section, a reconfigurable radiation pattern is achieved. Turning the PIN diodes to ON state and SPDT to OUTPUT2 leads to a directional beam, and switching the PIN diodes to OFF state and SPDT to OUTPUT1 produces a bidirectional pattern. The maximum peak gain and the maximum radiation efficiency for both states have been measured as shown in Figure 15, reaching values up to 6.75 dBi and 64.31% at 2.5 GHz, respectively. It should be noted that the efficiency is slightly low due to the diodes, SPDT switch, and particularly the nanocontroller platform that was incorporated in the measurement environment.

The performance of the proposed design is compared in Table 3 with some recently published designs featuring radiation pattern reconfigurable antenna performances. It is clear that the proposed antenna has fewer PIN diodes, which means less energy consumption and a low cost configuration. Moreover, it has the smallest size, except for the design presented in reference [31]. In comparison with the antenna having the same beam number [30, 31], the proposed antenna has different beams at the same resonant frequency which gives it toughness in terms of adaptation to the environment. Furthermore, the fabrication of our design is robust and the complexity is modest in comparison to the selected references.

5. Conclusion

The CM theory is able to provide a physical interpretation of the radiating behavior of an antenna. A radiation pattern reconfigurable antenna has been proposed in this paper based on the information provided by the CMA. The design of the antenna started from the modal analysis, in which the first case of two parallel plates with the same size shows a domination of mode $J1'$ and therefore a bidirectional pattern when the structure is excited. The second case, with a small difference in size in one plate, presents a unidirectional pattern, which arises from the contribution of two modes $J1$ and $J1'$. After the analysis, a reconfigurable antenna with the same structure has been proposed with the aim of changing the radiation pattern, and two different patterns are achieved by switching ON/OFF state of the PIN diodes. By means of introducing a SPDT switch, the operating frequency at both states is adjusted to 2.45 GHz. The bias voltage used is low, which is a significant interest for IoT sensors and mobile stations.

Abbreviations

CM: Characteristic mode
CMA: Characteristic mode analysis
IoT: Internet of Things
RA: Reconfigurable antenna
PIN: P-type layer, intrinsic layer, and N-type layer
SPDT: Single pole, double throw
DC: Direct current
VDD: DC supply voltage
VCTL: DC control voltage.

Data Availability

The data used to support the findings of this study are available from the corresponding author upon request.

Conflicts of Interest

The authors declare that they have no conflicts of interest.

Acknowledgments

This study was supported by the Spanish Ministry of Science and Innovation (Ministerio Ciencia e Innovación) under project no. PID2019-107885GB-C32 and Generalitat Valenciana under project no. AICO/2019/018.

References

[1] J. R. A. Garbacz, "Generalized expansion for radiated and scattered fields," Ph. D thesis, Ohio State University, Columbus, OH, USA, 1968.

[2] R. Garbacz and R. Turpin, "A generalized expansion for radiated and scattered fields," *IEEE Transactions on Antennas and Propagation*, vol. 19, no. 3, pp. 348–358, 1971.

[3] R. Harrington and J. Mautz, "Theory of characteristic modes for conducting bodies," *IEEE Transactions on Antennas and Propagation*, vol. 19, no. 5, pp. 622–628, 1971.

[4] E. Antonino-Daviu, M. Cabedo-Fabrés, M. Sonkki, N. Mohamed Mohamed-Hicho, and M. Ferrando-Bataller, "Design guidelines for the excitation of characteristic modes in slotted planar structures," *IEEE Transactions on Antennas and Propagation*, vol. 64, no. 12, pp. 5020–5029, 2016.

[5] M. Cabedo-Fabres, E. Antonino-Daviu, A. Valero-Nogueira, and M. Bataller, "The theory of characteristic modes revisited: a contribution to the design of antennas for modern applications," *IEEE Antennas and Propagation Magazine*, vol. 49, no. 5, pp. 52–68, 2007.

[6] J. Laheurte, *Compact Antennas for Wireless Communications and Terminals. Theory and Design*, John Wiley & Sons, Inc, Hoboken, NJ, USA, 2011.

[7] H. Al-Tamimi and S. Mahdi, "A study of reconfigurable multiband Antenna for wireless application," *International Journal of New Technology and Research*, vol. 2, pp. 125–134, 2016.

[8] Z. Mahlaoui, E. Antonino-Daviu, A. Latif, and M. Ferrando-Bataller, "Design of a dual-band frequency reconfigurable patch antenna based on characteristic modes," *International Journal of Antennas and Propagation*, vol. 2019, Article ID 512532, 12 pages, 2019.

[9] X. Zhao and S. Riaz, "A dual-band frequency reconfigurable MIMO patch-slot antenna based on reconfigurable microstrip feedline," *IEEE Access*, vol. 6, pp. 41450–41457, 2018.

[10] G. Jin, M. Li, D. Liu, and G. Zeng, "A simple planar pattern-reconfigurable antenna based on arc dipoles," *IEEE Antennas and Wireless Propagation Letters*, vol. 17, no. 9, pp. 1664–1668, 2018.

[11] J. Zhang, S. Yan, and G. A. E. Vandenbosch, "Metamaterial-inspired dual-band frequency-reconfigurable antenna with pattern diversity," *Electronics Letters*, vol. 55, no. 10, pp. 573-574, 2019.

[12] D. Chen, W. Yang, W. Che, Q. Xue, and L. Gu, "Polarization-reconfigurable and frequency-tunable dipole antenna using active AMC structures," *IEEE Access*, vol. 7, pp. 77792–77803, 2019.

[13] A. Bhattacharjee, S. Dwari, and M. K. Mandal, "Polarization-reconfigurable compact monopole antenna with wide effective bandwidth," *IEEE Antennas and Wireless Propagation Letters*, vol. 18, no. 5, pp. 1041–1045, 2019.

[14] E. González, J. Casanova-Chafer, A. Romero, X. Vilanova, J. Mitrovics, and E. Llobet, "LoRa sensor network development for air quality monitoring or detecting gas leakage events," *Sensors*, vol. 20, no. 21, p. 6225, 2020.

[15] M. Shirazi, J. Huang, T. Li, and X. Gong, "A switchable-frequency slot-ring antenna element for designing a reconfigurable array," *IEEE Antennas and Wireless Propagation Letters*, vol. 17, no. 2, pp. 229–233, 2018.

[16] C. Rick, "The nuts and bolts of tuning varactors," *High Frequency Electronics*, pp. 44–51, 2009.

[17] A. Zohur, H. Mopidevi, D. Rodrigo, M. Unlu, L. Jofre, and B. A. Cetiner, "RF MEMS reconfigurable two-band antenna," *IEEE Antennas and Wireless Propagation Letters*, vol. 12, pp. 72–75, 2013.

[18] I. F. Da Costa, S. A. Cerqueira, D. H. Spadoti, L. G. Da Silva, J. A. J. Ribeiro, and S. E. Barbin, "Optically controlled reconfigurable antenna array for mm-wave applications," *IEEE Antennas and Wireless Propagation Letters*, vol. 16, pp. 2142–2145, 2017.

[19] M. Konca and P. A. Warr, "A frequency-reconfigurable antenna architecture using dielectric fluids," *IEEE Transactions on Antennas and Propagation*, vol. 63, no. 12, pp. 5280–5286, 2015.

[20] A. Jouade, M. Himdi, A. Chauloux, and F. Colombel, "Mechanically pattern-reconfigurable bended horn antenna for high-power applications," *IEEE Antennas and Wireless Propagation Letters*, vol. 16, pp. 457–460, 2017.

[21] Z. Mahlaoui, E. Antonino-Daviu, A. Latif, and M. Ferrando-Bataller, "Radiation pattern reconfigurable antenna design using characteristic modes," in *Proceedings of the 12th European Conference on Antennas and Propagation (EuCAP 2018)*, pp. 1–4, London, UK, April 2018.

[22] Skyworks Solutions, Inc, *SKY13585-679LF: 1.0 to 6.0 GHz SPDT Switch*, Skyworks Solutions, Inc, Irvine, CA, USA, 2017, https://www.skyworksinc.com.

[23] FEKO Softwaer, "Solving connectivity, compatibility, and radar challenges," 2021, https://altairhyperworks.com/product/FEKO.

[24] CST Studio Suite Software, "Software de simulación de campo electromagnético," 2021, https://www.3ds.com/es/productos-y-servicios/simulia/productos/cst-studio-suite/.

[25] C. Yikai and W. Chao-Fu, *Characteristic Modes: Theory and Applications in Antenna Engineering*, John Wiley & Sons, Inc., Hoboken, NJ, USA., 1 edition, 2015.

[26] B. A. Austin and K. P. Murray, "The application of characteristic-mode techniques to vehicle-mounted NVIS antennas," *IEEE Antennas and Propagation Magazine*, vol. 40, no. 1, pp. 7–21, 1998.
[27] E. Newman, "Small antenna location synthesis using characteristic modes," *IEEE Transactions on Antennas and Propagation*, vol. 27, no. 4, pp. 530-531, 1979.
[28] A. G. Infineon Technologies, "Low signal distortion, surface mount RF PIN diode," 2018, https://www.infineon.com.
[29] Arduino, "User manual arduino nano (V2.3)," 2021, https://www.arduino.cc/en/uploads/Main/ArduinoNanoManual23.pdf.
[30] W. Lin, H. Wong, and R. W. Ziolkowski, "Wideband pattern-reconfigurable antenna with switchable broadside and conical beams," *IEEE Antennas and Wireless Propagation Letters*, vol. 16, pp. 2638–2641, 2017.
[31] L. Han, C. Wang, W. Zhang, R. Ma, and Q. Zeng, "Design of frequency- and pattern-reconfigurable wideband slot antenna," *International Journal of Antennas and Propagation*, vol. 20187 pages, Article ID 678018, 2018.
[32] S.-A. Malakooti and C. Fumeaux, "Pattern-reconfigurable antenna with switchable wideband to frequency-agile bandpass/bandstop filtering operation," *IEEE Access*, vol. 7, pp. 167065–167075, 2019.
[33] X. Yang, H. Lin, H. Gu, L. Ge, and X. Zeng, "Broadband pattern diversity patch antenna with switchable feeding network," *IEEE Access*, vol. 6, pp. 69612–69619, 2018.

Hindawi
International Journal of Antennas and Propagation
Volume 2019, Article ID 4512532, 12 pages
https://doi.org/10.1155/2019/4512532

Research Article

Design of a Dual-Band Frequency Reconfigurable Patch Antenna Based on Characteristic Modes

Zakaria Mahlaoui,[1,2] **Eva Antonino-Daviu**,[1] **Adnane Latif**,[2] **and Miguel Ferrando-Bataller**[1]

[1]*Instituto de Telecomunicaciones y Aplicaciones Multimedia, Universitat Politècnica de València, 46022, Spain*
[2]*Information Technology and Modeling Laboratory, National School of Applied Sciences, Cadi Ayyad University, 40000, Morocco*

Correspondence should be addressed to Zakaria Mahlaoui; mahza@doctor.upv.es

Received 30 November 2018; Accepted 4 February 2019; Published 31 March 2019

Academic Editor: Yuan Yao

A frequency reconfigurable patch antenna design based on the characteristic mode analysis is presented. The antenna presents a reconfigurable lower band and a steady band at higher frequencies. A slot is etched on the ground plane of the antenna, where two varactor diodes are placed on each side of the slot in order to tune the lower band. The first resonant frequency shifts down by varying the reverse voltage of the varactor, whereas the second operating frequency keeps stable. The proposed antenna is designed to cover WLAN bands, offering a first band operating at 2 GHz and a second band ranging from 5.3 GHz to 5.8 GHz. A prototype has been fabricated and measurements are provided, which validate the proposed analysis, method, and design procedure.

1. Introduction

In a wireless system, the antenna is a decisive component. A simple and appropriate design can fulfil the system requirements and improve the global system performance. Patch antennas are one of the simplest antenna structures, and they have been widely used over the years due to their characteristics of low cost, lightweight, low profile, and ease of integration.

Nevertheless, interference to the communication systems can exist because of the presence of different wireless applications who are using the same frequency band. As an example, in the Industrial, Scientific, and Medical (ISM) radio bands and the Unlicensed National Information Infrastructure (referred to as U-NII) bands used by IEEE 802.11 devices, the use of those bands is sometimes excessive by the Wi-Fi customers and leads to the presence of interferences because the access to this radio spectrum is without the need of restrictions and regulations that might be applicable elsewhere.

In addition, this unlicensed band operates over many frequencies, and from an antenna design perspective, UWB antenna with a band suppression feature can be one solution [1], but the cost and the difficulty here are increased. To overcome this issue, frequency reconfigurable antennas are proposed, where a dynamic modification of the operating frequency of the antenna brings flexibility to the communication system. This kind of antenna will not cover all the frequency bands simultaneously but provides several dynamically selectable narrow frequency bands and, within these bands, exhibits higher flexibility than that achievable with conventional wide-band and multiple band antenna solutions [2, 3]. Reconfigurability can be achieved by using electronic components to tune antenna characteristics such as PIN diodes [4–6], varactors [7, 8], and MEMS switches [9, 10] or changing material properties [11].

Hence, this paper presents an antenna with two bands suitable for WLAN applications. Work done in [3] proposed a similar simulation approach but only at 5 GHz band. However, the antenna proposed here operates at 2 GHz band, which will be a reconfigurable band, and at a second one that ranges from 5.3 GHz to 5.8 GHz, which is a steady band. A Defected Ground Structure (DGS) [12] consisting in a rectangular shape slot embedded in the ground plane is

proposed and has been studied using characteristic mode analysis (CMA), which provides interesting physical insight into the antenna behavior [13]. Varactor diodes are used to perform the selectivity over the frequency band. In this part, two simulation approaches are followed: the ideal case and the equivalent circuit case. At the end, a prototype has been fabricated and measurements have been made to validate the simulation results.

2. Characteristic Mode Analysis

2.1. Brief Introduction to the Theory of Characteristic Modes. Characteristic mode analysis (CMA) provides understanding into the physical phenomena associated to the radiating behavior of an antenna with arbitrary shape. Therefore, it helps to simplify the analysis, synthesis, and optimization of antennas [13]. By solving a generalized eigenvalue problem shown in equation 1, involving the impedance matrix of the Method of Moments (MoM), a set of orthogonal eigencurrents together with their associated eigenvalues are obtained. Due to the orthogonality of the eigencurrents, the total current on the surface of the conductor can be expanded into those modes. The eigenvalues provide information about the radiating behavior of the associated mode. Also, the quantities characteristic angle α_n in equation 2 and modal significance MS_n in equation 3 can be calculated, which are associated to the eigenvalue λ_n in equation 1.

As defined in [14], the following generalized eigenvalue equation is expressed by

$$X(J_n) = \lambda_n R(J_n), \tag{1}$$

where λ_n are the eigenfunctions, J_n are the eigencurrents, and R and X are, respectively, the real and imaginary parts of the impedance matrix of the MoM.

The characteristic angle provides a way to better show the mode behavior near resonance, and it is defined as

$$\alpha_n = 180^\circ - \tan^{-1}(\lambda_n). \tag{2}$$

The modal significance (MS_n) measures the contribution of each mode in the total electromagnetic response to a given source. It is described by

$$\mathrm{MS}_n = \left| \frac{1}{1 + j\lambda_n} \right|. \tag{3}$$

2.2. Characteristic Mode Analysis of a Patch Antenna over a Finite Ground Plane. Let us perform the characteristic mode analysis (CMA) of a metallic rectangular plate of 29 mm × 31 mm over a rectangular ground plane of 35 mm × 50 mm. Figure 1 shows the geometry of the structure to analyze, where the separation between the two plates is $h = 1.524$ mm. No substrate is used.

The characteristic angle α_n associated to the first six CM of the structure is shown in Figure 2. Current distribution corresponding to these six modes at its resonance frequency ($\alpha_n = 180^\circ$) is plotted in Figure 3, where arrows have been included for the sake of understanding to indicate the direction of the current in the ground plane and dashed lines represent nulls of current. As can be observed, each mode presents a specific current distribution, with vertical and/or horizontal currents.

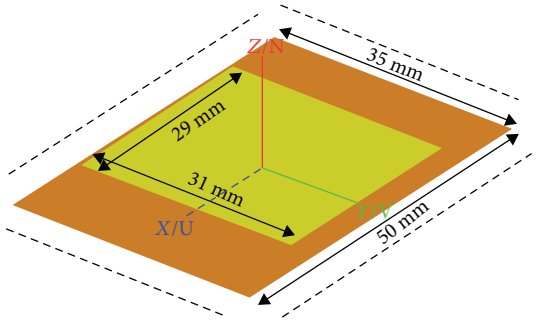

Figure 1: Patch antenna over a finite rectangular ground plane to analyze with CMA. Separation between the two plates is 1.524 mm.

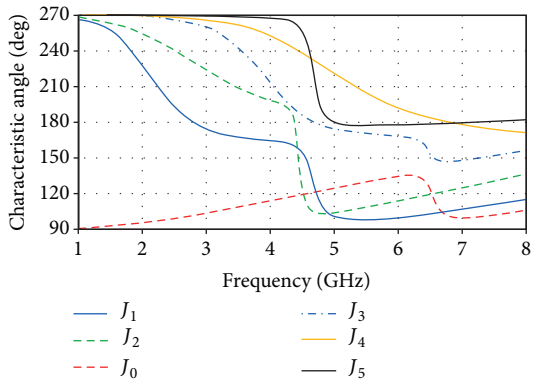

Figure 2: Characteristic angle associated to the first six CM of the patch antenna shown in Figure 1.

CM are intrinsic to any structure but their excitation depends on the feeding mechanism used. If the patch antenna is excited at its longer edge by a microstrip line, modes with current distributed along the x-axis and with opposite flow direction in the patch and in the ground plane will be excited. Therefore, according to Figure 3, modes J_1 and J_4 are the ones that will be excited. As each mode resonates at a different frequency ($\alpha_n = 180^\circ$), two operating bands will be achieved, obtaining a dual-band antenna.

Now, in order to create a tunable band for the first operating band, a narrow rectangular slot with two tunable capacitors should be inserted in the antenna at the appropriate place, so as to not disturb the second operating band that should be fixed. Looking at the current distribution associated to modes J_1 and J_4, we can see that the slot should be inserted in the center of the ground plane. Remark that the unidirectional radiation behavior of the patch is lost when the slot is etched in the ground plane, as back radiation will appear in this case. For applications where bidirectional radiation is needed, the proposed antenna with defected ground plane (slotted ground plane) can be used.

Figure 4 depicts the geometry of the proposed defected ground plane of the patch antenna. As a null of current is present at the position of the slot for mode J_4, this mode will

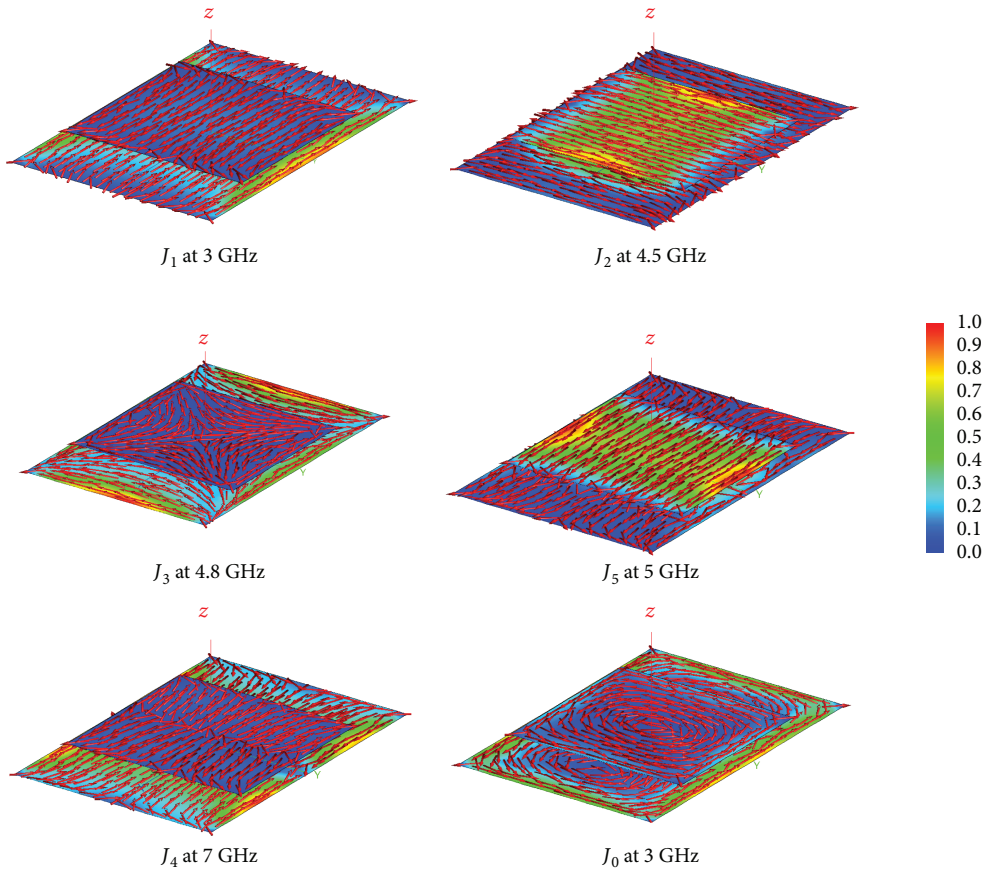

Figure 3: Current distribution of the first six CM of a patch antenna over a rectangular ground plane, near the resonance frequency. Arrows indicate the direction of the current in the ground plane and dashed lines indicate nulls of current.

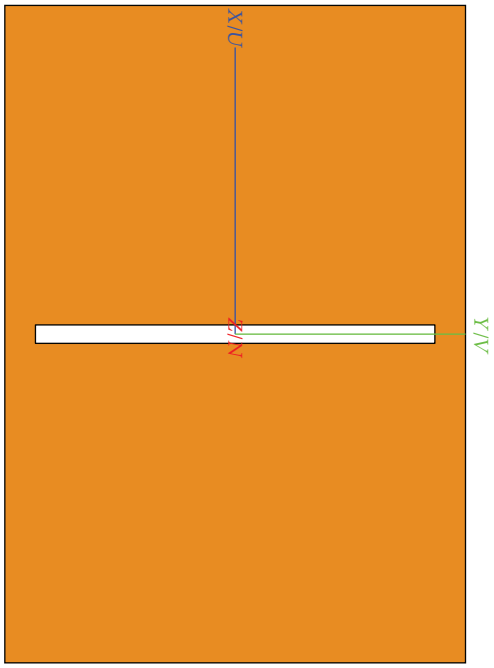

Figure 4: Defected ground plane (DGP) for the reconfigurable dual-band antenna.

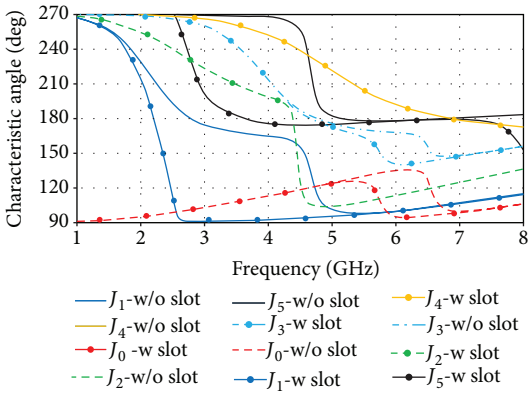

Figure 5: Comparison of the characteristic angle associated to the first six CM of the patch antenna over a ground plane with and without slot.

not be affected by the presence of the slot, while mode J_1 will be. This fact can be observed in Figure 5, where a comparison of the characteristic angle of the original structure and the structure including the slot is shown. As it can be seen, the resonant frequency of mode J_1 is shifted down due to the presence of the slot, while mode J_4 is not perturbed.

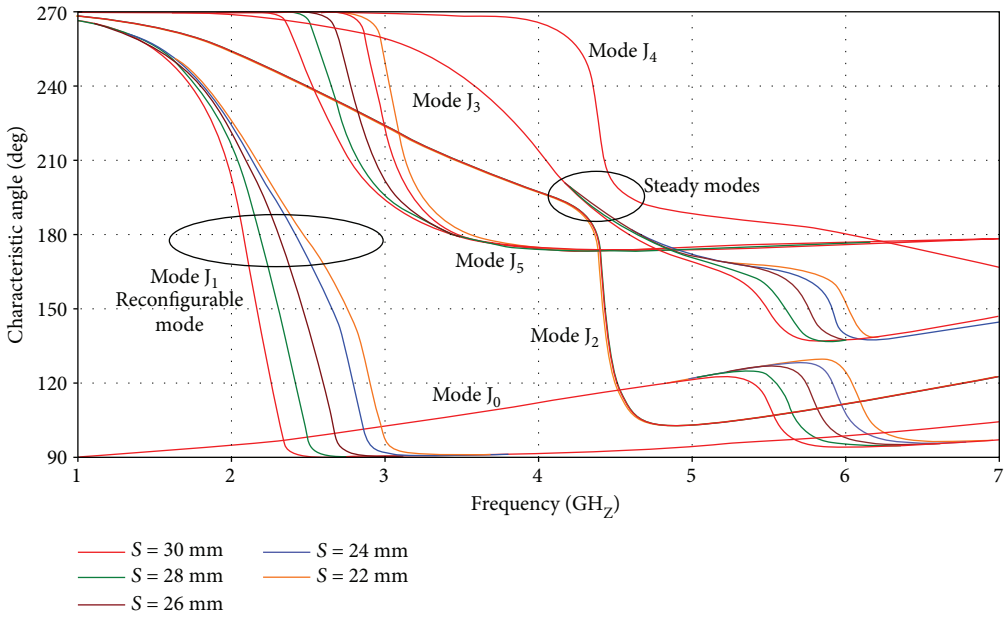

Figure 6: Characteristic angle variation with the slot length (S) for the first six CM over frequency.

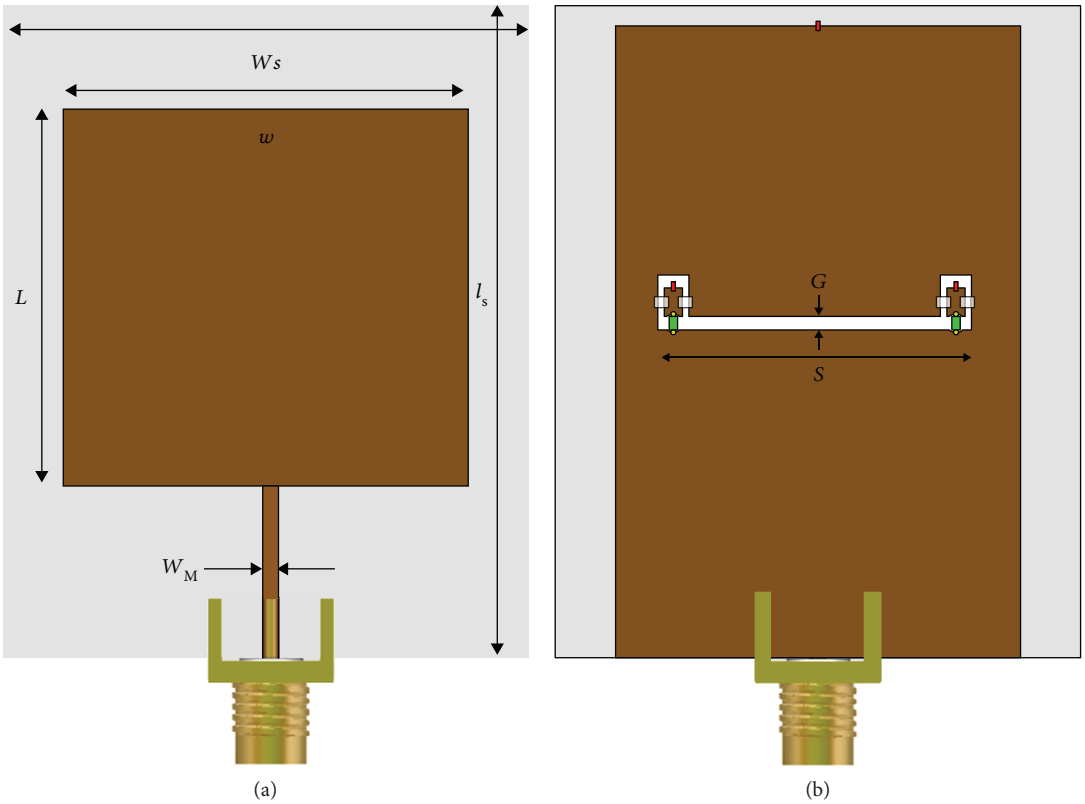

Figure 7: Antenna geometry. (a) Front view. (b) Back view.

Moreover, Figure 6 shows the characteristic angle of the first six modes when varying the slot length (S). As seen, the variation of the slot length affects modes J_1 and J_5, modifying their characteristic angle. Modes J_0, J_2, J_3, and J_4

Table 1: Dimension of the designed antenna.

Parameter	W	L	Ws	Ls	W_M	G	S	h
Value (mm)	31	29	35	50	1.25	1	30	1.524

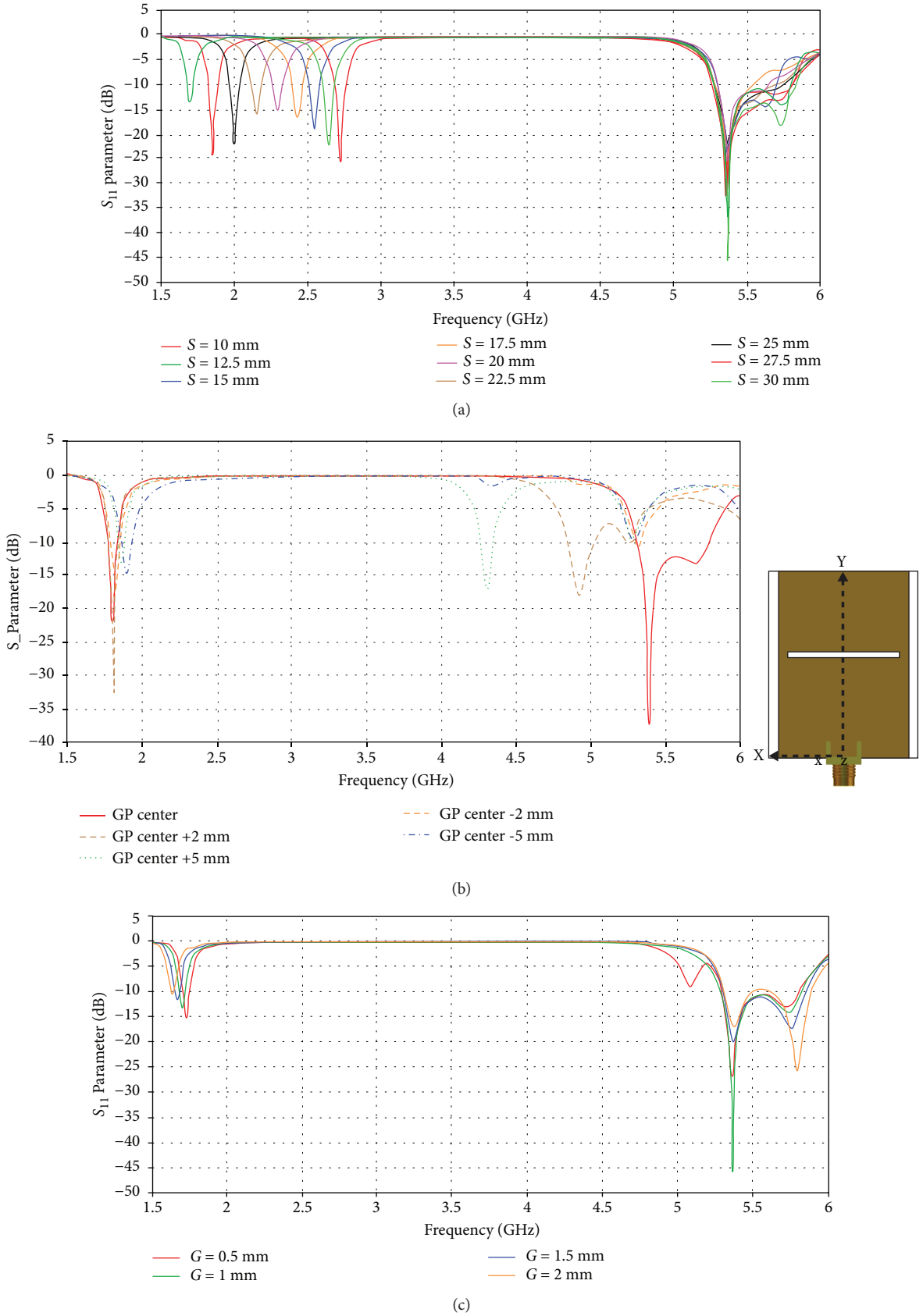

Figure 8: S_{11} parameter variation with (a) the slot length (S), (b) the slot position along the y-axis (*GP center*), (c) the slot width (g).

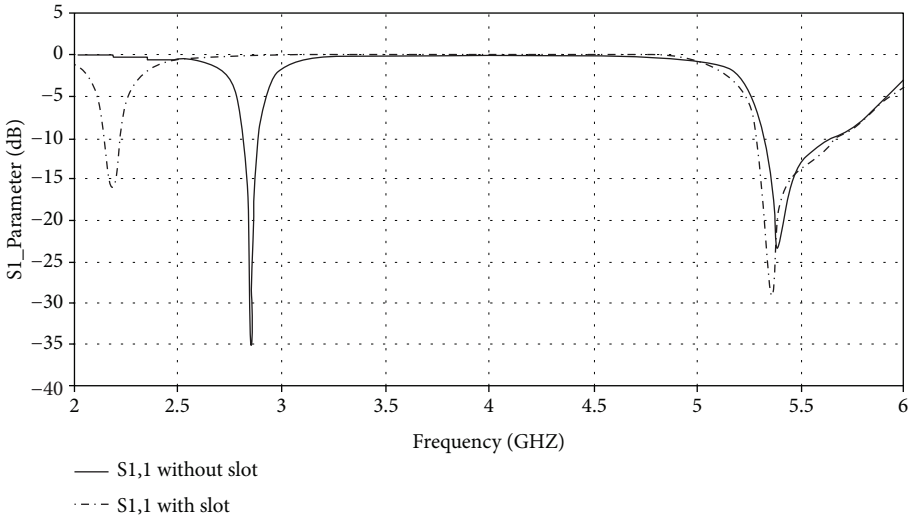

Figure 9: S_{11} parameter of the antenna without slot and with slot.

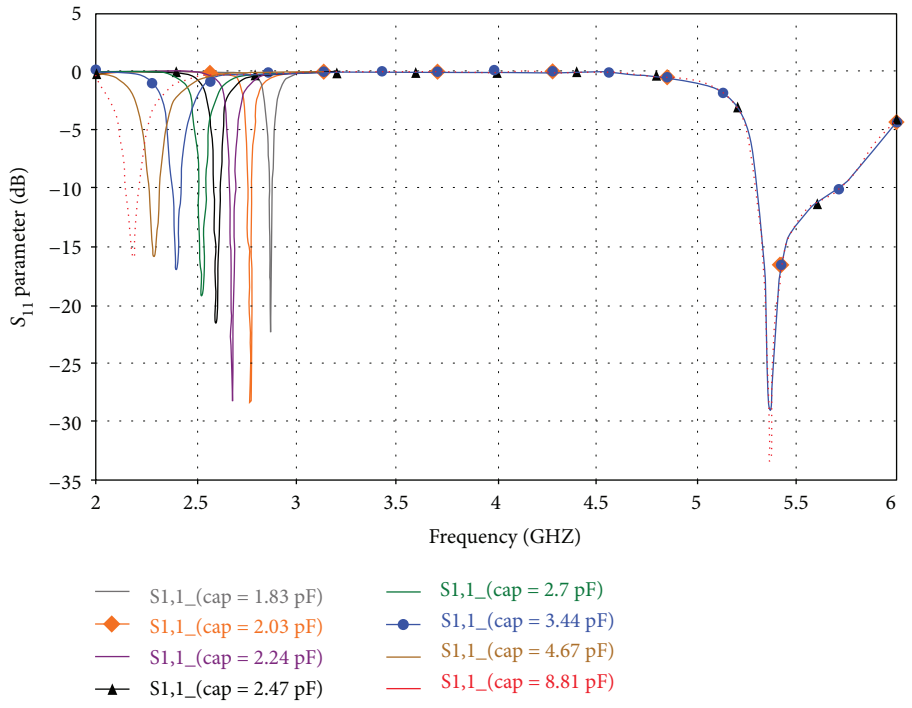

Figure 10: S_{11} parameter of the ideal case using capacitors.

are showing a constant behavior as they are conserving the same characteristic angle and resonant frequency even though the slot length is changing.

As modes J_1 and J_4 are excited in the proposed antenna, if the slot is loaded with variable capacitors, the resonance frequency of mode J_1 can be tuned, keeping the resonance frequency of mode J_4 steady. This will be shown in the next section.

3. Antenna Description and Simulations

3.1. Antenna Geometry. Figure 7 shows the geometry of the proposed reconfigurable dual-band antenna. As observed, the antenna consists of a rectangular patch with length L and width W, where entire dimensions of the ground plane are $Ls \times Ws$. The substrate used is Rogers RO3003, which is a lossy substrate with a dielectric constant of $\varepsilon_r = 3$ and loss tangent $\tan\delta = 0.001$. The patch antenna is fed at the longer edge by a microstrip line of width W_M connected to a coaxial SMA port of 50 Ω. As the objective is to obtain two bands (lower band at 2 GHz and upper band centered at 5 GHz), a slot of length S and width G is etched in the ground plane as described in the previous section. Each side of the slot is loaded with a varactor diode, to keep the symmetry. The model of the varactor adopted in this work is the SMV2025

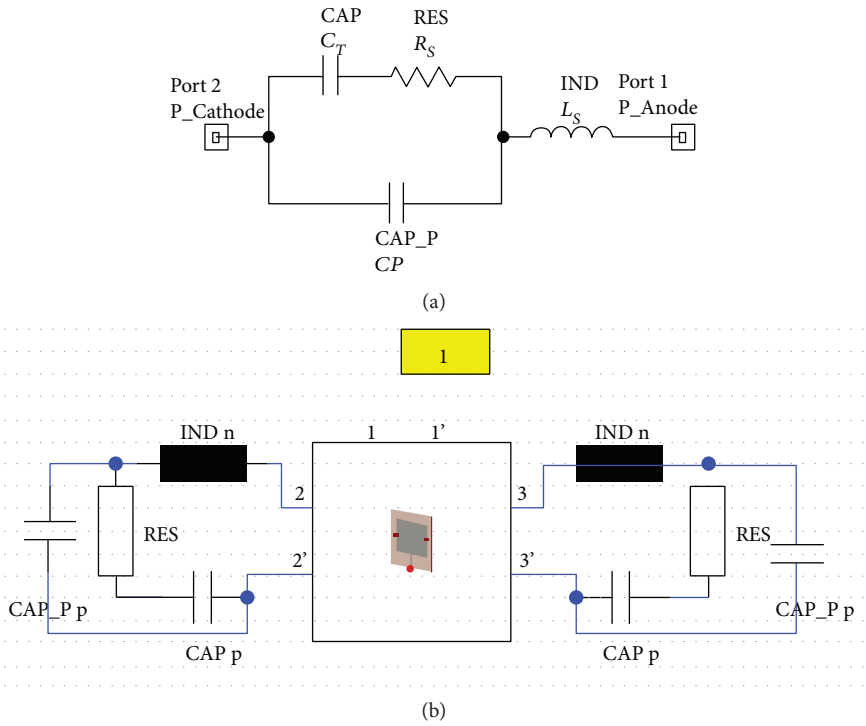

Figure 11: (a) Equivalent circuit of the diode varactor. (b) Schematic design of the antenna.

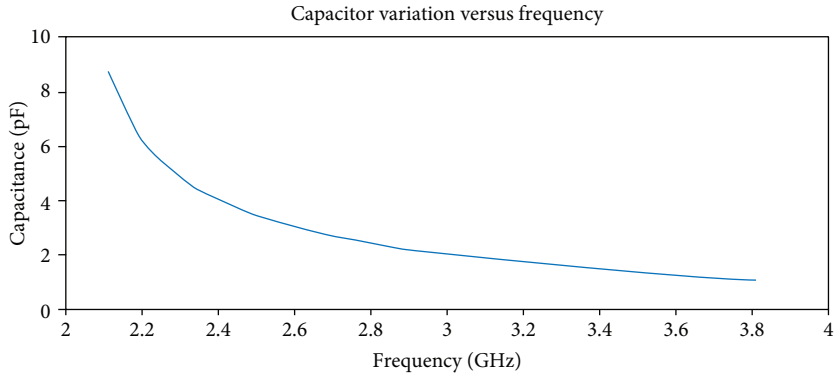

Figure 12: Variation of the varactor capacitance over frequency [15].

surface mount, hyperabrupt tuning varactor diode [15]. The simulation design is performed by using CST software, based on the simplified theoretical formulations that have been described in [16]. The final dimensions are shown in Table 1.

3.2. Simulation Results

3.2.1. Parametric Study of the Slot. In Figure 6, it has been presented the characteristic angle variation of the modes when varying the slot length (S), showing a variation in the resonance frequency of mode J_1 (mode of the tunable band). In Figure 8(a), the S_{11} parameter for different slot lengths is shown. As it can be observed, the slot length affects the first frequency band (reconfigurable band).

In order to obtain good results, the slot should be inserted in the center of the ground plane. Figure 8(b) shows the S_{11} parameter for different slot positions on the y-axis, with respect to the center of the ground plane (i.e., GP center is the distance from the center of the ground plane along the y-axis).

Finally, Figure 8(c) presents the S_{11} parameter for different slot widths. As observed, the slot width affects the matching of the frequency bands.

3.2.2. Reconfigurable Antenna Simulation Methods. Figure 9 shows the return losses of the antenna without slot and with slot. As shown by the CMA and as can be observed in Figure 9, the effect of adding a slot in the ground plane of the antenna shifts down the lower band, from 2.8 GHz to 2.2 GHz. It should be mentioned that the band achieved by the slot could be obtained by using the length of 0.165λ. Likewise, the second frequency band holds in a steady regime without any disturbance coming from the slot, as seen before.

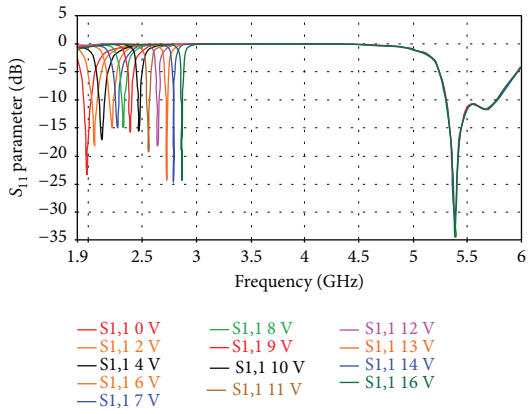

FIGURE 13: S_{11} parameter of the antenna using the varactor equivalent circuit.

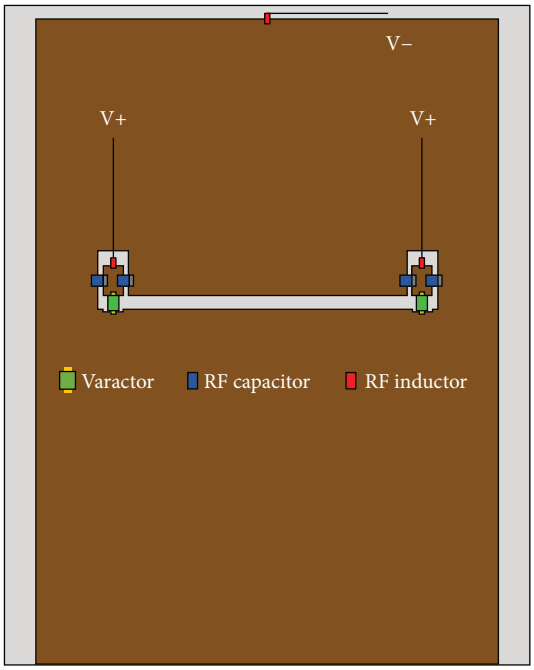

FIGURE 14: Biasing circuit configuration.

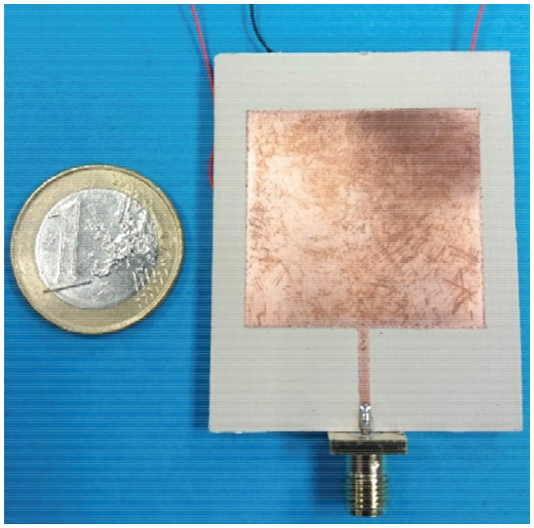

(a)

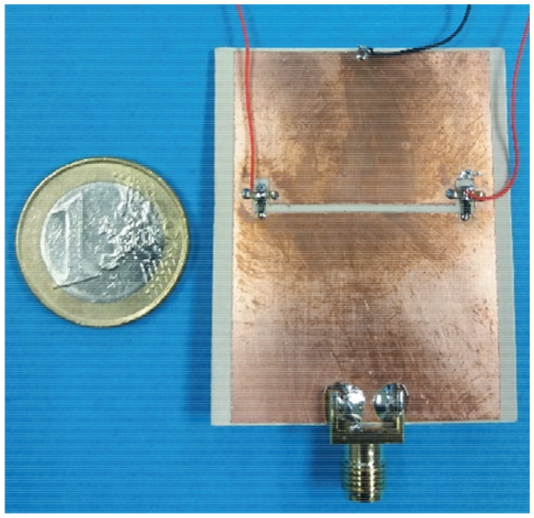

(b)

FIGURE 15: Fabricated antenna with DC bias circuit. (a) Front view. (b) Back view.

To be noted, the second band is a combination of several modes as seen in the previous section, and it is observed that the length and the width of the rectangular patch affect this band. As a suggestion, this band could be tuned as well by following the approach in [17] by embedding a pair of capacitors in the two opposite corners of the rectangular patch.

For the simulation of the structure including varactors, two approaches are followed in order to obtain good simulation performance. The first method consists of using the fundamental lumped element of the varactor diode, which is purely a capacitor. The second manner is based on using the equivalent circuit of the diode varactor given by the manufacturer, which include capacitors, inductance, and resistance.

(1) Case1: Ideal Circuit. Base on the typical capacitance of each voltage in the datasheet of the SMV2025 varactor diode model, a capacitor is used to simulate the diode varactor function. In Figure 10, by altering the capacitance values, the frequency of the first band is shifted reversely to the capacitor value and a smooth variation in a wide frequency range achieved. The second band keeps it constancy while the capacitors are varied. Remark that this simulation approach is called ideal case which did not include any parasitic element.

(2) Case2: Equivalent Circuit. For better simulation performance, this case includes the lumped elements in the equivalent circuit of the varactor. The tuning capacitance C_T ranges from 8.81 pF to 1.15 pF and can be achieved by the means of the reverse bias from 0 V to 20 V. The varactor diode model adopted in this antenna offer very low parasitic inductance and capacitance. Figure 11 shows the equivalent circuit of the varactor diode and antenna

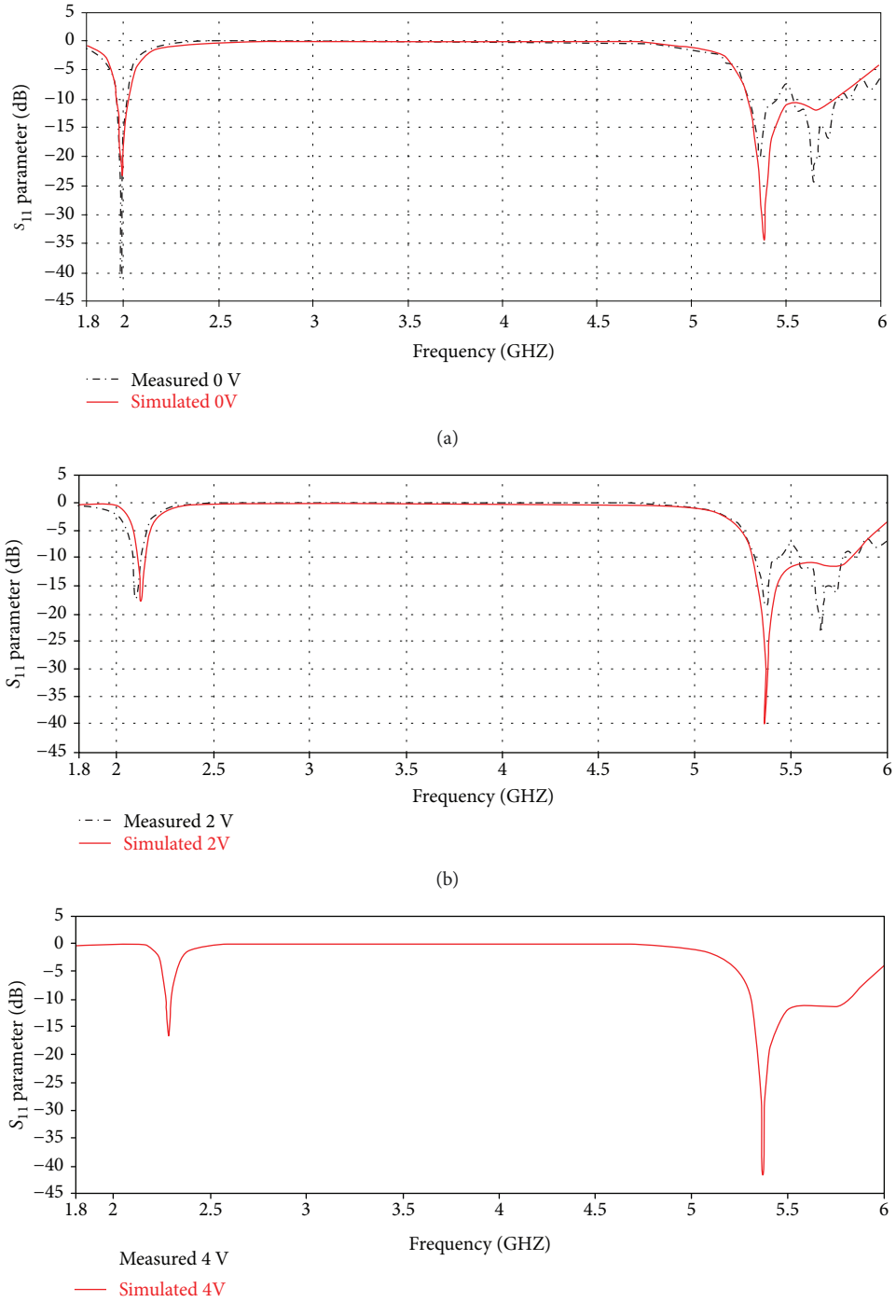

FIGURE 16: Simulated vs. measured S_{11} parameter for different biasing voltages: (a) 0 V, (b) 2 V, and (c) 4 V.

schematic model, where L_S is the parasitic inductance, R_S is the series resistance of the diode, C_T is the variable junction capacitance of the diode, and C_P is the parasitic capacitance arising from the installation of the package material. Figure 12 shows the variation of the frequency according to the capacitor variation. It can be seen that with this varactor model, a wide reconfigurable frequency band is achieved, from 2 GHz to 3.8 GHz.

The S_{11} parameter for both approaches are shown in Figures 10 and 13, showing a good agreement. The first band is a reconfigurable band, while the second is a steady band. A small shift in frequency can be observed in the second case, due to the additional parasitic components added. It can be seen that the impedance matching is below -10 dB for all the bands. The -10 dB bandwidth for the reconfigurable bands varies from 50 to 10 MHz,

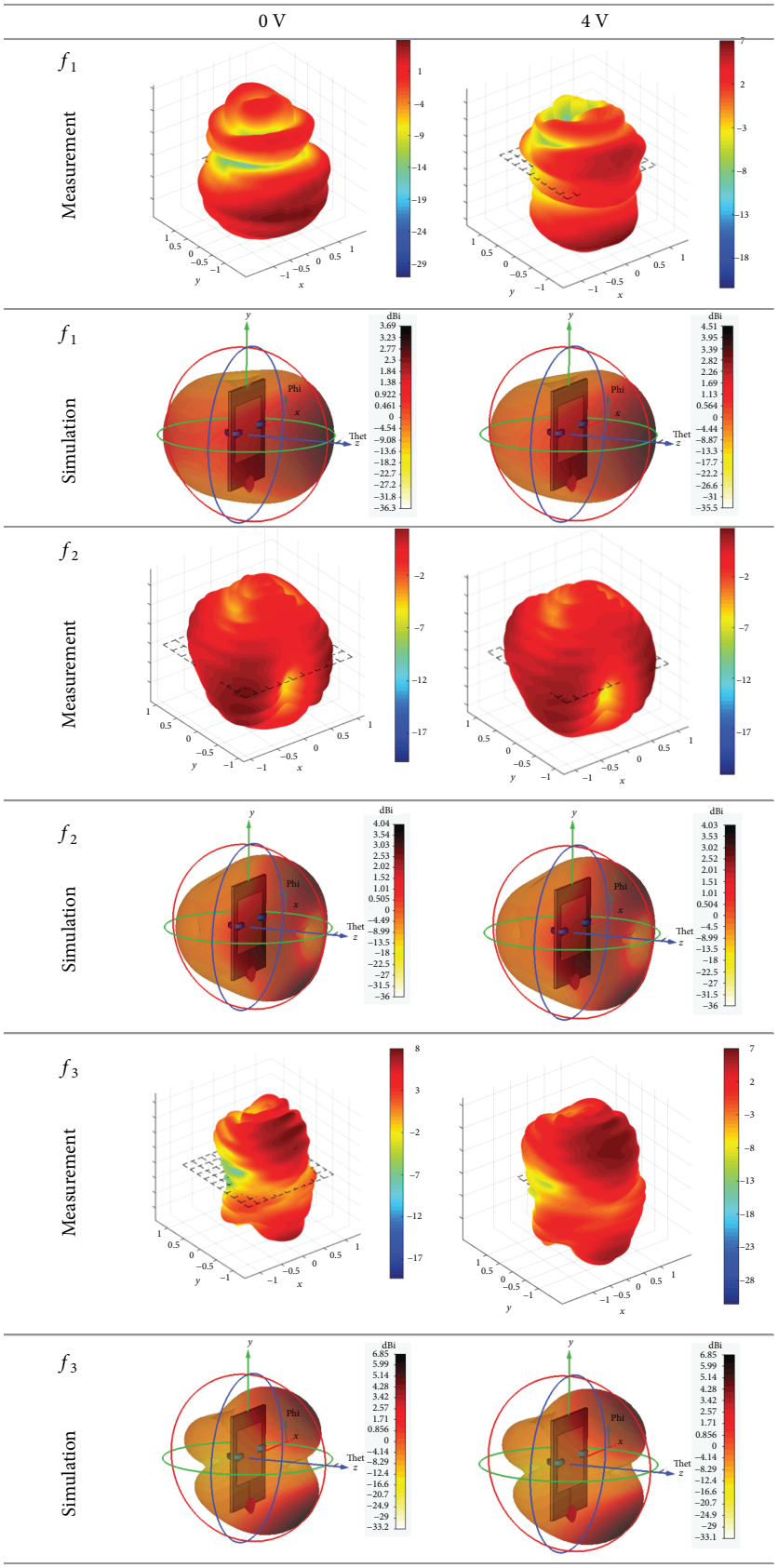

Figure 17: Simulated and measured 3D radiation patterns.

whereas for the steady band the impedance bandwidth reaches 500 MHz.

4. Prototype and Measurement Results

The bias circuit of the varactor diodes is loaded in a suitable manner, and DC components for controlling the varactor diodes are fitted in the ground plane. As illustrated in Figure 14, four DC block capacitors of 40 pF are used, in order to conserve the continuity of the RF current in the ground plane and provide DC blocking. DC voltage is isolated from the RF signal using three RF inductors of 40 nH. The cathode of the varactor diodes is connected to a small copper area and supplied with the positive DC voltage, while the anodes of the varactor diodes are connected to the ground plane, where the negative terminal is connected. The prototype of the antenna as depicted in Figure 15 is tested and analyzed.

Figure 16 illustrates a comparison between simulated and measured S_{11} parameter for three different biasing voltages 0 V, 2 V, and 4 V, as the bias increase, the capacitance decrease and the frequency shifted to the upper bands. It can be seen that at the reconfigurable band (lower band), a good agreement in the first configuration shown in Figure 16(a) (lower band centered at 2 GHz) and second configuration shown in Figure 16(b) (lower band centered at 2.15 GHz) is observed. The corresponding equivalent capacitance to the biasing voltages of 0 V and 2 V is 8.81 pF and 4.67 pF, respectively. The third configuration in Figure 16(c) (lower band centered at 2.25 GHz) does not meet a perfect match between simulation and measurement, due to the unstable behavior of bias circuit as the frequency increases. However, any selectable frequency at 2 GHz band can be achieved slightly by biasing reversely the varactor.

The radiation patterns of the prototype antenna were measured for the two configurations of biasing voltages (0 V and 4 V). The 3D patterns were taken at three selected operating frequencies within the reconfigurable band ($f_1 = 2$ GHz for 0 V and $f_1 = 2.3$ GHz for 4 V and two frequencies (f_2 and f_3) within the steady band ($f_2 = 5.4$ GHz and $f_3 = 5.67$ GHz)).

As shown in Figure 17, the majority of the measured patterns agree well with the simulated ones. Remark that some difference between the simulated and measured patterns for the first configuration (f_1, 0 V) exists, due to slight differences between the simulated and physical feeding adjustments.

Measured efficiency for the antenna in the steady band is above 66%, whereas the efficiency of the reconfigurable bands when the varactor is biased with 0 V and 4 V is 49% and 89%, respectively. These values are acceptable for real applications. In addition, the measured gains of the first and second bands are 3.16 dB and 6.56 dB (when 0 V is applied) and 6.33 dB and 5.67 dB (when 4 V is applied).

5. Conclusions

A practical approach to design dual-band frequency reconfigurable antenna is proposed. Based on the characteristic mode analysis, the ability to tune a particular mode instead of the rest of modes is demonstrated. Two simulation methods have been proposed, ideal case and equivalent circuit case. The interpretation is successfully applied to design a reconfigurable antenna that entirely covers the 2 GHz band and with a steady band centered at 5 GHz. The simulated results using the equivalent circuit of the varactor diode and the measured results are in good agreement.

Data Availability

The results used to support the findings of this study will be supplied under request to the corresponding author.

Conflicts of Interest

The authors declare that they have no conflicts of interest.

Acknowledgments

This work has been supported by the Spanish Ministry of Science, Innovation and Universities (Ministerio Ciencia, Innovación y Universidades) under the project TEC2016-78028-C3-3-P.

References

[1] F. Zhu, S. Gao, A. T. S. Ho et al., "Multiple band-notched UWB antenna with band-rejected elements integrated in the feed line," *IEEE Transactions on Antennas and Propagation*, vol. 61, no. 8, pp. 3952–3960, 2013.

[2] H. M. Al-Tamimi and S. Mahdi, "A study of reconfigurable multiband antenna for wireless application," *International Journal of New Technology and Research*, vol. 2, no. 5, pp. 125–134, 2016.

[3] Z. Mahlaoui, E. Antonino-Daviu, M. Ferrando-Bataller, H. Benchakroun, and A. Latif, "Frequency reconfigurable patch antenna with defected ground structure using varactor diodes," in *2017 11th European Conference on Antennas and Propagation (EUCAP)*, pp. 2217–2220, Paris, France, March 2017.

[4] Y. H. Cui, P. P. Zhang, and R. L. Li, "Broadband quad-polarisation reconfigurable antenna," *Electronics Letters*, vol. 54, no. 21, pp. 1199-1200, 2018.

[5] K. Boonying, C. Phongcharoenpanich, and S. Kosulvit, "Polarization reconfigurable suspended antenna using RF switches and P-I-N diodes," in *The 4th Joint International Conference on Information and Communication Technology, Electronic and Electrical Engineering (JICTEE)*, pp. 1–4, Chiang Rai, Thailand, March 2014.

[6] P. Y. Qin, Y. J. Guo, and C. Ding, "A dual-band polarization reconfigurable antenna for WLAN systems," *IEEE Transactions on Antennas and Propagation*, vol. 61, no. 11, pp. 5706–5713, 2013.

[7] I. T. E. Elfergani, A. S. Hussaini, C. H. See et al., "Printed monopole antenna with tunable band-notched characteristic for use in mobile and ultra-wide band applications," *International Journal of RF and Microwave Computer-Aided Engineering*, vol. 25, no. 5, pp. 403–412, 2015.

[8] N. Nguyen-Trong, L. Hall, and C. Fumeaux, "A frequency and pattern reconfigurable center shorted microstrip antenna,"

IEEE Antennas and Wireless Propagation Letters, vol. 15, pp. 1955–1958, 2016.

[9] M. D. Wright, W. Baron, J. Miller, J. Tuss, D. Zeppettella, and M. Ali, "MEMS reconfigurable broadband patch antenna for conformal applications," *IEEE Transactions on Antennas and Propagation*, vol. 66, no. 6, pp. 2770–2778, 2018.

[10] Q. Liu, N. Wang, C. Wu, G. Wei, and A. B. Smolders, "Frequency reconfigurable antenna controlled by multi-reed switches," *IEEE Antennas and Wireless Propagation Letters*, vol. 14, pp. 927–930, 2015.

[11] R. B. V. B. Simorangkir, Y. Yang, R. M. Hashmi, T. Bjorninen, K. P. Esselle, and L. Ukkonen, "Polydimethylsiloxane-embedded conductive fabric: characterization and application for realization of robust passive and active flexible wearable antennas," *IEEE Access*, vol. 6, pp. 48102–48112, 2018.

[12] D. Guha, S. Biswas, and C. Kumar, "Printed antenna designs using defected ground structures: a review of fundamentals and state-of-the-art developments," *Forum for Electromagnetic Research Methods and Application Technologies*, vol. 2, pp. 1–13, 2014.

[13] E. Antonino-Daviu, M. Cabedo-Fabres, M. Sonkki, N. Mohamed Mohamed-Hicho, and M. Ferrando-Bataller, "Design guidelines for the excitation of characteristic modes in slotted planar structures," *IEEE Transactions on Antennas and Propagation*, vol. 64, no. 12, pp. 5020–5029, 2016.

[14] R. Harrington and J. Mautz, "Theory of characteristic modes for conducting bodies," *IEEE Transactions on Antennas and Propagation*, vol. 19, no. 5, pp. 622–628, 1971.

[15] Skyworks Solution inc, "SMV2025 series: surface mount, silicon hyperabrupt tuning varactor diodes," *SMV2025 Series Data sheet*, 2015, http://www.skyworksinc.com/uploads/documents/SMV2025_Series_201431E.pdf.

[16] C. A. Balanis, *Antenna Theory: Analysis and Design*, Wiley, Hoboken, NJ, USA, 3rd edition, 2005.

[17] I. Rouissi, I. B. Trad, J.-M. Floc'h, H. Rmili, and H. Trabelsi, "Design of frequency reconfigurable triband antenna using capacitive loading for wireless communications," in *2015 Loughborough Antennas & Propagation Conference (LAPC)*, Loughborough, UK, November 2015.

2020 IEEE International Symposium on Antennas and Propagation and North American Radio Science Meeting | 978-1-7281-6670-4/20/$31.00 ©2020 IEEE | DOI: 10.1109/IEEECONF35879.2020.9329761

Radiation Pattern Agile Antenna using PIN Diodes and SPDT Switches

Zakaria Mahlaoui[1,2], Eva Antonino-Daviu[1], Miguel Ferrando-Bataller[1]
[1]Instituto de Telecomunicaciones y Aplicaciones Multimedia, Universitat Politècnica de València, Spain
[2]National School of Applied Sciences, Cadi Ayyad University, Marrakesh, Morocco
mahza@doctor.upv.es

***Abstract*—In this paper, a new design of a reconfigurable antenna is proposed. The antenna structure is using two PIN diodes for switching between two radiation patterns (directional and bidirectional) and a SPDT switch to achieve good impedance matching. The simulated results show a good impedance matching, with S_{11} below -10 dB using the SPDT switch configuration. In addition, the far-field directivity for both configurations is around 5 dB.**

***Index Terms*—Reconfigurable antenna, CMA, Radiation pattern, PIN Diode, SPDT.**

I. Introduction

Reconfigurable antennas are required by a significant number of modern wireless communication systems. Their excellent ability to modify some antenna parameter such as radiation pattern [1], polarization [2] and operating frequency [3], makes them a good solution to beat space volume, wireless standard diversity and user-effect problems.

The Characteristic Mode (CM) theory [4], [5] has an enormous potential in antenna engineering, since it delivers an easy approach to physically understand the characteristics of an antenna, such as the radiation pattern, polarization and bandwidth. In many designs [3]–[6], the CM theory has proved its great potential and insight toward physical behavior understanding, what leads to devise antenna systems with high performance.

This work is an improvement of the previous design presented in [1]. Based on the Characteristic Mode Analysis (CMA) shown in the previous work, two PIN diodes were used in two parallel plates to switch between two radiation pattern directions. In the earlier design, the antenna port was located at the the direction of the radiation pattern. In the current design, the antenna port was located at the edge of the plates, far away from the direction of the radiation pattern maximum. A SPDT (Single Pole Double Throw) [7] switch is inserted in order to perform the adequate impedance matching. One of the two outputs of the SPDT is connected directly to the antenna to obtain a bidirectional radiation pattern (case 1), whereas a circuit matching located between the second output of the SPDT and the antenna is adjusted to produce a directional radiation pattern (case 2).

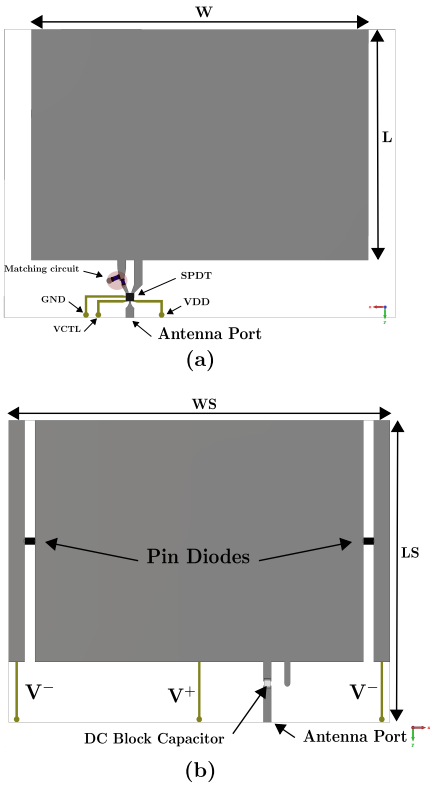

Fig. 1. (a) Antenna top view: (b) Antenna bottom view.

II. Proposed Antenna Design

The basic structure was proposed based on a CMA in [1]. It consists in two PEC parallel rectangular plates with the same size. The CMA showed that there are two main modes: Antenna mode J_1 (where current flows in the same direction in both plates) and transmission line mode J_1' (where current flows in opposite direction in both plates). However, by exciting the structure using a probe, it is observed that the resulting radiation pattern gets varied from a bidirectional beam to a directional pattern by means of slightly expanding the dimension of one plate.

A. Antenna geometry

The new proposed structure for the antenna is shown in Fig. 1 and its dimensions are presented in the Table I. The top

TABLE I
ANTENNA DIMENSION PARAMETERS.

Parameter	W	L	WS	LS	H	ϵ_r
Value (mm)	28	41	47.6	35	1.524	2.2

plate of the antenna contains the matching switching network. It consists of the main antenna input port of 50 Ω that is connected to a SPDT in order to choose the appropriate line to feed the antenna, depending on the desired configuration (case 1 or case 2, see Table II). The lower plate is considered as the ground plane, and its dimension can be increased by means of two PIN diodes connected at the two edge arms located at each side, as shown in Fig. 1(b).

B. Bias circuit configuration

The antenna switches are divided in two roles: the PIN diodes are controlling the switching between the two cases that provide the two different radiation patterns, whereas the SPDT switch is intended to match switching. To perform a good DC biasing supply to the PIN diodes, a DC block capacitor is introduced between the port and the ground plane. To decrease the matching lumped elements in the structure, case 1 is matched by putting the input transmission line at the appropriate position. Case 2 is matched by a series and a shunt capacitors both of them of 0.6 pF.

TABLE II
ANTENNA SWITCHES CONFIGURATION.

Case	Mode	PIN Diodes	SPDT
1	J_1'	OFF	VDD = 5 V, VCTL = 0 V
2	J_1' + J_1	ON	VDD = 5 V, VCTL = 3.3 V

C. Results and discussions

After presenting the configuration of the proposed structure, a full-wave simulation is carried out using CST Microwave Studio. All electronic components are taken into consideration in the simulation in order to provide the most precise results. The antenna design and the switches setup are optimized to be controlled with a microcontroller. The antenna radiation pattern structure is based on the two configurations shown in Table II:

Case 1: To excite mode J_1', the PIN diodes are reverse biased and a nought is given to the SPDT V_{CTL} (0 V). The S_{11} parameter in Fig. 2, with blue line, shows the band obtained at 2.44 GHz with this configuration. As a result, a bidirectional radiation pattern is achieved, with a directivity of 4.8 dB at both directions (θ = 0° and θ = 180°), as presented in Fig. 3(a).

Case 2: The combination of modes J_1' and J_1 is excited through the forward bias of the PIN diodes and by altering the V_{CTL} of the SPDT to 3.3 V. This second configuration shows a S_{11} parameter with a bandwidth larger than the first configuration, as shown in Fig. 2. Both configurations go along with the 2.4 GHz band. As a consequence, a directional radiation pattern is obtained with a directivity of 5 dB, as displayed in Fig. 3(b).

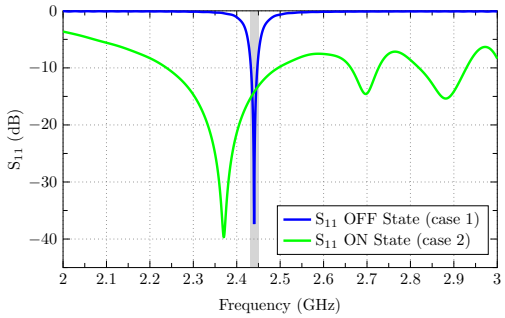

Fig. 2. S_{11} parameters of the case 1 and case 2.

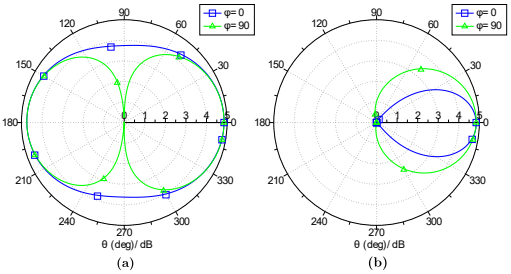

Fig. 3. Simulated radiation patterns: (a) Case 1; (b) Case 2.

III. CONCLUSION

In this design, the issues of the feeding cable and the matching of the design presented earlier in [1] are resolved. A radiation pattern reconfigurable antenna is proposed with a suitable control of the pattern, without drastically changing the antenna structure.

REFERENCES

[1] Z. Mahlaoui, E. Antonino-Daviu, A. Latif, M. Ferrando-Bataller and C. R. Peñafiel-Ojeda "From the Characteristic Modes Analysis to the Design of a Radiation Pattern Reconfigurable Antenna" *The 13th European Conference on Antennas and Propagation* (EuCAP) 2019.

[2] A. Bhattacharjee, S.Dwari and M.K Mandal, Polarization-reconfigurable compact monopole antenna with wide effective bandwidth. *IEEE Antennas and Wireless Propagation Letters*, vol 18(5), pp.1041-1045, 2019.

[3] Z. Mahlaoui, E. Antonino-Daviu, M. Ferrando-Bataller and A. Latif, "Design of a Dual-Band Frequency Reconfigurable Patch Antenna Based on Characteristic Modes," *International Journal of Antennas and Propagation*, vol 2019, Article ID 4512532, 12 pages, 2019.

[4] P. Futter, "Changing Design with Characteristic Mode Analysis" *Microwave journal* Altair Engineering Inc, 2016.

[5] R. F. Harrington and J. R. Mautz, "Theory of characteristic modes for conducting bodies," *IEEE Transactions on Antennas Propagation*, vol. AP-19, no. 5, pp. 622-628, Sept. 1971.

[6] E. Antonino-Daviu, M. Cabedo-Fabres, M. Gallo, M. Ferrando-Bataller and Bozzetti "Design of a Multimode MIMO Antenna Using Characteristic Modes",*The 3rd European Conference on Antennas and Propagation* (EuCAP) 2009.

[7] Data Sheet "SKY13585-679LF: 1.0 to 6.0 GHz SPDT Switch", *Skyworks Solutions*, 2015-2017.

From the Characteristic Modes Analysis to the Design of a Radiation Pattern Reconfigurable Antenna

Zakaria Mahlaoui[1,2], Eva Antonino-Daviu[2], Adnane Latif[1], Miguel Ferrando-Bataller[2]
[1] Information Technology and Modeling Laboratory, National School of Applied Sciences, Cadi Ayyad University, Marrakesh, Morocco
[2] Instituto de Telecomunicaciones y Aplicaciones Multimedia, Universitat Politècnica de València, Valencia, Spain, mahza@doctor.upv.es

***Abstract*— A reconfigurable radiation pattern antenna is proposed. Preliminary investigations are performed with the characteristic modes analysis to understand the physical behavior of the antenna. The presented antenna has the ability to switch from a directional beam to a bidirectional pattern by turning PIN diodes from ON to OFF state. A varactor diode is placed at the top plate to adjust the frequency and match the impedance. A prototype has been designed, fabricated, and measured. Results show good radiation pattern agreement on XZ plane, S_{11} parameter of the antenna is below −10 dB in the common band from 5.45 to 5.55 GHz.**

***Index Terms*—Characteristic Modes, Reconfigurable antenna, Radiation pattern, PIN diode, Varactor diode.**

I. INTRODUCTION

In several designs, the Characteristic Modes Analysis (CMA) has proved its great potential and insight towards physical behavior understanding, what leads to devise antenna systems with high performance. In the last decade, studies on the CM theory have affirmed its promising potential in a variety of antenna designs. The CM theory makes antenna design much easier, as it does not depend massively on personal experience or brute force optimization algorithms [1-2].

Reconfigurable antennas (RA) are conceived to change antenna basic characteristics such as the radiation pattern shape, beamwidth and direction, polarization or even the operating frequency [3]-[6]. RA can be classified into several types, depending on the use of semiconductors PIN or varactor diodes, RF MEMS, photoconductive components or reconfiguration by changing material properties [7]. As an example, the PIN diode is a silicon semiconductor with a high resistivity intrinsic area I interceding between a doped P type and N type region. However, the PIN diode is a current controlled resistor at radio frequencies and microwave circuits or can be defined as a switch that open or close the current flow. When the PIN diode is forward biased, a very low resistance is generated, the state labeled ON and the current flow reaches the required path. On the other hand, reverse bias generates a high resistance and causes an open circuit, as a result, there is no current flow and the case is identified as OFF state [7].

This work presents a pattern-reconfigurable antenna based on the use of two rectangular parallel metallic plates. The CMA was previously presented in [8], and here a real implementation of the antenna will be presented. A reconfigurable radiating structure using semiconductors PIN diode switches is proposed to activate or deactivate the lateral parts of the antenna. The aim of the proposed design is to control the radiation pattern of the antenna, switching between a bidirectional and unidirectional pattern, depending on the state of the PIN diodes. The reason of using a varactor diode is to reach a common operating frequency without drastically modifying the basic geometry. In this way, the proposed antenna suggests a convenient solution as it can be employed in different beam conditions without changing physically the antenna structure.

Characteristic modes analysis of the structure has been performed by means of FEKO software, whereas antenna simulation and design has been carried out by using CST simulator software.

II. CHRACTERISTIC MODES ANALYSIS

In [8], the characteristic modes analysis was performed on two rectangular PEC parallel plates as shown in Fig. 1, separated a distance of H=1.5 mm, and with initial dimensions of W1 x L1= 25 mm x 15 mm. The first analysis labeled as “case 1” consists of the two parallel plates with similar dimensions. The second analysis, labeled as “case2”, includes a small modification on one plate, which is increased 1 mm in length at both sides of the longer edges, being W2= 27 mm (see Fig. 1).

In [8], the CMA showed that there are two main modes at both cases: Antenna mode J_1 (where current flows in the same direction in both plates) and transmission line mode J_1’

(where current flows in opposite direction in both plates). At resonance frequency, it was observed that antenna mode J_1 and transmission line mode J_1' are presenting two different patterns, as shown in Fig. 2 (a) and (c). However, by exciting the structure using a probe, it is observed that the resulting radiation pattern gets varied from a bidirectional beam to a directional pattern by means of slightly expanding the dimension of one plate, as shown in Fig. 4 (b) and (d).

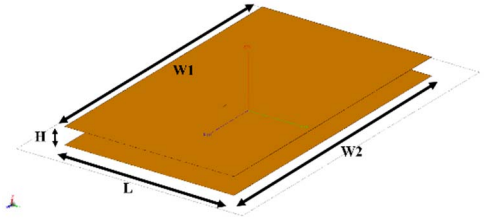

Fig. 1. Geometry of the structure

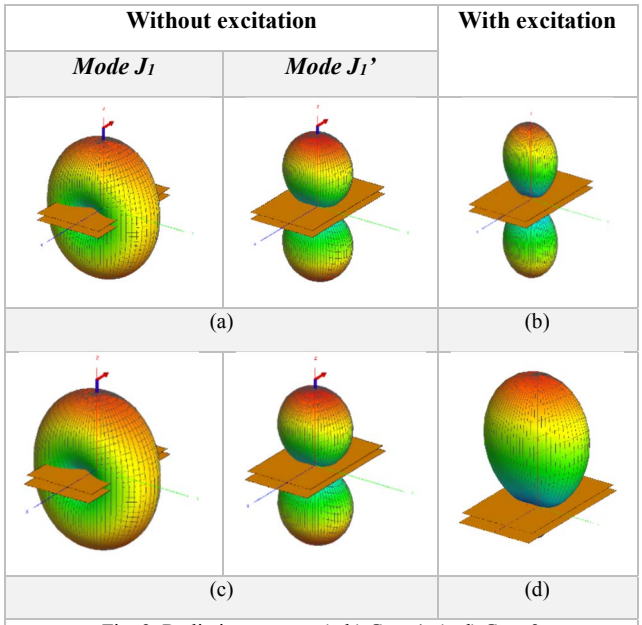

Fig. 2. Radiation pattern: (a-b) Case 1. (c-d) Case 2

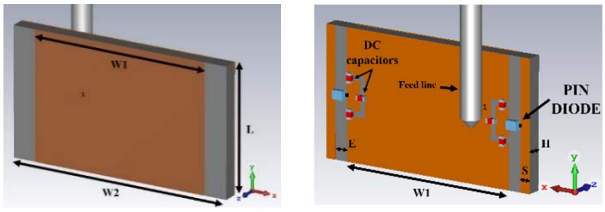

Fig. 3. (a): Top view, (b): Back view

From the CM perspective, this transformation of the radiation pattern can be explained by the different modal contribution to the total radiated power in the two cases. Mode J_1' (narrowband transmission line mode [2]) dominates the total radiation power at 5 GHz frequency band and leads to a bidirectional radiation pattern, as shown in Fig. 2 (b). Conversely, when the dimensions of the parallel plates are slightly different, the total radiated power includes a combination of mode J_1 (antenna mode) and J_1' (transmission line mode) and, therefore, this double mode excitation produces a directional pattern, as shown in Fig. 2 (d) [8].

III. ANTENNA DESCRIPTION

A. Antenna geometry

The proposed radiation pattern reconfigurable antenna shown in Fig. 3, consists of a patch antenna printed on a Neltec substrate with the thickness of 1.524 mm, permittivity of 2.2 and tangent loss of 0.0009. The dimensions of the structure are W1= 18mm, W2= 22.6 mm, L= 13 mm, S= 1mm and E= 1.3 mm.

Simulation and design are performed by using CST simulator software. The idea is to prove the modal analysis in the part II on a substantive antenna; Two PIN diodes are connecting the bottom plate to the lateral edges as shown in Fig. 3 (b). The two PIN diodes states, labeled as ON and OFF, allow or disallow the current to flow through the lateral edges; hence, and as shown in the modal analysis, the radiation pattern can get varied.

By switching from ON to OFF state, it is observed a shift in the operating frequency, as shown in Fig. 4 (a); this is generally due to the increase on length of the edges of the lower plate of the antenna. To settle this issue, a second design is proposed by applying a minor modification, that consists of adding a varactor on the top plate, as show in Fig. 5 (a). Varactor diode is considered one of the most used techniques to overcome the inherent constraint of narrow bandwidth and therefore extending the operation frequency range. As shown in Fig. 4 (b), a common operating frequency is achieved at 5.44 GHz for the two PIN diode states ON and OFF.

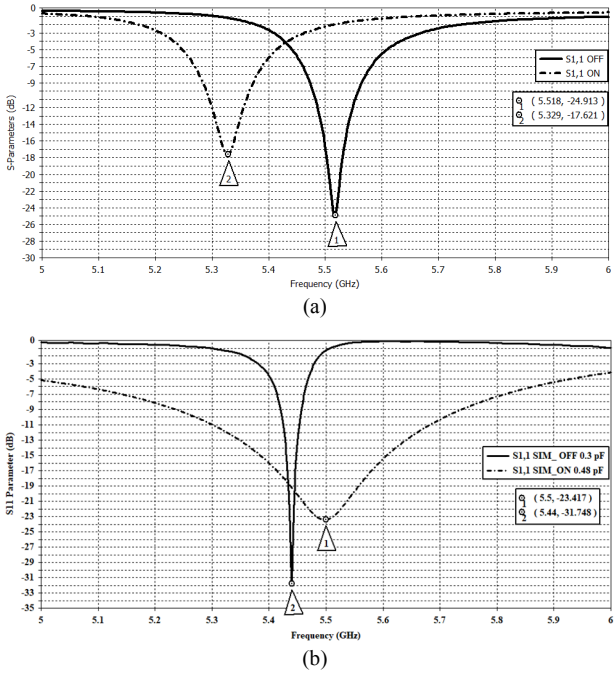

Fig. 4. Simulated S_{11} parameter: (a) without varactor, (b) with varactor

B. *Bias circuit configuration*

In this design shown in Fig. 5, the RF switch model adopted is the Infineon BAR50-02V silicon PIN diode. To perform the DC biasing supply, additional components are fitted around the PIN diodes and the Varactor diode. The DC voltage is isolated from the RF signal using four RF inductors of 27 nH. A total of eight DC block capacitor of 47 pF in order to conserve the continuity of the RF current crosswise the metal structure. The varactor diode model adopted in the design is MA46H120, has a tunable capacitance from 0.14 pF to 1.1 pF over the range 0-10V reverse bias voltage.

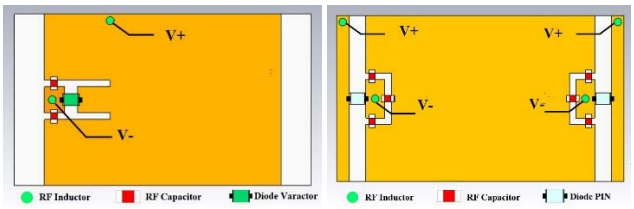

(a) (b)

Fig. 5. (a) Antenna top view, (b) Antenna back view

IV. PROTOTYPE AND MEASUREMENT RESULTS

The proposed radiation pattern reconfigurable antenna is fabricated and assembled with the electronic components as presented in Fig. 6. In this first prototype, wires are adopted in a classic manner to bias the diodes. Fig. 7 shows the measured versus simulated S_{11} parameter of the proposed radiation pattern reconfigurable antenna, when the PIN diodes are at the ON/OFF state. Besides, the varactor is reverse biased with 6 V when the state is OFF and 3 V at the ON state in order to match the impedance and to obtain a common frequency. From this figure, it is observed that the proposed antenna shows good measured impedance matching at the band 5.4-5.6 GHz that is suitable for WLAN applications.

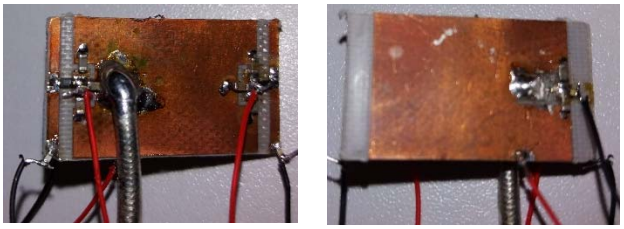

(a) (b)

Fig. 6. Fabricated antenna.

The measured radiation patterns of the reconfigurable antenna are plotted in Fig. 8. As shown by the analysis of section II, the two directions are achieved. By turning the PIN diodes to ON state leads to a directional beam and by switching the PIN diodes to OFF state conducts to a bidirectional pattern.

At the XZ plane, good agreement between the simulation and measurement are obtained. For the YZ plane, a notable distortion due to the position of the feeding cable and bias wires is observed.

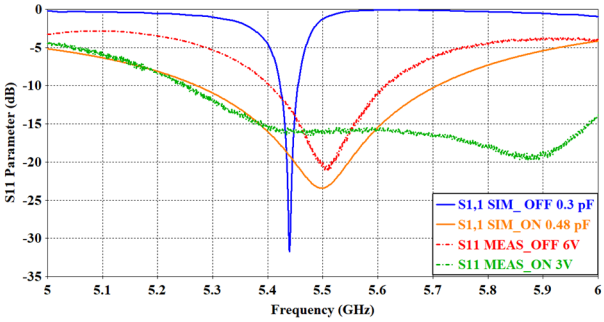

Fig. 7. Simulated and measured S11 Parameter of the two cases ON/OFF

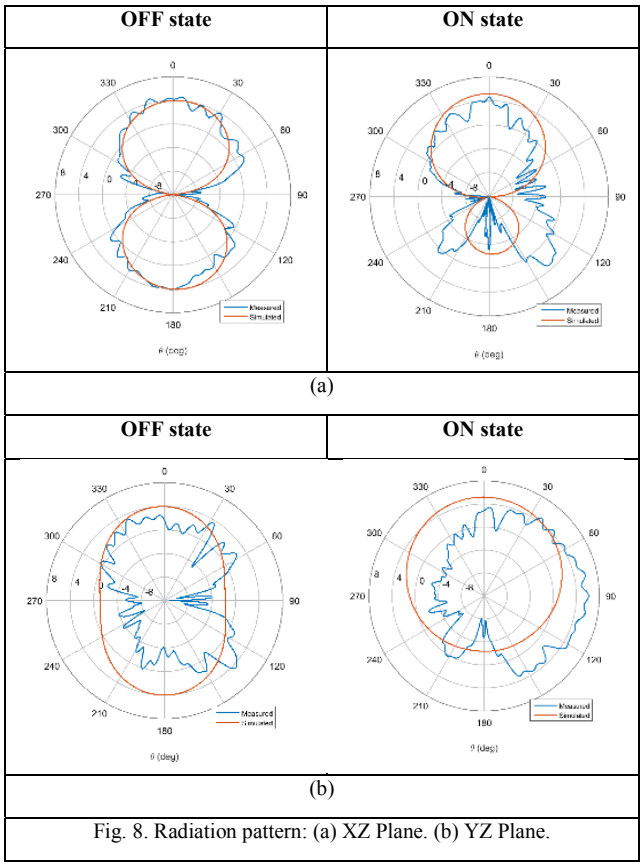

Fig. 8. Radiation pattern: (a) XZ Plane. (b) YZ Plane.

V. CONCLUSION

The presented work shows a methodical way to devise a reconfigurable antenna, starting by the characteristic modes analysis to the design and simulation, and ending by the fabrication and results validation. This approach has approved the stiffness of understanding antenna's structure.

As a result, two different patterns are achieved by tuning ON/OFF the state of PIN diodes. As a first prototype, good results obtained in term of S_{11} parameter and radiation pattern, especially at XZ plane. Further research is required to avoid cable effect on the antenna radiation pattern. Future work also includes new design with less bias wires.

REFERENCES

[1] M. Cabedo-Fabres. "Systematic Design of Antennas using the Theory of Characteristic Modes". PhD dissertation, Polytechnic University of Valencia, Spain, 2007

[2] M. Cabedo-Fabres, E. Antonino-Daviu, A. Valero-Nogueira, and M. Ferrando-Bataller, "The theory of characteristic modes revisited: A contribution to the design of antennas for modern applications," IEEE Antennas and Propagation. Magazine, vol. 49, no. 5, pp. 52–68, 2007

[3] M. N. Osman, M. K. A. Rahim, P. Gardner, M. R. Hamid, M. F. Yusoff and H. A. Majid "An Electronically Reconfigurable Patch Antenna Design for Polarization Diversity with Fixed Resonant Frequency" Radioengineering, vol. 24, no. 1, April 2015

[4] W. Lin, Hang Wong, and R. W. Ziolkowski "Wideband Pattern-Reconfigurable Antenna With Switchable Broadside and Conical Beams" IEEE Antennas and wireless propagation letters, vol. 16, 2017

[5] Z. Mahlaoui, E. Antonino-Daviu, A. Latif, M. Ferrando-Bataller and C. R. Peńafiel-Ojeda "Frequency Reconfigurable Patch Antenna Using Pin Diodes with Directive and Fixed Radiation Pattern" International Conference on Selected Topics in Mobile and Wireless Networking (MoWNeT) 2018

[6] I. T. E. Elfergani, A. S. Hussaini, C. H. See, R. A. Abd-Alhameed, N. J. McEwan, S. Zhu, J. Rodriguez, R. W. Clarke "Printed Monopole Antenna with Tunable Band-Notched Characteristic for Use in Mobile and Ultra-Wide Band Applications" International Journal of RF and Microwave Computer-Aided Engineering, November 2015

[7] H.M. Al-Tamimi, S. Mahdi, "A Study of Reconfigurable Multiband Antenna for Wireless Application", International Journal of New Technology and Research (IJNTR) ISSN: 2454-4116, Volume-2, Issue-5, May 2016 pp 125-134

[8] Z. Mahlaoui, E. Antonino-Daviu, A. Latif and M. Ferrando-Bataller "Radiation Pattern Reconfigurable Antenna Design Using Characteristic Modes" The12th European Conference on Antennas and Propagation (EUCAP) 2018

Radiation Pattern Reconfigurable Antenna Design Using Characteristic Modes

Zakaria Mahlaoui[1,2], Eva Antonino-Daviu[2], Adnane Latif[1], Miguel Ferrando-Bataller[2]
[1] Information Technology and Modeling Laboratory, National School of Applied Sciences, Cadi Ayyad University, Marrakesh, Morocco
[2] Instituto de Telecomunicaciones y Aplicaciones Multimedia, Universitat Politècnica de València, Valencia, Spain, mahza@doctor.upv.es

***Abstract*— In this paper, a radiation pattern reconfigurable antenna is presented, which is able to switch between a bidirectional and a unidirectional radiation pattern. The proposed antenna is conceived from the characteristic mode analysis of two parallel metallic plates, with the same and different sizes. By means of two PIN diodes, the size of the lower plate of the two parallel metallic plates can be modified, changing the behavior of the radiation pattern. During the ON/OFF switching, the operating frequency is shifted, what is solved by introducing a varactor diode in the antenna. Thus, the operating frequency is adjusted for the switching state.**

***Index Terms*—Characteristic Modes, Reconfigurable antenna, Radiation pattern, PIN diode, Varactor diode.**

I. INTRODUCTION

Many new techniques, design and concepts have been developed in the last few decades to beat the new challenges in the antenna engineering field. Nowadays, from a general view, numerical electromagnetic (EM) modeling techniques provide an accurate manner to examine the antenna performance before beginning the manufacturing and measurement procedures. However, from a physical point of view, numerical EM modeling techniques provide little information about physical behavior of the antenna. This lack of physical insight turns the forthcoming modification and optimization of the antenna difficult to achieve. In this insufficiency, the Characteristic Mode (CM) theory has a great potential in antenna engineering, since it hands over an easy way to physically understand many characteristics of an antenna, such as the radiation pattern, bandwidth and polarization [1][2].

In several designs [3][4], the CM theory has proved its great potential and insight toward physical behavior understanding, what leads to devise antenna systems with high performance.

Reconfigurable antennas (RA) are conceived to change antenna basic characteristics such as the radiation pattern shape, beamwidth and direction, polarization or even the operating frequency [5][6]. RA can be classified into several types, depending on the use of semiconductors PIN or varactor diodes, RF MEMS, photoconductive components or reconfiguration by changing material properties [7].

The ability to modify some antenna parameters increases flexibility and fulfills the requirements of communication systems. Antennas with reconfigurable radiation pattern increase the efficiency of indoor communication systems by reducing significantly the level of fading and it is suitable to be controlled by software programs.

This paper presents a pattern-reconfigurable antenna based on the use of two parallel metallic plates. Firstly, the geometry is proposed and a CM analysis is performed in order to explain the behavior of the antenna from a modal perspective. Then, a reconfigurable radiating structure using semiconductor switches is proposed. The aim of the proposed design is to control the radiation pattern of the antenna, switching between a bidirectional and unidirectional pattern, depending on the state of the PIN diodes.

II. ANALYSIS USING CHARACTERISTIC MODE THEORY

A. Physical Interpretation of Characteristic Modes

The eigenvalue λ_n is a quantity solved immediately from the following generalized eigenvalue equation [8]:

$$X(J_n) = \lambda_n R(J_n)$$

where $J_n$the eigenfunctions or eigencurrents, and R and X are, respectively, the real and imaginary parts of the impedance operator. Eigenvalues λ_n range from +∞ to -∞ and the sign of the eigenvalue determines whether the mode contributes to store magnetic energy ($\lambda_n > 0$) or electric energy ($\lambda_n < 0$). The mode is at resonance when its associated eigenvalue is zero.

Moreover, characteristic angles can be defined as:

$$\alpha_n = 180° - \tan^{-1}(\lambda_n)$$

From a physical point of view, a characteristic angle presents the phase angle between the characteristic current J_n and its associated characteristic field E_n. As can be seen, the phase angle α_n can be calculated from the eigenvalue λ_n directly. If the modal current and the tangential electric field on a surface *S* are 180° out of phase ($\alpha_n = 180°$), the mode is said to be in external resonance and the PEC shape is a more effective radiator, whereas when the modal current and the tangential electric field on a surface S are 90° or 270° out of phase($\alpha_n = 90°$ or $270°$), the mode mainly stores energy.

B. *Characteristic Modes of Two Rectangular Parallel Plates*

Fig. 1 shows two rectangular metallic plates, separated a distance H=1.5 mm. As seen, two cases are analyzed, corresponding to two plates with the same dimension (*W1* x *L1* = 25 mm x 15 mm) in Fig. 1 (a), and two plates with a small difference in the inferior plate length (*W2* x *L1* = 27 mm x 15 mm) in Fig. 1 (b).

Let us now analyze these two parallel plates using the CM theory. Fig. 2 shows the characteristic angle analysis carried out over the 2-10 GHz frequency band. The observation of the curves at $\alpha_n = 180°$ confirms that the antenna mode J_1', which is a transmission antenna mode, presents good radiating behavior. Fig. 2 also shows the total radiation pattern obtained for both structures when they are excited using a probe. As observed, the radiation pattern gets varied from a bidirectional beam in Fig. 2 (a) to a directional one in Fig. 2 (b), by means of slightly expanding the dimension of the one plate.

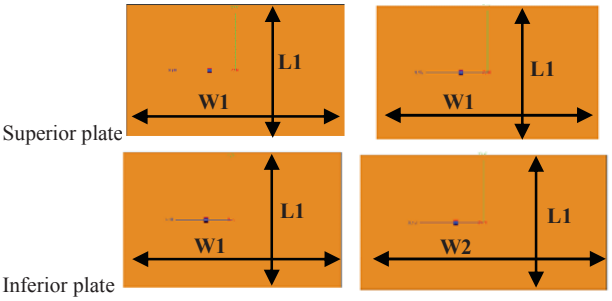

(a) (b)

Fig. 1. Geometry of the proposed structure: (a) rectangular parallel plates with same size, (b) rectangular parallel plates with small diffrence in size

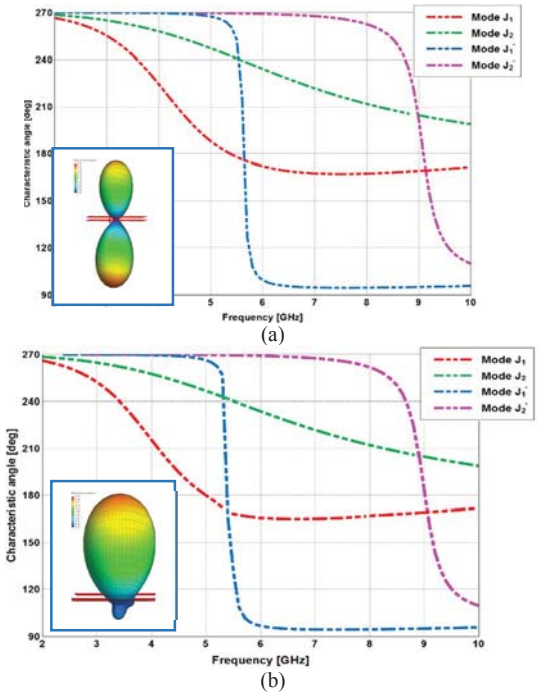

(a)

(b)

Fig. 2. Characteristic angle versus frequency for the first four modes of: (a) Two rectangular parallel plates with the same size; (b) Two rectangular parallel plates with a small diffrence in size.

From a CM perspective, this transformation of radiation pattern has a cause. Fig. 3 depicts the modal contribution to the total radiated power for the two cases. As seen in Fig. 3 (a), for the case of two rectangular parallel plates with the same size, mode J_1' (narrowband transmission line mode [2]) dominates the total radiation power at 5 GHz frequency band, and leads to a bidirectional radiation pattern. Conversely, as it can be observed in Fig. 3 (b), when the dimensions of the parallel plates are slightly different, the total radiated power consists of a combination of the mode J_1 (antenna mode) and J_1' (transmission line mode) and, therefore, this double mode excitation produces a directional pattern.

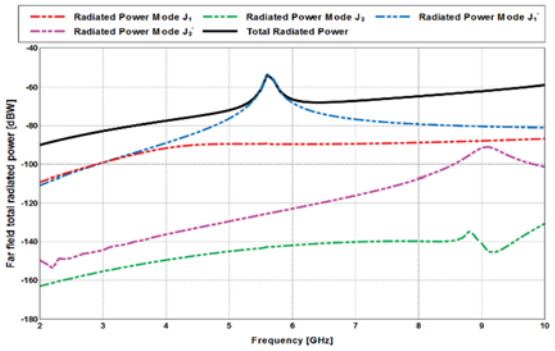

(a)

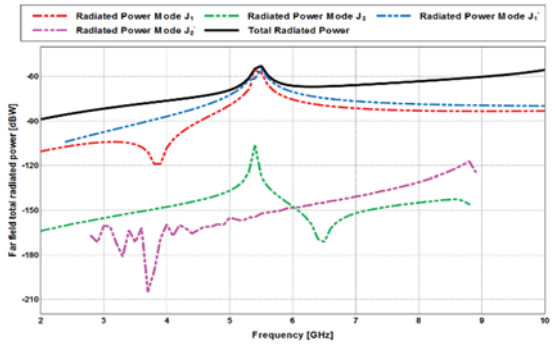

(b)

Fig. 3. Total radiated power and modal radiated power: (a) For the first four modes of two rectangular parallel plates with the same size; (b) For the first four modes of two rectangular parallel plates with a small difference in size.

III. RECONFIGURABLE ANTENNA

A. *Antenna Geometry*

As shown in the previous section, two parallel metallic plates with the same dimension present a bidirectional radiation pattern, which can be turned to a unidirectional pattern by means of slightly increasing the dimension of the lower plate.

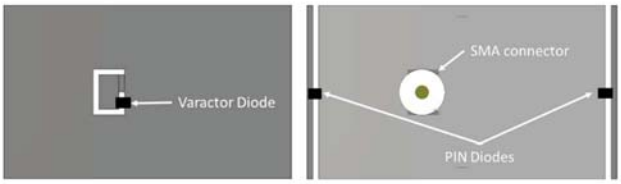

(a) (b)

Fig. 4. Antenna structure: (a) Top plate; (b) Lower plate.

Fig. 4 shows the geometry of the proposed radiation pattern reconfigurable antenna. The lower plate acts as the ground plane, and its dimension can be increased by means of using two PIN diodes connected to two metallic strips at the edges (edge arms). The top plate operates as the radiating element, where a varactor is used to tune the antenna.

In order to excite mode J_1' and mode J_1, the antenna is fed from underneath via a probe, as shown in Fig.4. The total size of the proposed antenna is WxLxH =27 mm x 15 mm x 1.5 mm.

It should be noted that the SMA port is not affecting the radiation pattern.

B. Results and discussion

After understanding the behavior of the proposed structure, a full-wave simulation is carried out using CST Microwave Studio. On one side, at the semiconductor switches (PIN diodes) placed at the both edges, forward biasing generates a very low resistance at higher frequencies that leads to the ON state, allowing the current to spread on the edge arms. In the other side, reverse biasing generates a very high resistance and causes an open circuit, which leads to an OFF state, where currents cease to flow in the edge arms.

As expected from the CM analysis performed in section II, the directional radiation pattern when the PIN diodes are in the ON-state changes to a unidirectional radiation pattern by turning the PIN diodes to the OFF-state, resulting a reconfigurable radiation pattern (see Fig. 5). As the length of the ground plane is increased in the ON-state, the operating frequency shifts down in frequency. Therefore, two different operating frequencies appear from the switching between ON/OFF state, as shown in Fig. 6.

The addition of a varactor diode next to the feeding point on the top plate solves the problem of shifting in the operating frequency when the switches are ON or OFF. As the varactor is a variable capacitor, the increase or decrease of the reverse biasing voltage moves the operating frequency and broadens the bandwidth at some reverse biases. Fig. 7 shows the equivalent circuit for the PIN diode (model BAR50-02V), which is composed by an inductor of 0.6 nH and a parallel capacitor of 0.15 pF with a resistance of 5 kΩ for the OFF state and 3 Ω for the ON state. The varactor diode (model SMV1232) circuit is based on the S-parameters data files provided by the manufacturer.

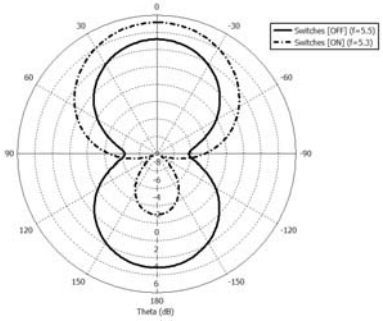

Fig. 5. Simulated radiation patterns corresponding to the OFF/ON state.

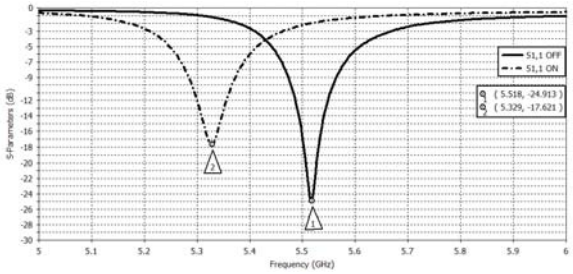

Fig. 6. Simulated S_{11} parameter for the OFF/ON state.

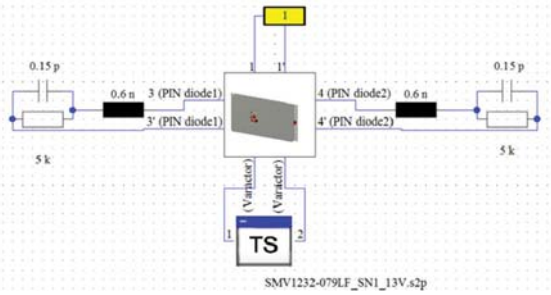

(a)

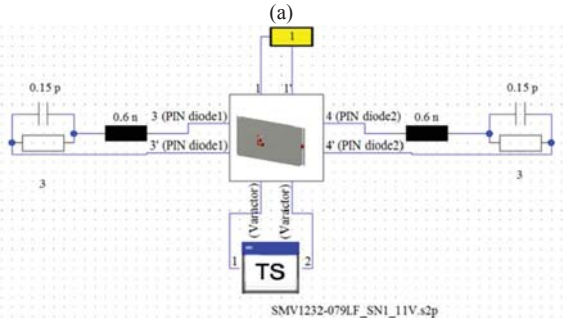

(b)

Fig. 7. Schematic of the equivalent circuit when PIN diode at: (a) OFF state; (b) ON state.

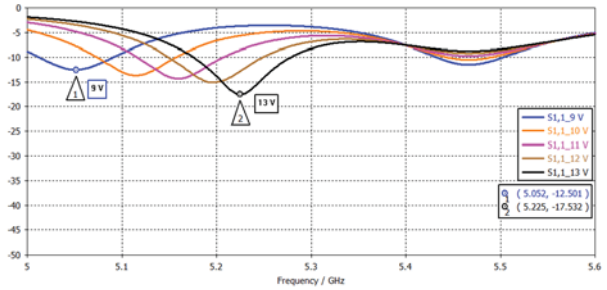

(a)

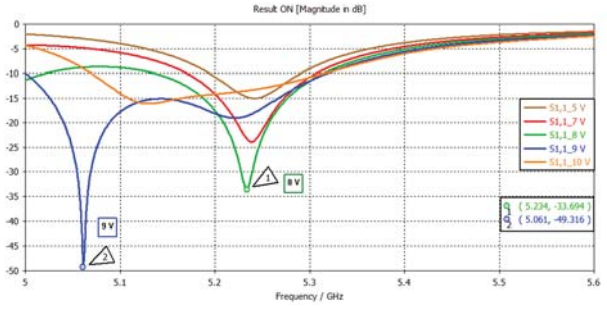

(b)

Fig. 8. Simulated S_{11} parameter for the different varactor diode reverse biasing: (a) When switches OFF; (b) When switches ON.

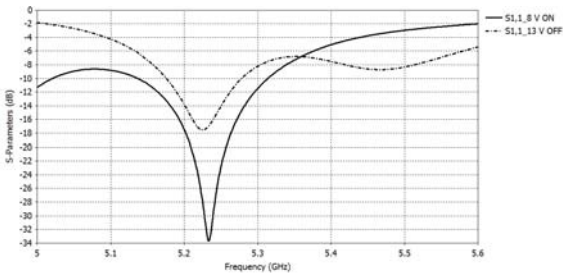

Fig. 9. Simulated S_{11} parameter for the optimum combination.

At the OFF state Fig. 8 (a), a wide bandwidth is achieved when the reverse bias is 13 V, leading to 105 MHz bandwidth. Moreover, at the ON state shown in Fig. 11, a wide bandwidth of 180 MHz can be achieved when the reverse biasing is 8 V and a reverse bias of 9 V, leading to 270 MHz bandwidth. By choosing the optimum values, Fig. 9 shows the operating frequencies for the two cases when switching ON or OFF. As observed, a 100 MHz bandwidth is achieved using the following combinations of "Switch state/reverse biasing": "Switch ON/8 V" and "Switch OFF/13 V".

The front-to-back ratio (F/B) describes the ratio between the E-field radiated from the main lobe to the back lobe. As shown in Fig. 10, in the ON state, the antenna concentrates the radiation in one direction, showing a high F/B ratio. In the OFF state, the antenna shows a F/B ratio of 2.5 (4 dB) at 5.2 GHz, which means that the difference between the two fields on both directions is convenient.

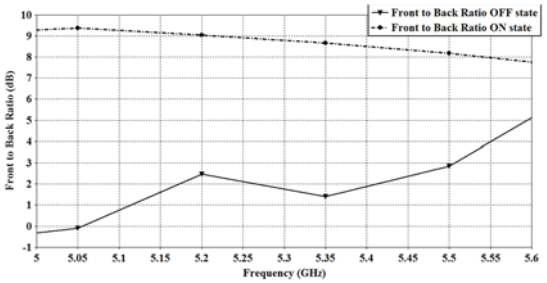

Fig. 10. Front to back ratio of the stat OFF and ON.

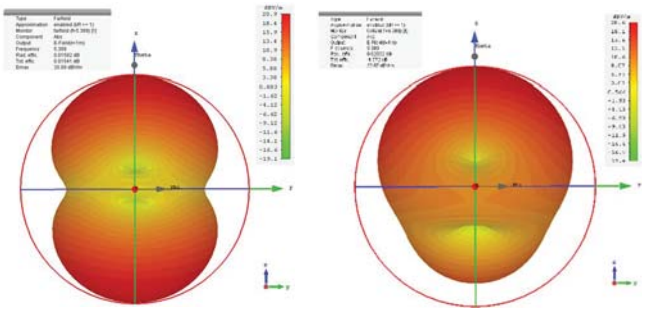

(a) (b)

Fig. 11. 3D Radiation Patterns for the states: (a) Pin Diodes OFF, (b) Pin Diodes ON.

The simulated 3D radiation patterns are shown in Fig. 11. simulation is based on the ideal cases, which include a fixed capacitor as the varactor diode, and a piece of metal as a PIN diode. The corresponding frequency for both states ON/OFF is 5.36 GHz. As can be seen, the configurability of the radiation is achieved, obtaining a total field focused at one direction or a bidirectional radiation pattern.

IV. Conclusions

The CM theory is able to provide a physical interpretation of the radiating behavior of an antenna. A radiation pattern reconfigurable antenna has been proposed with the aim of adjusting the radiation pattern of two parallel plates, from a bidirectional to a unidirectional pattern. PIN diodes are used to switch between the OFF and ON state, and by means of introducing a varactor diode, the operating frequency at both states is adjusted.

Acknowledgment

This work has been supported by the Spanish Ministry of Economy and Competitiveness under the project TEC2016-78028-C3-3-P.

References

[1] M. Cabedo-Fabres, E. Antonino-Daviu, A. Valero-Nogueira, and M. Ferrando-Bataller, "The theory of characteristic modes revisited: A contribution to the design of antennas for modern applications," *IEEE Antennas and Propag. Magazine*, vol. 49, no. 5, pp. 52–68, 2007.

[2] M. Cabedo-Fabes. "Systematic Design of Antennas using the Theory of Characteristic Modes". PhD dissertation, Polytechnic University of Valencia, Spain, 2007.

[3] R. Martens, D. Manteuffel. "Systematic design method of a mobile multiple antenna system using the theory of characteristic modes". *IET Microw. Antennas Propag.*, 2014, Vol. 8, Iss. 12, pp. 887–893 doi: 10.1049/iet-map.2013.0534.

[4] Q. Zhang, Y. Gao."Compact low-profile UWB antenna with characteristic mode analysis for UHF TV white space devices". *IET Microw. Antennas Propag.*, 2017, Vol. 11 Iss. 11, pp. 1629-1635.

[5] H.M. Al-Tamimi, S. Mahdi, "A Study of Reconfigurable Multiband Antenna for Wireless Application", *International Journal of New Technology and Research (IJNTR)* ISSN: 2454-4116, Volume-2, Issue-5, May 2016 pp 125-134.

[6] Z. Mahlaoui, E. Antonino-Daviu, M. Ferrando-Bataller, H. Benchakroun, A. Latif, "Frequency Reconfigurable Patch Antenna with Defected Ground Structure Using Varactor Diodes", 2017 11th European Conference on Antennas and Propagation (EUCAP), pp 2217-2220.

[7] Jean-Marc Laheurte, *Compact Antennas for Wireless Communications and Terminals*, John Wiley & Sons Inc, 2011. pp 169-202.

[8] R. F. Harrington and J. R. Mautz, "Theory of characteristic modes for conducting bodies," *IEEE Transactions on Antennas Propagation*, vol. AP-19, no. 5, pp. 622-628, Sept. 1971.

Frequency Reconfigurable Patch Antenna Using Pin Diodes with Directive and Fixed Radiation Pattern

Zakaria Mahlaoui[1,2], Eva Antonino-Daviu[2], Adnane Latif[1], Miguel Ferrando-Bataller[2], Carlos Ramiro Peñafiel-Ojeda[2,3]
[1] Information Technology and Modeling Laboratory, National School of Applied Sciences, Cadi Ayyad University, Marrakesh, Morocco
[2] Instituto de Telecomunicaciones y Aplicaciones Multimedia, Universitat Politècnica de València, Valencia, Spain, mahza@doctor.upv.es
[3] Universidad Nacional de Chimborazo (UNACH), Riobamba, Ecuador

***Abstract*__ This paper presents a frequency reconfigurable antenna, based on four PIN diodes implemented on one of each corner of a rectangular patch antenna. A combination of three switching configurations of the PIN diodes provides a current path modification, and consequently a variation on the operating frequencies. Simulated results are presented based on two approaches, the ideal case using a metal portion and the schematic case employing the equivalent circuit of the PIN diode. The proposed antenna is suitable for 5 GHz U-NII band. Results are obtained by using CST-MW simulator.**

***Index Terms*— Reconfigurable antenna, PIN diode, Directive, Patch antenna, Radiation pattern.**

I. INTRODUCTION

The evolution of wireless communication systems in the last years requests many techniques and concepts to design antennas that beat the challenges. Reconfigurable antennas (RA) have greatly contributed over recent years to provide to the market or the customer what they claimed. RA modifies dynamically the antenna performance such as the frequency, polarization or radiation pattern [1-3]. Many electronic components are used to tune antennas characteristics such as PIN diodes [3], varactors [1], MEMS switches [4] or tunable material properties [2].

The PIN diode is a silicon semiconductor with a high resistivity intrinsic area **I** interceding between a doped **P** type and **N** type region. However, the PIN diode is a current controlled resistor at radio frequencies and microwave circuits or can be defined as a switch that open or close the current flow. When the PIN diode is forward biased, a very low resistance is generated, the state labeled ON and the current flow reaches the required path. On the other hand, reverse bias generates a high resistance and causes an open circuit, as a result, there is no current flow and the case is identified as OFF state [5].

The presented antenna covers the 5 GHz U-NII band using PIN diodes switching between three configurations. As it is known, many applications use only one range of four from this unlicensed band in order to avoid the communication in the same frequency range as some other application. In this way, the proposed antenna suggests a convenient solution as it can be employed in different frequency bands without changing physically the antenna structure.

II. RECONFIGURABLE ANTENNA

A. *Antenna geometry*

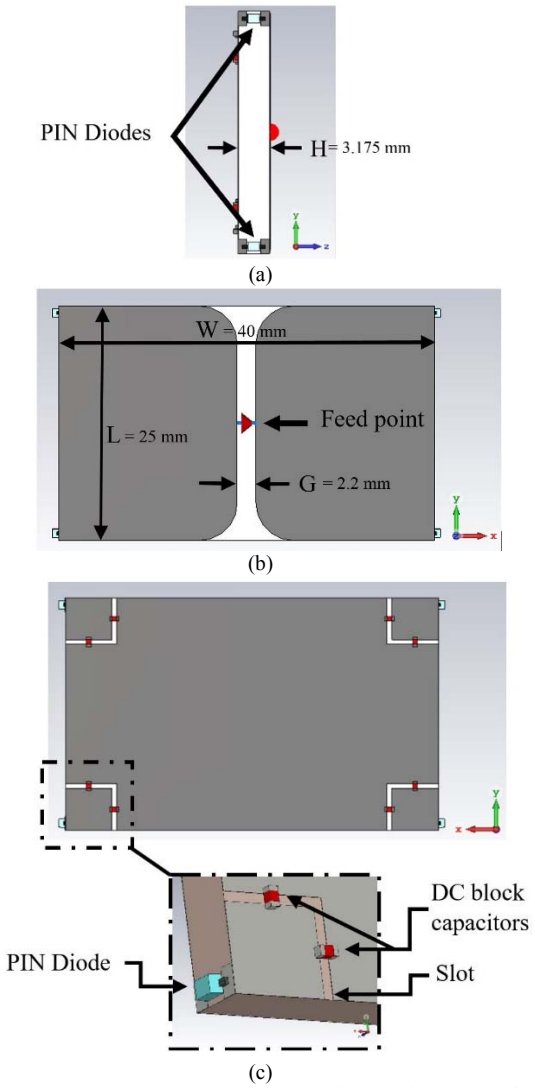

Fig. 1. Antenna structure : (a) Lateral view; (b) Top view; (c) Back view

978-1-5386-4248-1/18/$31.00 ©2018 IEEE

Fig. 1 shows a rectangular patch antenna with a substrate height of H = 3.175 mm and dielectric constant of 2.2. The feed point is positioned at the top plate on a gap of G = 2 mm that separate the negative from the positive side. It should be noted that the bending in the gap slot is for matching purposes and the full dimension of the antenna is W x L= 40 mm x 25 mm.

The reconfigurable antenna has four PIN diodes at each corner as presented in Fig. 1.(c). Because of the different path of the current flow achieved by the among three configurations, the frequency is altered.

B. Biasing circuit configuration

The biasing circuit consists of four narrow slots surrounding the PIN diodes to separate between DC area and RF zone, and eight DC Block capacitors to preserve the continuity of the RF current across the structure. As a first approach, wires replaced the DC block capacitors during the simulation, Additional six RF inductors to improve isolation between RF current and DC supply will be implemented in the manufactured prototype in further work.

III. SIMULATION RESULTS

Table1 shows the appropriate configurations to obtain the successive frequency bands. The first configuration consists of turning OFF all the PIN diodes, the second configuration contains two PIN diodes are ON and the two that are OFF, and the last configuration includes all the PIN diode in an ON state.

A. Equivalent circuit simulation

The PIN diode model adopted in the simulation is "infineon BAR50-02V". For the forward bias, the equivalent circuit shown in Fig. 2 comprises a serie inductance of 0.6 nH and a parallel capacitor of 0.15 pF with a resistance of 3 Ω. In reverse bias state, the parallel resistor turns to 5 kΩ.

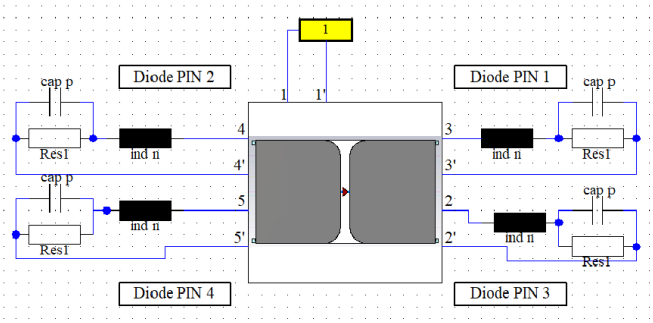

Fig. 2. Antenna schematic with equivalent circuit of the four PIN diodes

B. S11 Parameters

As shown in Fig. 3, a comparaison has been made between the ideal case using short/open representing the ON/OFF states of the PIN diode and the equivalent circuit of the diode model. The results show an agreement for the first and second configuration, while the third configuration presents a sligth shifting at the central frequency.

TABLE1. PROPOSED PIN DIODES CONFIGURATION

	First configuration	Second configuration	Third configuration
Diode PIN 1	OFF	ON	ON
Diode PIN 2	OFF	ON	ON
Diode PIN 3	OFF	OFF	ON
Diode PIN 4	OFF	OFF	ON
Central frequency	5.25 GHz	5.50 GHz	5.70 GHz
Bandwidth	480 MHz	380 MHz	370 MHz

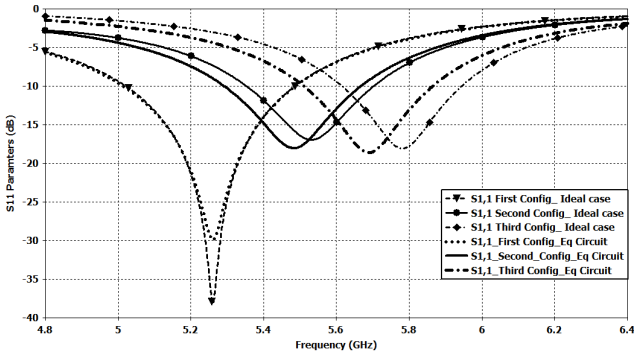

Fig. 3. S11 Parameters

C. Radiation pattern and feed cable effect

The simulation of the radiation pattern in Fig. 4 takes into account the feed cable effect, as it is positionned in the direction of the beam. Comparing to other paper [6], it is observed that the antenna shows a good radiation patterns, with a directivity of 8 dB for the first and third configuration and 7.5 dB for the second configuration. As it is presented in Fig. 4, the pattern is identical for the three configurations and the feed cable does not disturbe the radiation patterns.

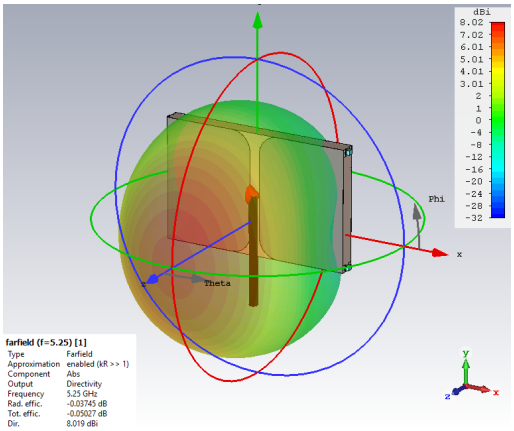

(a)

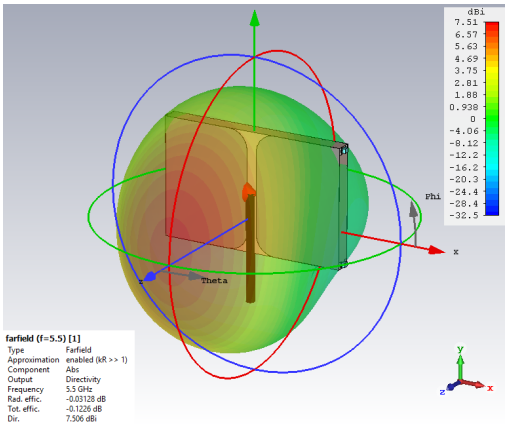

(b)

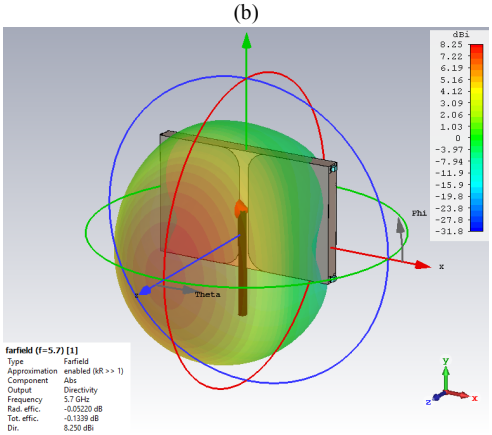

(c)

Fig. 4. 3D Radiation patterns: (a) First configuration; (b) Second configuration; (c) Third configuration

D. Gain and efficiency

The reconfigurable antenna shows a good performance such as the simulated gain in Fig. 5, that it is arround 8 dB at the central frequency for each configuration. The simulated efficiency results presented in Fig. 6 shows a high efficiency for the three configurations, meaning that the antenna delivers the most of the radiated power in the radiated electromagnetic waves.

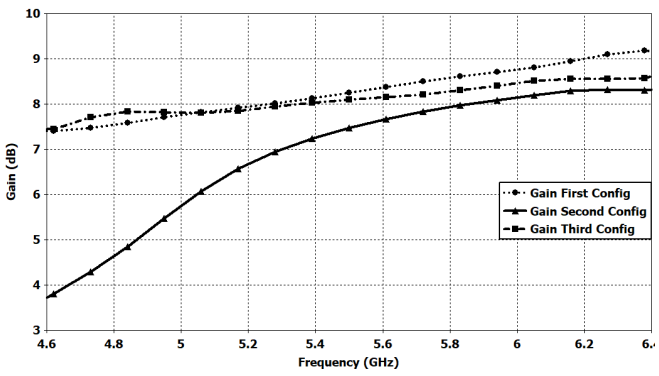

Fig. 5. Antenna simulated gain for the three configurations

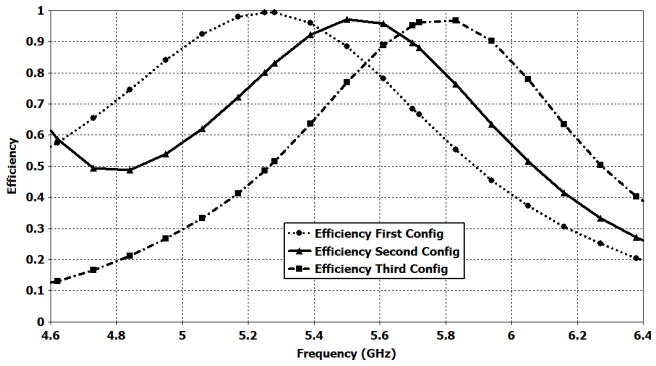

Fig. 6. Simulated antenna efficiency for the three configurations

IV. CONCLUSION

The antenna was based on PIN diodes embbeded on the edges to achieve frequency reconfigurability. Three configurations have been proposed to have a consecutive frequency ranges along the 5GHz band. A comparison between the ideal case simulation and the equivalent circuit simulation shows an acceptable agreement. Good results have been obtained in terms of directivity, gain and efficiency, showing that the feed cable has no effect on the radiation pattern.

ACKNOWLEDGMENT

This work has been supported by “Centre National pour la Recherche Scientifique et Technique (CNRST, Maroc)” as part of the research excellence scholarships program and by the Spanish Ministry of Economy and Competitiveness under the project TEC2016- 78028-C3-3-P..

REFERENCES

[1] Z. Mahlaoui, E. Antonino-Daviu, M. Ferrando-Bataller, H. Benchakroun, A. Latif, “Frequency Reconfigurable Patch Antenna with Defected Ground Structure Using Varactor Diodes”, 2017 11th European Conference on Antennas and Propagation (EUCAP), pp 2217-2220.

[2] D. Rodrigo, L. Jofre, B.A. Cetiner “Circular Beam-Steering Reconfigurable Antenna With Liquid Metal Parasitics” IEEE Transaction On Antennas and Propagation, Vol.60,No.4,April 2012 pp 1796-1802

[3] M.N. Osmani, M.K. Rahim, P. Gardner, M.R. Hamid, M.M. Yusoff, H.A. Majid “An Electronically Reconfigurable Patch Antenna Design for Polarization Diversity with Fixed Resonant Frequency”, radioengineering, Vol. 24, NO. 1, April 2015 pp 45-53

[4] S.Pioch, N. Adellan, J.M Laheurte, P. Blondy, A Pothier, “Integration of MEMS in frequency-tunable cavity- backed slot antennas” Journées Internationales de Nice sur les Antennes (JINA 2002), Nov 2002, Nice, France. 2, pp.153-156, 2002

[5] H.M. Al-Tamimi, S. Mahdi, “A Study of Reconfigurable Multiband Antenna for Wireless Application”, International Journal of New Technology and Research (IJNTR) ISSN: 2454-4116, Volume-2, Issue-5, May 2016 pp 125-134.

[6] N. Sood, K. Goodwill, M.V. Kartikeyan,“Frequency Reconfigurable Fabry Perot Cavity Antenna using Modulated Metasurface for WiMAX/WLAN Applications”, 2017 IEEE Applied Electromagnetics Conference (AEMC).

Frequency Reconfigurable Patch Antenna with Defected Ground Structure Using Varactor Diodes

Zakaria Mahlaoui[1], Eva Antonino-Daviu[2], Miguel Ferrando-Bataller[2], Hamza Benchakroun[1], Adnane Latif[1] [1] Information Technology and Modeling Laboratory, National School of Applied Sciences, Cadi Ayyad University, Marrakesh, Morocco, zakaria.mahlaoui@ced.uca.ma

[2] Instituto de Telecomunicaciones y Aplicaciones Multimedia, Universitat Politècnica de València, Valencia, Spain

***Abstract*— This paper presents an approach that combines two methods for reducing the size of a patch antenna and obtaining a wide tunability frequency range. The addition of a slot in the ground plan helps to shift down the basic frequency of the patch from 7.273 GHz to 4.267 GHz without modifying the basic geometry of the antenna. By modifying the varactor values, a series of successive bands are obtained, ranging from 4.65 GHz to 6.18 GHz. Accurate simulations are performed by using S-Parameter varactor data files. The patch antenna is suitable for U-NII band applications.**

***Index Terms*— reconfigurable antenna, DGS, varactor, patch.**

I. INTRODUCTION

Wireless communications have advanced very quickly in recent years, several wireless devices are becoming smaller than its preceding, and then antennas must have their dimensions reduced in a suitable way. Planar antenna, such as printed and microstrip antennas, have the attractive features of low profile, small size, and are very promising candidates to meet these miniaturization requirement.

Recently, an enormous interest has appeared toward miniaturizing microwave components such as antennas, amplifiers, filters…. A Defected Ground Structure (DGS) is performed by engraving some shape in the ground plane. The defected structure can be altered depending on the performance desired making the surface current distribution in the ground plane to get disturbed and resulting a controlled excitation and propagation of the electromagnetic waves through the substrate layer. DGS have many advantages such as antenna size reduction, harmonics reduction, cross polarization reduction, mutual coupling reduction, etc [1, 2].

Reconfigurable antennas use active components such as PIN diodes, varactors, (RF MEMS), photoconductive components or reconfiguration by changing material properties; one example is liquid crystal, which permittivity changes when a static field is applied [3]. Therefore, those components are able to change the antenna basic characteristics like the operating frequency, type of polarization and the radiation pattern.

The purpose of using a varactor diodes for tuning is to enable the radiator to be resonant over a greater frequency band without exceptionally modifying its basic geometry.

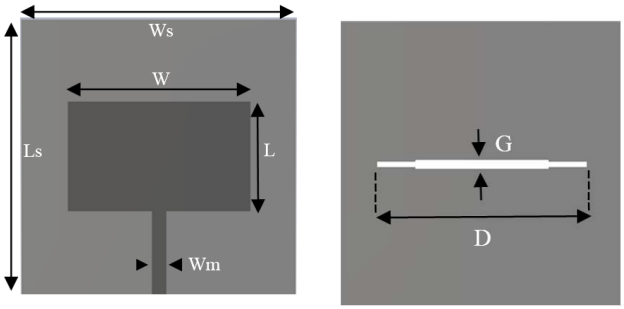

Fig. 1. Antenna structure: (a) Front view, (b) back view

II. ANTENNA CONFIGURATION

The basic antenna consists of a rectangular microstrip patch antenna (see Fig.1), whose parameters can be obtained by using the formulas in [4]. The proposed antenna is designed on a RT/duroid 5880 substrate with a thickness h = 1.575 mm and a dielectric constant ε_r = 2.2. The length and width of the rectangular resonator are L = 12 mm, and W = 20 mm, respectively. The width of the 50 Ω microstrip feeding line Wm is 1.5 mm. The total dimensions of the antenna are 30 x 30 mm^2.

Conventionally, in a planar microstrip circuit, the DGS is located underneath the microstrip feeding line [1, 2 and 5], and it disturbs the current distribution around the defect. As shown in Fig. 1, the defected shape in our case is a rectangular slot with variable width, with a width of G = 1 mm and a length of D = 22 mm. The slot is located under the rectangular resonator, and at each side of the slot, a varactor is positioned to change the antenna capacitance when reversed bias voltage is applied. The capacitance is inversely proportional to the reversed bias.

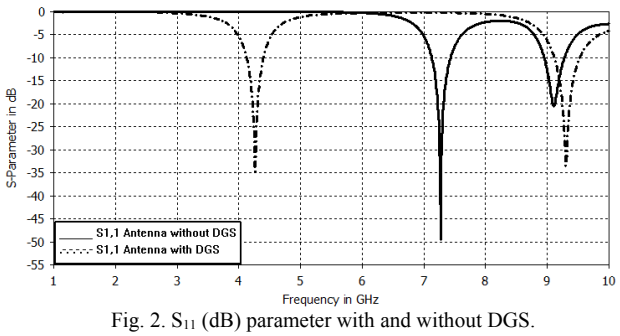

Fig. 2. S_{11} (dB) parameter with and without DGS.

III. RESULTS AND DISCUSSION

A. *Rectangular patch antenna with defected ground structure*

As presented in Fig. 2, the addition of a slot in the ground plane disturbs the current distribution, resulting the fact that, the basic operating frequency at 7.273 GHz is shifted down to 4.267 GHz without modifying the basic geometry of the antenna. Moreover, the frequency shift depends not only on the values of the capacitance, but also their locations along the slot.

As shown in Fig.3, the radiation pattern also gets disturbed by the DGS, turning from a directive beam to an omnidirectional pattern.

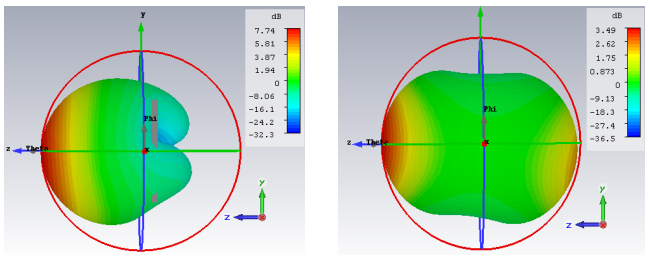

(a) (b)

Fig. 3. Radiation pattern: (a) without DGS, (b) with DGS.

B. *Rectangular patch antenna with reconfigurable DGS*

The simulations of the antenna are done in three different manners. The first case consists of using lumped elements, a pair of capacitances located at each side of the slot in the point on the antenna where the electric field is highest, as shown in Fig. 4 and Fig. 5.

Based on the datasheet of the varactor diode SMV1232-079LF [6], a series of simulations have done by varying the capacitance value. Fig. 6 shows the frequency tuning range achieved, from 5 GHz to 6.7 GHz.

Second approach include the equivalent circuit of the varactor diode, depicted in Fig. 7 and Fig. 8, where $C_J(V)$ is the variable junction capacitance of the diode, and can be varied from 4.15 pF to 0.72 pF, with a reverse voltage between 0 and 15 V, $R_S(V)$ is the variable series resistance of the diode, L_P is the parasitic inductance and C_P is the parasitic capacitance arising from the installation of the package material, geometry and the bonding wires or ribbons. C_P has been neglected in the equivalent circuit of the simulation, as seen in Fig. 8. The values of R_S and L_P are 1.5 Ω and 0.7 nH, respectively [7].

The third approach is based on the S-Parameter data files provided by the manufacturer of the varactor [6]. Each file contains the S-Parameter measure data for one voltage value. As shown in Fig. 11, different operating frequencies are obtained by switching between files from 0 to 13 V.

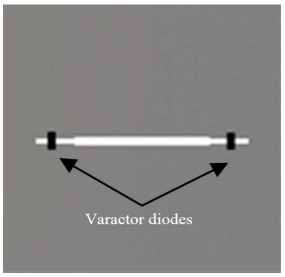

Fig. 4. Position of the varactor diodes.

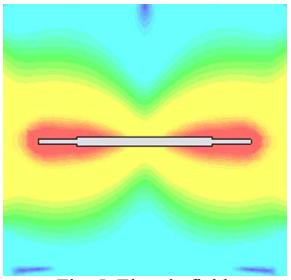

Fig. 5. Electric field.

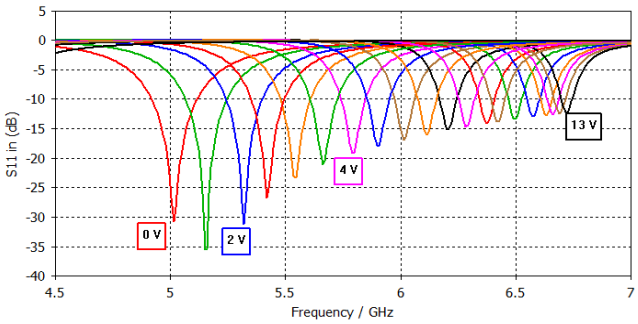

Fig. 6. S_{11} (dB) for different capacitance values.

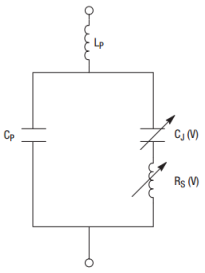

Fig. 7. Varactor diode equivalent circuit.

By comparing the three cases, reflection coefficient in the first case does not match perfectly with the others cases (Fig. 7, 9, and 11). This is due to the fact that the first case is an ideal case with no parasitic effects.

Comparing to other reconfigurable antenna papers [8, 9, and 10], it is observed that the antenna shows a good tunability range, a small size and a simple design with low coast and low power consumption.

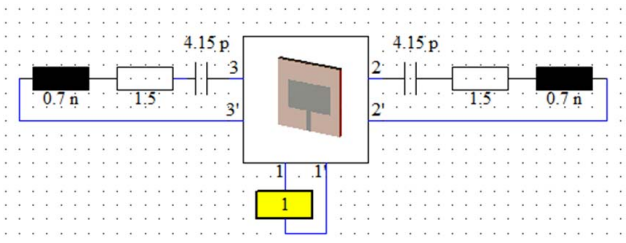

Fig. 8. Schematic of the varactor diode.

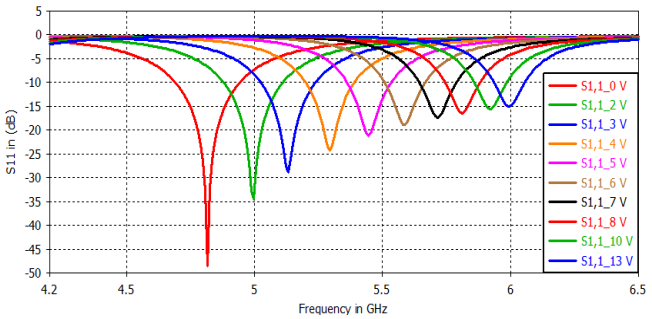

Fig. 9. S_{11} parameter using varactor diode equivalent circuit.

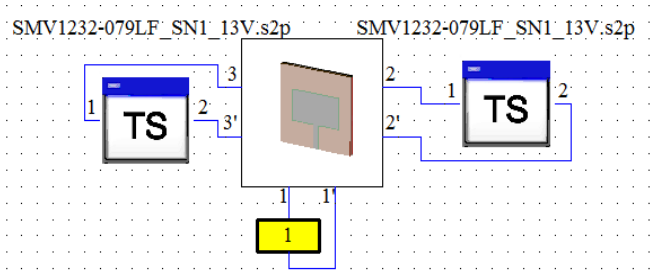

Fig. 10. Schematic of the s2p files.

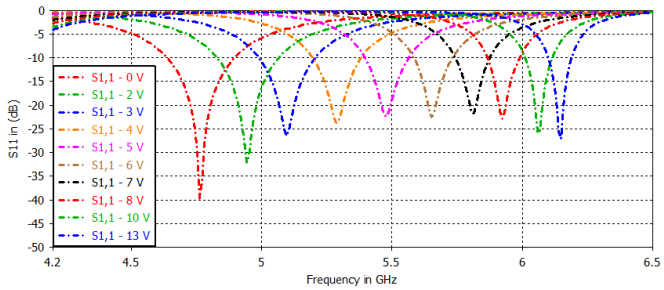

Fig. 11. S_{11} (dB) parameter using data files.

C. *Surface current distribution*

In previous section it is observed that a wide frequency tuning range (from 5 GHz to 6.7 GHz) was achieved by means of the use of varactor. However, as depicted in Fig. 12, the second resonance of the at 9.2 GHz stays stable despite of the variable capacitance values of 4.15 pF, 1.97 pF, 1.22 pF and 0.94 pF which correspond to 0, 2, 4 and 6 V reverse bias values, respectively. This is an interesting feature to get a stable band with the possibility to tune other bands.

In order to understand the behavior of the antenna, the current surface distribution both in the patch surface and the defected ground plane are investigated in Fig. 13 at the frequencies of 2.251 GHz, 5.014 GHz and 9.224 GHz for the reference case of a reverse bias voltage of 0V.

As shown in Fig. 13-(f), horizontal current distribution in the ground plane is not affected by the presence of the slot, which means that the DGS does not affect the patch antenna resonance at this frequency. Otherwise, the ground slot acts as a resonator and a strong current intensity appears around the capacitances position, as observed in Fig. 13(d) and (e).

The radiation patterns (with side and perspective view) of the patch antenna with DGS at the frequencies mentioned above are presented in Fig. 14 for the reference case of a reverse bias voltage of 0V. The results show that the radiation patterns are nearly omnidirectional for the tunable frequencies as shown in Fig. 14-(d) and (e). It is observed that in the stable band (around 9.224 GHz), the null of current surface around the defected ground slot provides a radiation pattern towards the z axis.

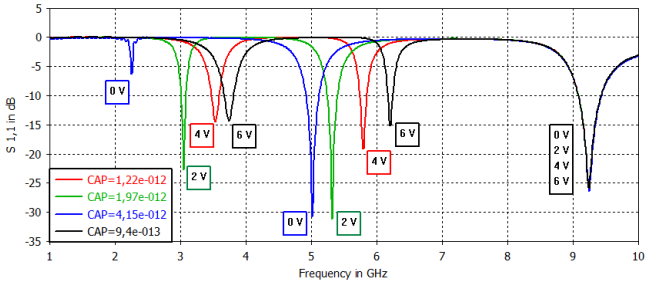

Fig. 12. S_{11} (dB) at 1 to 10 GHz band.

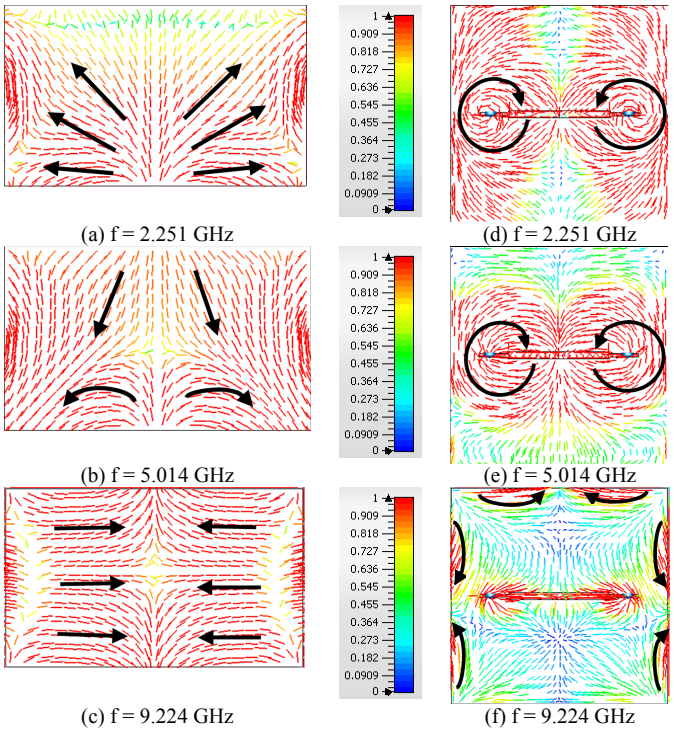

(a) f = 2.251 GHz (d) f = 2.251 GHz

(b) f = 5.014 GHz (e) f = 5.014 GHz

(c) f = 9.224 GHz (f) f = 9.224 GHz

Fig. 13. Surface current distribution of the: Patch in (a), (b) and (c); ground plane in (d), (e) and (f).

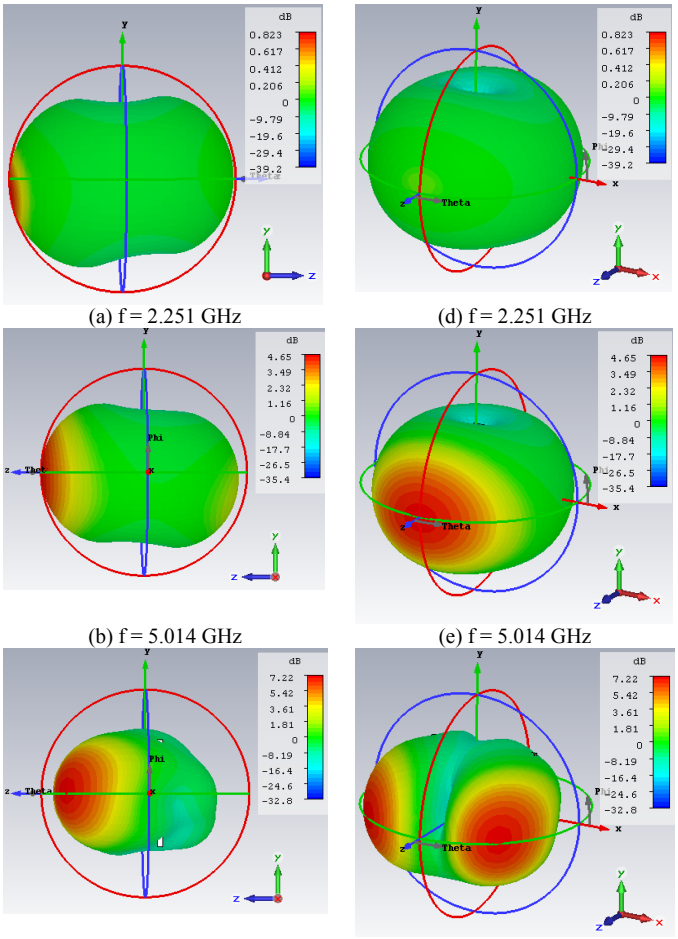

(a) f = 2.251 GHz (d) f = 2.251 GHz

(b) f = 5.014 GHz (e) f = 5.014 GHz

(c) f = 9.224 GHz (f) f = 9.224 GHz

Fig. 14. Radiation patterns: Side view in (a), (b) and (c); perspective view in (d), (e), and (f).

IV. CONCLUSIONS

In the work presented, the performance of a reconfigurable antenna with a defected ground structure (DGS) is improved. The purpose of this paper is to reduce size and to achieve a wide tunable frequency range. The possibility to obtain a stable frequency band has been observed. By following this approach, it is feasibly to obtain in further work a steady band in the 5 GHz band and a reconfigurable 2 GHz band.

REFERENCES

[1] K. Ashwini Arya, M.V. Kartikeyan , and A.Patnaik, "Defected Ground Structure in the perspective of Microstrip Antennas: A Review" Frequenz, Berlin, pp 79-81, June 2010.

[2] D. Guha, S. Biswas, and C. Kumar, "Printed Antenna Designs Using Defected Ground Structures: A Review of Fundamentals and State-of-the-Art Developments", Forum for Electromagnetic Research Methods and Application Technologies.

[3] Jean-Marc Laheurte, "Compact Antennas for Wireless Communications and Terminals", John Wiley & Sons Inc, 2011. pp 169-202.

[4] Constantine A . Balanis, "Antenna Theory Analysis and design", 2005 by John Wiley & Sons, Inc. pp 816-843.

[5] L. Hai-Wen, L. Zheng-Fan, S. Xiao-Wei, S. KURACHI2, J. Chen, and T. Yoshimasu, "Theoretical Analysis of Dispersi on Characteristics of Microstrip Lines with Defected Ground Structure", J. of Active and Passive Electronic Devices, Vol. 2, pp. 315–322.

[6] Data sheet, "SMV123x Series: Hyperabrupt Junction Tuning Varactors Applications", http://www.skyworksinc.com/Product/531/SMV1232_Series.

[7] Application note, "Varactor Diodes". Skyworks Solution inc.

[8] A. Hany Atallah, B. Abdel-Rahman, K. Yoshitomi and K. Ramesh Pokharel, "Design of Miniaturized Reconfigurable Slot Antenna Using Varacctor Diodes for Cognitive Radio Systems", 2016 Fourth International Japan-Egypt Conference on Electronics, Communications and Computers (JEC-ECC), pp 63-66.

[9] E. Antonino-Daviu, M. Cabedo-Fabres, M. Ferrando-Bataller and Vicent M. Rodrigo-Pefiarrocha, "Active UWB Antenna with Tuneable Band-notched Behaviour", Antennas and Propagation. EuCAP 2007.

[10] I. T. E. Elfergani, A. S. Hussaini, C. H. See, R. A. Abd-Alhameed, N. J. McEwan, S. Zhu, J. Rodriguez, R. W. Clarke, "Printed Monopole Antenna with Tunable BandNotched Characteristic for Use in Mobile and Ultra-Wide Band Applications", International Journal of RF and Microwave Computer-Aided Engineering · November 2014

6.8 Radiation Pattern Reconfigurable Antenna 3D video and Job Circuit

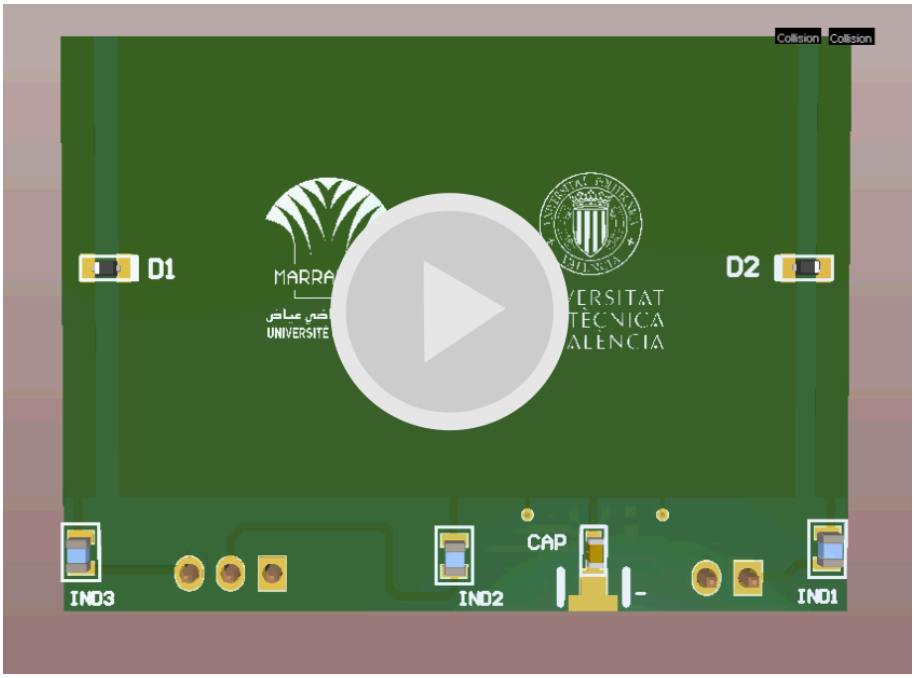

zakaria

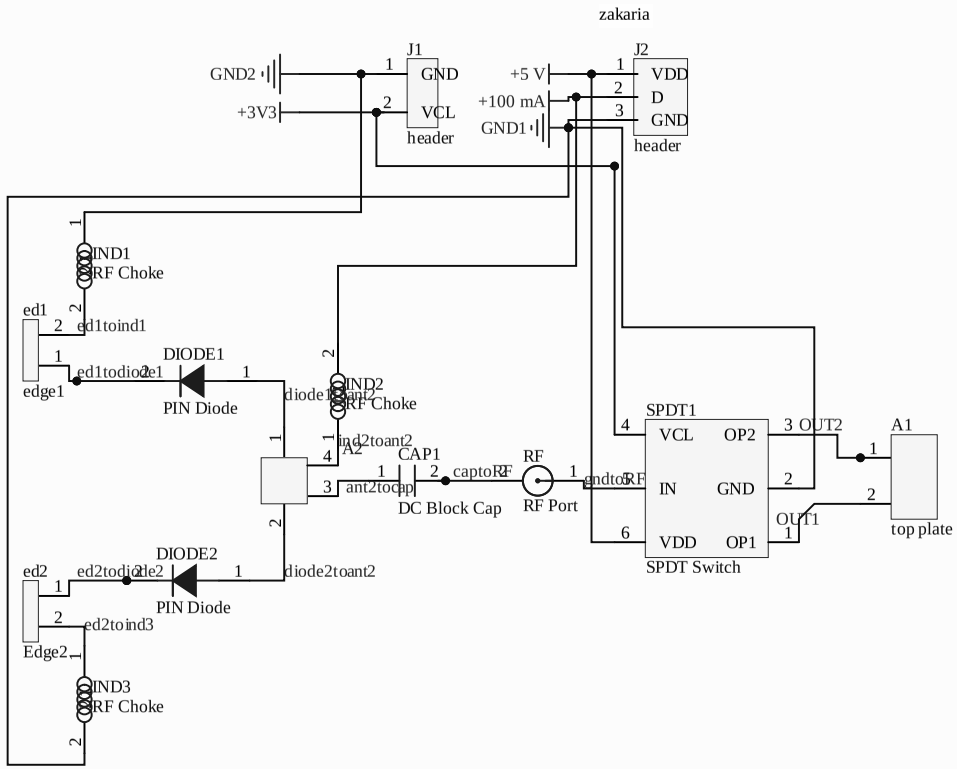

Title		
Size A4	Number	Revision
Date: 2/11/2020	Sheet of	
File: C:\Users\..\Antenna_Schematic.SchDoc	Drawn By:	